



SECTION 5: THESIS DETAILS

NUMBER OF PAGES

This thesis consist of 184 pages in total.

DEDICATION

To My Beloved Grandmother

ACKNOWLEDGMENTS*

I would like to express my special thanks to my advisor Assoc. Prof. Dr. Mecit Halil Öztop for his continuous support, understanding, guidance, energy and encouragement throughout this study. He always tried to make everything easy for me and helped me in my stressful days. Additionally, I am very grateful to my co-advisor Prof. Dr. Behiç Mert for his all suggestions about the study and the selection of correct academic path.

I would like to express my thanks also to Asst. Prof. Ilkay Sensoy for her advices. I would like to extend my gratitude to members of my thesis committee, Prof. Dr. M. Esra Yener, Assoc. Prof. Dr. Özge Şakıyan Demirkol and Assist. Prof. Dr. Elif Yolaçaner. Very special thanks go to Prof. Dr. Alexander Pines for accepting me to his lab as 1 year visiting student researcher in UC Berkeley. During my research, Danila Barskiy was the leading labmate in my studies so I am very grateful to him. My thanks also go to Dr. Jeff Pelton, technical expert who helped me so much during my analyses. I would like to appreciate other Pines Lab members owing to their friendships, helpfulness and kindness throughout my research.

I would also like to thank our all research assistants at our department, Özge Güven for her trustable friendship, Esmanur İlhan and Kübra Ertan for their delicious dishes and good humour, Selen Güner for her energy, help and thoughtful behavior, Barış Özel and Seren Oğuz for also their friendships. My special thanks continue with Eda Yıldız, Cansu Kabakçı, Şahin and, Serap Namlı for their faithful sense and never letting me alone during this period. I also feel very lucky to work with Hande-Cem Baltacıoğlu and Sezen Dinçel. Moreover, I should indicate that this study would not be completed without motivations of Ayça Aydoğdu, Emrah Kırtıl and Bade Tonyalı. I also want to express my special thanks to Bade Tonyalı, Eda Yıldız and Derya Uçbaş for sharing same office by spending good time. I also want to express my gratitude to the most enjoyable labmates Pelin Poçan, Damla Dağ and others for their friendships during the time I spent at the department. My sincerest appreciation goes out to Elçin Bilgin, one of my best friends, for her helpfulness and unconditional love. Finally, I want to mention the days that I was working with Hazal-Oğuz Öztürk, with unforgottable, funny days.

Finally, I would like to express my deepest appreciation to my family; my grandmother, Nuriye Çıkrıkçı, my father, Remzi Özkan Çıkrıkçı and my mother Şule Çıkrıkçı for their endless support, unconditional love, encouragement and patience. Any word can express my gratitude and love to them. They have respected all my decisions through my life and they made me feel so lucky. I dedicate this work to them.

The last but not least, I would like to express my deepest love and appreciation to my beloved boyfriend İzzet Kağan Erünsal with whom we overcame difficulties together despite the long distances. He always supported me with his love and patience; and encouraged and advised me to do my best at every step of my thesis writing and defense.

I would like to acknowledge and thank to TUBİTAK 2228-B Graduate Students Scholarship Program. Additionally, I would like to thank to TUBİTAK 2214-A Graduate Scholarship International Program for funding of the study conducted in UC Berkeley.

* If you have received project support from TUBİTAK, you must mention about it.



ORTA DOĞU TEKNİK ÜNİVERSİTESİ
FEN BİLİMLERİ ENSTİTÜSÜ MÜDÜRLÜĞÜ

EXPERIMENTAL AND MATHEMATICAL INVESTIGATION OF MASS
TRANSFER IN FOOD AND HYDROGEL SYSTEMS USING MAGNETIC
RESONANCE IMAGING AND NMR RELAXOMETRY

A THESIS SUBMITTED TO
THE GRADUATE SCHOOL OF NATURAL AND APPLIED SCIENCES
OF
MIDDLE EAST TECHNICAL UNIVERSITY

BY

SEVİL ÇIKRIKCI

IN PARTIAL FULFILLMENT OF THE REQUIREMENTS
FOR
THE DEGREE OF DOCTOR OF PHILOSOPHY
IN
FOOD ENGINEERING

SEPTEMBER 2019

Approval of the thesis:

**EXPERIMENTAL AND MATHEMATICAL INVESTIGATION OF MASS
TRANSFER IN FOOD AND HYDROGEL SYSTEMS USING MAGNETIC
RESONANCE IMAGING AND NMR RELAXOMETRY**

submitted by **SEVİL ÇIKRIKCI** in partial fulfillment of the requirements for the degree of **Doctor of Philosophy in Food Engineering Department, Middle East Technical University** by,

Prof. Dr. Halil Kalıpçılar
Dean, Graduate School of **Natural and Applied Sciences**

Prof. Dr. Serpil Şahin
Head of Department, **Food Engineering**

Assoc. Prof. Dr. Mecit Halil Öztop
Supervisor, **Food Engineering, METU**

Prof. Dr. Behiç Mert
Co-Supervisor, **Food Engineering, METU**

Examining Committee Members:

Prof. Dr. Meryem Esra Yener
Food Engineering, METU

Assoc. Prof. Dr. Mecit Halil Öztop
Food Engineering, METU

Assoc. Prof. Dr. İlkay Şensoy
Food Engineering, METU

Assoc. Prof. Dr. Özge Şakıyan Demirkol
Food Engineering, Ankara University

Assist. Prof. Dr. Elif Yolaçaner
Food Engineering, Hacettepe University

Date: 02.09.2019

I hereby declare that all information in this document has been obtained and presented in accordance with academic rules and ethical conduct. I also declare that, as required by these rules and conduct, I have fully cited and referenced all material and results that are not original to this work.

Name, Surname: SEVİL ÇIKRIKCI

Signature:

ABSTRACT

EXPERIMENTAL AND MATHEMATICAL INVESTIGATION OF MASS TRANSFER IN FOOD AND HYDROGEL SYSTEMS USING MAGNETIC RESONANCE IMAGING AND NMR RELAXOMETRY

ÇIKRIKCI, SEVİL

Doctor of Philosophy, Food Engineering
Supervisor: Assoc. Prof. Dr. Mecit Halil Öztop
Co-Supervisor: Prof. Dr. Behiç Mert

September 2019, 184 pages

Nuclear magnetic resonance (NMR) and Magnetic Resonance Imaging (MRI) are well-known non-invasive characterization methods used in a wide range of areas; from medical to food applications. NMR experiments are conducted either through spectroscopy with high resolution systems or with relaxometry (Time Domain NMR) through mid or low field systems. Time domain NMR is primarily based on relaxation times and diffusion measurements from the signal coming from the whole sample while MRI enables to visualize the inside of the materials on a macroscopic scale without disturbing the sample based on the differences on relaxation and diffusion. For biological imaging, proton NMR (^1H) is used mostly. Since the signal comes from protons, this technique could easily be employed to monitor different transport processes in food systems that include moisture or oil transport. In this dissertation, model food and gel systems were selected and mass transport was analyzed through both NMR and MRI in which mathematical models of the transport were developed and validated.

Monitoring oil migration from hazelnut paste layer to chocolate layer (sweetened with sucrose, stevia, splenda or with their combinations) and developing the mathematical

models were the first section of the study. Oil migration is a common problem in chocolate confectionery products leading to quality defects, particularly fat bloom. So, knowing the migration model for the product could have enabled us to predict the shelf life of the chocolate.

In the second section, a hydrogel system was selected as the system of interest and alginate-gum tragacanth (ALG-GT) hydrogels at different ALG replacement ratios were designed for controlled release of insulin in simulated gastrointestinal (GIT) conditions and characterized by NMR/MRI to analyze mass transfer and water-polymer, polymer-polymer interactions. Since insulin is a therapeutic protein, it could not have given such a high signal to be observed in MRI but insulin was confirmed by NMR spectroscopy and its interactions were studied by NMR relaxometry. When hydrogels are placed in a solution, they usually respond to the environment by swelling and thus modelling mass transport becomes challenging due to moving boundaries. However, the studied hydrogels did not show significant swelling which were also validated by MR images. On the other hand, insulin release was quantified by High Performance Liquid Chromatography (HPLC). In both sections of this dissertation, effective diffusion coefficients (D) of the systems were predicted by fitting experimental data to the assumed mathematical model by MATLAB.

In the first part of the study, for five chocolate formulations stored at 30 °C over a time frame of 22 days, experimental data acquired through MRI were modeled using a Fickian based mathematical model to calculate D values. Using two different equations for boundary condition at upper chocolate surface, two models were evaluated and logistic type boundary model was shown to exhibit a better fit. In addition, associated constants (C_0 , β , t_0) for time dependent upper boundary conditions were determined. Average diffusivities of all samples varied in the order of 10^{-11} m²/s. This study addressed the potential use of MRI for visualization and quantification of migration for different chocolate formulations.

In the second part of the study, insulin entrapped alginate-gum tragacanth (ALG-GT) hydrogels at different ALG replacement ratios (100, 75, 50, 25) were prepared through an ionotropic gelation method, followed by polyelectrolyte complexation (PEC) with chitosan (CH). Retention of almost the full amount of entrapped insulin in a simulated gastric environment and sustained insulin release in simulated intestinal buffer indicated the pH sensitivity of the gels. Insulin release from hydrogels with different formulations showed significant differences ($p < 0.05$). D values of the gel samples were predicted in the order of 10^{-10} m²/s. Time domain (TD) NMR relaxometry experiments showed the differences for different formulations, and the presence of CH revealed that ALG-GT gel formulation could be used as an oral insulin carrier at optimum concentrations. Texture, FTIR and SEM analyses supported less firm structure, interactions between polymers and more heterogenous structure with the increase of GT ratio in the formulations. The hydrogels formulated from biodegradable, biocompatible, and nontoxic natural polymers were seen as promising devices for potential oral insulin delivery.

In summary, this dissertation referred the potential of magnetic resonance for validation of transport processes, identification of molecular interactions and characterization of conformational changes occurred in a food and gel matrix. This study could give an insight for further studies undergoing in food and biomedical applications.

Keywords: Magnetic Resonance Imaging (MRI), Nuclear Magnetic Resonance (NMR), Oil migration, Insulin release, Hydrogel

ÖZ

GIDA VE HİDROJEL SİSTEMLERİNDE KÜTLE TRANSFERİ SÜRECİNİN MANYETİK REZONANS GÖRÜNTÜLEME VE NMR RELAKSOMETRE İLE DENEYSEL VE MATEMATİKSEL İNCELENMESİ

ÇIKRIKCI, SEVİL

Doktora, Gıda Mühendisliği

Tez Danışmanı: Doç. Dr. Mecit Halil Öztop

Ortak Tez Danışmanı: Prof. Dr. Behiç Mert

Eylül 2019, 184 sayfa

Nükleer Manyetik Rezonans (NMR) ve Manyetik Rezonans Görüntüleme (MRG), medikal alanlardan gıda uygulamalarına kadar pek çok alanda kullanılan tahribatsız bir tekniktir. NMR deneyleri, ya yüksek çözünürlüklü sistemler içeren spektroskopi ya da orta ya da düşük alanlı sistemler aracılığıyla relaksometre ölçümleriyle (Zamansal Alanlı NMR) gerçekleştirilir. Zamansal alanda NMR, esasen bütün numuneden gelen sinyalden gelen gevşeme ve difüzyon ölçümlerine dayanırken, MRG, gevşeme ve difüzyondaki farklılıklara dayanarak numuneye zarar vermeden makroskopik bir ölçekte numunenin iç yapısı hakkında bilgi edinmeyi sağlar. Biyolojik görüntüleme için çoğunlukla proton NMR (¹H) kullanılmaktadır. Numuneden alınan sinyal proton kaynaklı olduğundan, bu teknik rutubet ve yağ taşınımı gibi farklı transfer sistemlerini izlemede kolaylıkla uygulanabilir. Bu çalışmada, farklı gıda ve jel sistemleri seçilmiş olup bu sistemlerdeki kütle transferi NMR / MRG tekniği ile incelenip analiz edilmiştir. Ayrıca kütle transfer sistemi matematiksel olarak da modellenmeye çalışılmıştır.

Model gıda olarak farklı tatlandırıcılar (sükroz, stevya, splenda ve kombinasyonları) kullanarak hazırlanan çikolata formülasyonlarında yağ migrasyonunun takibi ve

matematiksel modellerin geliştirilmesi çalışmanın ilk kısmını oluşturmuştur. Yağ migrasyonu çikolata sektöründe kalite problemine neden olan yaygın bir sorundur. Bu nedenle, ürüne özel migrasyon modeli elde etmek ürün raf ömrünü önceden tahmin etmeye yardımcı olmuştur.

Çalışmanın ikinci kısmında ise, hidrojel hedef model olarak seçilmiş olup farklı aljinat (ALG) yüzde oranları ile hazırlanmış insülin yüklü aljinat-kitre gamı (ALG-GT) hidrojelleri sindirim sisteminde kontrollü insülin salınımı amacı ile hazırlanmıştır. İnsülin ve su transferi ile polimerlerin etkileşimini karakterize etmek için NMR/MRG teknikleri kullanılmıştır. İnsülinin proton kaynaklı sinyali düşük olduğundan MRG yöntemi ile gözlemlenmeye uygun olmayıp, NMR spektroskopisi ile moleküler yapısı hakkında detaylı bilgi elde edilebilmiştir. İnsülin yüklü hidrojellerde meydana gelen etkileşimler ve su transferi ise NMR relaksometre ile analiz edilmiştir. Hidrojeller bir çözeltiye batırıldıklarında genellikle şişerler ve bu da kütle transferinde sabit olmayan sınırların olmasına neden olur. Ancak yapılan çalışmada hidrojellerin önemli ölçüde şişme eğilimine sahip olmadığı görülmüş olup bu sonuç MR görüntüleri ile de desteklenmiştir. Hidrojellerden insülin salınımı ise Yüksek Performanslı Sıvı Kromatografisi (HPLC) yöntemi ile analiz edilmiştir. Çalışmanın iki kısmında da sistemin difüzyon katsayısı (D) MATLAB programı kullanılarak deneysel sonuçların matematiksel modele eşleştirilmesi ile tahmin edilmiştir.

Çalışmanın ilk kısmında, 30°C’de 22 gün boyunca bekletilen çikolata sisteminin üst tabakasını oluşturan fındık ezmesi bölgesinden alt tabakayı oluşturan çikolata bölgesine gerçekleşen yağ migrasyonu MRG ile takip edilmiş ve yağın transferindeki difüzyon katsayı değeri (D), Fickian bazlı matematiksel model ile tahmin edilmiştir. Çikolata üst yüzeyinde iki farklı sınır koşulu kullanılmış olup lojistik tipli koşulun deneysel sonuçlar ile daha yakın sonuç verdiği görülmüştür. Ayrıca, zamana bağlı üst sınır koşulları için ilişkili sabitler (C_0 , β , t_0) de bu çalışmada belirlenmiştir. Ortalama D değerleri 10^{-11} m²/s düzey aralığında elde edilmiştir.

Çalışmanın ikinci kısmında ise, model jel sistemi olarak kitozan (CH) ile polielektrolit kompleks oluşturmuş ya da oluşturmamış ve de farklı aljinat (ALG) yüzde oranları (100, 75, 50, 25) ile hazırlanmış insülin yüklü aljinat-kitre gamı (ALG-GT) hidrojelleri hazırlanmıştır. İnsülin transferindeki D değeri Fickian bazlı matematiksel modelleme ile 10^{-10} m²/s düzeyinde tahmin edilmiştir. NMR relaksometre sonuçları jel formülasyonuna göre değişiklik göstermiştir. Tekstür, FTIR ve SEM analiz sonuçları, formülasyonda GT oranının artmasıyla örneklerde daha yumuşak bir yapının oluştuğunu, kullanılan polimerler arası etkileşimin varlığını ve GT varlığı ile mikroskobik açıdan daha heterojen yapıda jeller elde edildiğini desteklemiştir. Bu çalışma, CH ile kompleks oluşturmuş optimum konsantrasyonda ALG-GT hidrojellerinin ağız yoluyla insülin alım sistemi olarak kullanılabileceğini göstermiştir.

Sonuç olarak, yapılan bu çalışmalar manyetik rezonansın gıda ve jel sistemlerinde meydana gelen kütle transferi, moleküller arası etkileşim ve konformasyonel değişikliklerin belirlenmesi ve karakterizasyonunda kullanılabileceğini desteklemiştir. Bu çalışma, gıda ve biyomedikal uygulamalarda yapılan daha ileri çalışmalar için fikir verme niteliği sunmaktadır.

Anahtar Kelimeler: Manyetik Rezonans Görüntüleme (MRG), Nükleer Manyetik Rezonans (NMR), Yağ migrasyonu, İnsülin salınımı, Hidrojel

To My Beloved Grandmother

ACKNOWLEDGMENTS

I would like to express my special thanks to my advisor Assoc. Prof. Dr. Mecit Halil Öztop for his continuous support, understanding, guidance, energy and encouragement throughout this study. He always tried to make everything easy for me and helped me in my stressful days. Additionally, I am very grateful to my co-advisor Prof. Dr. Behiç Mert for his all suggestions about the study and the selection of correct academic path.

I would like to express my thanks also to Asst. Prof. Ilkay Sensoy for her advices. I would like to extend my gratitude to members of my thesis committee, Prof. Dr. M. Esra Yener, Assoc. Prof. Dr. Özge Şakıyan Demirkol and Assist. Prof. Dr. Elif Yolaçaner. Very special thanks go to Prof. Dr. Alexander Pines for accepting me to his lab as 1 year visiting student researcher in UC Berkeley. During my research, Danila Barskiy was the leading labmate in my studies so I am very grateful to him. My thanks also go to Dr. Jeff Pelton, technical expert who helped me so much during my analyses. I would like to appreciate other Pines Lab members owing to their friendships, helpfulness and kindness throughout my research.

I would also like to thank our all research assistants at our department, Özge Güven for her trustable friendship, Esmanur İlhan and Kübra Ertan for their delicious dishes and good humour, Selen Güner for her energy, help and thoughtful behavior, Barış Özel and Seren Oğuz for also their friendships. My special thanks continue with Eda Yıldız, Cansu Kabakcı, Şahin and, Serap Namlı for their faithful sense and never letting me alone during this period. I also feel very lucky to work with Hande-Cem Baltacıoğlu and Sezen Dinçel. Moreover, I should indicate that this study would not be completed without motivations of Ayça Aydoğdu, Emrah Kırtıl and Bade Tonyalı. I also want to express my special thanks to Bade Tonyalı, Eda Yıldız and Derya Uçbaşı for sharing same office by spending good time. I also want to express my gratitude to the most enjoyable labmates Pelin Poçan, Damla Dağ and others for their friendships during the time I spent at the department. My sincerest appreciation goes out to Elçin Bilgin, one of my best friends, for her helpfulness and unconditional love. Finally, I want to mention the days that I was working with Hazal-Oğuz Öztürk, with unforgottable, funny days.

Finally, I would like to express my deepest appreciation to my family; my grandmother, Nuriye ıkırcı, my father, Remzi zkan ıkırcı and my mother Őule ıkırcı for their endless support, unconditional love, encouragement and patience. Any word can express my gratitude and love to them. They have respected all my decisions through my life and they made me feel so lucky. I dedicate this work to them.

The last but not least, I would like to express my deepest love and appreciation to my beloved boyfriend İzzet Kaęan Erünsal with whom we overcame difficulties together despite the long distances. He always supported me with his love and patience; and encouraged and advised me to do my best at every step of my thesis writing and defense.

I would like to acknowledge and thank to TUBITAK 2228-B Graduate Students Scholarship Program. Additionally, I would like to thank to TUBITAK 2214-A Graduate Scholarship International Program for funding of the study conducted in UC Berkeley.

TABLE OF CONTENTS

ABSTRACT	v
ÖZ	viii
ACKNOWLEDGMENTS	xii
TABLE OF CONTENTS	xiv
LIST OF TABLES	xvii
LIST OF FIGURES	xviii
LIST OF SYMBOLS AND ABBREVIATIONS	xxi
1. INTRODUCTION	1
1.1. Background	1
1.2. Oil Migration In Hazelnut Paste / Chocolate Systems Using Magnetic Resonance Imaging (MRI)	4
1.2.1. Characteristics of chocolate	4
1.2.2. Fundamentals of NMR / MRI	11
1.2.3. Oil Migration in chocolate systems	17
1.2.3.1. Oil Migration mechanism in chocolate	19
1.2.3.2. Modelling of oil migration	27
1.2.3.3. Oil migration in chocolate system with MRI	29
1.3. Development of pH Sensitive Alginate / Gum Tragacanth Based Hydrogels for Oral Insulin Delivery	41
1.3.1. Overview of controlled drug delivery systems	41
1.3.2. Hydrogels for drug delivery	44
1.3.3. Polymers used in drug delivery	45
1.3.3.1. Alginate	45

1.3.3.2. Gum Tragacanth	46
1.3.3.3. Chitosan	47
1.3.4. Protein drugs for oral delivery	48
1.3.4.1. Insulin	48
1.3.5. Modelling of drug release from delivery systems.....	49
1.3.6. Mass transfer in gel system with NMR/MRI.....	54
1.4. Objectives of The Study	58
2. MATERIALS AND METHODS	59
2.1. Materials	59
2.1.1. Hazelnut Paste / Chocolate System.....	59
2.1.2. Insulin Loaded Hydrogel System.....	59
2.2. Methods.....	60
2.2.1. Hazelnut Paste / Chocolate System.....	60
2.2.1.1. Two-Layer chocolate confectionery system preparation	60
2.2.1.2. NMR/MRI measurements	61
2.2.1.3. Mathematical modelling	63
2.2.2. Insulin Loaded Hydrogel System.....	67
2.2.2.1. Gel preparation	67
2.2.2.2. Zeta potential measurement	68
2.2.2.3. pH dependent insulin release studies	68
2.2.2.4. Modelling release behavior of gel samples	69
2.2.2.5. Texture profile analysis.....	71
2.2.2.6. Scanning Electron Microscopy (SEM)	72
2.2.2.7. Fourier Transform Infrared (FTIR) Spectroscopy.....	72

2.2.2.8. NMR/MRI Measurements.....	72
2.2.3. Statistical Analysis	74
3. RESULTS AND DISCUSSION.....	75
3.1. Hazelnut Paste / Chocolate System	75
3.1.1. NMR/MRI Results	75
3.1.2. Mathematical Modelling	83
3.2. Insulin Loaded Hydrogel Systems.....	92
3.2.1. Release Profiles.....	92
3.2.2. NMR / MRI Results	99
3.2.2.1. 0.32 T NMR relaxometry results	99
3.2.2.2. 1.4 T Benchtop NMR relaxometry results	103
3.2.2.3. High-Field NMR results.....	106
3.2.2.4. MRI Results.....	109
3.2.3. Texture Profiles.....	110
3.2.4. Mathematical Modelling of Hydrogels	112
3.2.5. FTIR	113
3.2.6. Microstructure of Hydrogels.....	116
4. CONCLUSION AND RECOMMENDATIONS	119
5. APPENDICES	141
A. Additional Results for Chocolate System.....	141
B. Statistical Analysis	148

LIST OF TABLES

TABLES

Table 1.1. Factors and their effects on oil migration (Ghosh et al. 2002; Smith et al. 2007).	17
Table 1.2. Common properties of alginate (Kaygusuz, 2011).....	46
Table 1.3. Exponent n of power law for drug release from polymeric devices (Siepmann & Peppas, 2001).....	52
Table 2.1. Composition of 5 chocolate formulations.	60
Table 2.2. Expressions for the mathematical model.	66
Table 2.3. Composition of hydrogels.	68
Table 2.4. Parameters used in 60 MHz Benchtop NMR.	73
Table 3.1. Estimated Diffusion coefficient (D) and nonlinear curve fitting for interface constants of 5 chocolate formulations in Model 1, $C(\text{interface}) = C_0 [1 + \exp(-\beta t)]$, over days 1 to 22 at 30 ± 0.5 °C.	84
Table 3.2. Estimated Diffusion coefficient (D) and nonlinear curve fitting for interface constants of 5 chocolate formulations in Model 2, $C(\text{interface}) = C_0 / [1 + \exp(-\beta(t-t_0))]$, over days 1 to 22 at 30 ± 0.5 °C.....	87
Table 3.3. Self diffusion coefficient (SDC) values of gel samples. Results are mean values and errors are represented as standard deviation for at least two replicates in each gel sample. Lettering was done for each subgroup separately ($p < 0.05$).	102
Table 3.4. Textural properties of fresh gel samples. Results are mean values and errors are represented as standard deviation for at least two replicates in each gel sample (n=5). Lettering was done for each subgroup separately ($p < 0.05$).	111
Table 3.5. Diffusion coefficients of gel samples. Results are mean values and errors are represented as standard deviation for at least two replicates in each gel sample. Lettering was done for each subgroup separately ($p < 0.05$).	113

LIST OF FIGURES

FIGURES

- Figure 1.1.** Several properties in six polymorphic forms of cocoa butter (Afoakwa 2010; Beckett 2008)..... 6
- Figure 1.2.** Chocolate tempering cycle (Afoakwa 2010). 7
- Figure 1.3.** a) Chocolate, oil and two layer chocolate systems. From left to right: dark chocolate, peanut butter over chocolate, replicate of peanut butter over chocolate, peanut oil-sugar, peanut oil b) 2D MR images of two-layer chocolate system. (A) Day 1. (B) Day 5. (C) Day 11. (D) Day 14. (E) Day 18. (F) Day 29. CH; chocolate region. PB; peanut butter region. POS; peanut-oil-sugar 16
- Figure 2.1.** Representative system and coordinates 64
- Figure 2.2.** Model hydrogel system for insulin release modelling 70
- Figure 3.1.** 2-D MR images of reference oil, F1, F2 and F3 and reference oil (from right to left) (a) at day 1 (b) at day 2 (c) at day 3 (d) at day 4 (e) at day 5 (f) at day 11 (g) at day 15 (h) at day 22. 77
- Figure 3.2.** 2-D MR images of oil, F4 and F5 (from right to left) (a) at day 1 (b) at day 2 (c) at day 3 (d) at day 4 (e) at day 5 (f) at day 11 (g) at day 15 (h) at day 22. 78
- Figure 3.3.** Representative MRI information for one set of 2-layer chocolate sample F1 stored at 30 °C at day 1. (a) MR image (b) 1D signal intensity profile for F1 at day 1. (c) at day 3. (d) at day 4. (e) at day 15. (f) at day 22. HP: hazelnut paste. CH: chocolate. HO: hazelnut oil. 82
- Figure 3.4.** Data and curve fitting in Model 1 for days 1 to 22 at interface between chocolate-and hazelnut paste at 30 °C. (a) for F1 ($R^2=0.88$). (b) for F2 ($R^2=0.97$). (c) for F3 ($R^2=0.96$). (d) for F4 ($R^2=0.82$). (e) for F5 ($R^2=0.83$). Experimental and their fitting results were represented by dot point and solid line, respectively. (These figures are examples for each formulation. To find out the final result, averages of the replicates were taken in all samples). 85
- Figure 3.5.** Data and curve fitting in Model 2 for days 1 to 22 at interface between chocolate-and hazelnut paste at 30 °C. (a) for F1 ($R^2=0.98$). (b) for F2 ($R^2=0.96$). (c)

for F3 ($R^2=0.95$). (d) for F4 ($R^2=0.96$). (e) for F5 ($R^2=0.99$). Experimental and their fitting results were represented by dot point and solid line, respectively. (These figures are examples for each formulation. To find out the final result, averages of the replicates were taken in all samples). 86

Figure 3.6. Representative experimental and fitting dimensionless signal intensity profiles. From left to right and top to bottom: F1 sample over position and time at day 4 ($R^2=0.91$), for F2 at day 11 ($R^2=0.94$), for F3 at day 15 ($R^2=0.89$), for F4 at day 2 ($R^2=0.83$) and for F5 at day 4 ($R^2=0.93$) in Model 1. Fitted models were represented by dashed line. (These selected days are the examples for each formulation. To find out the final result, averages of the replicates were taken in all samples). 88

Figure 3.7. Representative experimental and fitting dimensionless signal intensity profiles. From left to right and top to bottom: F1 sample over position and time at day 4 ($R^2=0.93$), for F2 at day 11 ($R^2=0.92$), for F3 at day 15 ($R^2=0.90$), for F4 at day 2 ($R^2=0.98$) and for F5 at day 4 ($R^2=0.92$) in Model 2. Fitted models were represented by dashed line. (These selected days are the examples for each formulation. To find out the final result, averages of the replicates were taken in all samples). 89

Figure 3.8. Chromatographs of a) Humulin b) insulin c) m-cresol and d) representative insulin loaded gel in buffer of SIF (pH 6.8). 93

Figure 3.9. Release profile of a representative hydrogel (100A-CH) in SGF (pH 1.2). 94

Figure 3.10. Release profile of hydrogels a) without CH coating b) with CH coating in SIF (pH 6.8). 96

Figure 3.11. T_1 results of a) hydrogels without CH and b) hydrogels with CH. 100

Figure 3.12. T_2 results of a) hydrogels without CH and b) hydrogels with CH. 101

Figure 3.13. T_1 results of a) hydrogels without CH and b) hydrogels with CH. 105

Figure 3.14. T_2 results of a) hydrogels without CH and b) hydrogels with CH. 106

Figure 3.15. 18.8 T High-Field NMR results for insulin solution at pH 9 in D_2O a) Insulin spectra in the range of 0-15 ppm b) Insulin released buffer medium at pH 6.8 c) DOSY experiment of insulin solution. 108

Figure 3.16. a) Gel samples b) gel samples prepared for MR analysis and 2D MR images of gel samples c) before and d) 6 hours after immersion into intestinal fluid (pH 6.8). 110

Figure 3.17. FTIR spectra corresponding to a) polymers in powder form and b-c) all gel formulations. 115

Figure 3.18. SEM images of hydrogels From a1) to a4): 100A, 75A, 50A, 25A. From b1) to b4): 100A CH, 75A CH, 50A CH, 25A CH, respectively. 118

LIST OF SYMBOLS AND ABBREVIATIONS

A	contact area
C	concentration
C_0	equilibrium concentration over time
$C_{FP}(t)$	Hazelnut concentration in filter paper
D	diffusion coefficient or diffusivity
D_{eff}	effective diffusion coefficient
D_0	diffusion coefficient in the liquid phase of the cocoa butter
g	gravity
h	height
h_∞	equilibrium height
J	molar diffusion flux of the migrating molecules
k	Boltzmann constant ($1.38 \times 10^{-23} \text{ J K}^{-1}$)
k'	kinetic rate constant
K	partition distribution constant
l	thickness
L	distance
$L(t)$	slab thickness expressed as a function of time
M	observed pixel intensity in MRI
M_0	total pixel liquid proton intensity in MRI
m_s	amount of migrated oil at infinity

m_t	amount of migrated oil at time t
r	molecular radius of the diffusing material
t	time
T	absolute temperature
T_1	longitudinal relaxation time (spin-lattice relaxation time)
T_2	transverse relaxation time (spin-spin relaxation time)
TE	echo time
TR	repetition time
V	volume
ε	void volume
v^v	volume average velocity
x	position
α	aspect ratio
Ω	angle between the capillary and a reference horizontal datum plane
β	time constant
ρ	density
θ	contact angle between the fluid and the capillary wall
γ	surface tension of the fluid
μ	viscosity
η	viscosity of the medium
τ	global tortuosity factor

\emptyset	volume fraction in chocolate
\emptyset_{LF}	volume fraction of liquid fat in chocolate
\emptyset_{NF}^T	volume fraction of non-fat solid in chocolate
\emptyset_{SF}^{Fat}	volume fraction of solid fat in the cocoa butter phase
ALG	alginate
GT	gum tragacanth
CH	chitosan
PEC	polyelectrolyte complexation
M_t	released agent at time t
M_{inf}	released agent at long times

CHAPTER 1

INTRODUCTION

1.1. Background

Mass transfer is a well-studied phenomena that has been mathematically analyzed in a wide range of areas from food industry to biomedical applications. It plays an important role in unit operations of food processing such as extraction, distillation, drying and absorption which requires to be understood for optimization of operating conditions (Farid, 2013). In the absence of this understanding, it could result in quality loss in the product. For instance, drying of food stuffs is a critical process to extend the product shelf life by minimizing microbial spoilage and unwanted reactions (Ruiz-López, Martínez-Sánchez, Cobos-Vivaldo, & Herman-Lara, 2008). Additionally, it provides food stability and helps to reduce packaging requirements and cost. Since drying is both heat and mass transfer based operation, the optimization of these mechanisms are important to obtain a good quality product and to achieve an efficient process by saving time and energy.

Similarly, the design of drug delivery system could be given as an example for biomedical application. It is based on the controlled release of the required amount of active agent to target site action of the body at desired time. In this regard, several systems have been emerged as promising devices such as microcapsules, hydrogels, etc. At this point, responsive behavior of the system to environmental conditions (swelling, release, etc.) could be analyzed considering unique mass transfer mechanism and could be optimized by considering numerous mathematical approaches.

In last decades, modelling of mass transfer or other phenomenological aspects is among certain areas for research. Mathematical modelling of such kind of dynamic

systems enables to predict the future of the process and product with good accuracy considering model structure and variables. Depending on your goal (structural understanding, optimized control, simulation or others), the complexity of the model can vary from simplified models (e.g. empirical kinetics) to complicated approaches (e.g. dynamics coupled with reactions) (Trystram, 2012). At this point, theoretical background becomes very important to describe food or similar systems having complex dynamic nature. Methods that would be used to obtain experimental data plays also critical role. Rather than 1D or 2D geometrical information, 3D visualization of the systems could be more useful for multiscale analyses and for generation of models. Therefore, techniques like X-ray or MRI could be helpful to introduce both quantitative and qualitative information about internal structure of the products (Ho et al., 2013).

Mass transfer occurs either due to bulk fluid motion (convection) or random motion of molecules (diffusion) (Swarbrick, Hill, & Carolina, 2000) . However, the emphasis of the current study would be dominantly for diffusional transport. Diffusion is the process resulting from random molecular motions by which matter is transported from one part of a system to another (Crank, 1975). Based on thermodynamic approach, free energy interpretation of diffusion helps to describe the phenomena. Chemical potential is the real driving force of mass transfer but activity-based diffusivity (D) in this expression requires much more accurate and extensive activity data thereby its use is not so widespread. The expression of concentration is simpler to analyze and solve, it is mostly preferred rather than chemical potential.

There is an analogy between diffusion and heat conduction due to random molecular motions. Fick became a pioneer scientist by putting diffusion on a quantitative basis. He adopted the Fourier's mathematical equation for heat conduction into mass transfer equation (Crank, 1975). In isotropic substances, diffusion is based on the principle that transfer rate of diffusing substance per unit area of a section is in proportion with the concentration gradient measured normal to the section. Thus, for one dimensional diffusion, Fick's first law is expressed as;

$$J = -D \frac{\partial C}{\partial x} \quad (1.1)$$

where J is the molar flux or the rate of flow per unit area of the diffusing molecules ($\text{mol cm}^{-2} \text{ s}^{-1}$), $\partial C/\partial x$ is concentration gradient, C is concentration (mol/cm^3), x is space coordinate measured normal to the section and D is the diffusion coefficient ($\text{cm}^2 \text{ s}^{-1}$). The negative sign results from the fact that diffusion occurs in the opposite direction to that of concentration increase. Another point is that this general mathematical expression is valid for isotropic medium which means that diffusion and structure properties in the neighborhood of any point are equal relative to all directions. On the other hand, for anisotropic medium, diffusion properties become dependent to direction (Crank, 1975).

If the system is at steady state conditions, Fick's first law would be enough to describe diffusional process. If the system is under unsteady state conditions (concentration is changing with time (t)), the mass flow will change continuously and it is described by Fick's second law;

$$\frac{\partial C}{\partial t} = D \frac{\partial^2 C}{\partial x^2} \quad (1.2)$$

D value could be constant or the function of some parameters such as concentration, temperature, porosity etc. There are so many factors affecting mass transfer rate and diffusivity but all of these concepts were explained in detail in further sections. For now, it should not be forgotten that the solution of these equations require initial and boundary conditions and it is important to define them correctly. Detailed explanations of mechanisms and mass transfer models will also be explained in the latter sections.

In order to analyze experimental and mathematical validation of mass transfer in different food systems, this study has comprised of two parts; oil migration in chocolate and controlled release in hydrogel systems.

The next part of introduction will cover a brief description about chocolate, theoretical aspects of migration and use of NMR/MRI in migration studies and the latter section

will focus on fundamental information about hydrogels for drug delivery, modelling drug release and application of NMR/MRI in this field.

1.2. Oil Migration In Hazelnut Paste / Chocolate Systems Using Magnetic Resonance Imaging (MRI)

1.2.1. Characteristics of chocolate

Chocolate is a mixture of solid cocoa particles, chocolate liquor, sugar, lecithin and in the case of milk chocolate, milk solids dispersed in a continuous fat phase. Continuous fat phase in chocolate includes both solid and liquid fat in which the ratio changes with temperature and composition (Andrae-Nightingale, Lee, & Engeseth, 2009; Y J Choi, Mccarthy, Mccarthy, & Kim, 2007). Continuous cocoa butter phase has a hydrophobic nature and tends to show impermeability to moisture in comparison to cocoa and sugar particles (Hondo, 2013). On the other hand, sugar is hydrophilic and cocoa particles also contribute slightly to the hydrophilicity of chocolate. Thus, moisture can diffuse through these solid particles (Ghosh, Duda, Ziegler, & Anantheswaran, 2004; Ghosh, Ziegler, & Anantheswaran, 2005).

Composite chocolate products (chocolate-enrobed biscuits, chocolate bars, etc.) are very popular in confectionery industry. The presence of an additional ingredient with chocolate makes these products more susceptible to oil migration. Migration is defined as the movement of oil coming from an added ingredient to chocolate matrix. One of the major problems in chocolate confectionery systems is oil migration and it mainly occurs from nut pastes, truffles or bakery products with chocolate coating and causes quality defects in products during storage such as fat bloom (Ghosh, Ziegler, & Anantheswaran, 2002).

Chocolate enrobed products are produced by coating of the main food with chocolate. In filled products, on the contrary, products are manufactured by filling the inside of the coating with the ingredient. If the two primary domains (chocolate and ingredient) are in contact with each other, it is inevitable that migration will occur between the systems resulting in changes on chemical and physical properties of the filled product.

Cocoa butter is mainly composed of triglycerides that contain the fatty acids; oleic (C18:1), stearic (C18:0), palmitic (C16:0). Additional free fatty acids, polar lipids, fat-soluble compounds, mono-glycerides and di-glycerides are also present (Miquel, Carli, Couzens, Wille, & Hall, 2001b). Providing a unique melting behavior and desired mouthfeel, 1,3-distearoyl-2-oleoylglycerol (SOS), 1-palmitoyl-2-oleoyl-3-stearoylglycerol (POS) and 1,3-dipalmitoyl-2-oleoylglycerol (POP) are the main triacylglycerols (TAGs) found in cocoa butter with percentages of around 25%, 40% and 20%, respectively (Khan and Rousseau 2006). The type of cocoa tree and geographical growth area are also among the factors affecting TAG composition in cocoa butter (Lonchamp & Hartel, 2004).

The presence of crystals is the most important structural property of chocolate. Different crystalline forms of cocoa butter cause different physical properties like melting or stability characteristics and different appearance (Toro-vazquez & Marangoni, 2004). As shown in Fig.1, six different crystalline forms (I-VI) with increasing order of melting points and stability could exist in cocoa butter (Dahlenborg, Millqvist-Fureby, Bergenståhl, & Kalnin, 2010). In chocolate literature, these forms are shown by the Greek letters; γ , α , $\beta'2$, $\beta'1$, $\beta2$ and $\beta1$, respectively. They differ in distance between fatty acid chains, manner in which triglycerides pack in crystallization and angle of tilt relative to plane of chain-end methyl group (Talbot, 2010). Form I to form V show double chain packing, form V and VI have triple chain system enabling greater thermodynamic stability and closer packing. Although form VI is the most stable one it could not be obtained directly from the melted chocolate (except by the addition of form VI cocoa butter seeds and under controlled conditions) and also it has high melting temperature and large crystals giving a gritty texture on tongue. Generally, the most desirable crystal in a well-tempered chocolate is the form V providing glossy appearance, good contraction and resistance to bloom parameters (Afoakwa, 2010). It is relatively stable and obtained after appropriate cooling of melted chocolate depending on several (sometimes unknown) parameters (Lonchamp & Hartel, 2004). For those interested in the phase behavior of cocoa butter, Van

Malsen et. al (1999) presented a phase diagram using the data obtained from real-time x-ray powder diffraction.

Transformation in different polymorphic forms may take place due to several reasons such as temperature changes or storage time (De Graef et al., 2005). As given in Fig.1.1, Form IV and Form V have range of melting points as 26-28 °C and 32-34 °C, respectively. Form IV may be transformed into form V over time and this occurs faster (in an uncontrolled way) at higher temperatures (Beckett.T.Stephen, 2008). However, at room temperature, a part of the cocoa butter becomes still liquid and energy is given off during transformation to a lower energy state. The free energy of the newly formed crystals is lower than that of the original crystalline state hence it occurs spontaneously possibly causing bloom (Ziegler, 2009). Some fat may go onto the chocolate surface with the form of large crystals giving white or greyish haze which is known as ‘fat bloom’. Fat bloom results in color changes and non-uniform color patterns (Beckett.T.Stephen, 2008; Briones & Aguilera, 2005; Dahlenborg et al., 2010).

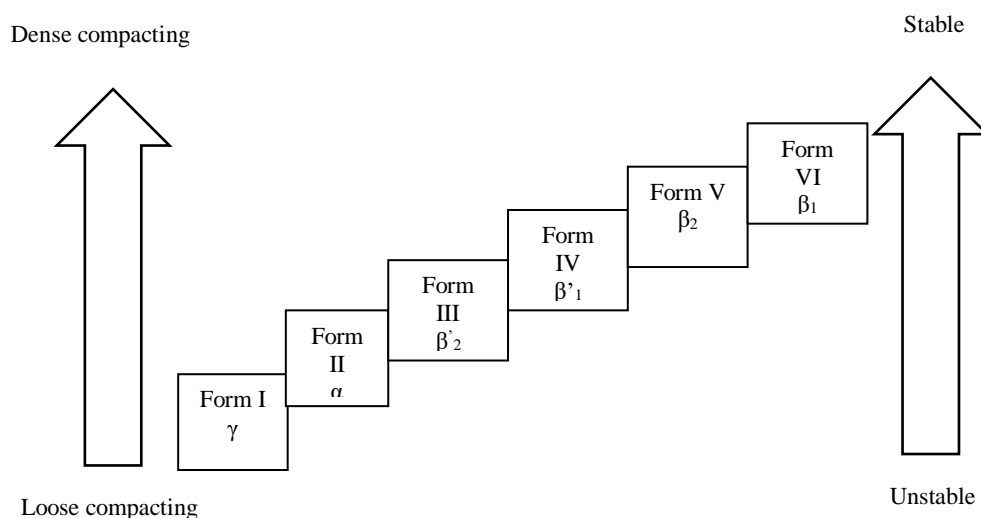


Figure 1.1. Several properties in six polymorphic forms of cocoa butter (Afoakwa 2010; Beckett 2008).

In order to obtain sufficient amount of nucleation sites for stable fat crystals to grow on, pre-crystallization is usually considered. External addition of solid cocoa butter crystals as seeds or application of temper with controlled temperature profile in combination with shearing could introduce primary nucleation sites (Hondo, 2013). Tempering is a very crucial step for chocolate production since it is responsible for obtaining fine homogenous sized crystals in the correct form (β -modification) (Beckett.T.Stephen, 2008; Lipp & Anklam, 1998). As seen in Fig. 1.2, chocolate is first melted (at 50 °C) to remove all the crystals and then temperature is decreased for crystal formation (27 °C). However, both stable and unstable crystals occur in the chocolate at that point. By increasing the temperature slightly (to 29-31 °C), only stable crystals are obtained and the unstable forms are eliminated (Afoakwa, 2010; L. Svanberg, Ahrné, Lorén, & Windhab, 2011a). As another method, seeds can be added to promote crystallization. For this purpose, Form VI cocoa butter seeds can be utilized as a new tempering procedure and it leads to a higher quality final product. Seed crystals are formed during tempering and surround liquid TAG for rapid crystallization in the correct form (Lonchamp & Hartel, 2004).

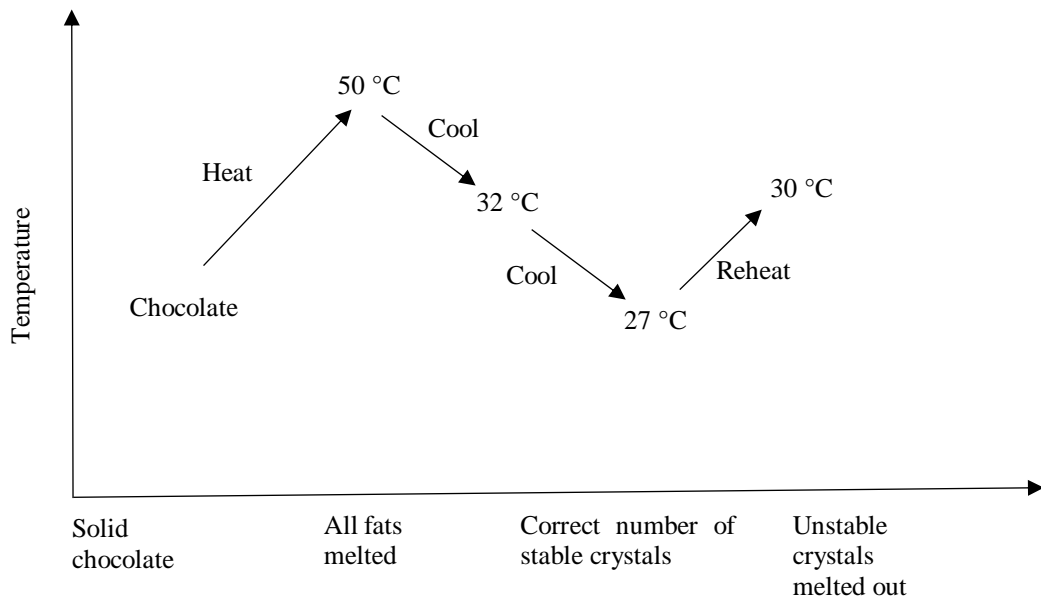


Figure 1.2. Chocolate tempering cycle (Afoakwa 2010).

The success of tempering influences final physical properties and shelf life characteristics of the chocolate. Well-tempered high fat barrier coatings can slow down oil migration in composite confectionery products (Motwani, Hanselmann, & Anantheswaran, 2011). Furthermore, poor tempering may induce fat bloom during storage due to existence of less form V crystals (Miquel et al., 2001b). Cooling curves before molding for low and high tempered chocolates were examined in the study of Miquel et al. (2001). Higher form V seed crystals were gathered in high tempered ones. Slope of the cooling curve presented in research of Miquel et al. (2001) became positive at low tempered chocolate at the inflection point owing to the release of higher heat of crystallization (Miquel et al., 2001b). Similarly, De Graef et al. (2005) observed that under-tempered chocolates bloomed quicker than well-tempered samples and over temper process delayed bloom formation.

The impacts of seed addition on cocoa butter crystallization was investigated by Kinta and Hartel (2009). Their findings indicated that over 270 ppm seeds (fat basis) were required to achieve good tempering (Kinta & Hartel, 2009). As seed addition increased, the number of circular β crystals increased whereas crystal size and time needed for crystals to grow decreased. When the number of seeds reached to a level needed for well-tempering process, small circular cocoa butter crystals rapidly overlapped to form a continuous surface of stable cocoa butter crystals. When adequate number of seeds existed for bloom prevention, β crystallization required less time to attain equilibrated solid fat content (SFC) at that temperature. Nevertheless, insufficient number of seeds increased the formation time of β crystals. As the seeds grew to a larger size, equilibrated solid fat content (SFC) was attained.

In the aforementioned study, two new forms of visual fat bloom were also stated. One of them was associated with the uneven distribution of fat content when no seed crystal formation occurred, and the other form resulted from porosity or roughness of the microstructure caused by coarsened fat crystal network and liquid fat migration. It was shown that the kind of bloom on poor tempered and untempered chocolate were same whereas time to observe the bloom to appear differed. While bloom occurred just after

cooling in poor tempered one, it was formed several days after in untempered products. The difference was related to the rate of stable polymorph formation. In poor tempered chocolate, the existence of even a few stable crystals decreased the time for bloom formation because nucleation was not needed and only growth of the present seeds took time. However, in untempered chocolate, β seeds crystallized first and this required additional time.

Svanberg et al. (2011b) carried out analyses to observe the effect of seeded/non-seeded procedures and also solid particle addition to a chocolate model system. Confocal laser scanning microscopy (CLSM) was used to analyze the structure of β VI-seeded chocolate. It was seen that seeded samples showed a more homogenous microstructure forming multiple nucleation sites which enhanced faster crystal growth. On the other hand, non-seeded samples gave a more random structure. Some parts had large spherical crystals but other areas were more heterogeneous with large inclusions of liquid fat and small compact crystals (L. Svanberg, Ahrné, Lorén, & Windhab, 2011b). Moreover, non-seeded chocolates experienced extensive post-crystallization during storage and became denser like seeded samples. Nevertheless, initially non-seeded chocolates were less compact and no seed addition resulted in a more appropriate environment for diffusion. Additional research of Svanberg et al. (2013) also supported these results (L. Svanberg, Ahrné, Lorén, & Windhab, 2013; Lina Svanberg, Lorén, Ahrné, & Windhab, 2013).

Another study to discuss the impact of tempering and fat crystallization in textural properties of chocolate was performed by Afoakwa et al. (2008). Optimal, over and under temper processes were evaluated in dark chocolates having different particle size ranging from 18 to 50 μm . In three-stage temper machine, both temperature of chocolate and coolant fluid were recorded and it was set as 26:24:32 °C, 21:19:32 °C and 18:16:32 °C, respectively for attaining the under-tempered, optimally-tempered and over-tempered regimes in coolant fluids (Zones 1:2:3). The degree of pre-crystallization and tempering curves were evaluated. Temper readings in chocolate temper index (slope) corresponded over-temper (slope as -1.0), under-temper (slope

as 1.0) and optimal-temper (slope as 0). It was found that samples experienced by over-temper process showed higher hardness, stickiness values but less glossy structure and lower darkness on the chocolate surface than optimal process (Afoakwa, Paterson, Fowler, & Vieira, 2008). In under-tempered samples, quality defects were observed on the product. Such kind of quality loss on color, texture and surface gloss was considered as fat bloom (Bricknell & Hartel, 1998; Dahlenborg, Millqvist-Fureby, Brandner, & Bergenstahl, 2012; Frazier & Hartel, 2012; Marty & Marangoni, 2009; Nattress, Ziegler, Hollender, & Peterson, 2003). In the study of Afoakwa et al. (2008), the results of micrographs showed differences in surface and internal crystal network structure of different temper regimes. Under-tempered samples were bloomed causing whitening of both internal sides and surface of products with impact on appearance and texture. Similarly, Afoakwa et al. (2009) also analyzed variations in texture, microstructure, appearance and melting properties during storage in under-tempered dark chocolate. The most rapid fat bloom was observed in the samples having the largest particle size (50 μm). Both temper regime and particle size influenced bloom formation (Afoakwa, Paterson, Fowler, & Vieira, 2009).

James and Smith (2009) demonstrated that temper degree could affect resulting surface composition (fat, sugar, etc.) during bloom development. Well-tempered chocolate developed surface bloom consisting only fat composition (from cocoa butter extrusion onto the surface) whereas while on poor tempered or untempered chocolate, surface bloom was comprised of both fat and sugar (James & Smith, 2009a). Another previous study by Lonchamp and Hartel (2006) had similarly shown that bloom on the surface of untempered chocolate consisted of sugar crystals and cocoa solids, whereas surface bloom on the over tempered chocolate was mainly due to growth of cocoa butter crystals. Moreover, it was shown that bloom on untempered chocolate developed more quickly than over tempered sample (Lonchamp & Hartel, 2006).

Campos and Marangoni (2014) analyzed the effect of shear rates applied (with maximum value of 120 s^{-1}) on crystallization dynamics of cocoa butter. Shear demonstrated a significant impact on crystallization, microstructure of polycrystalline

materials and physical properties such as melting point (Campos & Marangoni, 2014; Maleky & Marangoni, 2011a, 2011b; Maleky, Smith, & Marangoni, 2011). In tempering, time-temperature relation and also the effect of shear were important factors according to Jovanovic' et al. (1995). Since high shear enabled TAGs to come together and to integrate onto nuclei crystal surfaces, it had an impact on nucleation. In fact, shorter induction times for crystallization in cocoa butter and chocolate when processed under shear influenced nucleation. Further, it provided acceleration of polymorphic transformations. Campos and Marangoni (2014) found that shear reinforced mixed crystal formation in the growing crystals. It induced more rapid crystallization kinetics and higher number of smaller crystal formation and also stronger crystal network mechanically.

Crystal structures, fat bloom and oil migration are all related concepts in chocolate literature. Determination of the crystal structure or presence of fat bloom could be detected by x-ray scattering, differential scanning calorimeter and microscopic techniques. However, to obtain information about the rate of migration on a macroscopic scale which will be helpful to estimate the shelf life of chocolate requires other techniques to be used. At that point, Magnetic Resonance Imaging (MRI) becomes an alternative tool.

1.2.2. Fundamentals of NMR / MRI

Magnetic resonance imaging (MRI) is a non-destructive method enabling visual differentiation of various components (Guiheneuf, Couzens, Wille, Hall, & Way, 1997). Spatial regions (positions) are designated and used to obtain average signal intensity over time (temporal information). It could be widely used for so many foods such as fruit and vegetables, dairy products, confectionery products, baked products and others. MRI is also successful on efficient visualization of oil migration monitoring and quantification in chocolate systems.

Nuclear magnetic resonance (NMR) involves the application of radio frequency (RF) pulses in order to create a temporary disturbance on a sample placed into another static

magnetic field (Kirtil & Oztop, 2016). On the other hand, NMR imaging (MRI) requires NMR instrument equipped with magnetic field gradients to obtain two or three dimensional images of the samples giving both internal and external information on the whole sample (d'Avila et al., 2005; Miquel & Hall, 1998). A gradient is simply a magnetic field which varies from point to point in a linear fashion and information could be obtained by creating magnetic field nonuniformity in linear manner (Duerk, 2007). Thus, MRI could give spatial distribution of the signal with the help of gradient in three axes (Kirtil & Oztop, 2016). Depending on the orientation axis, the magnetic field gradients G_x , G_y and G_z are defined as frequency-encoding, phase-encoding and slice-select gradients with the units of magnetic field divided by length, respectively (d'Avila et al., 2005).

Nuclear magnetism emerging from the spins of nucleons (protons or neutrons) is the basic principle behind NMR/MRI techniques. Since hydrogen proton is abundant in organic samples (presence in oil and water) and has a high MR sensitivity, it is mostly preferred element for these experiments (Kirtil & Oztop, 2016). To get a signal, sample is placed into a large static magnetic field (B_0). If spinning, unpaired protons within the sample line up with that magnetic field. If an RF (radio-frequency) wave of a very specific frequency is then sent into sample, some spins change their alignment owing to this magnetic field. After applying RF pulse, signal is generated as they return to their original alignment and this is MR signal that we measure (Duerk, 2007).

There are several sequences used in MRI such as spin echo, gradient echo, inversion recovery sequences. An MRI sequence is a combination of radiofrequency pulses and gradients to acquire data from images. Sequence parameters are chosen in regard to particular application. In food science, spin echo (SE) pulse sequence is the most commonly used sequence to obtain an MR image and it is comprised of 90° excitation pulse followed by one or more 180° rephrasing pulses (Duerk, 2007). By rephrasing spins, dephasing effects due to external magnetic field inhomogeneities are eliminated. This point is the major difference between SE and gradient echo (GRE) pulse sequence because this 180° pulse is not used in GRE imaging. GRE uses small flip angles

providing reduction in scan time. Thus, 3D imaging could be evaluated due to its higher speed (Duerk, 2007). CPMG (Carr-Purcell-Meiboom-Gill), modified SE technique, is also another sequence used in MRI. It applies 90° RF pulse along x axis followed by an echo train induced by successive 180° pulses along y axis and is useful to measure T₂ weighted images that will be explained later.

For SE image, each pixel intensity of an image is expressed as given in Eq. (1.3) with the condition TR (repetition time) is longer than TE (echo time) and where M is the observed pixel intensity across the image, M₀ is the total pixel liquid proton intensity.

$$M = M_0 e^{-\frac{TE}{T_2}} (1 - e^{-\frac{TR}{T_1}}) \quad (1.3)$$

T₁ and T₂ represent longitudinal relaxation time (spin-lattice relaxation time) and transverse relaxation time (spin-spin relaxation time), respectively. TR is the recovery delay between each acquisition. Observed pixel intensity M depends on the relaxation parameters; T₁ and T₂. When TR is five times higher than T₁, the term becomes negligible and yields:

$$M = M_0 e^{-TE/T_2} \quad (1.4)$$

Where TE (the echo time) approximately represents the delay between the radiofrequency excitation and the collection of the signal. In experiments where the echo time (TE) is fixed, the relative intensity of each pixel is characterized by the liquid proton density M₀ and the transverse relaxation time T₂ (Guiheneuf et al., 1997).

T₁ is related to the exchange of energy between the spins and their molecular environment. Proton T₁ values are obtained as long in solid and liquid fats while it can become relatively short in the intermediate viscous state. T₂ which is spin-spin relaxation time arises from the loss of phase coherence between neighboring spins. It is relevant to an increase in the entropy of the spin system. Since hydrogen protons in water molecule have higher motional frequencies than hydrogen protons in solids, water has longer T₁ than solids. Fat and proteinaceous materials on the other hand show short T₁ values. To determine T₂ characteristics of tissues, how fast proton spins in that tissue dephase are determined. As they dephase more slowly, longer T₂ is

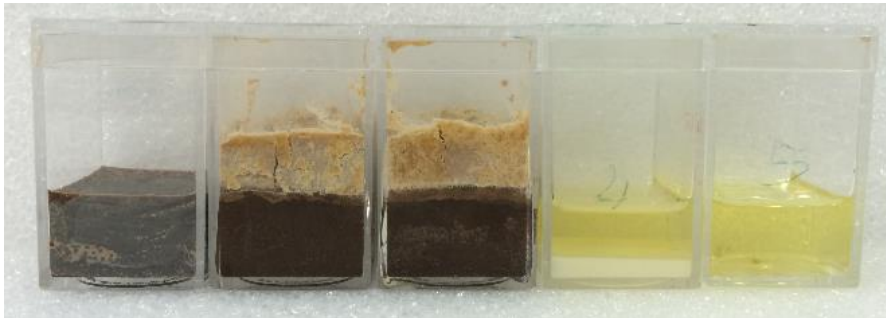
obtained. Owing to less dephasing, water has long T_2 but solids have short T_2 with the result of most dephasing. Fat and proteinaceous materials give intermediate T_2 (Duerk, 2007). As dealing with different tissues, tissue contrast helps to distinguish different parts from each other. Changing TR and TE parameters, the effect of T_1 or T_2 values could be changed. For instance, long TR decreases T_1 effect while short TE reduces T_2 effect of image. Thus, T_1 or T_2 weighted images might be acquired with different parameters. T_1 weighted images are obtained if both TR and TE are short. Opposite condition gives T_2 weighting. Other than these, long TR and short TE give proton density weighting in SE imaging (Duerk, 2007).

Since spin-spin relaxation is strongly enhanced by slow rotational motion of the triacylglycerol molecules, proton T_2 values are very short in solid cocoa butter fats (of the order of tens of microseconds) (Guiheneuf et al., 1997). T_2 values of chocolate lies between 9- 17 ms, however the T_2 values for nuts and fat fillings are usually higher (> 40 ms), and thereby they show high intensity in spin echo sequences with an echo time of (TE) 6 ms (Miquel & Hall, 1998). Compared to chocolate, caramel, another ingredient used in chocolate products exhibits a wide range of T_2 values (25-40 ms) varying depending on the water and fat content. Furthermore, dried fruits such as raisin or cereals like puffed rice have low signal intensity due to low proton density and short T_2 times, as well as biscuits and wafers. On the other hand, in the case of honeycomb, nougat or mousse, the main reason of low signal intensity is the high magnetic susceptibility difference associated with the distribution of air bubbles (Miquel & Hall, 1998).

Photos and 2D MR images of a two layer chocolate system (peanut butter over chocolate layer) that was stored for 29 days at 30 °C were given in Fig. 1.3a, b respectively. The MRI experiments were performed using a spin echo sequence with a TR of 600 ms and TE of 13 ms with a 3T clinical scanner (SIEMENS MAGNETOM Trio, Germany). As illustrated in Fig. 1.3b, it was clearly seen that oil was so bright indicating high signal intensity, while chocolate was seen as darker having low signal intensity. During the storage, oil migrated from peanut butter to the chocolate region

and resulted in a brighter visualization in chocolate layer starting from the top of chocolate surface. Due to incompatibility of the migrating oil, cocoa butter would be dissolved in the migrating oil and could contribute to signal intensity significantly. When Fig. 1.3b was examined carefully, another interesting behavior was observed. A depletion zone at the interface (signal intensity being very low thus seen as a black zone) between the peanut butter and the chocolate developed during storage. This type of zone was also observed by other researchers (Y J Choi et al., 2007; McCarthy & McCarthy, 2008). Reason of the presence of the depletion zone was previously explained by Ziegleder (2009). Depletion could have occurred due to oil diffusion through the filling to the interface being slower than the diffusion of oil into the chocolate away from the interface (Ziegleder, 2009). A detailed microstructural analysis at the interface would also be helpful to understand the real behavior on this zone.

a)



b)

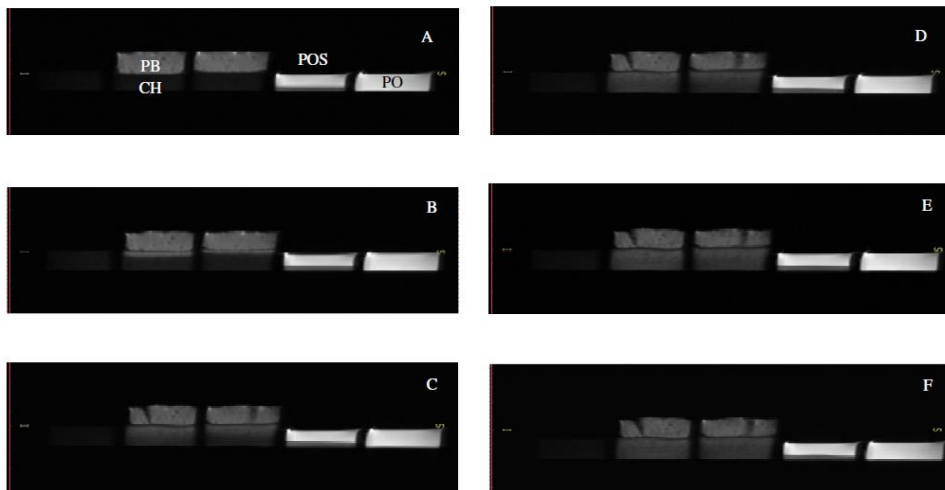


Figure 1.3. a) Chocolate, oil and two layer chocolate systems. From left to right: dark chocolate, peanut butter over chocolate, replicate of peanut butter over chocolate, peanut oil-sugar, peanut oil b) 2D MR images of two-layer chocolate system. (A) Day 1. (B) Day 5. (C) Day 11. (D) Day 14. (E) Day 18. (F) Day 29. CH; chocolate region. PB; peanut butter region. POS; peanut-oil-sugar

Before elaborating the studies of MRI on oil migration, it is worth mentioning migration mechanisms and modelling approaches followed in chocolate literature.

1.2.3. Oil Migration in chocolate systems

When chocolate enrobes a lipid containing material, oil migration is observed through the outer chocolate layer. Since liquids migrate more rapid than solids, liquid lipid migration is mainly explored in literature (Guiheneuf et al., 1997; McCarthy & McCarthy, 2008; Miquel et al., 2001b; Miquel & Hall, 2002a; Rumsey & Mccarthy, 2012; Walter & Cornillon, 2002b). As a result of migration, chocolate region softens while the filling or enrobed part becomes hard. The reason of softening is due to decrease in solid fat content, which may result from the dissolution of fat crystals (Brake & Fennema, n.d.; Reinke et al., 2015). If TAG migrating into chocolate is incompatible with cocoa butter, additional softening occurs (Baker, Dibildox-alvarado, Neves, & Marangoni, 2005; Depypere, De Clercq, Segers, Lewille, & Dewettinck, 2009; K. Smith, Cain, & Talbot, 2007).

It is known that anything changing solid fat content in chocolate will have an impact on oil migration. Ratio of two phases, fat level and non-fat solid particles, particle size, viscosity and storage temperature are among parameters influencing oil migration. Significant factors and their impact on oil migration rate were listed in Table 1.1.

Table 1.1. Factors and their effects on oil migration (Ghosh et al. 2002; Smith et al. 2007).

Factor	Response
Contact area	Migration becomes faster as the ratio of surface to volume increases. The shape of the product changes migration rate.
Ratio of the two fat phases	The higher ratio of filling relative to chocolate leads to higher liquid fat migration rate as well higher softening effect.
Solid fat content	It is inversely proportional with migration rate.

Fat level and non-fat solid particles	Absorption of oil by sugar particles is higher compared to absorption by cocoa solid particles (Ziegleder, 2000) . Non-fat solids increase tortuosity and cause reduction in diffusion coefficient resulting decrease in migration rate ($D_{\text{eff}} = (\varepsilon/\tau)D$). The effective diffusivity D_{eff} is a function of the molecular diffusivity, D_0 , times the ratio of the liquid fat content (liquid phase volume fraction, ϕ_l) to the tortuosity, τ . Nevertheless, due to the limitations set by the chocolate processing and formulation, tortuosity is not altered significantly and liquid phase volume fraction dominates. This is the reason for little effect of non-fat particle size on oil migration rate (Ziegler 2009).
Particle size	The decrease in non-fat particle size may increase tortuosity, entraps liquid oil and migration occurs at a slower rate (K. . Smith, 1998).
Viscosity	Liquid lipid phase viscosity becomes important and it is inversely related to diffusivity as described by Stokes-Einstein equation (Hondo, 2013).
Storage temperature	Temperature rise enhances migration rate by increasing diffusion coefficient. Stokes-Einstein equation asserts this relation (Hondo, 2013).
Fat type	Incompatible fats with TAG of cocoa butter promotes eutectic interactions makes migration faster (Eutectic Effect is defined as the phase separation between two physically incompatible fats. In a eutectic mixture, melting point of the mixture is lower than the melting points of either of the two pure fats (Hartel, 1996).
Concentration gradient of TAGs	Migration might be driven by concentration gradient between differing TAG compositions of the adjacent fat phases until reaching thermodynamic equilibrium. As the concentration gradient is steeper, migration rate becomes faster (Ghosh et al., 2002).
Structure	Tempering affects chocolate structure and thereby migration rate. A densely packed crystalline structure produced by proper tempering slows down migration (Ghosh et al., 2002).

1.2.3.1. Oil Migration mechanism in chocolate

It is generally supported that different migration mechanisms contribute to oil migration in an extent. The mechanism of oil migration through chocolate confectionery system has still not been clearly understood due to its complexity. Molecular diffusion based on TAG concentration difference is mainly considered as the dominant migration mechanism in most studies. On the other hand, capillary flow which is sensitive to microstructure may also play a role in migration rate. Pressure driven convective flow and interphase migration are other possible mechanisms that are discussed in the literature.

Molecular diffusion: Diffusion is a transport phenomenon in which matter is moved from one part of a system to another as a consequence of random molecular motion. Migration occurs when there is a concentration gradient between the species and it continues until thermodynamic equilibrium is achieved. Diffusion rate is described by the proportion of chemical potential difference as driving force to resistance of the movement encountered by diffusing molecules (Ergun, Lietha, & Hartel, 2010). However, instead of chemical potential, concentration gradient is more preferably used due to its simplicity. Diffusion coefficient is expressed as fundamental diffusion coefficient (area²/time) when diffusion rate is governed by chemical potential gradient whereas it is defined as mutual binary diffusion coefficient (area²/time) as diffusion rate is explained by concentration gradient (Ghosh et al., 2002).

Diffusion mechanism could be described more easily by referring polymer behavior (Hondo, 2013). Swelling and relaxation are the two substantial terms in diffusion. Swelling is related to increase in volume owing to the adsorption of diffusing molecules within polymer. Svanberg et al. (2012a, b) analyzed moisture and fat migration in chocolate confectionery systems in both studies and it was stated that migrating fat induced a more pronounced swelling (50% higher in terms of normalized height change) than the same amount of absorbed moisture by displaying different mechanisms (L Svanberg, Lorén, & Ahrné, 2012; L. Svanberg, Ahrné, Lorén, &

Windhab, 2012). Besides swelling, relaxation is a measure of stress relief in polymers under constant strain. It is the consequence of viscoelasticity of polymers and also influences the microstructure of the material. Since microstructure is a significant factor on diffusion, relaxation plays an important role in diffusion (Hondo, 2013).

According to Alfrey et al. (2007), diffusion could be expressed with three different types; Case I, Case II and Non-Fickian diffusion:

- i. **Case I (Fickian diffusion):** It occurs if diffusion rate is much slower than that of relaxation (Alfrey, Gurnee, & Lloyd, 2007). Sorption equilibrium is attained fast and causes time independent boundary conditions. In this case, swelling of particles has no effect on diffusion. Diffusion in rubbery polymers usually follows this behavior since these polymers respond changes rapidly.
- ii. **Case II (Supercase II):** Diffusion occurs very fast compared to relaxation. Swelling kinetics influence sorption.
- iii. **Non-Fickian / Anomalous Diffusion:** Both diffusion and relaxation occur with the same order of magnitude. Simultaneous phase change from amorphous to crystalline state is involved in this case. Penetrant results in extensive swelling of the polymer. Since the properties of the glassy polymer are prone to be time-dependent, it can be given as an example to this category (Hondo, 2013). While a single parameter is adequate to explain Case I and II, two or more parameters are needed to depict diffusion and relaxation in Non-Fickian / Anomalous diffusion.

The most common mathematical representation of diffusion is explained by Fick's first law. At steady state conditions, for a one dimensional system and for a single component diffusion over a material of thickness x , Fick's 1st law was written as (Crank, 1975):

$$J = -D \frac{\partial C}{\partial x} \quad (1.5)$$

where J is the molar flux or the rate of flow per unit area of the diffusing molecules ($\text{mol cm}^{-2} \text{s}^{-1}$), $\partial C/\partial x$ is concentration gradient, C is concentration (mol/cm^3) and D is the diffusion coefficient ($\text{cm}^2 \text{s}^{-1}$).

For the system of oil or moisture migration through chocolate, unsteady state diffusion (since concentration changes with time) is required and Fick's 2nd law for the conditions described above (for a one dimensional system and for a single component diffusion over a material of thickness) becomes valid as:

$$\frac{\partial J}{\partial x} = - \frac{\partial C}{\partial t} \quad (1.6)$$

Flux term could be written as Eq. (1.6) and gives:

$$\frac{\partial C}{\partial t} = \frac{\partial}{\partial x} \left(D \frac{\partial C}{\partial x} \right) \quad (1.7)$$

If D is constant, final equation is obtained as:

$$\frac{\partial C}{\partial t} = D \frac{\partial^2 C}{\partial x^2} \quad (1.8)$$

These equations have been conducted in so many studies to model oil migration and to predict diffusion coefficient of oil through different chocolate systems (Ghosh et al., 2002; Khan & Rousseau, 2006a; Miquel et al., 2001b).

If experimental data is not available, the diffusion coefficient (D) is required to solve the equations (Eqs. (3-6)). A number of methods such as light scattering, diaphragm cell, Gouy interferometer, infinite couple method, Taylor dispersion, capillary method could be used to measure diffusion coefficient (Ghosh et al., 2002).

There are two main types of diffusion coefficient; mutual- and self-diffusion coefficient. Mutual diffusion coefficient (effective diffusion coefficient) is the ratio of mass transfer to resistance and generally it is the one that is calculated (Hondo, 2013). On the other hand, self-diffusion coefficient is a kind of the rate of diffusion of one

component in another of uniform chemical composition. As a result, it is important which method is used for determining diffusion coefficient because it may give either effective or self-diffusion coefficient. Nuclear Magnetic Resonance (NMR) Pulse Gradient Spin Echo (PGSE) method determines self-diffusion coefficient, whereas Magnetic Resonance Imaging (MRI) could provide information to find out effective diffusion coefficient (Ghosh et al., 2002). The ability estimating diffusion coefficient with MRI makes it a powerful tool in studying mass transfer of foods (Kirtil & Oztop, 2016).

Stokes-Einstein equation is one of the first theories for a large spherical molecule diffusing into a liquid solvent that correlates diffusivity with viscosity (η) and temperature (T) as shown below (Geankoplis 2003):

$$D = \frac{kT}{6\pi\eta R} \quad (1.9)$$

(k is the Boltzmann constant; R is the radius of a particle)

As shown in Eq. (1.9), diffusivity is directly proportional to temperature while it is inversely proportional to viscosity. However, determination of diffusion coefficient through Stokes-Einstein approach gives only 20% accuracy (Cussler, 1997).

Ziegleder (1998) proposed the following equation for oil migration in chocolate including diffusion coefficient;

$$\frac{m_t}{m_s} = \frac{A\sqrt{Dt}}{V} \quad (1.10)$$

where m_t is the amount of migrated oil at time t, m_s is the migrated amount at infinity, A is the contact area, V is the chocolate volume, and D is the diffusion coefficient.

Capillary flow: Since chocolate is a multicomponent system with a complex microstructure, diffusion may not be sufficient to explain and model oil migration (Altimiras, Pyle, & Bouchon, 2007a; Y J Choi et al., 2007). In the presence of capillaries, cavities, porous matrices and crystallized fat networks, capillary flow

should also be considered for migration modelling. Capillary action is explained as the tendency of liquids to rise up in capillary tubes due to surface tension (Atkins & Depaula, 2006). There are many studies in which it was reported that capillary flow might play a role in oil migration in chocolate systems (Aguilera, Michel, & Mayor, 2004; Altimiras et al., 2007a; Baker et al., 2005; Bouzidi, Omonov, Garti, & Narine, 2013; Hamraoui & Nylander, 2002; Omonov, Bouzidi, & Narine, 2010; Quevedo, Brown, Bouchon, & Aguilera, 2005). Aguilera et al. (2004) stated that capillary penetration into pores is a spontaneous process driven by an interfacial pressure gradient (that is, there is a meniscus inside the capillary), thereby flow induced by capillary forces should not be confused with flow through porous media driven by external pressure gradient. So-called Lucas-Washburn equation that would be described below is related to capillary pressure, on the other hand, so-called Poiseuille equation is relevant to average velocity under stationary flow conditions in pores of circular cross-section when there is a pressure gradient but capillary forces are absent. Impregnation of fruit pieces by sugar solutions could be given as an example where bulk flow under the impetus of a pressure gradient is relevant (Aguilera et al., 2004).

Microstructure also plays an important role in migration (Marty & Marangoni, 2009). It was suggested by Sonwai and Rousseau (2010) that chocolate's microstructural heterogeneity was responsible for the distinct surface fat crystallization pathways. Two pore scales exist for capillary flow; the interparticle channels, as migrating mass includes total phase of fat (liquid and crystals) and capillaries between fat crystals for the liquid fat (Aguilera et al., 2004).

Surface and chocolate porosity may influence lipid migration positively or vice versa. Liquid lipids may arrive to the surface due to capillarity and then fat bloom occurs owing to crystallization of liquid lipid. When there is no pressure difference, liquid lipid does not attain to surface and thus prevents blooming (Lonchamp & Hartel, 2004). The existence of a porous matrix partly filled with liquid cocoa butter fractions (1% and 4% of the total chocolate volume) in dark chocolate and a network of cavities was confirmed in the research of Loisel et al. (1997) (Loisel, Lecq, Ponchel, Keller,

& Ollivon, 1997). Khan et al. (2003) determined the pores on chocolate surface having depths in the range of 1-2.5 μm . To mimic capillary formation in the model system, Van der Weeën et al. (2013) assumed the existence of vertical capillaries by grouping the cavities. According to the work, capillary could have a role on migration of nut oil present in the upper layers of chocolate coating at early stages during storage, since gradient-driven diffusion was found as a slower mechanism (Maleky & Marangoni, 2011a; Van Der Weeën et al., 2013).

Another common mechanism to explain capillary flow is Lucas-Washburn expression (Eq. (1.11)). Similar to the diffusion, Lucas-Washburn equation exhibits a square root of time dependence at early stages of the migration as given in Eq. (1.11).

$$\frac{2}{r_c} \gamma \cos\theta = \frac{8}{r_c^2} \mu h \frac{dh}{dt} \mp \rho_L g h \cos\Omega \quad (1.11)$$

$$h(t \rightarrow 0) = \sqrt{\frac{r_c \gamma \cos\theta t}{2 \mu}} \quad (1.12)$$

As the time goes to infinity, equation becomes;

$$h(t \rightarrow \infty) = h_\infty \left[1 - \exp\left(-\frac{\rho g \cos\Omega r_c^2}{8 \mu h_\infty} t\right) \right] \quad (1.13)$$

h represents the distance the fluid is drawn into the capillary and γ term is the surface tension of the fluid. θ shows the contact angle between the fluid and the capillary wall, Ω is the angle between the capillary and a reference horizontal datum plane ($h = 0$, is set at the bottom of the capillary). While r_c is the radius of the capillary, ρ_L and μ are the density and the viscosity of the liquid, respectively, and g is the acceleration due to gravity. ‘ h_∞ ’ is the equilibrium height reached by the liquid within the capillary when the hydrostatic pressure is balanced by the interfacial pressure difference. The \pm sign shows the dependence of capillary as an upward (+) or a downward orientation with regard to the datum plane. Since these parameters could change with conditions

present within the chocolate microstructure, their measurements are difficult. For instance, distribution of pore sizes within matrix should be known to obtain ‘average’ pore radius. Moreover, it would not be easy to determine contact angle if surface is heterogeneous or rough. Another parameter, viscosity, referring viscosity of mass flowing in the pores might contain fat crystals and liquid fat (Quevedo et al., 2005). Shortly, these difficulties are relevant to chocolate structure rather than measurement methods.

Ziegler (2009) declared that the flow of liquid into a capillary network (dh/dt in Eq. (1.11)) is relatively faster “in the order of seconds to hours” than the time scale of oil migration which was usually days to months. As an example, Carbonell et al. (2004) measured the capillary flow of sunflower oil into a bed of chocolate crumb with a mean porosity of 0.43 and observed the movement of oil as 4 cm in 4 hours. On the other hand, Maleky and Marangoni (2011b) used timescale in the order of days for capillary motion through pores in cocoa butter. Thus it is better to express that migration with capillary rise highly depends on material parameters defined in Eq. (1.11) such as radius.

In Lucas-Washburn expressions (Eq. (1.11-1.13)), it was assumed that viscous drag and gravity compensate capillary pressure in a cylindrical capillary that is in contact with an infinite liquid reservoir. While gravitational force is the driving force for oil loss; viscous drag, capillary and surface interactions are opposing forces. Thus, competing action of driving and retarding forces is resulted in oil transport. If higher unbound liquid exists, morphological specifications do not have a significant impact on transport phenomena and gravitational pressure becomes a driving force for flow. Viscous drag still acts and weak Van der Waals interactions (crystal–crystal, liquid–liquid and liquid–crystal) are still considered (Bouzidi et al., 2013). However, it was seen that the physical state inside the chocolate does not conform to ideal cases such as infinite liquid reservoir and cylindrical uniform pores as described in Lucas-Washburn equation. Nevertheless, the equation has been held for various physical situations which involved a porous media characterized by assembly of cylindrical

capillaries and etc. (Aguilera et al., 2004; Hamraoui & Nylander, 2002). Rousseau (2006) investigated the surface porosity of chocolate, however no evidence was obtained about the fact that these pores extended throughout the bulk. Altimiras et al. (2007) found that capillary theory estimated higher migration rate for bigger capillaries at short times than experimental observations.

It is better to indicate that transport mechanism for oil migration is a combination of both capillary and molecular diffusivity and it still needs to be supported by experiments and more work to eliminate unexplained phenomena. Detailed microstructural analysis of chocolate particulate systems is required to understand it completely.

Other mechanisms: Although molecular diffusion and capillary flow are discussed for possible mechanisms of oil migration in chocolate confectionery systems, other mechanisms such as pressure driven convective flow that is based on density difference could also be responsible for migration. When the amount of liquid cocoa butter increases due to temperature rise or dissolution owing to eutectic effect or Ostwald ripening, volume expansion occurs due to decrease in density. Afterwards, liquid is pumped to the surface through the pores and cracks and also towards the interface of the filling and chocolate. This becomes a potential factor for fat bloom and oil migration. Temperature variations also induce chocolate bloom, which might also support for the so called pumping effect. Thereby, protrusions which are in the form of imperfections on chocolate surface could be another reason for oil migration and this theory was evaluated in several studies (Altimiras, Pyle, & Bouchon, 2007b; Dahlenborg et al., 2010, 2012; Loisel et al., 1997; Sonwai & Rousseau, 2008).

It was stated in the study of Sonwai and Rousseau (2008) that after tempering and development of form V crystals in chocolate, contraction of the chocolate network created pressure inside and significant microscale reorganizations took place by namely;

- i. The inward movement of liquid fat around the dispersed particles during contraction.

ii. Ensuing generation of surface imperfections (cracks, pores, etc.).

iii. Generated pressure within the chocolate matrix pushing molten fat back toward the surface via newly formed channels and pores.

Over time, continued crystallization and the onset of the form V-VI transition will lead to further matrix contraction, more liquid fat will be driven toward the surface through these “active” channels by promoting cone formation and bloom crystals (Sonwai & Rousseau, 2008).

As another migration mechanism, interphase migration was proposed for oil migration between a filling and chocolate at the interphase region. The distribution coefficient K is helpful to understand migration between two components or interphase mass transfer. It is mainly described as relative concentration of a compound in phase x and y , (c_x/c_y). It may be associated with the relative attraction each phase has for the compound. To induce oil migration to a chemical potential gradient should exist in the system (Ziegler, 2009). Since chemical potential is lower in the solution state than the pure liquid state, oil behaves as a solvent for the solid phase of cocoa butter thus attracts to chocolate.

There exists several observations in chocolate-filling interfaces which are complex to interpret (Y J Choi et al., 2007; Walter & Cornillon, 2002a). Although it is not clear yet why such interface would occur during migration, it could be based on differences in diffusion rate of oil through chocolate and filling parts. The diffusion of oil through the filling to the interface is slower than the diffusion of oil into the chocolate away from the interface and consequently interface becomes depleted in oil (Ziegler, 2009).

1.2.3.2. Modelling of oil migration

Since mathematical modelling provides advantages in terms of time and experiment, it is preferred and used in so many areas to model changes in food systems such as in chocolate crumbs (Edmondson, Grammatika, Fryer, & Handy, 2005), in frozen foods

(Pham, 2006), in porous foods and other foods (Aguiar & Gut, 2014; Chen & Opara, 2013; Peralta, Rubiolo, & Zorrilla, 2012; Ruiz-López et al., 2008).

In dilute solutions, diffusion coefficient could be assumed as constant; whereas concentration may influence the diffusion coefficient in other cases. Diffusion coefficient in the Fickian diffusion model is generally considered as a concentration independent parameter. However, it may vary with concentration and this could make it more complex to solve the diffusion equation. Diffusion coefficient may be directly or inversely proportional to the concentration. The mathematical solution could be solved numerically or analytically depending on the type of concentration dependency and medium (e.g. infinite, semi-infinite etc.).

Since Fickian diffusion requires the solution of partial differential equation with different boundary conditions depending on the system, there has been many studies conducted in the literature to simplify the model. One of these approaches includes the power law model. In this model, the amount sorbed or desorbed is directly proportional to the square root of time in early stages of diffusion essentially in a semi-infinite medium. If the amount sorbed at time t is represented as Kt^n (K and n are constants), type of the diffusion mechanisms are determined based on the n value and geometry. Peppas and Brannon-Peppas (1994) gave the limits of 'n' for determining the diffusion mechanism for modelling in cylindrical and spherical coordinates. For rectangular coordinates, if n value equals to 0.5, it indicates Fickian diffusion (Case I) (N. A. Peppas & Brannon-Peppas, 1994). The n value of 1 refers to Case II. If n value is between 0.5 and 1, it corresponds to Case III diffusion. The n value less than 0.5 is associated with pseudo-Fickian diffusion where sorption curves are similar to Fickian curves, but the approach to final equilibrium is very slow (Clercq et al., 2014; K. Lee et al., 1999).

Several mathematical models have also been evaluated for anomalous diffusion behavior. History dependence, two-stage theories, strain-dependent models and irreversible thermodynamic model are among these mathematical models to model

anomalous diffusion behavior (Crank, 1975). According to Crank (1975), the history dependence model was based on the concentration dependent diffusion coefficient as given by the following equations;

$$D_i = D_0 e^{aC} \quad (1.14)$$

where D_i represents instantaneous component of diffusion coefficient, C is penetrant concentration and D_0 and a are the constant values.

$$D_e = D_0 e^{bC} \quad (1.15)$$

D_e is the final equilibrium value and b value is another constant that is greater than a .

Finally, diffusion coefficient is obtained as:

$$\left(\frac{\partial D}{\partial t}\right)_x = \left(\frac{\partial D_i}{\partial C}\right) \left(\frac{\partial C}{\partial t}\right)_x + \sigma(D_e - D) \quad (1.16)$$

In history dependent model, internal relaxation affects diffusion coefficient but in the second stage of two-stage sorption it has been hypothesized that internal relaxation has only impact on the solubility (Crank, 1975).

1.2.3.3. Oil migration in chocolate system with MRI

Numerous analytical techniques have been conducted to study oil migration in chocolate other than MRI in the use of oil migration. High-performance liquid chromatography (HPLC), fourier transform infrared spectroscopy (FTIR) and X-ray diffraction (XRD) are among these methods. Molecular based analyses such as chromatographic methods achieve quantification of oil migration by emerging fatty acid distribution within sample, this means that additional technique is also required for structural information. Therefore, XRD (polymorphic form), scanning electron microscopy (SEM), polarized light microscopy (PLM) or confocal laser scanning microscopy (CLSM) could be used with these techniques (Green & Rousseau, 2015). The study of Khan and Rousseau (2006) supported these perception by using HPLC, atomic force microscopy and X-ray diffraction to study the migration behaviour of

hazelnut oil into simulated filled confections. Surface topography by microscopic technique, polymorphic transition by diffraction method enhanced this study. Similarly, James and Smith (2009) acquired excellent images of the structure of bloom by using cryo-SEM complimented by a combination of environmental scanning electron microscopy (ESEM) and X-ray photoelectron spectroscopy (XPS) to eliminate limitations of cryo-SEM. Firstly, cryo-SEM need a conducted metal coating to allow SEM imaging of an insulating sample, but this condition prevents further analysis of the same sample (James & Smith, 2009b). Secondly, cryo-SEM prevents observation of dynamic process in sample since it both figuratively and literally freezes the sample. ESEM eliminates these procedures by performing under suitable pressures maintaining water in liquid phase and insulating samples with no requirement for conductive coating. Moreover XPS having a surface sensitivity is an ultra high vacuum technique. Hence, structure of bloom was examined on the surface of fresh and bloomed chocolate by these measurements. Another method, flatbed scanner, was used by Marty et al. (2009a) for oil migration in palm kernel oil based filling to cocoa butter. Image acquisition using a flatbed scanner was obtained, then it was followed by normalization and plotting data with respect to time. The migration of lipid soluble dye (nile red) into cocoa matrix was monitored to correlate migrated oil with obtained pixel intensity (Marty, Schroeder, Baker, Mazzanti, & Marangoni, 2009). However, non-linear migration and matrix structure did not allow to fit data to Fick's second law. Dahlenborg et al. (2012) was used another technique, Confocal Raman microscopy, in white chocolate and hazelnut filling. Confocal Raman microscopy combines both Confocal microscopy and Raman spectrometry. It creates relationship between surface topology and fat migration like atomic force microscopy, laser scanning microscopy, optical profilometry and scanning electron microscopy. It has the ability to scan a sample to acquire a Raman spectrum providing chemical information, with a resolution down to the optical diffraction limit (Dahlenborg et al., 2012).

However, these methods are mostly destructive and sometimes requires large sample preparation. Thus, non-destructive methods are more advantageous to investigate oil migration in composite chocolate products. Electron spin resonance (ESR) as being non-destructive technique is sensitive to fat migration but its quantification is hard (Miquel, Carli, Couzens, Wille, & Hall, 2001a). MRI has wide use to model oil and moisture migration in food systems.

Monitoring Oil Migration In Chocolate System With MRI: MRI has been conducted by several researchers to follow oil migration into chocolate (Y J Choi et al., 2007; Young J. Choi, McCarthy, & McCarthy, 2005; Deka et al., 2006; Guiheneuf et al., 1997; Miquel & Hall, 1998; Walter & Cornillon, 2002b).

Miquel and Hall (2002) supported the use of MRI over chromatographic methods for analysis of oil migration. While traditional methods were much more relevant to provide information about specific fatty acid or triglyceride, MRI technique gave the opportunity to deal with multi-component systems. Miquel and Hall (2002) determined T_2 values by using Carr–Purcell–Meiboom–Gill–(CPMG) sequence and assessed for migration of lipids from the fillings into the chocolate. T_2 values showed similar pattern with oil migration, for instance in first 5 weeks T_2 of filling changed linearly from 26.8 ms to 21.2 ms and then 20.6 ms after 7 weeks. The MR images were also helpful to obtain spatial information on the lipid migration.

It was seen in most of the studies that in order to correlate MR signal intensity with oil concentration, a calibration curve had been generated by plotting signal intensity against the oil content which had been added to the chocolate at varying amounts (Guiheneuf et al., 1997; W. L. Lee, McCarthy, & McCarthy, 2010a). The type of this curve gave information about the effects of oil on the samples and about relationship between signal intensity and oil content.

Lipid migration kinetics in composite chocolate product were carried out by Miquel et al. (2001) by using magnetic resonance imaging. Migration was monitored using a spin echo pulse sequence and the signal intensity was quantified in terms of oil content

through the use of MRI and a correlation was accomplished with calibration curve as stated before. Two temper degrees (low temper, high temper), three storage temperatures (20, 23, 28 °C) and the presence of thermal treatment (post-crystallization) (24 h at 30 °C followed by 24 h at 4 °C) were used as experimental factors to work on hazelnut oil migration through chocolate from the filling. To produce low temper chocolate, from the molten state (> 38 °C), chocolate mass was cooled gradually to 29 °C, maintained at that temperature for 5 min, heated gradually to 30.5 °C and then maintained at that temperature for 10 min. On the other hand, in high temper chocolate production, cooling was done up to 27 °C and 5 min duration was repeated. Then, samples were heated gradually to 30.5 °C and then maintained at that temperature for 5 min.

Since signal mainly came from liquid lipid, signal intensity of chocolate region increased while signal intensity of filling region was diminished during storage as expected. Eq. (8) was used to fit MRI data for fat migration as previously mentioned. ‘ m_t ’ represents the concentration of fat migrating within chocolate by time t . ‘ m_s ’ is the migrating fat concentration within chocolate at saturation point. Eutectic interactions were not considered for the system. It was again understood that migration occurred linearly as function of square root of time at early stages (Altimiras et al., 2007b; Quevedo et al., 2005; Van der Weeën et al., 2013). In the study of Miquel et al. (2001), all MR image data were fitted to the model in Eq. (1.17). Tempering degree did not affect migration speed significantly but less stable polymorphs were present in low temper processed chocolate. Moreover, thermal treatment decreased saturation concentration of hazelnut oil in chocolate most probably due to the composition and structural alterations developed by post-crystallization. Diffusion coefficient was calculated according to the equation used by Miquel (2000).

$$D = \left(\frac{R}{r}\right)^4 l^2 \left(\frac{\varphi}{m_s}\right)^2 \quad (1.17)$$

where χ was slope of linear part of curves; R and r were radius of chocolate disk and filling washer, respectively; l was the thickness of chocolate disk, m_s was the saturation concentration and D was diffusion constant .

The results of this work showed that diffusion coefficient increased from 0.7×10^{-7} cm^2/s to 10×10^{-7} cm^2/s as temperature was changed from 20°C to 28°C . Although there was no significant difference between the diffusion constants of low and high tempered samples, the lowest value was obtained in the post-crystallized samples.

Another study of MRI related to oil migration in chocolate confectionery system was conducted by Choi et al. (2005). A chocolate confectionery system was modelled as a two layer system that contained chocolate and peanut butter paste. The influences of the particle size (45 and 60 μm), temper degree (under, well, over temper), storage temperature (20 and 30 $^\circ\text{C}$), emulsifier concentration (lecithin or PGPR with varying percentage between 0% and 0.11%) and milk fat content (in the range from 0 to 10%) on migration rate were explored with the relative signal intensity values obtained from MR images. It was concluded that storage temperature, milk fat content and particle size affected migration rate significantly ($p \leq 0.05$). Additionally, overall change in signal intensity was significantly influenced by temperature and milk fat content. Looking at the one dimensional signal intensity profiles of the samples, both chocolate and peanut butter region were easily differentiated in MR images. Peanut butter had higher relative signal intensity than chocolate due to high oil content giving higher proton signal. Choi et al. (2005) stated that capillary flow might also be a factor for spatial variation other than Fickian diffusion. Similar results about spatial variations in the signal of liquid lipid were also obtained in the research of Walter and Cornillon (2002) in which a commercial peanut butter and dark chocolate were used as the sample.

Choi et al. (2007) examined oil migration in different chocolate formulations in another study. Spin echo pulse sequence without phase encoding was used for obtaining 1D signal intensity profiles of the samples. Mathematical modelling of the

migration was conducted through the use of Fick's second law with the appropriate initial and boundary conditions. The model equations were given as:

$$\frac{\partial C}{\partial t} = D \frac{\partial^2 C}{\partial x^2} \quad (\text{Eq. (1.8) as mentioned before})$$

Concentration at upper boundary (x=l) was assumed as:

$$C(l, t) = C_0 [1 - e^{-\beta t}] \quad (1.18)$$

$$\begin{aligned} & \frac{C(x, t)}{C_0} \\ = & 1 - e^{-\beta t} \frac{\cos x (\beta/D)^{\frac{1}{2}}}{\cos l (\beta/D)^{\frac{1}{2}}} \\ & - \frac{16\beta l^2}{\pi} \sum_{n=0}^{\infty} \frac{(-1)^n \exp[-D(2n+1)^2 \pi^2 t/4l^2]}{(2n+1)\{4\beta l^2 - D\pi^2(2n+1)^2\}} \cos \frac{(2n+1)\pi x}{2l} \end{aligned} \quad (1.19)$$

Choi et al. (2007) also found oil mass uptake as:

$$\begin{aligned} \frac{m_t}{m_{\infty}} = \frac{m_t}{lC_0} = & 1 - \{\exp(-\beta t)\} \left\{ \frac{D}{\beta l^2} \right\}^{\frac{1}{2}} \left[\tan \left(\frac{\beta l^2}{D} \right)^{\frac{1}{2}} \right] \\ & - \frac{8}{\pi^2} \sum_{n=0}^{\infty} \frac{\exp[-(2n+1)^2 \pi^2 D t/4l^2]}{(2n+1)^2 [1 - (2n+1)^2 \{\pi^2 D/4\beta l^2\}]} \end{aligned} \quad (1.20)$$

where C_0 is equilibrium concentration over time, $1/\beta$ is time constant. Finally, concentration profile was obtained given above.

Signal intensity obtained from MR Images was used to express liquid oil concentration in the diffusion equations. Normalized signal intensity (Eq. (21)) was determined by considering signal intensity (SI) values. Boundary condition parameters were found by nonlinear curve fitting. Besides Fick's law, capillary forces based on Lucas-Washburn equation were also considered for oil migration. According to Choi et al.

(2007), the effect of particle size could be explained both due to diffusion and capillary effect. Migration became faster as particle size increased due to diminished resistance and increased diffusivity. Sample prepared with anhydrous milk fat content of 3.57% and 0.38 % emulsifier concentration gave D_{eff} of $4.62 \times 10^{-12} \text{ m}^2 / \text{s}$ for 45 μm particle size, whereas D_{eff} increased to $7.79 \times 10^{-12} \text{ m}^2 / \text{s}$ as emulsifier concentration was increased to 0.51% at a particle size of 60 μm .

From the point of view of capillary effect, larger particle size produced larger effective pore radius and increased oil transport rate.

$$C \approx \text{Normalized } SI = \frac{SI - \langle SI \rangle_{CH,t_1}}{\langle SI \rangle_{PB,t_1} - \langle SI \rangle_{CH,t_1}} \quad (1.21)$$

The research of Deka et al. (2006) exhibited advantages of MRI for analysis of a complex migration phenomenon. They performed one-dimensional, centric-scan MRI technique for imaging both solid lipid and longer timescale components of the liquid lipid in a chocolate sample. Different from traditional MRI practice, this new technique enabled to acquire images from the short lived signal components from the solid lipid and one-dimensional solid and liquid distribution maps in a 5 mm thick chocolate sample. Corresponding spectrum gave a broad peak for solid lipid and a narrow peak for liquid lipid for chocolate before any exposure to oil. MR results showed typical characteristics of oil penetration into chocolate, in other words, diffusion was slow with the penetrating front barely moving (<1 mm) during storage. By observation of slow diffusion with time at exposed surface, capillary flow was seen as responsible mechanism for migration rather than diffusion mitigated migration. Deka et al. (2006) also explained the reason of observation of homogenous proton density except at absorbing surface as counter diffusion of lipid from the chocolate sample towards the surface.

McCarthy and McCarthy (2008) employed another study of oil migration in a 2-layer chocolate-peanut butter paste model system. MRI was again used to monitor spatial

and temporal oil content variations in the composite product. A Fickian-based model similar to the work of Choi et al. (2007) was assessed to determine diffusion coefficient over a time period of 17 days. Decrease in the signal intensity of peanut butter paste indicated the movement of peanut oil into the chocolate region. Low MR signal intensity at interface region was monitored in the 2-layer-model system. Phase separation showed different degrees between samples stored at different temperatures. In the samples stored at 30 °C, diffusion coefficient varied from 1.82 to 3.23 x 10⁻¹¹ m²/s. For the samples stored at 20 °C, no migration was observed.

Although there are a number of mass transfer studies based on the so-called Fickian diffusion it is believed that these simple solutions are inadequate to explain migration accurately. Galdámez et al. (2009) used a new diffusion-based model with more realistic solutions taking into account structural parameters such as fat crystal microstructure and tortuosity and considered chocolate swelling and partition distribution coefficient (Although MRI experiment has not been conducted in this work, it has been included due to its promising modelling ability). The model predicted liquid phase profiles inside the chocolate wafers that are in contact with hazelnut oil at different temperatures and compared it with published MRI data to create spatially resolved concentration profiles (Galdámez, Szlachetka, Duda, & Ziegler, 2009). Mass transfer was governed by molecular diffusivity, and existence of solid particles influenced diffusion through a tortuosity term that differs with temperature and oil concentration. Diffusion within chocolate slab was evaluated in terms of volume average velocity. This model had also some limitations due to several assumptions such as elimination of convective terms, considering one-directional diffusion, negligible crystal formation on chocolate surface, negligible counter diffusion of cocoa butter into filter paper. Model was set up based on the assumption of local equilibrium between solid fat and the migrating oil resulting in another assumption of diffusion as the rate-limiting mechanism although it might not be valid, especially at low temperatures.

Galdámez et al. (2009) used a non-Fickian diffusion model by taking into account swelling of chocolate slab with moving boundary conditions. Different than the assumption of constant diffusivity preferred in many models, effective diffusion coefficient included a tortuosity term (τ) which was dependent on volume fraction of non-fat and fat solids as given below:

$$D_{eff} = D_0\tau = D_0f_{T1}(\phi_{NF}^T)f_{T2}(\phi_{SF}^{Fat}) \quad (1.22)$$

D_0 represents diffusivity of hazelnut in liquid fat (It was taken as 2×10^{-10} m²/s). τ is given as the product of tortuosity that the diffusing species “sees” by the presence of nonfat solids, f_{T1} , and the tortuosity that the diffusing species experiences within the fat phase due to fat crystals, f_{T2} . They were expressed in Eqs. (1.23) and (1.24).

$$f_{T1} = \frac{1 - \phi_{NF}^T}{1 + 0.5\phi_{NF}^T} \text{ for spheres} \quad (1.23)$$

$$f_{T2}^{-1} = 1 + \frac{(\alpha\phi_{SF}^{Fat})^2}{1 - \phi_{SF}^{Fat}} \text{ for flakes} \quad (1.24)$$

In different works, it was observed that in MRI measurements, signal intensity values at the interface of two layer systems exhibited differences with regard to filling type, the position of chocolate layer and temperature. Guiheneuf et al. (1997) performed migration profiles of a two layer system with chocolate over icing sugar/hazelnut oil layer at 19 °C and 28 °C. High signal intensity was observed at the interface at 19 °C most probably due to settling of icing sugar that resulted from pooling of the hazelnut triacylglycerols. At 28 °C, however, high signal intensity values were not observed in the samples. Walter and Cornillon (2002) used MR images to calculate migration time of fat from fatty filling (peanut butter) over a dark chocolate layer. At 28 °C, low signal intensity appeared at the interface region. Moreover, Miquel et al. (2001) acquired high signal intensity at interface region of the sample which was chocolate over icing sugar/hazelnut oil filling. Likewise, Lee et al. (2010) observed that peanut butter over

cocoa butter layer had an interface region with higher signal intensity but peanut butter over chocolate layer did not show such a high signal value in MRI measurements. Possible reasons for high intensity were attributed to changes in composition of interface region and partition coefficient owing to the chemical composition of two layers.

Another research of oil migration was carried out in two-component confectionery systems of peanut oil/cocoa butter, peanut butter paste/chocolate and peanut butter paste/cocoa butter by Lee et al. (2010). Migration was monitored by MRI, signal from liquid oil as a function of position was obtained during 193 days at 25 °C storage. Three samples gave different patterns for oil migration. Similar to other studies, Fick's 2nd law (Eq. (6)) was used to determine the transfer of oil. Lee et al. (2010) took the time constant β for the boundary condition as an input value and C_0 as an adjustable term. By conducting curve fitting at the upper boundary of chocolate layer, β value was found and then it was used for further fitting routine. Effective diffusivities changed insignificantly from 1.10 to 2.01×10^{-13} m²/s for the samples. They were much smaller than the results of McCarthy and McCarthy (2008) most probably owing to differences in milk chocolate formulation and temperature.

Effective diffusion coefficient was mentioned as:

$$D_{eff} = (\varepsilon/\tau)D \quad (1.25)$$

Void volume (ε) depended on cocoa butter percentage in the liquid phase which meant that void volume increased with higher liquid cocoa butter thereby increased effective diffusivity. The report of McCarthy and McCarthy (2008) also supported these findings. Distinctions between the Fickian-based model and other works related to non-Fickian model arose due to swelling attribution and effective tortuosity. Since volume change due to swelling was lower than 3% in the samples and there was no significant difference in the effective diffusivities of the samples, Fickian model was found adequate in this study.

In order to evaluate spatial and temporal changes of liquid lipid content in a two component- system, MRI was also utilized by Altan et al. (2011). Images were obtained by using a multislice spin echo pulse (MSSE) sequence with a 1000-ms repetition time and a 7.8-ms echo time at 1 T. Signal intensity data were corrected to eliminate variations in temperature and MRI gain settings and became in the order of 10^{-3} (arbitrary units/mm³). It was aimed to quantify oil migration from six types of almond products (filling cream, cream turner, confectioners paste, bakers paste, almond praline, and unblanched almond butter) over a dark chocolate that was stored at 20, 25 and 30 °C for several months. Since unblanched almond butter had the highest fat content (57.7% (db) fat), it showed the highest migration and signal intensity at 21.4×10^{-3} /mm³ for all storage temperatures. Similar to Lee (2006), a calibration curve was used to quantify the signal intensity in terms of concentration of the added almond oil.

The linear relationship was associated with the dilution effect rather than monotectic or eutectic effect. Monotectic effect is related to the phase change of solid cocoa butter due to foreign fat addition, dilution effect, on the other hand, does not show a phase change (Altan, Lavenson, Mccarthy, & Mccarthy, 2011). On the other hand, in a eutectic mixture SFC decreases below the level of either fat, whereas in dilution reduction in SFC changes linearly with amount of low-melting component (Lonchamp & Hartel, 2004). This means that eutectic formation occurs with a lower solid fat content (SFC) than either one of the two pure fats if fats are incompatible. Otherwise, even for compatible fats, dilution causes softening if there is significant difference in SFC. Therefore, as nut oils are liquid at room temperature and they are blended with solid fat, cocoa butter is simply diluted in those liquid oils rather than forming eutectics (Lonchamp & Hartel, 2004).

Oil uptake of chocolate was expressed by the following kinetic expression (Altan et al., 2011);

$$\frac{m_t}{m_\infty} = k't^{1/2} \quad (1.26)$$

MRI allowed to calculate uptake values using signal intensity/volume value in the samples. The results of kinetic rate constant k' , belonging to almond praline, cream turner, filling cream and unblanched almond butter which showed oil migration varied from 1.25×10^{-2} to $8.01 \times 10^{-2} \text{ hr}^{-0.5}$ being at least two times higher at 30°C when compared to 25°C . At 30°C , almond praline and filling cream products had the highest kinetic constant as $8.01 \times 10^{-2} \text{ hr}^{-0.5}$ and $8.00 \times 10^{-2} \text{ hr}^{-0.5}$, whereas unbalanced almond butter and cream turner were the two almond products revealing the lowest k' values as $5.50 \times 10^{-2} \text{ hr}^{-0.5}$ and $6.29 \times 10^{-2} \text{ hr}^{-0.5}$, respectively.

Rumsey and McCarthy (2012) conducted a similar work to predict diffusion coefficient in chocolate-almond confectionery product. Liquid oil concentration, which was proportional to the MR signal intensity was governed by “C”. 1D signal intensity profiles were figured out and changes in signal intensity during migration time were obtained as chocolate showed higher signal with reduction in almond region. Major difference of this approach was the inclusion of both chocolate and almond regions for mass transfer equations separately. While diffusion equations were solved for only chocolate region in the previous studies, partial differential equations were also solved for the almond region by Rumsey and McCarthy (2012) through appropriate initial and boundary conditions. In the study, oil migration in four almond products (unblanched almond butter, filling cream, cream turner, almond praline) over chocolate layer was monitored by using MRI. Diffusion coefficients of the samples were found between 3×10^{-11} and $6 \times 10^{-11} \text{ m}^2/\text{s}$ by obtaining higher values for almond regions. Unblanched almond butter having the highest fat content had the highest diffusivity as $7.82 \times 10^{-10} \text{ m}^2/\text{s}$ at almond region while other samples had the result lower than $6.5 \times 10^{-10} \text{ m}^2/\text{s}$ (mostly around the value of $3 \times 10^{-10} \text{ m}^2/\text{s}$). Similar to the result of Altan et al. (2011), the samples with almond praline and unblanched almond butter gave higher diffusion coefficients as $5.97 \times 10^{-11} \text{ m}^2/\text{s}$ and $5.34 \times 10^{-11} \text{ m}^2/\text{s}$ at

chocolate regions and lower partition coefficients as 0.729 and 0.758, respectively. Since double bonds lead to greatest fluidity (Rumsey & Mccarthy, 2012); higher composition of oleic and linoleic acids was expressed as the possible reason for the results. It was concluded that oil migration from the filling part to chocolate region could provide an insight for the estimation of fatty acid composition in the filling products.

Maleky et al. (2012) studied the impact of cocoa butter structure on oil migration. The main experimental factor evaluated was the cocoa butter preparation method (static, seeded, sheared). Signal intensity data were fitted to Eqn. (24). Kinetic constants in the sheared, seeded, static samples were found as 0.91×10^{-3} , 2.5×10^{-3} and 5.3×10^{-3} AU d^{-0.5}, respectively. The lowest constant was obtained in the sheared sample due to the impact of particle size and distribution on liquid oil diffusivity. MRI analysis demonstrated that liquid oil movement through a solid matrix depended on both concentrations of particle and also other factors such as particle size, shape, distribution and geometry of dispersed phase.

1.3. Development of pH Sensitive Alginate / Gum Tragacanth Based Hydrogels for Oral Insulin Delivery

1.3.1. Overview of controlled drug delivery systems

Controlled drug delivery systems are special designs enabling the control on the action of therapeutic substances such as peptides, drugs and hormones in the body. These systems could eliminate the barriers encountered in the application of free drug. Enzymatic degradation, low drug solubility, environmental degradation or toxicity could be given as examples to these barriers (Erdemli, 2013). Two main goals could be featured for controlled drug delivery. Firstly, controlled drug delivery systems can be designated to release therapeutic proteins from natural or synthetic polymers in a controlled manner, for predefined periods of time at predetermined rates (Pinardag, 2006). When difficulties are encountered in traditional injectable or oral drug delivery,

controlled drug delivery becomes more important and secondly they are important systems to maintain the level of therapeutic protein in body within therapeutic range.

Several routes like oral, nasal, ocular, transdermal, parental or intra-articular administration could be applied as drug delivery approaches depending on your target site of action (Erdemli, 2013; Swarbrick et al., 2000). In traditional drug administration, drug blood level increases after each dose taking and it could exceed maximum effective dose causing adverse side effects and then decreases to minimum effective level to meet therapeutic need until next administration. However, in controlled delivery dosing, drug in blood could exist between desired maximum and minimum levels for a period of time (even like months or years). The design of drug delivery system should achieve as low as possible released drug concentration in undesired site of body while drug release should mainly occur at desired site of action (Gunbas, 2007). It should not be confused with sustained release which only extends drug level just for a prolonged period of time. Ideally, controlled release delivery targets not only to control its duration within therapeutic level but also to provide specific place of delivery in the body (Swarbrick et al., 2000).

In pharmaceutical industry, mathematical modelling of drug release requires a broad overview to elucidate the desired mass transfer profile. Both empirical and mechanistic models have an attractive interest in controlled release systems (Hsieh & Faculty, 2012).

Mainly; for drug transfer; diffusion controlled system (drug diffusion from non-degraded polymer), swelling controlled system (enhanced drug diffusion owing to polymer swelling) and erosion controlled system (drug release owing to polymer erosion and degradation) are introduced as major mechanisms (Arifin, Lee, & Wang, 2006).

Diffusion controlled release system are expressed based on Fick's second law with the appropriate boundary conditions. For one dimensional drug release from a spherical system, it is described as:

$$\frac{\partial C}{\partial t} = \frac{1}{r^2} \frac{\partial}{\partial r} \left[D r^2 \frac{\partial C}{\partial r} \right] \quad (1.27)$$

where C is concentration of drug, D is diffusion coefficient.

Depending on the diffusion region, it is divided as the reservoir and matrix (monolithic) systems. While in reservoir system, target drug is in core region and polymer is in outside; in matrix system, drug concentration is uniformly distributed. Constant concentration gradient occurs across polymer membrane by saturated drug core concentration. On the other hand, a challenging feature of such systems is the presence of a possible moving boundary which makes it difficult to solve the problem analytically for the matrix device (Hsieh & Faculty, 2012).

Matrix systems are usually divided into two categories; drug dissolved (if initial drug loading is lower than drug solubility in polymer) and drug dispersed system (if initial drug loading is higher than drug solubility in polymer). According to different initial conditions, boundary conditions and assumptions; Fick's second law could be resulted from simple to complicated solution.

Swelling controlled system considers not only diffusion but also dissolution and polymer matrix disentanglement. When drug diffusion is faster than hydrogel swelling, swelling driven release is taken into consideration. Swelling character of polymer network causes increase in hydrogel volume and polymer chain relaxation as external solvent (biological fluid or water) penetrates into the gel. In this mechanism, phase transition from glassy to rubbery state occurs separating the gel matrix as glassy and swollen region (Zarzycki, Modrzejewska, Nawrotek, & Lek, 2010). While glassy core region includes dissolved drug, rubbery region contains drug which dissolves with enhanced diffusivity. Swelling eventually ends up and then gel begins to dissolve when polymer entanglement is sufficiently weak (Hsieh & Faculty, 2012).

Erosion is another mechanism for the biodegradable polymers. It occurs whereby separation of polymer chains from the network by several ways such as scission reaction with a solvent or backbone cleavage, hydrolysis (Swarbrick et al., 2000).

Mainly, bulk erosion (homogenous) and surface erosion (heterogenous) are the basic types of this mechanism. In bulk erosion, surrounding fluid enters into the polymer causing the erosion within the polymer network but polymer shape does not change. On the other hand, in surface erosion, shrinkage effect induces size change (ex: diameter change for spherical polymer) by erosion of the polymer starting from the surface (Hsieh & Faculty, 2012).

1.3.2. Hydrogels for drug delivery

Especially, in reservoir based drug delivery systems, three main categories can be listed as drug carrier vehicles; injectable micro/nanospheres, implants and hydrogels (W. W. Yang & Pierstorff, 2012). In recent years, hydrogel has sparked a progressive interest in drug delivery applications and clinical practices. Its biocompatibility, biodegradability, bio-adhesive property, porous structure, crosslinking density, responsive attribute towards the changes in environmental conditions favor its use in pharmaceutical area, tissue engineering and regenerative medicine formulations, etc. Although it may have some disadvantages in mechanical properties, it may not be crucial in so many applications. The most important issue is probably related to drug delivery properties. To improve drug release kinetics and gel degradation time, some strategies such as gel diffusion control, surface control or polymer modifications are currently being demonstrated (Hoare & Kohane, 2008).

Hydrogels can be classified into two classes as physically and chemically crosslinked gels depending on linkages between polymer networks (Guti, 2018). Physically crosslinked gels may possess hydrophobic interaction, charge interaction, H bonding, stereo complexation form or supramolecular chemistry. These gels do not require cross linker or chemical modification. On the other hand, chemically crosslinked gels might have small molecule/polymer-polymer crosslinking. This type of gel may help to improve poor mechanical gel properties but it may have potential toxicity of unreacted residuals (Hoare & Kohane, 2008).

1.3.3. Polymers used in drug delivery

Controlled release systems can be categorized into diffusion controlled, chemically controlled or externally triggered systems (W. W. Yang & Pierstorff, 2012). In these systems, they can also be subdivided into further categories depending on biodegradability and the origin of the polymers used in hydrogel fabrication. Hydrogels can be prepared by natural or synthetic polymers. While natural hydrogels could be made from food grade polymers (carbohydrate, protein or lipid based polymers); hydrogels from polyvinyl alcohol (PVA), polyethylene glycol (PEG) can be given as example for synthetic ones (Guti, 2018). Alginate, chitosan, carrageenan, gelatin and whey protein are among the most common food grade polymers used in controlled release studies.

1.3.3.1. Alginate

Alginate is an unbranched polysaccharide copolymer consisting of two uronic acid residues as (1→4)-linked α -L-guluronic acid (G) and β -D-mannuronic acid (M) units. Alginic acid is water insoluble and includes the acid form of uronic acid groups as (-COOH), while sodium alginate is the sodium salt of alginic acid as (-COONa) showing higher water solubility (Milani & Maleki, 2012). Function of alginate is affected by sequential structure, composition and relative amount of these two building units G- and M- residues. G blocks are responsible for gel forming ability, while M blocks enable flexibility to uronic acid chains.

Alginate is a polyanionic polymer due to the existence of carboxylic acid. In hydrocolloid gelation, alginate undergoes ionotropic gelation process by electrostatic interaction with positively charged molecules, most commonly divalent cations such as Ca^{2+} . Primary interchain linkages aggregate into junction zones and create a basis for 3D network gel formation (Burey, Bhandari, Howes, & Gidley, 2008). Negatively charged carboxyl groups and divalent cation Ca^{2+} interacts via crosslinking of ions with polymer chains and egg-box model of network is formed. Chemical composition of alginate, pH and temperature of solution, Ca^{2+} concentration are among the factors

influencing gel formulation and properties. Higher level of G fractions makes stronger gels in egg box junctions. Conversely, M residues lead to softer and less porous gels. Higher temperature also slows down gelling process. Another parameter, higher Ca^{2+} concentration causes stiffer gel in a shorter time until excessive Ca^{2+} remains (Tirilmasi, 2013). However, there is an optimum condition for optimum gelling properties.

Alginate gels do not require heating or cooling for gelation but they form heat-stable gels. They are widely used as gelling agents in bakery fillings, puddings, dressings, fruit juices, yoghurt and meat (Saha & Bhattacharya, 2010). Its concentration used in different food formulations can vary between 0.5% and 2% (Tirilmasi, 2013). Other properties of alginate are listed in Table 1.2.

Table 1.2. Common properties of alginate (Kaygusuz, 2011).

Molecular formula	$(\text{C}_6\text{H}_8\text{O}_6)_n$
Molecular weight	10000 – 600000 $\text{g}\cdot\text{mol}^{-1}$
pKa	1.5-3.5

1.3.3.2. Gum Tragacanth

Gum tragacanth (GT), also known as *katira*, is a highly branched, heterogeneous, and hydrophilic anionic carbohydrate polymer. It is composed of D-galactose, D-galacturonic acid, D-xylose, L-fucose, and L-arabinose units giving special functionalities and small amount of protein (Shiroodi, Mohammadifar, Gorji, Ezzatpanah, & Zohouri, 2012). It has a molecular weight around 840 kDa (Balaghi Sima, Mohammadifar Mohammad Amin, Zargaraan Azizollaah, Gavlighi Hassan Ahmadi, 2011). It includes two major fractions as tragacanthin (water soluble) and bassorin or tragacanthic acid (water swellable). Tragacanthin, neutral fraction, has approximately molar mass of 104 Da including highly branched arabinogalactan groups. Bassorin, pectic component, composes 60-70% of total gum with molar mass of around 105 Da having ability of swelling and gel forming (Mostafavi, Kadkhodaei,

Emadzadeh, & Koocheki, 2016). It has (1→4)-linked α -D-galacturonic acid units and some parts are changed at O-3 with β -D-xylopyranosyl units and some of them are ended with D-Gal or L-Fuc (Balaghi Sima, Mohammadifar Mohammad Amin, Zargaraan Azizollaah, Gavlighi Hassan Ahmadi, 2011).

GT solutions are acidic mostly having a pH of 5-6. It has high stability in a wide range of pH (Milani & Maleki, 2012). Its pKa is around 3 (M. Nur, Ramchandran, & Vasiljevic, 2016). It has been demonstrated as GRAS in the range of 0.2-1.3%. It is used as thickening agent, water binding and gelling agent in so many food products such as confectionery, fillings, soft drinks, ice creams, fruit tablets, etc. (Balaghi Sima, Mohammadifar Mohammad Amin, Zargaraan Azizollaah, Gavlighi Hassan Ahmadi, 2011).

1.3.3.3. Chitosan

Chitosan is a biocompatible, non-immunogenic, nontoxic and biodegradable linear polysaccharide making it a preferred polymer for biomedical and oral drug delivery applications (Du, Liu, Yang, & Zhai, 2015; Mukhopadhyay, Mishra, Rana, & Kundu, 2012; Tahtat et al., 2013). Chitin is a homopolymer with β -(1,4)-linked N-acetyl-glucosamine units. When alkaline deacetylation is applied to chitin, chitosan is obtained. Chitosan is copolymer of glucosamine and N-acetyl-glucosamine (Sinha et al., 2004). It includes two free hydroxyl and one amino groups for each C6 unit. Free amino groups are responsible for cationic property of chitosan. Chitosan is a weak base and it cannot dissolve in water but its solubility is high in dilute aqueous acidic solution (pH<6.5) (Sinha et al., 2004). Its pKa is around 5.5-6.5 (Bayat, Larijani, Ahmadian, Junginger, & Rafiee-Tehrani, 2008; Mukhopadhyay, Sarkar, Soam, & Kundu, 2013).

Chitosan can be used as suspending agent, thickening, flocculating polymer to recover proteins, as adsorption enhancer for hydrophilic drugs and also as a carrier in peptide delivery. Chitosan is regarded as a desired drug carrier due to its excellent mucoadhesive properties. Since mucosal surface is usually negatively charged,

electrostatic interaction occurs with positive charges of chitosan. Strong hydrogen bond units such as –COOH and –OH, strong charges, high molecular weight, sufficient chain flexibility, surface energy properties attribute to these properties (Sinha et al., 2004).

Alginate gels as carrier for protein drugs have potential to lose its network and to loose drug through pores during gel preparation. When alginate is mixed with chitosan, carboxyl groups of alginate and amino groups of chitosan are interacted electrostatically by leading alginate-chitosan complex. This may reduce gel leakage and increase efficiency of drug encapsulation (Zhang, Wei, Lv, Wang, & Ma, 2011).

1.3.4. Protein drugs for oral delivery

1.3.4.1. Insulin

Insulin is a polypeptide hormone excreted from pancreas for regulating blood glucose levels (Sonia & Sharma, 2012). *Diabetes mellitus*, a major endocrine disorder is associated with chronic hyperglycemia with disturbances of protein, carbohydrate and protein metabolism owing to defects in insulin resistance, insulin secretion or both of them (Wong, 2010). Globally, it is one of the common non-communicable diseases and fourth or fifth reason of death in most developing countries (Park, 2004). There are four types of diabetes that have been defined. While Type I patients could not produce enough insulin and need to take exogenous insulin, Type II diabetic people could produce insulin but at a decreased level over time, disorder in insulin action, hence requiring exogenous insulin to regulate blood glucose level, especially during illness and a period of stress (Sonia & Sharma, 2012). In another type, gestational diabetes, the symptoms are first recognized during the pregnancy. In Type IV, genetic defects of beta cells, chemicals, drugs, or diseases inducing pancreatic damage and others are known to be the reasons (Wong, 2010). Type 1 and Type 2 are the most common forms of diabetes.

For treatment of diabetic patients, insulin is the most effective drug (Tahtat et al., 2013). Exogenous insulin administration is done by subcutaneous route due to some

barriers in oral route. Harsh acidic stomach environment, enzymatic degradation, poor absorption are among these encountered problems (Mukhopadhyay et al., 2012). However, subcutaneous administration requires multiple daily injections because duration of drug action changes with regard to insulin types but it is short as 4 to 8 hours. This may be uncomfortable and painful for patients (Sonia & Sharma, 2012).

Insulin could be produced from bovine, sheep, porcine in different ways such as semisynthetic conversion or human, by recombinant DNA technology. It is divided into groups; short, intermediate or long acting insulin regarding to intended duration of action (Sonaje et al., 2010).

Human insulin consisting 51 amino acid residues has an empirical formula $C_{257}H_{383}N_{65}O_{77}S_6$ and has a molecular weight of 5808 g/mol (at around 5.8 kDa) (N. A. Peppas & Kavimandan, 2006). In human insulin, Chain A with 21 amino acids and Chain B with 30 amino acids are linked by three disulfide linkages (Wong, 2010). Its pI lies between 5.3-5.4 (Reis, Ribeiro, Veiga, Neufeld, & Damgé, 2008). Insulin has amphiphilic property due to the presence of 6 positively and 10 negatively charged amino acid residues (Martins, Sarmiento, Souto, & Ferreira, 2007).

The insulin products that are sold in the pharmaceutical stores for injection are known as humulin. Humulin regular (100 IU/ml), a short acting insulin, is one type of insulin product used as an insulin source by the diabetes people. It is structurally identical to human insulin and it is synthesized through recombinant DNA technology. It contains human insulin (rDNA origin) 100 units/mL, glycerin 16 mg/mL and metacresol 2.5 mg/mL, endogenous zinc (approximately 0.015 mg/100 units) and water for injection (<http://www.accessdata.fda.gov>).

1.3.5. Modelling of drug release from delivery systems

Modelling of drug delivery has increasingly become a topic of both academic and industrial interest to optimize novel dosage designs by saving time and reducing cost. For the successful design of the drug delivery systems and description of complete mechanisms, there is a need for a rigorous mathematical modeling approach (Cikrikci,

Mert, & Oztop, 2018; Mani & Tulsi, 2016). It is clear that there is no universal valid mechanism for all kind of drug release systems. For better predictability of drug release, underlying mechanisms for each particular system should be elucidated well by considering each particular condition. It is crucial to make correct decisions for the optimization of the system with required assumptions. In some situations, you might need to identify the most important transport process and to neglect other mechanisms to simplify the model. However, in some conditions, you should consider several mechanisms together to obtain more reliable results. Thus, it depends on your system and factors influencing your system and also what you are looking for. As an example, empiric models may be sufficient if the aim is just to have a simple information to make comparison. On the other hand, mechanistic models would be more beneficial to have detailed information (Siepmann & Peppas, 2001).

In recent years, numerous models have been performed and it might be helpful to categorize them as four main classes; most used models as semi-empirical/empirical models (45.8 % of scientific works), then mechanistic models (31.4 %), statistical models (9.8 %) and neural networks models (8.5 %) (Caccavo, 2019; Siepmann & Siepmann, 2008). Empiric models, mainly zero order, first order, Higuchi or Peppas equations mainly rely on a basic, simple form as given as:

$$\frac{M_t(t)}{M_\infty} = k f(t) \quad (1.28)$$

where M_t and M_∞ represent total amount of drug released at time “t” and at infinite time, respectively. If $f(t)$ is taken equal to “t”, it is obvious that release rate is time independent and it corresponds to zero order release kinetics or termed as case II transport (Nokhodchi, Raja, Patel, & Asare-Addo, 2012).

In the first order, it has the form;

$$\frac{dM_t(t)}{dt} = k M_t(t) \quad (1.29)$$

and then, it becomes as;

$$\ln \left(\frac{M_t(t)}{M_\infty} \right) = k t \quad (1.30)$$

Professor Takeru Higuchi, the “father” of mathematical modelling of drug delivery proposed famous equations in this field (Takeru Higuchi, 1961). Especially, as given in Eq. (1.31), Higuchi’s equation demonstrated an analytical solution for a thin plane sheet (no edge effects) with thickness of $2l$ with special assumptions such as: diffusion as limiting step, constant diffusivity, constant total concentration, non-swelling system (constant dimension), etc. (T Higuchi, 1961).

$$\frac{M_t}{M_\infty} = 1 - \left(\sum_{n=0}^{\infty} \frac{8}{(2n+1)^2 \pi^2} \exp \left(- \frac{D(2n+1)^2 \pi^2 t}{(2l)^2} \right) \right) \quad (1.31)$$

This equation could be simplified to a square-root approximation for short time release (at only first 60 % of the total drug release). This approach is very appropriate to have a rough estimation but it should be used with caution for each system.

$$\frac{M_t(t)}{M_\infty} = 4 \left(\frac{Dt}{\pi(2l)^2} \right)^{\frac{1}{2}} = k t^{\frac{1}{2}} \quad (1.32)$$

Much more flexible than Higuchi’s equation, *Peppas’s equation* also known as “power law equation” is another and most widely used approximation to describe fractional release for different geometries (Eqn. (1.33)).

$$\frac{M_t(t)}{M_\infty} = k t^n \quad (1.33)$$

Table 1.3 summarizes the meaning of exponent “n” for drug release from polymeric devices regarding to geometry. Other than these commonly used models, it is possible

to find out other empirical and semi empirical models in the literature (Siepmann & Peppas, 2001).

Table 1.3. Exponent n of power law for drug release from polymeric devices (Siepmann & Peppas, 2001).

Thin Film	Cylinder	Sphere	Drug release mechanism
0.5	0.45	0.43	Fickian diffusion
$0.5 < n < 1.0$	$0.45 < n < 0.89$	$0.43 < n < 0.85$	Anomalous transport
1.0	0.89	0.85	Case-II transport (polymer swelling)

To characterize the nature of diffusive phenomena, the order of magnitude of *Deborah number* ($N_{De,D}$) given below could also be determined. If its order of magnitude is higher than 1 ($N_{De,D} \gg 1$), it means that diffusion is faster than relaxation so polymer remains in glassy state and system could be explained by Fick's law using constant diffusion coefficients independent from polymer/water concentrations. Oppositely, in the case of small values of *Deborah number* ($N_{De,D} \ll 1$), relaxation becomes faster and the process could be explained by Fick's law using diffusivity which is a function of polymer/water concentrations. In intermediate values of *Deborah number* ($N_{De,D} \approx 1$), both diffusion and relaxation occur on same time scale so anomalous which is non-Fickian transport becomes valid (Caccavo, 2019). While Fickian transport is concentration gradient driven process, non-Fickian is based on polymer network relaxation.

$$N_{De,D} = \frac{\text{stress relaxation time}}{\text{diffusion time}} = \frac{\tau}{\tau_D} \quad (1.33)$$

Besides empiric approaches, mechanistic models rely on more realistic phenomena including diffusion, swelling, erosion, dissolution and degradation (Haseeb, Hussain, Yuk, Bashir, & Nauman, 2016; Kikuchi, Onuki, Kuribayashi, & Takayama, 2012; N. Peppas, 2000; Siepmann & Siepmann, 2008).

When a dry, target agent loaded hydrogel is left into a dissolution medium, the solvent starts to penetrate into the polymer gel network. If the glass transition temperature of the polymer is higher than medium temperature, as the concentration of the solvent exceeds the threshold value, unfolding of polymer chains emerges and glass to rubbery transition occurs. A gel like layer covering the matrix core develops. The moving front at this stage is defined as “swelling front” that differentiates swollen matrix from non-swollen part. In this process, the active agent could coexist as both dissolved and dispersed form. The front which separates the swollen matrix with only dissolved agent from the swollen part with both dissolved and dispersed agent is defined as “diffusion front”. Another zone “erosion front” is the eroding matrix boundary that the swollen matrix is in contact with the outer medium and chains disentanglement take place, polymer network becomes hydrated as well (Caccavo, 2019). The most important mechanistic model studies conducted up to 2019 were listed and explained in detail in the review of Caccavo (2019). They are usually based on partial differential equations to be solved analytically or numerically with defined initial and boundary conditions depending on the system (reservoir or monolithic solution / dispersion) for water and/or drug. While single component approach is based on dissolved drug diffusing within the system through the external release medium, multicomponent advanced approaches consider the swelling/shrinkage approximation, the deformation under osmotic pressure, the effect of ionic species and the electrical potential, etc. (Caccavo, 2019).

“Sequential layer” model proposed by Siepmann (Siepmann & Peppas, 2000) is one example for the multicomponent approach with inhomogeneous swelling, polymer and drug dissolution consideration. The system is defined by Fick’s second law with time and position dependent diffusivity by sequential layers (sections) considering both water and drug diffusion in radial and axial mass transfer within cylindrical tablets. For polymer dissolution, reptation theory was considered and dissolution rate constant was included depending on the polymer mass loss velocity.

The study of Pareek et al. (2017) is a good example for the multicomponent mechanistic model. They combined three main equations which were “Nernst-Planck” equation for diffusion of ionic species, Poisson equation accounting electric potential and force balance equation for deformation of hydrogel under osmotic pressure (Pareek, Maheshwari, Cherlo, Thavva, & Runakana, 2017).

Hydrogels usually swell in water due to the penetration of a hydrophilic solvent caused by polymer chain relaxation and polymer–polymer and polymer–water interactions affecting this response (Ozel, Uguz, Kilercioglu, Grunin, & Oztop, 2016). Similarly, release ability also shows changes with regard to gel formulation. Diffusion, swelling, and chemical mechanisms could explain the release of active compounds (Je Lee & Rosenberg, 2000). The barriers encountered in analysis of full hydrogel based systems behavior have directed most of the researchers to define the system with “mass transport only” or with empirical models (Caccavo, 2019). Controlled release mechanisms had been summarized in Section 1.3.1. In this section, several models that have been found in the literature would be listed.

1.3.6. Mass transfer in gel system with NMR/MRI

Imaging, spectroscopic or relaxometry measurements in NMR is among the techniques to be used for modelling study and active agent / water transport behavior in drug delivery systems. Although polymer gels are usually characterized by their rheology, physical appearance, different spectroscopic methods should be used as a fingerprint for specific molecules.

For hydrogels, solid state NMR such as ^1H DQ magic angle spinning (MAS) could give structural insight for dried gels while high resolution (HR) MAS or static ^1H multiple-quantum (MQ) could enable analysis of gel samples in wet state (Brown, 2018). NMR/MRI could be even performed on the stage of gel formation. Transport processes in colloidal systems to derive the information about dynamic processes have been evaluated in several studies (Chowdhury, Hill, & Whittaker, 2005; Cukier, 1984; Dahlberg, Fureby, Schuleit, Dvinskikh, & Furó, 2007; Duncan & Whitten, 2000;

Escuder, LLusar, & Miravet, 2006; Fyfe & Blazek-Welsh, 2000; McConville & Pope, 2000; Ozel et al., 2016; Oztop, Rosenberg, Rosenberg, McCarthy, & McCarthy, 2010; Östlund, Bernin, Nordstierna, & Nydén, 2010; P. D. Williams, Oztop, McCarthy, McCarthy, & Lo, 2011; Yoon, Gayathri, Gil, Kowalewski, & Matyjaszewski, 2010; Zeng et al., 2007). Owing to rigid structure of the gel, NMR signal relax faster and monitoring water penetration becomes easier than investigating actual gel components, that is why most of the studies have been interested in water transport (Östlund et al., 2010).

Common approaches for dissolution and release behaviors of gels are based on macroscopic observations varying from simple gravimetric methods, texture analyses to more complicated and noninvasive methods such as MRI (Abrahmsén-Alami, Körner, Nilsson, & Larsson, 2007; Tajarobi, Abrahmsén-Alami, Carlsson, & Larsson, 2009; Viridén, Abrahmsén-Alami, Wittgren, & Larsson, 2011). For better understanding of the underlying mechanism, mathematical modelling of dissolving tablets, spheres, etc. is also proposed (Caccavo et al., 2017).

From early studies, NMR imaging has been used to comprehend drug release/swelling behaviors from the gels. Fyfe and Blazek-Welsh (2000) performed the measurement of relaxation time constants and self-diffusion coefficients at different polymer (HPMC) and model drug (triflupromazine-HCl and 5-fluorouracil) concentrations yielding calibration equations. ^{19}F NMR imaging was carried out for drug profile along the gel and ^{19}F molarities were found in swollen tablets with respect to time to compare two model drugs. Fractional drug release for both drugs were obtained linearly with respect to square root of the time demonstrating that the drug release was Fickian (Fyfe & Blazek-Welsh, 2000).

Slow-release drug delivery system including a compact of Eudragit polymer and Diltiazem hydrochloride drug was monitored by two dimensional slice selective MRI for water ingress in the non-swelling study of Karakosta and McDonald. They addressed the square root time dependent water progression and Fickian like ingress

behavior (Karakosta & McDonald, 2007). As an example to swelling system, Mikac et al. (2010) combined two MRI protocols, 2D multi-echo MRI with T_2 mapping and 1D single point imaging (SPI), to characterize swelling, penetration and erosion fronts of hydrophilic polymers. 1D SPI profile, T_2 value and signal intensity profile of 2D MRI were used for penetration, swelling and erosion front, respectively (Mikac, Sepe, Kristl, & Baumgartner, 2010). The study of Strübing et al. (2008) was among the first use of a benchtop MRI for these purposes (Strübing, Metz, & Mäder, 2008). Williams et al. (2011) also used MRI compatible benchtop setup for drug dissolution behavior of HPMC matrix formulation. Discrimination between water protons in gel layer and those in hydration medium and fat accumulation in gel surface were monitored (H. D. Williams et al., 2011). Similar MR studies for dissolution and hydration of non-swelling and swelling drug delivery systems were all listed in detail in the review of Mantle (2013) (Mantle, 2013).

Another study of Dahlberg et al. (2007) used ^1H NMR spectroscopy to investigate a released drug concentration (antipyrine, the hydrophilic drug) into aqueous phase with better understanding of its effect on polymer (HPMC) swelling dynamics. For this purpose, they constructed such a sample set up in NMR tube that it allowed only one-dimensional release. To hinder signals coming from water molecules, D_2O was used as a solvent instead of H_2O . Setting the imaging sequence parameters, spectra was obtained for tablets undergoing D_2O penetration from the top at different swelling and release times (0 min, 5 min, 2 h, 11 h). The area underneath the intensity profiles were used to calculate relative amount of swollen polymers while spectral integrals corresponding to antipyrine were used as release data. The position of hydration front as a function of time for each tablet was also represented to estimate molecular diffusion coefficient which was found as $3 \times 10^{-10} \text{ (m}^2 / \text{s)}$ with square root law (Dahlberg et al., 2007).

Relationship between drug release attribute and diffusivity of water molecules inside hydrating tablets were studied by Kikuchi et. al. (2012) by MRI. Proton density and diffusion weighted images of hydrating tablets were figured out at intervals for HPMC

matrix and poly-ion complex tablets. They concluded that penetration of water was faster in poly-ion complex tablets with high diffusivity. MRI was seen as a useful tool to provide a valuable information about the state of water molecules in hydrating tablets and about the release mechanism at a molecular level (Kikuchi et al., 2012).

López-Cebral et al. (2014) demonstrated the application of NMR spectroscopy as an biomimetic approach for hydrophobic drug association with physical hydrogels. Protein albumin was incorporated into the hydrogel and ketoconazole and prednisolone were used as two model hydrophobic drugs to study drug binding capacities derived from NMR (López-Cebral et al., 2014). Saturation transfer difference spectra (STD) and 1D T_2 -filtered watergate proton spectra obtained with double titration assay were acquired for NMR detection of weak to medium binding and strong binding affinity, respectively. Release experiments were followed by HPLC analysis. Finally, they proposed that weak binding was the reason of initial burst drug delivery while strong binding led a subsequent sustained drug release. NMR results supported HPLC results indicating its potential use for the design of new pharmaceutical dosage forms.

Caccavo et al. (2017) proposed a model for transport of water, polymer (HPMC) and drug (theophylline) considering pseudo-diffusion phenomenon. MRI was used to monitor water distribution and gel hydration by determining water concentrations at different positions inside swollen tablets (Caccavo et al., 2017). A NMR setup similar to the study of Abrahmsen-Alami et. al. (2007) were designed where tablets were left in dissolution media in a release cell in NMR device under *sink-conditions*. After the proton T_2 relaxation was correlated with water concentration in the solution by measuring it at known water concentrations, water fraction distributions in gel layer at different dissolution times were calculated from NMR images. In the modelling part, a transport model for 2D axial geometry (computational domain was built as half tablet in NMR tests) with coupled constitutive equations was developed. Fujita-type equation was used for the dependency of diffusion coefficients on hydration. Erosion velocity which was important for the polymer release and domain reduction was

described through an erosion constant. Then, water mass fraction and erosion constant were predicted and fitted to NMR data. This study enabled combined approach of modelling and experiment with a fruitful way to deepen gelling, hydration and release in hydrophilic matrices.

1.4. Objectives of The Study

The aim of the present study is to offer NMR / MRI as a tool to monitor and quantify mass transport phenomena in food and gel systems, effectively. For this purpose, the study was divided into two main parts. The first part focused on hazelnut paste layer over chocolate as a food system to quantify oil migration. The second part covered alginate-based hydrogel study as a controlled insulin delivery carrier. The characterization of polymer and water interactions was explored with the help of NMR/MRI. Moreover, additional chromatographic, textural and microstructural analyses were employed for explaining the process better.

CHAPTER 2

MATERIALS AND METHODS

2.1. Materials

2.1.1. Hazelnut Paste / Chocolate System

Cocoa liquor and cocoa butter were supplied from ETİ Food Industry and Co. Inc. (Eskişehir, Turkey). Hazelnut paste (Fiskobirlik, Giresun) and icing sugar (Bağdat Baharat, Ankara, Turkey) were purchased from local markets. Stevia containing stevia extract (Stevia in The Raw®, USA) and Splenda containing sucralose (Splenda®, USA) were used as sweeteners. In order to develop texture and taste of chocolate, inulin (Smart Kimya Ltd., Cigili, Turkey) was used. Lecithin (Cargill, Belgium) as emulsifying agent was used. As filler for stretching the taste of sweetness of chocolate containing sweeteners, maltodextrin (Sunar Co. Inc., Adana, Turkey) was also used.

2.1.2. Insulin Loaded Hydrogel System

The polysaccharides sodium alginate with low viscosity (viscosity of 1% aq. solution: <300 cps) (FMC, Scotland) and GT (C.E. Roeper GmbH, Hamburg, Germany) were kindly obtained by FMC group (FMC BioPolymer, Philadelphia, USA). CH (deacetylation degree > 75 % and medium molecular weight) was purchased from Sigma-Aldrich (St. Louis, MO) to be used in the experiments. Absolute hydrochloric acid (37%, with density of 1.19 g/cm³ at 20 °C, boiling point of 45 °C, melting point of -28 °C) and potassium dihydrogen phosphate (KH₂PO₄) (EMSURE® ISO) were obtained from Merck (Germany). Calcium chloride dihydrate, sodium hydroxide and sodium chloride were purchased from Sigma–Aldrich (St. Louis, MO). Standards, insulin human (≥27.5 units/mg, meets USP testing specifications) and m-cresol (99%) were purchased from Sigma–Aldrich (St. Louis, MO). Humulin R (100 IU/ml, Eli Lilly and Company, France) was used as insulin product in all experiments.

Double distilled water from a water purification system (Nanopure Infinity, Barnstead International, IA) was used for preparation of HPLC phase solutions. All other chemicals used were of analytical grade.

2.2. Methods

2.2.1. Hazelnut Paste / Chocolate System

2.2.1.1. Two-Layer chocolate confectionery system preparation

Samples were prepared as a 2-layer chocolate confectionery system with an initially deposited layer of chocolate and a subsequent layer of hazelnut paste on top. Five different chocolate formulations with sucrose, sweetener Splenda, sweetener Stevia and combination of sucrose with sweeteners (Table 2.1) and one type of hazelnut paste were used. The percentage of sweeteners was chosen considering desired sweetness and acceptable sensory quality. The amount of maltodextrin in samples with only sweeteners was increased to fix solid amount in all formulations. Hazelnut paste contained 11% protein, 42.2% carbohydrate and 44% fat and others (vitamins, calcium, ferrous, phosphorous) (Fiskobirlik, Giresun).

Table 2.1. Composition of 5 chocolate formulations.

Sample	Cocoa mass (gr)	Cocoa butter (gr)	Sugar (gr)	Splenda (gr)	Stevia (gr)	Inulin (gr)	Lecithin (gr)	Maltodextrin (gr)
F1	40	25	14	-	-	15	0.5	5
F2	40	25	14	0.5	-	15	0.5	5
F3	40	25	14	-	0.5	15	0.5	5
F4	40	25	-	0.5	-	15	0.5	19
F5	40	25	-	-	0.5	15	0.5	19

For chocolate production, cocoa butter was firstly melted and then cocoa mass was added. After that, other ingredients were also added. The process was achieved on a heater. The mixture was transferred to a grinder vessel for refining and conching steps together. The grinder machine was actually a ball mill and could be substituted for conching and refining on lab scale. The ball mill (Retsch, PM 100, Germany) was

adjusted at 250 rpm for 60 min. Tempering of the chocolate was achieved by controlled temperature process using an electronic thermometer. Firstly, chocolate was melted to 45-50 °C and then 2/3 portion of chocolate (66.6 g of 100 g sample mixture) was cooled by gradually to 27 °C on marble ground. Finally, remained portion of chocolate was put, mixed and temperature was increased to 30 °C on marble. After tempering step, the chocolate was checked for a smooth and glossy finish by spreading a thin layer on an aluminum foil and by waiting for cooling.

The sample container was a plastic rectangular container with an air- and moisture-tight lid. The dimensions were 3 cm x 3 cm x 3 cm. For hazelnut paste-chocolate samples, a layer of chocolate was deposited in the sample container. The thickness of the chocolate layer was approximately 1 cm. An equally thick layer of hazelnut product measured by ruler was then deposited on the chocolate layer. In previous studies, it was seen that oil migration into chocolate was insufficient at 20 °C (McCarthy & McCarthy, 2008). When fractional liquid lipid content in chocolate was compared between at 20 °C and at 30 °C, higher liquid lipid was obtained at 30 °C (McCarthy & McCarthy, 2008). Thus, the samples were stored in a controlled environment chamber at 30 ± 0.5 °C, thereby migration occurred faster. All sample types were made in replicates. In addition, a single layer of chocolate and pure hazelnut oil as a reference were also prepared as two separate samples. For MRI analysis, the sample containers were removed from their chambers and measurements were evaluated at ambient temperature (20 ± 0.5 °C). The samples were kept at room temperature no longer than 20 min and then returned to storage conditions. Data were collected over a time frame of 22 days as 1, 2, 3, 4, 5, 11, 15 and 22 days.

2.2.1.2. NMR/MRI measurements

MRI measurement: MRI was performed using a spin echo sequence (SE) with a repetition time (TR) of 800 ms and echo time (TE) of 13 ms on a 3T system (SIEMENS MAGNETOM Trio, Germany) at Bilkent University, UMRAM (National Magnetic Resonance Research Center). The field of view was 170 mm for a 256 x

256-pixel image. The slice thickness was set to 4 mm. Day-to-day signal variations of the instrument were addressed by normalizing the data with a time-invariant sample of hazelnut oil as the reference. Firstly, correction was performed for each sample according to signal intensity variations of reference pure hazelnut oil at each measurement day. Then, for normalization, a similar approach to McCarthy and McCarthy (McCarthy & McCarthy, 2008) was followed. Firstly, signal intensity (SI) of chocolate belonging to specific day was multiplied by the ratio of average SI (average of all days) of reference hazelnut oil (HO) to SI of HO belonging to specified day. Signal intensity values were then divided by 1D profile's own mean to attain values of order one. For MR image analysis and mathematical calculations, Radiant DICOM Viewer (Poznan, Poland) and MATLAB 7.9.0 software (Mathworks, Natick, Mass., U.S.A.) were used. One-dimensional signal intensity profiles across the center of the sample container were obtained from the MR images.

NMR measurement: Chocolate NMR experiments were performed on a 0.5 T Benchtop NMR system (Spin Track SB4, Mary El, Russia). For spin-lattice relaxation (T_1) measurements, a saturation-recovery pulse sequence with 10s time of observation was used with repetition time of 600 ms. For spin-lattice relaxation (T_2) measurements, Carr-Purcell- Meiboom-Gill (CPMG) sequence was used with 100 ms echo time, 3000 echoes.

Proton spectral information can be directly related with molecular mobility and so rigid and more mobile components in semi crystalline polymers could be readily discerned (Maus, Hertlein, & Saalwächter, 2006). To characterize the interface region in detail, ^1H NMR measurement were conducted by using magic sandwich echo (MSE) pulse sequence, offering insights into the chemical compositions with different mobilities in samples (Y. B. Grunin, Grunin, Talantcev, Nikolskaya, & Masas, 2015). Signals from solid and liquid phases were analyzed by fitting to Gauss-Lorentzian (Eq. 2.1) and Semicrystalline FID equation (Eq. 2.2), separately.

Gauss-Lorentzian FID:
$$FID(t) = a_{01} e^{-\left(\frac{t}{T_{21}}\right)^2} + a_{02} e^{-\left(\frac{t}{T_{21}}\right)^2} + y_0 \quad (2.1)$$

Semicrystalline FID:
$$FID(t) = a_{0cr} e^{-\left(\frac{t}{T_{2s}}\right)^2} \cos(2\pi bt) + a_{0m} e^{-\left(\frac{t}{T_{2m}}\right)^2} + a_{0l} e^{-\left(\frac{t}{T_{2l}}\right)^2} + y_0 \quad (2.2)$$

where amplitude a_{01} and a_{02} are proton population of solid and liquid parts, respectively. In detail, amplitude a_{0cr} , a_{0m} and a_{0l} represent proton population of crystalline region (protons with spatially ordered), amorphous region (protons with less ordered) and liquid phase (protons of absorbed water), respectively (Y. B. Grunin et al., 2015). Then, degree of crystallinity k was calculated as

$$k = \frac{a_{0cr}}{a_{0cr} + a_{0m}} \quad (2.3)$$

2.2.1.3. Mathematical modelling

As proposed by Deka et al. (2006), Lee et al. (2010) and others, diffusion was taken as dominant mechanism for oil migration. Transport of liquid lipid in food has been characterized as a diffusion process described by Fick's 2nd law;

$$\frac{\partial C}{\partial t} = D \frac{\partial^2 C}{\partial x^2} \quad (2.4)$$

where C is hazelnut oil content in the chocolate layer and D is diffusion coefficient. The partial differential equation Eqn. (2.4) was subjected to appropriate initial and boundary conditions for diffusion into a plane sheet (rectangular coordinates) (Fig. 2.1).

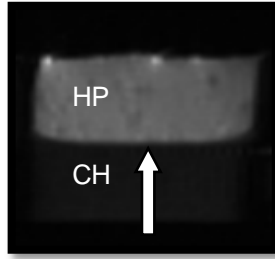


Figure 2.1. Representative system and coordinates

Boundary conditions were described in two ways. In Model 1, initial and boundary conditions were demonstrated as follows for a slab of thickness ‘l’ (Y J Choi et al., 2007; W. L. Lee, McCarthy, & McCarthy, 2010b; McCarthy & McCarthy, 2008);

$$\text{IC:} \quad C(x, 0) = 0 \quad (2.5)$$

$$\text{BC:} \quad \left. \frac{\partial C}{\partial x} \right|_{(x=0)} = 0 \quad (2.6)$$

$$\text{BC:} \quad C(l, t) = C_0 [1 - e^{-\beta t}] \quad (2.7)$$

Eq. (2.5) implied that initially there was no hazelnut oil content on chocolate layer. “x” coordinate was defined as “0” at the chocolate bottom (x=0) and “l” at the upper boundary of chocolate (x=l). Eq. (2.6) demonstrated that no flux existed at bottom of chocolate layer.

In order to describe a time varying concentration at the interface of the hazelnut paste and chocolate layers, Eq. (2.7) was used at the upper boundary of chocolate layer for

all chocolate formulations. This BC represented an initial hazelnut oil content of zero at the interface and approach to an equilibrium concentration C_0 over time with β as rate constant. C_0 and β values were firstly estimated by fitting the signal intensity at the interface ($C(l,t)$) to Eq. (2.7) by nonlinear fitting routine and later these findings of C_0 and β parameters were used as initial estimation to solve Eq. (2.8). With a no flux boundary condition at $x = 0$ (the container bottom) and the exponential condition at $x = l$ (the upper boundary of the chocolate layer), the analytical solution was (Crank, 1975):

$$\begin{aligned} \frac{C(x,t)}{C_0} & \quad (2.8) \\ &= 1 - e^{-\beta t} \frac{\cos x(\beta/D)^{\frac{1}{2}}}{\cos l(\beta/D)^{\frac{1}{2}}} \\ & - \frac{16\beta l^2}{\pi} \sum_{n=0}^{\infty} \frac{(-1)^n \exp[-D(2n+1)^2\pi^2 t/4l^2]}{(2n+1)\{4\beta l^2 - D\pi^2(2n+1)^2\}} \cos \frac{(2n+1)\pi x}{2l} \end{aligned}$$

Since experimental 1D MR signal intensity data have arbitrary units, normalized data explained in “MRI measurements” part was converted into dimensionless form to yield hazelnut oil concentration, C

$$C = \frac{SI - \langle SI \rangle_1}{\langle SI \rangle_1} \quad (2.9)$$

where the brackets indicated an average signal intensity (SI) over the chocolate region and the subscript $_1$ designated the SI at day 1, before the all the possible migration started. Thus, $\langle SI \rangle_1$ helped to obtain dimensionless form of concentration.

Experimental data acquired from MR images were fitted to Eqs. (2.7) and (2.8) and designated as Model 1. However, fitting results were not so convincing due to lower R^2 values and another fitting model was also evaluated by using a different boundary condition as follows:

$$C(l, t) = \frac{C_0}{1 + e^{-\beta*(t-t_0)}} \quad (2.10)$$

This empirical boundary condition was selected based on the shape of the signal intensity plot at the interface which showed a behavior similar to a logistic model which was a typical S shape, sigmoid curve. This logistic model was obtained using mathematical tool. Instead of Eq. (2.7), Eq. (2.10) was used at the upper boundary of chocolate layer for all chocolate formulations which required a numerical solution and the resulting model was designated as Model 2. The initial hazelnut oil content of zero at interface and an approach to an equilibrium concentration C_0 over time were still valid for Model 2. Obtaining better R^2 values was aimed in Model 2 and then two model fitting results were compared. Conditions and solutions for both models were summarized in Table 2.2.

Table 2.2. Expressions for the mathematical model.

Model 1	Model 2
Initial condition $C(x, 0) = 0$	$C(x, 0) = 0$
Boundary condition at $x=0$ $\left. \frac{\partial C}{\partial x} \right _{(x=0)} = 0$	$\left. \frac{\partial C}{\partial x} \right _{(x=0)} = 0$
Boundary condition at $x=l$ $C(l, t) = C_0[1 - e^{-\beta t}]$	$C(l, t) = \frac{C_0}{1 + e^{-\beta*(t-t_0)}}$
Applied Mathematical Solution	
Analytical solution $\frac{C(x, t)}{C_0}$ $= 1 - e^{-\beta t} \frac{\cos x(\beta/D)^{\frac{1}{2}}}{\cos l(\beta/D)^{\frac{1}{2}}}$ $- \frac{16\beta l^2}{\pi} \sum_{n=0}^{\infty} \frac{(-1)^n \exp[-D(2n+1)^2\pi^2 t/4l^2]}{(2n+1)\{4\beta l^2 - D\pi^2(2n+1)^2\}} \cos \frac{(2n+1)\pi x}{2l}$	Numerical solution

Parameters (C_0 , β , t_0) belong to time varying boundary conditions were estimated for the hazelnut oil content, C , at the upper boundary of the chocolate layer using MATLAB “Curve Fitting Toolbox” for both Model 1 and Model 2 respectively.

In Model 1, the diffusion coefficient D was found subsequently by using the MATLAB function “nlinfit”, Eq. (2.10) and experimental data. “nlinfit” depending on nonlinear regression predicted the coefficients using iterative least squares estimation, with initial estimations. C_0 was the 2nd adjustable parameter after D value although it was estimated using MATLAB “Curve Fitting Toolbox” before.

In Model 2, numerical solution and model fitting were obtained by using MATLAB “pdepe” solver and MATLAB “Optimization Toolbox”. Constants (C_0 , β , t_0) found by using boundary conditions and MATLAB “Curve Fitting Toolbox” were taken as initial guess and then all of the constants and D value were estimated finally by using MATLAB “Optimization Toolbox”. In “Optimization Toolbox”, “fminsearch (unconstrained nonlinear minimization)” was used as an equation solver giving initial estimations for the unknown coefficients. “fminsearch” depends on Nelder-Mead simplex algorithm. In MATLAB solutions, number of iterations, function tolerance (at least $1e-14$), exitflag values (>1) and R^2 values (> 0.90) were checked to provide stopping criteria.

2.2.2. Insulin Loaded Hydrogel System

2.2.2.1. Gel preparation

Hydrogels were prepared by immersing mesh baskets with gelation solution including alginate (ALG) and gum tragacanth (GT) at different ratios into the beaker with coating solution containing CaCl_2 (1.5% (w/w)) and with/out chitosan solution (0.5% (w/v)). The total concentration of polymers (ALG and GT) was kept at 1% (w/w). All formulations were presented in Table 2.3.

ALG and GT solutions were stirred at 10,000 rpm for 2 min using Ultra Turrax T-18 (IKA Corp., Staufen, Germany) separately and then combined in a beaker at the

magnetic stirrer. Polymer solutions were left at magnetic stirrer for 1 h at room temperature. Then 2.5 ml of Humulin (insulin agent) was added into 100 gr polymer solution and stirred at 5,000 rpm for 2 min using Ultra Turrax T-18. This ALG-GT solution was left at magnetic stirrer for 1 h again to obtained homogenized and uniform insulin concentration within gel matrix.

Chitosan solution was prepared by first dissolving 5.0 g of chitosan in 500 mL 1% HCl solution. The pH of the solution was then adjusted to 5.5 with 1 M NaOH and diluted to give a final volume of 1 L. At 25 °C, ALG-GT solution was poured into mesh plastic baskets by immersing into the binding solutions (with/out chitosan) at the same time. The resulting gels were allowed to harden in the gelation solution overnight. Gels were then washed with distilled water. Then they were cut into 2 cm length of cylinder (1.3 cm in diameter).

Table 2.3. Composition of hydrogels.

Sample	ALG : GT ratio (%)	Binding solution
100A	100:0	1.5% CaCl ₂
100A CH	100:0	1.5% CaCl ₂ + 0.5% Chitosan (at equal ratio)
75A	75:25	1.5% CaCl ₂
75A CH	75:25	1.5% CaCl ₂ + 0.5% Chitosan (at equal ratio)
50A	50:50	1.5% CaCl ₂
50A CH	50:50	1.5% CaCl ₂ + 0.5% Chitosan (at equal ratio)
25A	25:75	1.5% CaCl ₂
25A CH	25:75	1.5% CaCl ₂ + 0.5% Chitosan (at equal ratio)

2.2.2.2. Zeta potential measurement

Zeta potential of gelation and binding solutions were analyzed by using nano ZS90 (Malvern Instruments, UK). It was conducted at METU Central Laboratory.

2.2.2.3. pH dependent insulin release studies

All insulin loaded hydrogel samples were submitted to *in vitro* insulin release experiments in simulated gastric fluid (SGF) and simulated intestinal fluid (SIF), separately. The digestive media, SGF and SIF were prepared according to method used by Xu & Dumont (2015). Since preliminary experiments showed that enzymes

caused rapid degradation of insulin, SGF and SIF were prepared with free enzyme. SGF (pH 1.2) was prepared by dissolving 2.0 g of NaCl in 7 mL of concentrated HCl and setting the final volume to 1 L. For SIF (pH 6.8), 6.8 g of KH_2PO_4 was dissolved in 250 mL of distilled water, then 77 mL of 0.2 N NaOH solution was added and final volume of 1 L was diluted. The pH of SGF and SIF solutions were adjusted to 1.2 and 6.8 respectively (Xu & Dumont, 2015).

Each hydrogel was suspended in 40 ml of digestive medium by using mesh baskets at 37 °C under magnetic stirring at 80 rpm. At determined time intervals (0.5, 1, 2, 3, 4, 5, 6 and 24 h), an aliquot sample (1mL) was withdrawn from release medium and insulin content was estimated by Reverse-Phase High Performance Liquid Chromatography (HPLC) (Shimadzu, Japan).

In HPLC method, the mobile phase was a premixed isocratic mixture of 0.2 M sodium sulfate anhydrous solution adjusted to pH 2.3 with phosphoric acid and acetonitrile (72:28, v/v). The injection volume was 20 μl and flow rate was 1.0 ml min^{-1} at 40 °C. The eluent was monitored at 214 nm (J. Liu, Gong, Wang, Zhong, & Zhang, 2007). Then, to calculate the released amount, peak area corresponding to insulin was calculated. Calibration curve of insulin was prepared with insulin human standard solutions of known concentrations. All experiments were performed at least duplicate.

2.2.2.4. Modelling release behavior of gel samples

For modelling release behavior of the gels in intestine, the system given in Fig. 2.2 was considered. Although it was not shown in the Fig. 2.2 not to create crowded picture, magnetic stirrer was also used in the system to obtain uniform concentration in the medium. Additionally, mesh baskets were used to hang out the gels for diffusion from all directions.

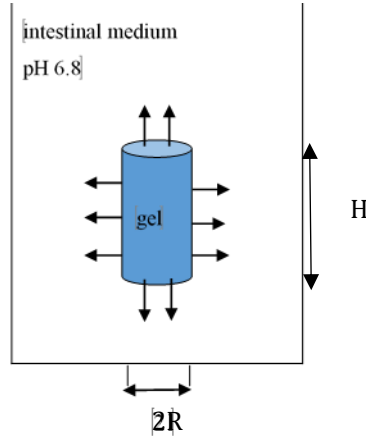


Figure 2.2. Model hydrogel system for insulin release modelling

Species conservation equation involving only diffusion is (Crank, 1975) :

$$\frac{\partial c_i}{\partial t} + \nabla \cdot (-D_i \nabla C_i) = G_i \quad (\text{i represents species}) \quad (2.11)$$

where C represents concentration of species (IU/cm^3), D is diffusion coefficient (cm^2/s), G is the homogenous generation term which is zero. Hence, Eqn. (2.11) was used for time dependent insulin transport through the gels.

Initial condition (IC) and boundary conditions (BC) were determined as:

$$\text{IC: } C = C_0 \quad \text{at } t = 0 \quad (2.12)$$

$$\text{BC.1: } N = -D \nabla C = \frac{\partial M}{A \partial t} \quad \text{at } r = R, x = H \quad (2.13)$$

$$\text{BC.2: } N = 0 \quad \text{at } r = 0 \quad (2.14)$$

where H and R represented gel height (cm) and radius (cm), respectively. N was the flux ($\text{IU}/\text{cm}^3\text{s}$), M was the amount of insulin at that determined time (IU), C_0 was initial insulin concentration in each gel (IU/cm^3) and A was exposed area (cm^2). “ x ” coordinate started from the bottom of gel layer. BC expressed the fact that the rate at which insulin left the gel over the surfaces was equal to that at which it entered into the medium.

To calculate effective diffusion coefficient for release of insulin from each gel samples with the shape of cylinder, mass transport equation for diffusion in infinite plane and infinite cylinder in a stirred solution of limited volume (Crank, 1975) were combined with product rule. Thus, the solution for finite cylinder geometry satisfied the conditions of “product type solution” as given;

$$\begin{aligned} & \frac{M_t}{M_{inf}} \\ & = 1 \\ & - \left(\sum_{m=1}^{\infty} \frac{4\gamma(1+\gamma)}{4+4\gamma+\gamma^2q_m^2} \exp\left(-\frac{Dq_m^2}{R^2}t\right) \right) \cdot \left(\sum_{n=1}^{\infty} \frac{2\gamma(1+\gamma)}{1+\gamma+\gamma^2p_n^2} \exp\left(-\frac{4Dp_n^2}{H^2}t\right) \right) \end{aligned} \quad (2.15)$$

where M_t/M_{inf} is the ratio of the diffusing agent at time t as fraction of the instantaneous released amount (M_t) to the released agent at long times (M_{inf}). M_{inf} was found as an average value for each formulation by using total released amount of insulin after 6 h (approaching steady state). R and H are the radius and height of the sample respectively. γ represents ratio of the volume of the solution to the volume of sample. D is the effective diffusion coefficient. The q_m 's are the nonzero positive roots of

$$\gamma q_m J_0(q_m) + 2J_1(q_m) = 0 \quad (2.16)$$

and p_n 's are the nonzero positive roots of

$$\tan(p_n) = -\gamma p_n \quad (2.17)$$

HPLC results were fitted to Eq. (2.15) and diffusion coefficients were found by using Matlab function “lsqnonlin”.

2.2.2.5. Texture profile analysis

A textural property of gel was evaluated by the Texture Analyzer (The TA.XTPlus, England). 1 cm diameter cylindrical probe was used for gel samples having dimensions of 3 cm x 3 cm x 2 cm. Gel samples were compressed to 80% of their

initial height at a 1 mm/s pre-test speed, at 1 mm/s test speed and at 10 mm/s post-test speed with 60 s holding time. From texture profile curve, firmness and springiness values were obtained. Six replicates from three different sets of gel solutions were measured and averages of them were taken.

2.2.2.6. Scanning Electron Microscopy (SEM)

Morphological properties of hydrogels were analyzed with scanning electron microscope (FEI Nova NanoSEM 430, Oregon, USA). Samples undergoing SEM were first freeze dried (Christ, Alpha 2-4 LD plus, Germany) at 48h after refrigeration period. Samples were coated with thin layer of gold and analyzed at acceleration voltage of 20 kV. Images were observed at magnification levels of 80X, 300X and 10000X. Analyses were done at Metallurgical and Materials Engineering Laboratory of METU (Ankara, Turkey).

2.2.2.7. Fourier Transform Infrared (FTIR) Spectroscopy

FTIR spectra of hydrogels, alginate, gum tragacanth and chitosan powders were analyzed by IR Affinity-1 Spectrometer with Attenuated Total Reflectance (ATR) attachment (Shimadzu Corporation, Kyoto, Japan). The measurements were recorded in 4000-400 cm^{-1} region at 4 cm^{-1} resolution for 32 scans. The analyses were replicated for three times for each gel. Before the analysis, the gel samples were freeze dried (Christ, Alpha 2-4 LD plus, Germany) at 48h after refrigeration period.

2.2.2.8. NMR/MRI Measurements

Some part of this study were conducted at METU, Department of Food Engineering and some were performed at University of California Berkeley, Department of Bioscience, CA, USA.

NMR experiments were performed using a 0.32 T NMR system (Spin Track SB4, Mary El, Russia). For spin-lattice relaxation (T_1) measurements, a saturation-recovery pulse sequence with 15s time of observation with 8 scans, with a delay time changing in the range of 0.5 ms-2 s with 1024 acquisition points, and 2 scans with 3 replicates

was used. For spin-spin relaxation (T_2) measurements, Carr-Purcell- Meiboom-Gill (CPMG) sequence was used with 1 ms echo time, 800 echoes, 6s relaxation period with 32 scans. Self-diffusion coefficients (SDCs) of hydrogels were determined by a pulse gradient spin echo sequence with three 22 us, 90° pulses. The time intervals between the first and the second pulses and between the second and the third pulses were 2 ms and 60 ms, respectively, with an acquisition time of 500 us. The duration of the pulsed gradient field was 1 ms and the gradient strength was $1.66e^{-2}$ T/m. All NMR measurements of hydrogels were conducted at determined time intervals of 0 h and 6 h and all NMR results were analyzed using MATLAB.

NMR experiments @ UC Berkeley

Same gel formulations were also analyzed by a 1.4 T (60 MHz) Benchtop NMR (NMReady-60PRO, Calgary, Alberta, Canada) in Pines NMR Laboratory, UC Berkeley. Different than 0.32 T NMR measurements in Turkey, bead form of the gels was used to put them into 5 mm NMR tubes as this was the size for the instrument. To form beads, 20 ml polymer solution was introduced in a 1-ml syringe and then extruded through a needle with an internal diameter of 0.45 mm into a 40 ml of agitated gelation solution. T_1 and T_2 measurements were performed through an inversion-recovery pulse and spin echo sequences respectively, by setting parameters as given below.

Table 2.4. Parameters used in 60 MHz Benchtop NMR.

<u>Inversion recovery pulse sequence for T_1 experiment</u>	
Delay time between pulses	15.000 ms
Repetition time	20 s
Number of scans	4
Number of points	1024
<u>Spin-echo sequence for T_2 experiment</u>	
Delay time	2.000 ms
Repetition time	20 s
Number of scans	16
Number of points	8

In addition to TD-NMR experiments, High field NMR measurements were also conducted in Bruker 18.8 T (800 MHz) device in NMR facility in Pines Laboratory, UC Berkeley:

¹H NMR spectra for insulin was obtained using Bruker 800 MHz device at room temperature by applying water suppression. For sample preparation method, the study of Lin and Larive (1995) was followed and some modifications were done. 6 mg/ml of insulin solution was prepared with pure D₂O and pH was adjusted to 9.4 by using NaOH (Lin & Larive, 1995). This experiment was just done to obtain the NMR spectrum of the insulin used in the study.

T₁ of insulin was also obtained using this high resolution system with an inversion-recovery pulse sequence with 16 τ values in the range of 0.001-6.5 ms. For T₂ measurement, CPMG sequence was used with delay time varying from 2 to 60 ms. To calculate relaxation parameters for insulin, peak obtained at around 7.112 was considered. For SDC measurement, Diffusion Ordered Spectroscopy (DOSY) was applied.

Similar to chocolate samples, MRI experiments were also conducted at Bilkent UMRAM. Imaging experiments were performed using a spin echo sequence (SE) with a repetition time (TR) of 800 ms and echo time (TE) of 13 ms on a 3T system (SIEMENS MAGNETOM Trio, Germany). The field of view was 170 mm for a 256 x 256-pixel image. The slice thickness was set to 8 mm. For MR image analysis Radiant DICOM Viewer software (Poznan, Poland) were used.

2.2.3. Statistical Analysis

Analysis of variance (ANOVA) was performed to determine whether there was a significant difference on model constants and diffusivities among chocolate formulations. If significant difference was detected, means were compared by the Tukey test ($p \leq 0.05$) using MINITAB (Version 16) software.

CHAPTER 3

RESULTS AND DISCUSSION

3.1. Hazelnut Paste / Chocolate System

3.1.1. NMR/MRI Results

The extent of oil migration in five chocolate formulations given in Table 2.3 was followed by MRI as a function of position and time. In order to establish relationship between liquid oil content and MR signal intensity, a calibration curve was plotted by using the MR images (Appendix A) (W. L. Lee et al., 2010a; Rumsey & Mccarthy, 2012). Varying amounts of hazelnut oil were mixed into each chocolate formulations and imaged. The signal intensity values from samples on a per volume basis were then plotted against the amount of hazelnut oil per sample volume. Since the relationship between two variables was linear with nearly R^2 being higher than 0.90, it was concluded that signal intensity from the images data could be used instead of concentration for all chocolate formulations.

To control the constancy of MR signal intensity values from the sample over time, 2 replicates of 5 types of two-layer chocolate samples were evaluated in terms of signal intensity. In order to eliminate day-to-day variations between samples, signal intensity (SI) data of each sample were standardized by hazelnut oil reference as described before and then calculations were proceeded.

One set of 2-D MR images of formulations F1, F2, F3, F4 and F5 during storage times of 1, 2, 3, 4, 5, 11, 15 and 22 days were represented in Figs. 3.1 and 3.2. The chocolate (CH) and hazelnut paste (HP) regions were clearly identifiable in MR images. While hazelnut region was so bright giving high signal intensity, chocolate region was so dark with low signal intensity. Hazelnut oil, designated as HO was used as the reference material for correction step of all data. As mentioned before, correction was

performed for each sample according to signal intensity variations of reference pure hazelnut oil at each measurement day. Average signal values were taken from all day data for HO and then it was divided to selected day and signal value was corrected.

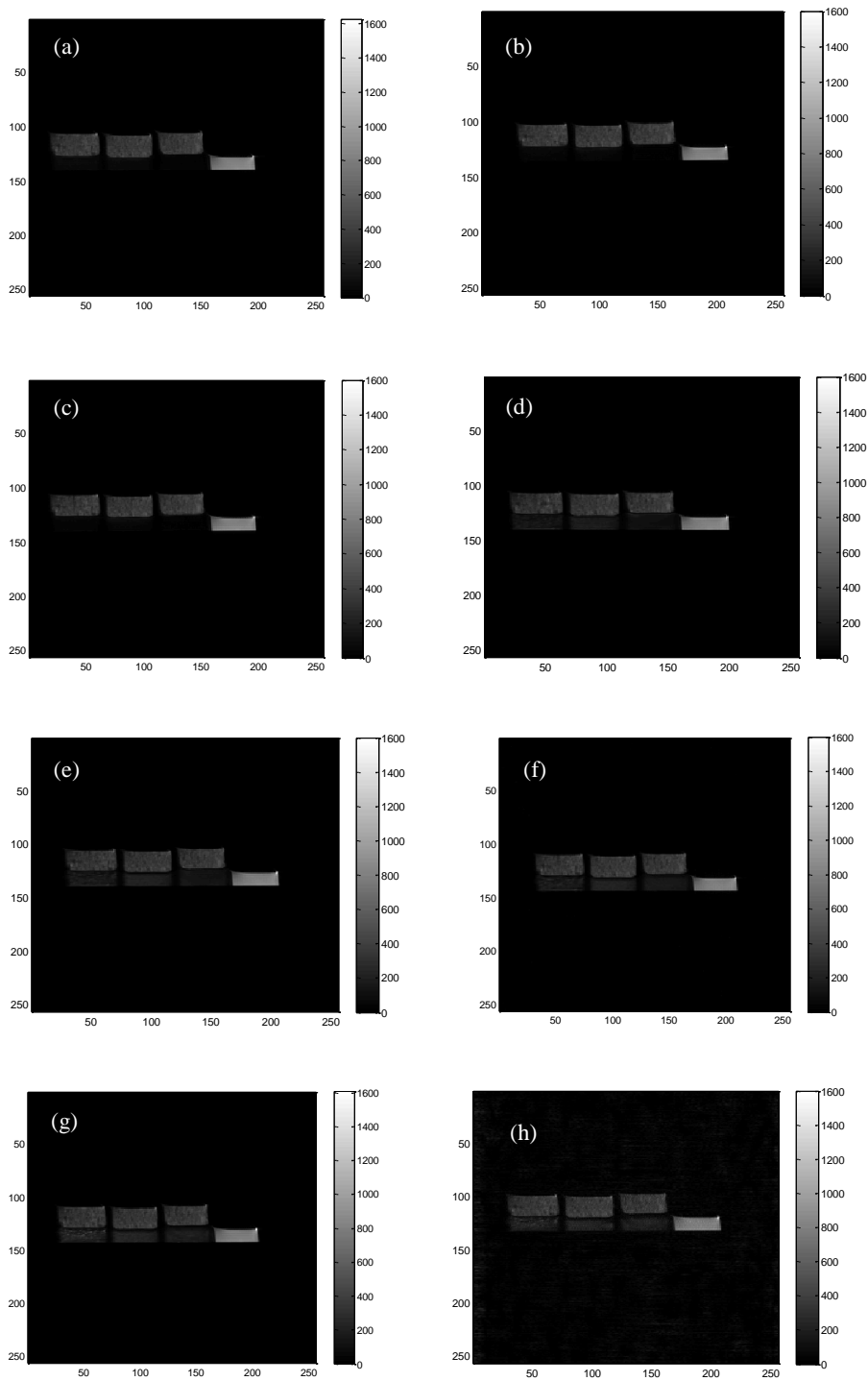


Figure 3.1. 2-D MR images of reference oil, F1, F2 and F3 and reference oil (from right to left) (a) at day 1 (b) at day 2 (c) at day 3 (d) at day 4 (e) at day 5 (f) at day 11 (g) at day 15 (h) at day 22.

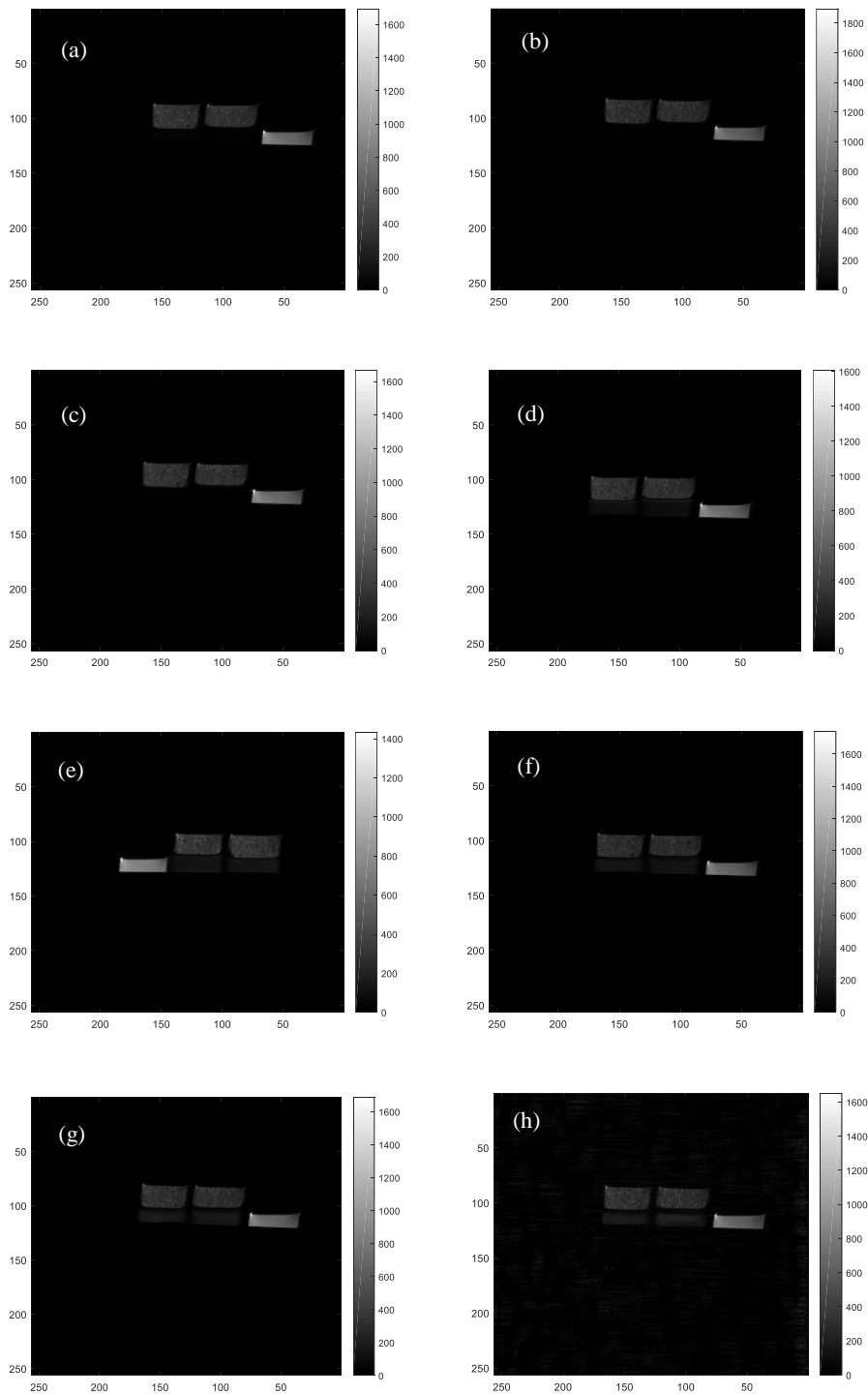


Figure 3.2. 2-D MR images of oil, F4 and F5 (from right to left) (a) at day 1 (b) at day 2 (c) at day 3 (d) at day 4 (e) at day 5 (f) at day 11 (g) at day 15 (h) at day 22.

During storage, hazelnut oil migrated from hazelnut paste into the chocolate leading to increase in signal through CH region and gave brighter color due to existence of liquid hazelnut oil at 30 °C. Interface region was dynamic in all samples. After the 3rd day, a dark layer started to occur between CH and HP region. Miquel and Hall (1998) observed dark regions at border between different materials and explained the possible reason as magnetic susceptibility artefacts. Such a different region with low or high signal between chocolate and filling was also observed in other studies (Y J Choi et al., 2007; McCarthy & McCarthy, 2008; Walter & Cornillon, 2002a) but the reason was not clearly explained. The presence of this zone was ignored during modelling similar to previous studies since the exact mechanism was unclear. The composition of the interface region changed so that it did not resemble neither bottom nor upper layer. During migration, the most mobile triacylglycerols might have left CH-HP interface going through bottom layer. Another possible explanation could be related to the occurrence of fat bloom at chocolate surface. Since fat bloom is the solid transformation, recrystallization form of fats, by phase separation it could increase solid to liquid fat ratio in cocoa butter giving low signal (Walter & Cornillon, 2002a).

It is hypothesized in the study of Ziegler (2009) that the depletion zone could be associated with interphase migration. But this is still an unresolved discussion. Microstructural analysis at the interface or a higher resolution MRI instrument would be helpful to understand the real behavior. In this case, analyzing solid and liquid fractions in interface region, differences in proton characteristics with different arrangements in chocolate was proposed by measurement of NMR crystallinity for mobile fraction as an improved approach.

MSE sequence results were fitted to Gauss-Loarentz and Semicrystalline FID equations and fitting parameter constants were analyzed. Since semicrystalline function consisted of three components that were related to crystalline (a_{0cr}), amorphous (a_{0m}) and liquid (a_{0l}) phases of the sample, its results were mainly considered. It was of particular interest to study how the degree of crystallinity varied during oil migration. Thereby, degree of crystallinity of interface region was

characterized and compared with other parts of chocolate. According to the results, fractions of crystalline (a_{0cr}) and amorphous (a_{0m}) nature at interface were obtained different than other chocolate region. As amorphous fraction was obtained higher (1.35 ± 0.27), degree of crystallinity (k) (as given in Eq. (2.2)) of chocolate interface was found lower (0.54 ± 0.10) than bottom chocolate layer (0.67 ± 0.07) and also for control chocolate (0.86 ± 0.03). It is obvious that upon migration, a rearrangement in microstructure of chocolate surface occurs and corresponding amorphization develops with the dispersion of the structure (decline in crystallinity) (L. Y. Grunin, Grunin, Nikolskaya, Sheveleva, & Nikolaev, 2017). With migrating oil, surface region of crystallites might have been less restricted by hydrogen bonds having higher reactivity compared to inner molecules. The percentage of amorphous phase showed an increase for this depletion zone. This was in agreement with findings of Grunin et al. (2015) that obtained increase in specific surface of cellulose during defibring upon adsorption. Another approach behind of the reason of relative increase of amorphous phase may be wedging pressure deepening the pores between molecules and possibly causing a rise in packing density of surface molecules Grunin et al. (2017). The pressure effect in crystallite dispersion causing decrease in crystallinity has also reported in the study of Grunin et al. (2015). Additionally, NMR relaxometry was used to characterize the mobility of protons in chocolate and hazelnut paste. As expected, time constants; T_1 , and T_2 , were found as lower values than constants of gel samples (high amount of water absorbed) that would be given in Part 2. T_1 and T_2 , values of chocolate were obtained at as 115 ± 5.4 ms and 57.1 ± 6.8 ms, respectively.

Fig. 3.3 illustrated a representative MR image of 2 layer samples stored at 30 °C and the extracted SI data. In Figs. 3.3 (b-f), signal intensities of one set of F1 samples as a function of position over time were given. One dimensional (1D) signal intensity profiles were taken in vertical direction from bottom (chocolate layer) to top (hazelnut paste layer). The demarcation between two regions was identifiable by the sharp vertical gradient. That vertical line introduces qualitative observation of oil migration from hazelnut region on right to chocolate region on left. It was clearly seen that there

was a sharp increase in SI profile from CH region to HP region. HP region had higher signal intensity than CH region in all images and had a much lighter gray color. As a general comment, in several samples, signal intensity variations in both CH and HP regions were observed; the reason could be heterogeneity due to small amount of air entrapped during sample preparation of viscous paste and the variation in materials (Y J Choi et al., 2007; Young J. Choi et al., 2005). During storage, signal intensity of CH region showed an increase due to migration of hazelnut oil.

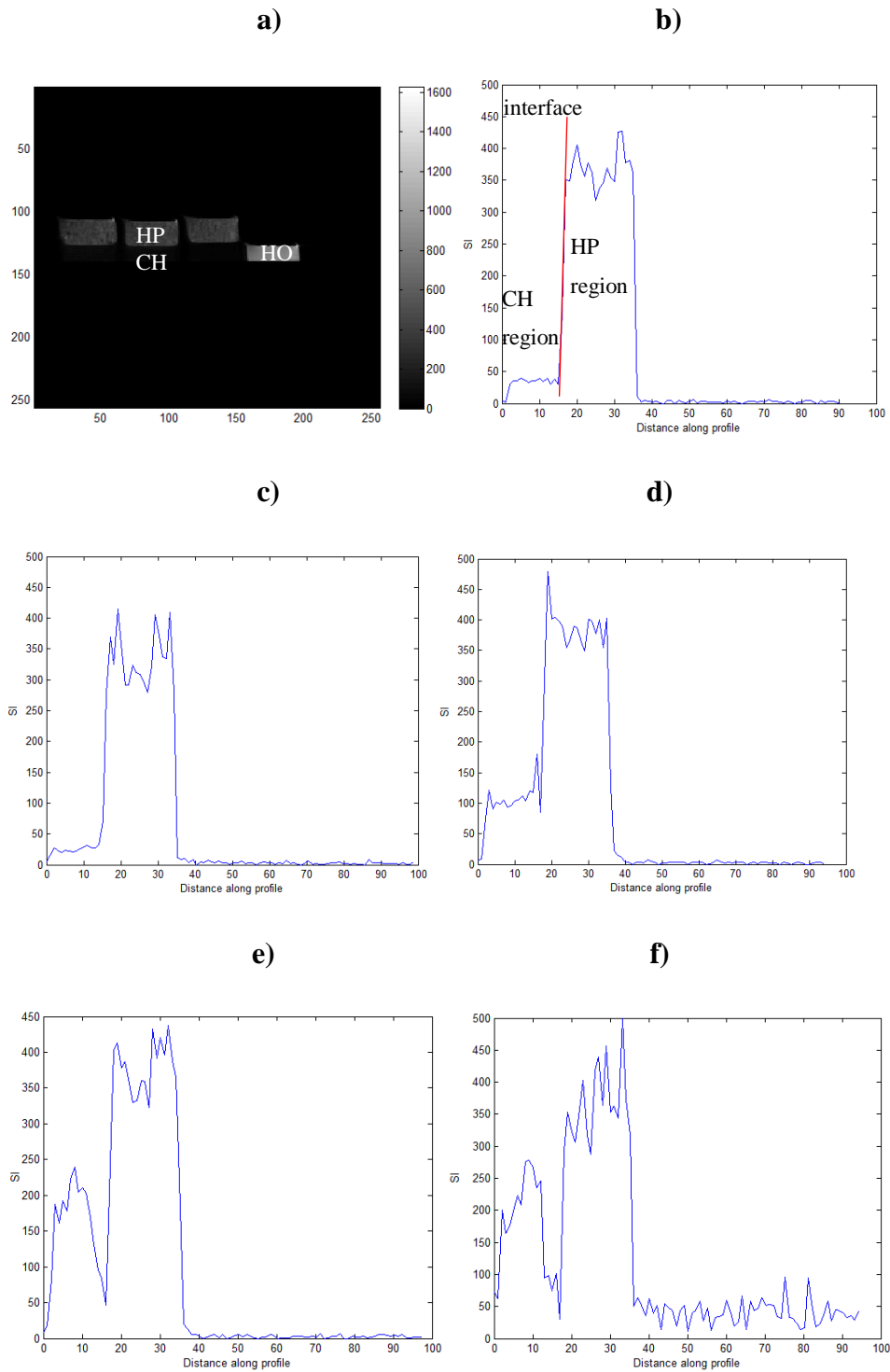


Figure 3.3. Representative MRI information for one set of 2-layer chocolate sample F1 stored at 30 °C at day 1. (a) MR image (b) 1D signal intensity profile for F1 at day

1. (c) at day 3. (d) at day 4. (e) at day 15. (f) at day 22. HP: hazelnut paste. CH: chocolate. HO: hazelnut oil.

3.1.2. Mathematical Modelling

Although exact mechanism has not been understood clearly, diffusion has been preferred as a theory for oil migration in chocolate products for so many studies (Altan et al., 2011; Khan & Rousseau, 2006b; McCarthy & McCarthy, 2008; Miquel & Hall, 2002b; Rumsey & Mccarthy, 2012). Similar to peanut butter/chocolate, cream/cocoa butter and almond products/chocolate systems studied by Lee et al. (2010), Maleky et al. (2012) and Altan et al. (2011), diffusion was expected to be dominant mechanism for oil migration. Following the same approach, 1D mass transfer of liquid oil to chocolate was characterized by Fick's second law in this study.

To understand transport behavior and whether obtained data fit the model, results were analyzed using both analytic and numerical solutions. Five formulations were used in this study to assess additional insight for oil migration phenomena. The models tested yielded values of diffusivity, equilibrium hazelnut oil concentration at the interface and time constants. For modeling of hazelnut oil migration into chocolate region, two-pixel signal intensity values at interface were averaged for upper boundary condition. Using Eq. (2.9), normalized SI data was converted to dimensionless form. The dimensionless SI values plotted against time at upper boundary of chocolate were figured out in Figs. 3.4 and 3.5 to find out constants of Eqs. (2.7) and (2.10) for Model 1 and Model 2, respectively. C_0 was equilibrium concentration. β value represented time constant and t_0 was the midpoint time. The parameter β quantified the rate of approach to equilibrium value C_0 . In Model 1, Eq. (2.8) belonging to analytical solution was used for parameter estimations. C_0 was the 2nd adjustable parameter after D value estimation. They were listed on Table 3.1. Eq. (2.10) that was considered as the boundary condition of Model 2 was best fitted to experimental results with $R^2 \geq 0.94$.

Table 3.1. Estimated Diffusion coefficient (D) and nonlinear curve fitting for interface constants of 5 chocolate formulations in Model 1, $C(\text{interface}) = C_0 [1 + \exp(-\beta t)]$, over days 1 to 22 at 30 ± 0.5 °C.

Formulation	D (m ² /s)	C ₀	β (1/day)	R ²
F1	(20.2 ± 13.9) x 10 ⁻¹¹ ab	5.12 ± 2.22 ^a	0.18 ± 0.06 ^a	≥ 0.81
F2	(13.8 ± 2.7) x 10 ⁻¹¹ ab	3.04 ± 1.91 ^a	0.11 ± 0.04 ^a	≥ 0.91
F3	(6.5 ± 2.05) x 10 ⁻¹¹ a	4.82 ± 2.66 ^a	0.06 ± 0.03 ^a	≥ 0.88
F4	(22.7 ± 6.8) x 10 ⁻¹¹ b	8.24 ± 4.74 ^a	0.16 ± 0.07 ^a	≥ 0.83
F5	(15.3 ± 5.4) x 10 ⁻¹¹ ab	6.88 ± 3.60 ^a	0.17 ± 0.01 ^a	≥ 0.90

Results are the mean and standard deviation for two replicates in each formulation.

Lettering was done for each subgroup separately ($p < 0.05$).

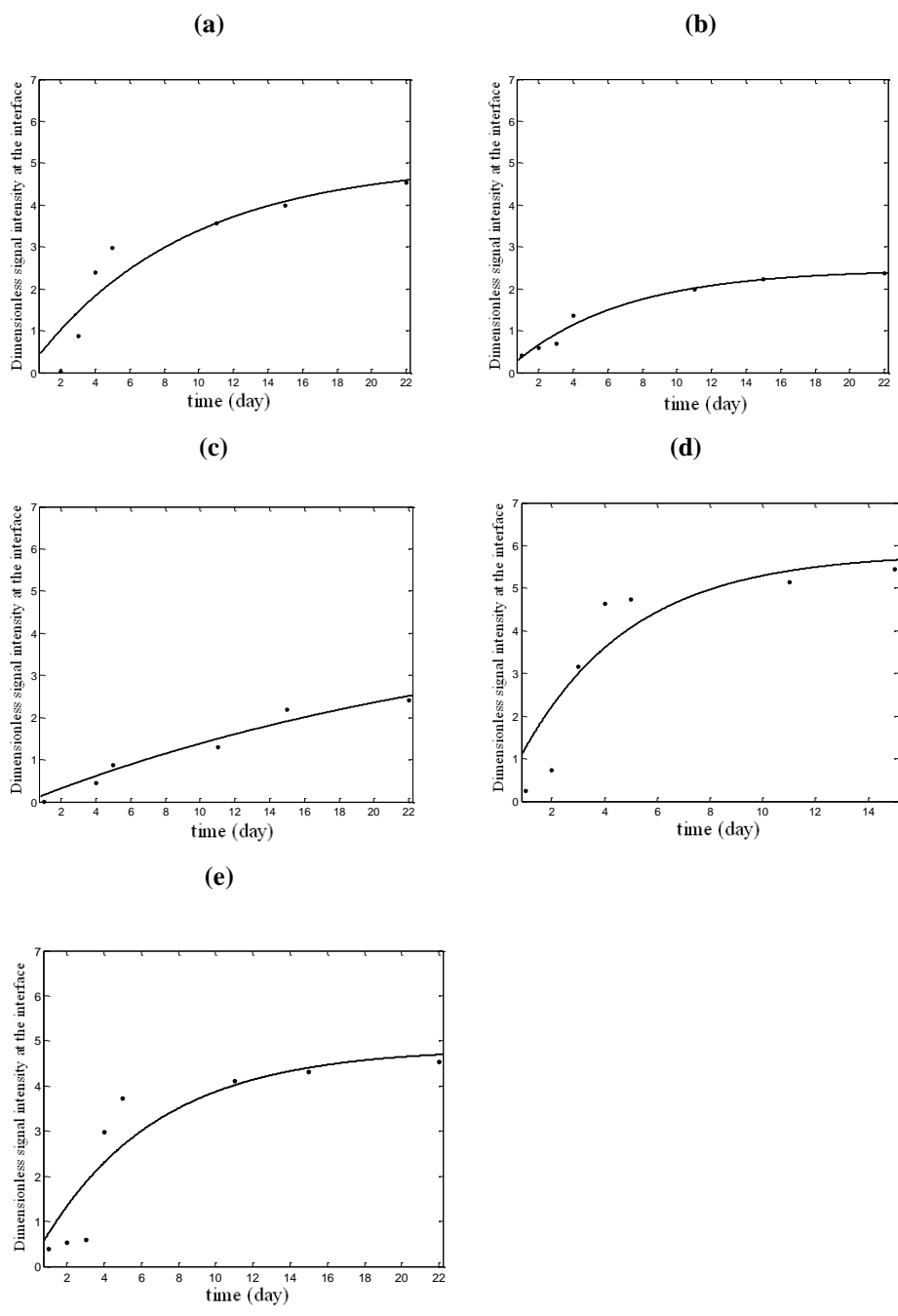


Figure 3.4. Data and curve fitting in Model 1 for days 1 to 22 at interface between chocolate-and hazelnut paste at 30 °C. (a) for F1 ($R^2=0.88$). (b) for F2 ($R^2=0.97$). (c) for F3 ($R^2=0.96$). (d) for F4 ($R^2=0.82$). (e) for F5 ($R^2=0.83$). Experimental and their fitting results were represented by dot point and solid line, respectively. (These figures are examples for each formulation. To find out the final result, averages of the replicates were taken in all samples).

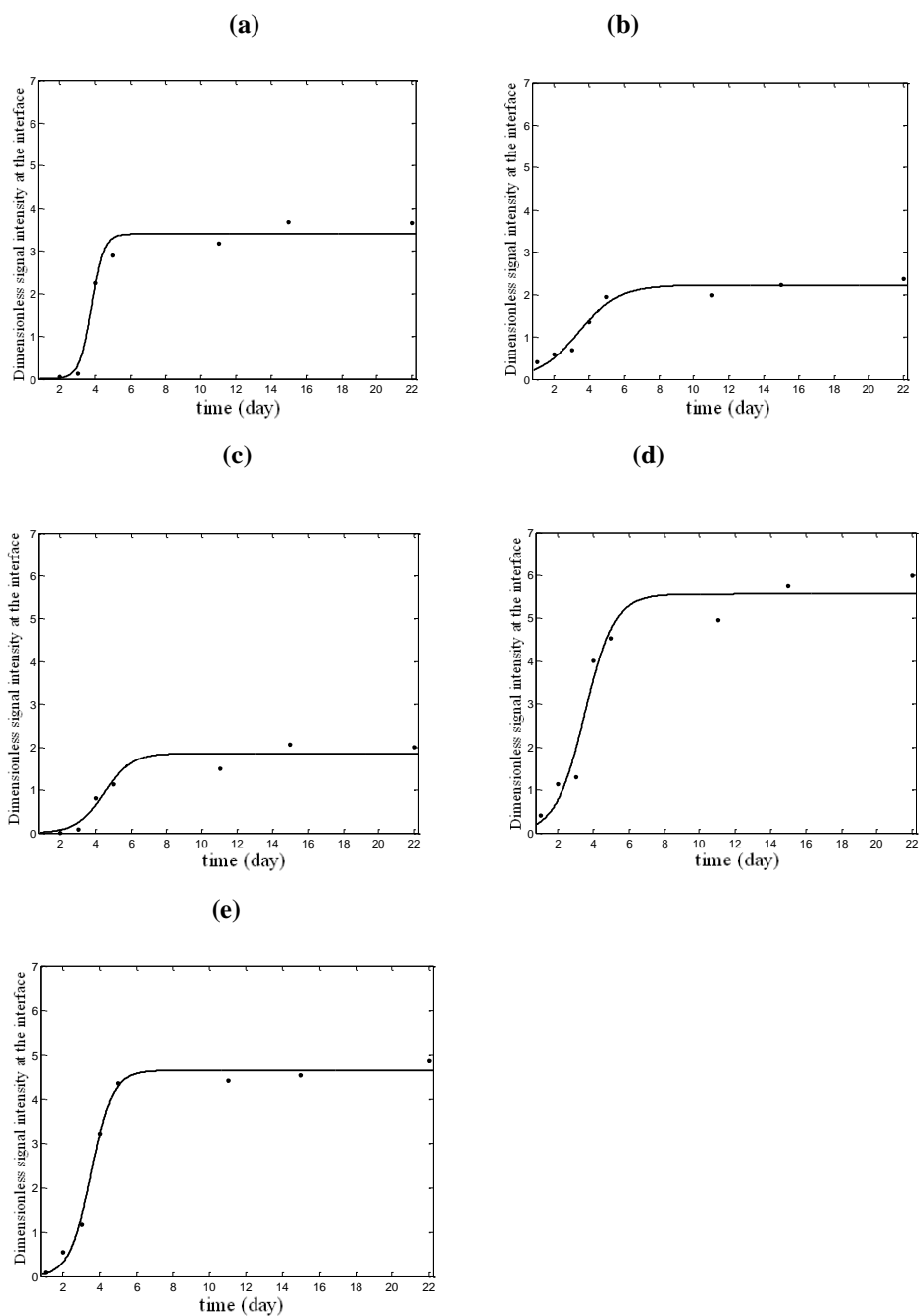


Figure 3.5. Data and curve fitting in Model 2 for days 1 to 22 at interface between chocolate-and hazelnut paste at 30 °C. (a) for F1 ($R^2=0.98$). (b) for F2 ($R^2=0.96$). (c) for F3 ($R^2=0.95$). (d) for F4 ($R^2=0.96$). (e) for F5 ($R^2=0.99$). Experimental and their fitting results were represented by dot point and solid line, respectively. (These figures are examples for each formulation. To find out the final result, averages of the replicates were taken in all samples).

Diffusion coefficient (D) values were fitted using 2 sets of experimental MR signal data belonging to chocolate region from day 1 to day 22. Fick's 2nd law given in Eq. (2.4) was used for both Model 1 and Model 2, however time depending boundary conditions differed and led unequal solutions for two models. After fitting results were evaluated for both replicates and storage times, an average diffusivity value was found for each chocolate system as given in Table 3.1 and Table 3.2 for Model 1 and Model 2, respectively. Representative data and curve fits were also shown in Figs. 3.6 and 3.7 for all chocolate formulations. Fit values of diffusivity were demonstrated in the order of 10^{-11} as showing consistency with literature (Table 3.1 and Table 3.2). For instance, in the study of Rumsey and McCarthy (2012) diffusion coefficients of four almond products types (unblanched almond butter, filling cream, cream turner, almond praline) over chocolate layer were found between 3×10^{-11} and 6×10^{-11} m²/s by obtaining higher values for almond regions most probably due to higher unsaturated fatty acid composition.

Table 3.2. Estimated Diffusion coefficient (D) and nonlinear curve fitting for interface constants of 5 chocolate formulations in Model 2, $C(\text{interface}) = C_0 / [1 + \exp(-\beta(t-t_0))]$, over days 1 to 22 at 30 ± 0.5 °C.

Sample	D (m ² /s)	C ₀	β (1/day)	t ₀ (day)	R ²
F1	(20.0 ± 2.0) x 10 ⁻¹¹ a	3.88 ± 1.27 ^b	0.88 ± 0.82 ^{ab}	2.87 ± 1.13 ^b	≥ 0.93
F2	(3.7 ± 1.22) x 10 ⁻¹¹ b	2.87 ± 0.75 ^b	2.25 ± 0.85 ^a	2.47 ± 1.75 ^b	≥ 0.92
F3	(1.2 ± 0.01) x 10 ⁻¹¹ b	3.49 ± 1.31 ^{ab}	0.45 ± 0.21 ^b	10.39 ± 2.44 ^a	≥ 0.99
F4	(6.5 ± 2.52) x 10 ⁻¹¹ b	9.30 ± 3.77 ^a	0.52 ± 0.17 ^b	2.84 ± 1.47 ^b	≥ 0.91
F5	(22.2 ± 6.0) x 10 ⁻¹¹ a	6.78 ± 2.14 ^{ab}	0.82 ± 0.40 ^{ab}	2.09 ± 1.35 ^b	≥ 0.92

Results are the mean and standard deviation for two replicates in each formulation. Lettering was done for each subgroup separately (p < 0.05).

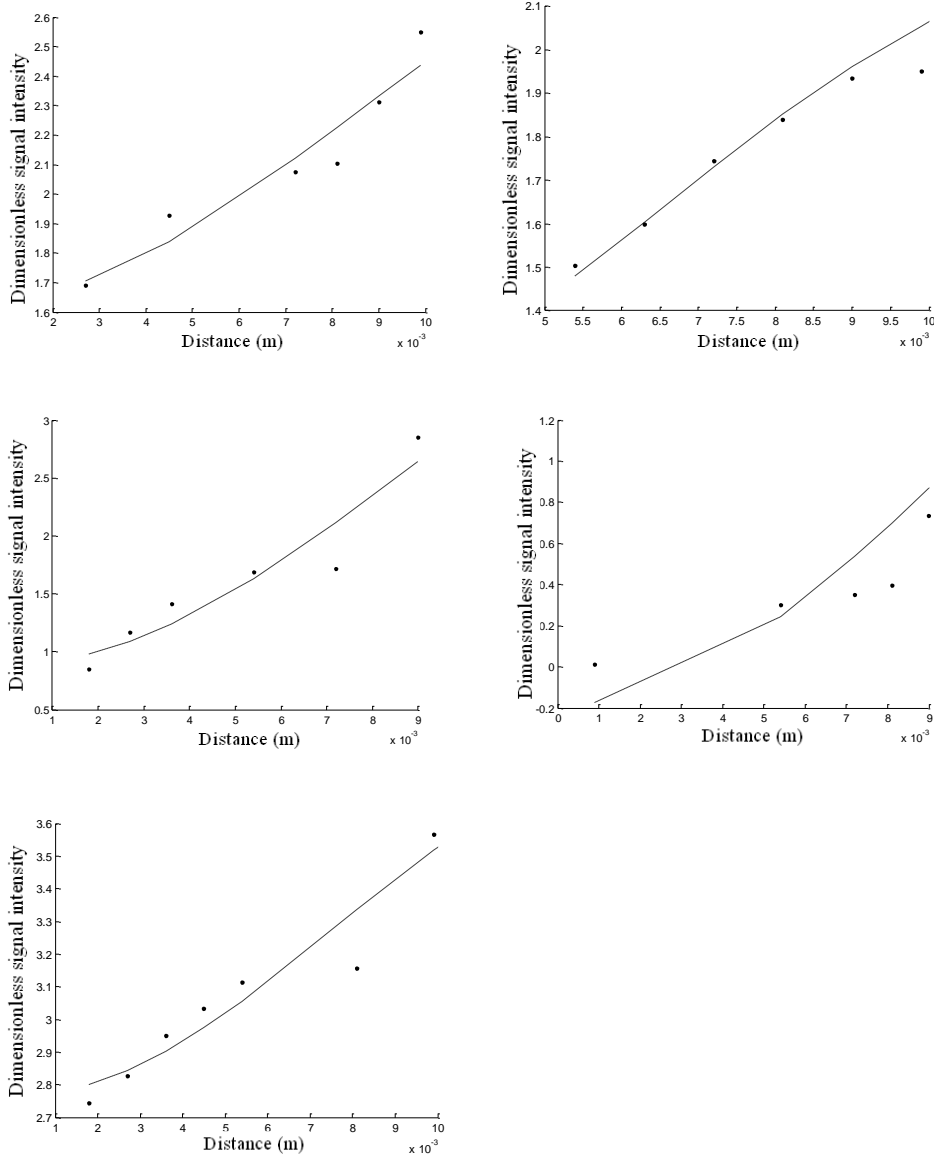


Figure 3.6. Representative experimental and fitting dimensionless signal intensity profiles. From left to right and top to bottom: F1 sample over position and time at day 4 ($R^2=0.91$), for F2 at day 11 ($R^2=0.94$), for F3 at day 15 ($R^2=0.89$), for F4 at day 2 ($R^2=0.83$) and for F5 at day 4 ($R^2=0.93$) in Model 1. Fitted models were represented by dashed line. (These selected days are the examples for each formulation. To find out the final result, averages of the replicates were taken in all samples).

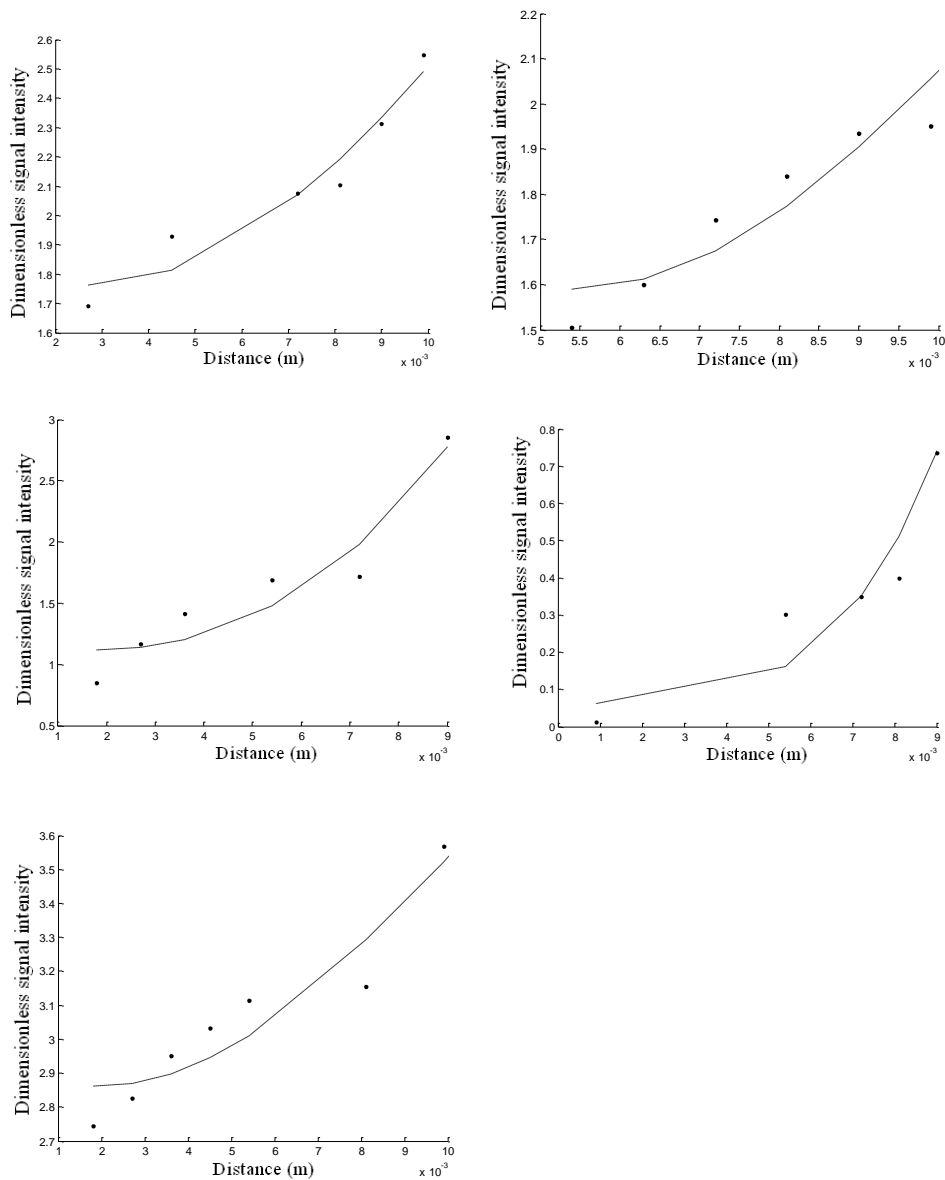


Figure 3.7. Representative experimental and fitting dimensionless signal intensity profiles. From left to right and top to bottom: F1 sample over position and time at day 4 ($R^2=0.93$), for F2 at day 11 ($R^2=0.92$), for F3 at day 15 ($R^2=0.90$), for F4 at day 2 ($R^2=0.98$) and for F5 at day 4 ($R^2=0.92$) in Model 2. Fitted models were represented by dashed line. (These selected days are the examples for each formulation. To find out the final result, averages of the replicates were taken in all samples).

No difference was obtained statistically ($p \leq 0.05$) for D values in F1, F2 and F5 samples in Model 1; in addition F2 and F3 samples gave the lowest D values. In Model 2, F1 and F5 gave higher diffusivity results than other samples, significantly ($p \leq 0.05$). The lowest D value was found for F3 sample prepared with sucrose-stevia combination in both Model 1 and Model 2. This meant that the lowest affinity of chocolate for hazelnut oil was obtained in the presence of sucrose-stevia combination which showed potential for low fat bloom formulations.

Chocolate matrix may be considered as an analogue for polymer membrane. The principles applied for interactions between organic solvents and polymers might be similar with filled confection system as studied under the conditions that maintain the integrity of the confectionery matrix. Concentration-independent form of Fick's Law with constant boundary conditions can explain diffusional behavior of solvents in semi-crystalline polymers when mass transfer is propagated with structural relaxation (Khan & Rousseau, 2006a). Molecular transport governing ingress of liquid fat into chocolate depends on temperature, physical and chemical nature and dimensions of penetrating fats and chocolate matrix (Khan & Rousseau, 2006a).

It has been explained by Kariduraganavar et al. (2003) that beside the size of migrating liquids, transport phenomena also depended on molecular interactions between liquids and membrane. Each ingredient reveals different interactions (Kariduraganavar, Kulkarni, & Aminabhavi, 2003). For instance, absorption of oil by sugar particles is higher compared to absorption by cocoa solid particles (Ziegleder, 2000). In the study of Kariduraganavar et al. (2003), other than size of the migrant, molecular interactions between filling and chocolate likely changed with regard to chocolate formulations thus affecting hazelnut oil diffusivity. This is due to specific liquid property that it could lead to more or less interactions in membrane systems (Kariduraganavar et al., 2003). Moreover, emulsifiers could act as bloom inhibitor affecting chocolate viscosity, cocoa butter crystallization and also interaction between fat and sugar (Lonchamp & Hartel, 2004). In our study, chocolate formulation with different type of sweeteners was considered as main role in the extent of migration rate ($p \leq 0.05$).

In order to investigate the presence/absence of sucrose, its amount was kept constant in formulations. Combination of sucrose with sweeteners presented much more barrier for liquid fat penetration compared to samples consisting of only sucrose as sweetening agent. The additional existence of stevia/sucralose most probably led to lower interstitial spaces and higher tortuosity due to higher nonfat solid ratio in F2 and F3 samples compared to F1 sample giving lower diffusivity results (Table 3.2). Non-fat solids increase tortuosity and cause reduction in diffusion coefficient resulting decrease in migration rate ($D_{eff} = (\varepsilon/\tau)D$). However, it has usually little effect on migration occurring in chocolate (Ghosh et al., 2002). Diffusion through sucrose particles was statistically similar ($p \leq 0.05$) with diffusion through stevia recipe when F1 and F5 samples were compared with each other (Table 3.2).

Since stevia has higher molecular weight than sucralose, number of sucralose molecules will be much more than stevia molecules at same weight leading higher tortuosity (accounts for longer path in porous medium) and so lower diffusivity. This expectation was obtained in F4 and F5 samples while there was not such an agreement between F2 and F3 samples ($p \leq 0.05$). It is possible to say that there are so many factors influencing migration rate thereby diffusivity. In this study, contact area, storage temperature, ratio of two phases, fat type were kept same for all samples. Then, it was shown that chocolate structure prevailed among migration affect. Due to interaction with sweeteners, bulking agents and cocoa butter and resulting lubricating action, particle–particle interactions and mobility differed (Glicerina, Balestra, Rosa, & Romani, 2013). It was concluded that chocolate prepared with only stevia (F5) gave similar results with only sucrose formulation (F1) by leading high diffusivity values. On the other hand, synergistic effect of sucrose and stevia reduced diffusion coefficient in F3 sample. Similarly, ideal acceptance in sensory, texture and rheology analyses was obtained for chocolates prepared with partial replacement of sucrose with stevia in the study of Cikrikci et al. (2016). Chocolate matrix is very complex and so it is difficult to explain migration mechanism occurred there (Cikrikci,

Yucekutlu, Mert, & Oztop, 2016). It is still a phenomenon which has not been explained clearly in the literature.

3.2. Insulin Loaded Hydrogel Systems

3.2.1. Release Profiles

The HPLC chromatogram of Humulin (as two peaks) released from gels after incubation in the biological fluids gave similar retention time with insulin and m-cresol standards (Fig. 3.8). It was confirmed that first peak belonged to insulin while second peak represented m-cresol. The insulin release study of gel samples was initially conducted in both SGF and SIF, separately. Since initially small amount of insulin in buffer was obtained but then no considerable cumulative release rate was observed in SGF (Fig. 3.9), due to the acidic pH and gels not releasing out insulin at that pH, release behavior in SGF were just evaluated for further experiments (Figs. 3.9). In order to understand whether the reason of not detecting insulin in SGF was either low release rate or destruction of insulin due to low pH, insulin loaded gels were completely disintegrated in SGF using Ultraturax and HPLC analysis was conducted for the medium. Since the samples gave identifiable insulin content, this implied that hydrogel created a controlled release system protecting insulin from burst release in SGF, on the other side showing cumulative release up to 70% in SIF. Although the release study was continued for 24 h, only 6 h release was figured out due to insulin degradation after that period.

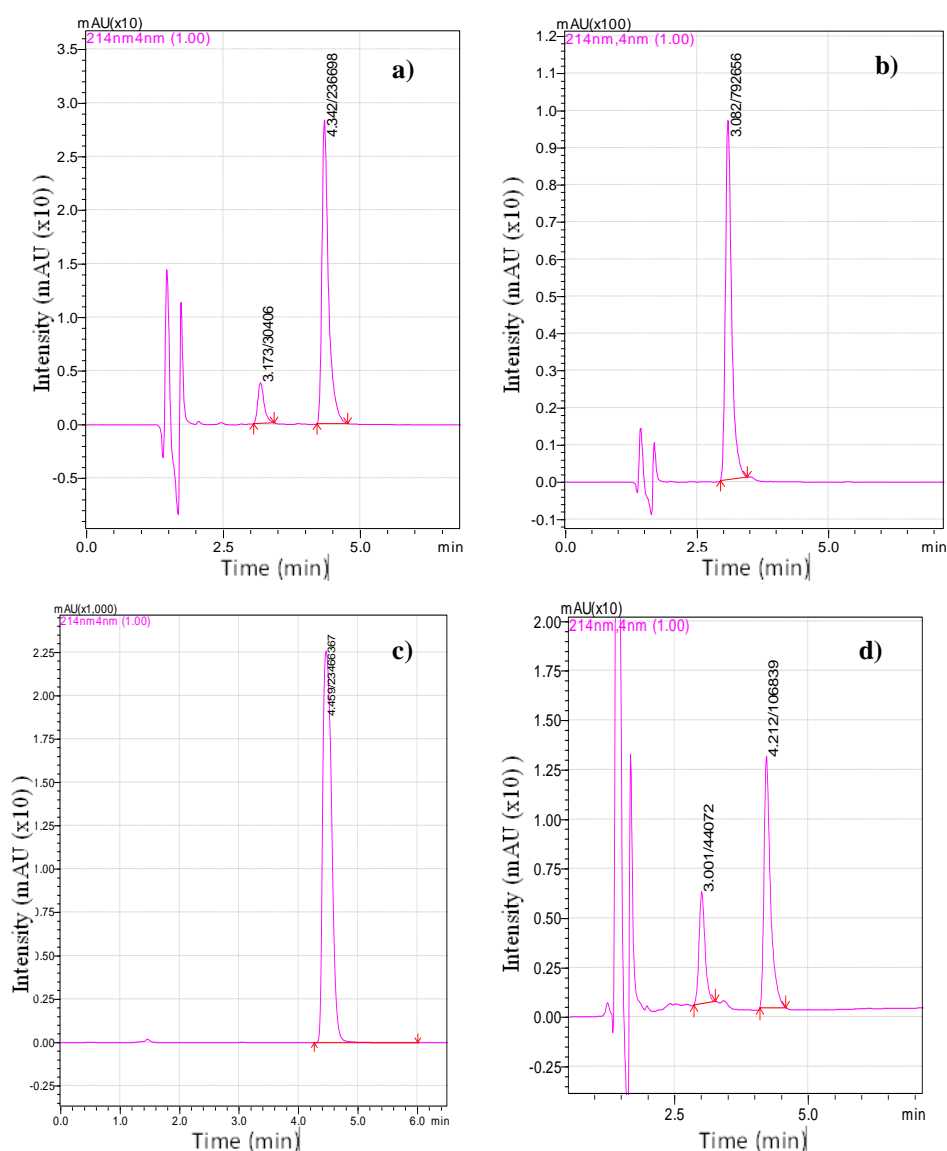


Figure 3.8. Chromatographs of a) Humulin b) insulin c) m-cresol and d) representative insulin loaded gel in buffer of SIF (pH 6.8).

The intestine is usually seen as the main absorption site for oral formulations, thus it is meaningful to focus on intestine-targeted delivery system that remains intact at acidic pH of stomach but dissociates and releases the drug at alkaline pH of small intestine (Guo et al., 2013). In intestinal media, calcium ions are also lost from the gels due to formation of calcium phosphate salts in SIF (Xu & Dumont, 2015) causing

weakening in the structure thereby increasing release. It is possible to list other possible interactions that contribute to the three-dimensional cross-linked gel networks: the guluronic and mannuronic acid units and interchain hydrogen bonds, the junction formed by the calcium ion; electrostatic interactions (between opposite charges of the biopolymers), GT-ALG interactions, interactions between insulin and polymers (Reis et al., 2008; Sankalia, Mashru, Sankalia, & Sutariya, 2007). Like alginate, GT has a carboxyl group due to the existence of galacturonic acid and this means that the charge differences in GT are induced by this carboxyl group (M. Nur et al., 2016). This carboxyl group (COO^-) could interact with the amino group (NH_3^+) of cationic polymer (chitosan or a protein) and proceeds ionic complexation between the two polymers via polyelectrolytes interactions and peptide entrapment depending on medium pH (M. Nur et al., 2016; Sarmiento, Ferreira, Veiga, & Ribeiro, 2006). Considering intestinal pH, electrostatic repulsion between polymers and insulin due to having same charge could be another reason for mechanism of insulin release in intestinal simulation (Woitiski, Neufeld, Ribeiro, & Veiga, 2009).

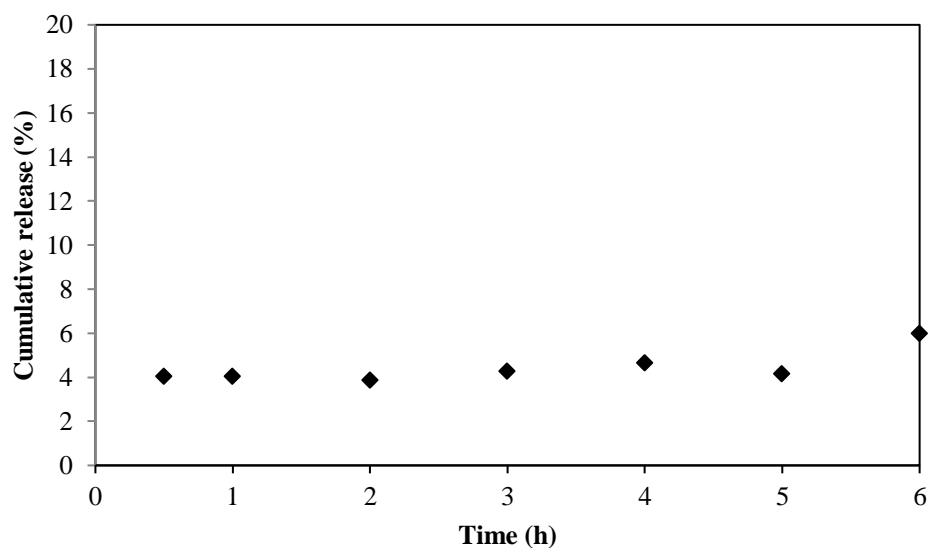


Figure 3.9. Release profile of a representative hydrogel (100A-CH) in SGF (pH 1.2).

The ionizable groups present in the polymer backbone are mainly responsible for pH responsive behavior of the hydrogels. When gels are exposed to an aqueous solution of an appropriate pH and ionic strength, these groups would ionize and emerge a fixed charge along the polymer (Koetting, Peters, Steichen, & Peppas, 2015). Anionic hydrogel network had potential to swell in solutions at $\text{pH} > \text{pKa}$ (dissociation constant) due to presence and repulsions of ions, while cationic hydrogels were swollen at $\text{pH} < \text{pKa}$ since cationic pendant groups are protonated at pH less than pKa (Koetting et al., 2015). Due to its structure, alginate gel is stable in acidic pH of stomach, while it swells and begins dissolving in the intestinal alkaline $\text{pH} > 6$ (Tahtat et al., 2013). At SIF, pH (6.8) is higher than pKa of ALG (3.38-3.65) and GT (at around 3) making them negatively charged. Thereby, hydrogel network composed of both anionic and cationic polymers had a complex nature that differs regarding to composition. At intestine media, both polysaccharides were strongly negatively charged thus steric and electrostatic repulsions between the side chains played an important role in the release of insulin. ALG, GT and CH underwent physical crosslinking owing to charge or hydrophobic interactions, electrostatic repulsions, as well and their interactions shaped release mechanism. Furthermore, isoelectric point (pI) of the target protein, insulin (pI of 5.5-6.4), also played an important role in gel response to environmental conditions. Insulin is a relatively small hydrophilic, water soluble protein with molecular weight of approximately 6000 (Hara & Miyake, 2001). Since insulin is composed of 10 amino acid residues capable of attaching a negative charge and the 6 amino acid residues capable of attaining a positive charge, it has an amphiphilic character (Martins et al., 2007). When $\text{pH} > \text{pI}$, charge status of insulin becomes negative (Mokhammad Nur & Vasiljevic, 2017). Although insulin becomes negatively charged at intestinal pH, it could still include a few positive charges in its own structure. These properties were, thereby, possibly responsible for the entrapment of insulin in the hydrogel network (Tahtat et al., 2013).

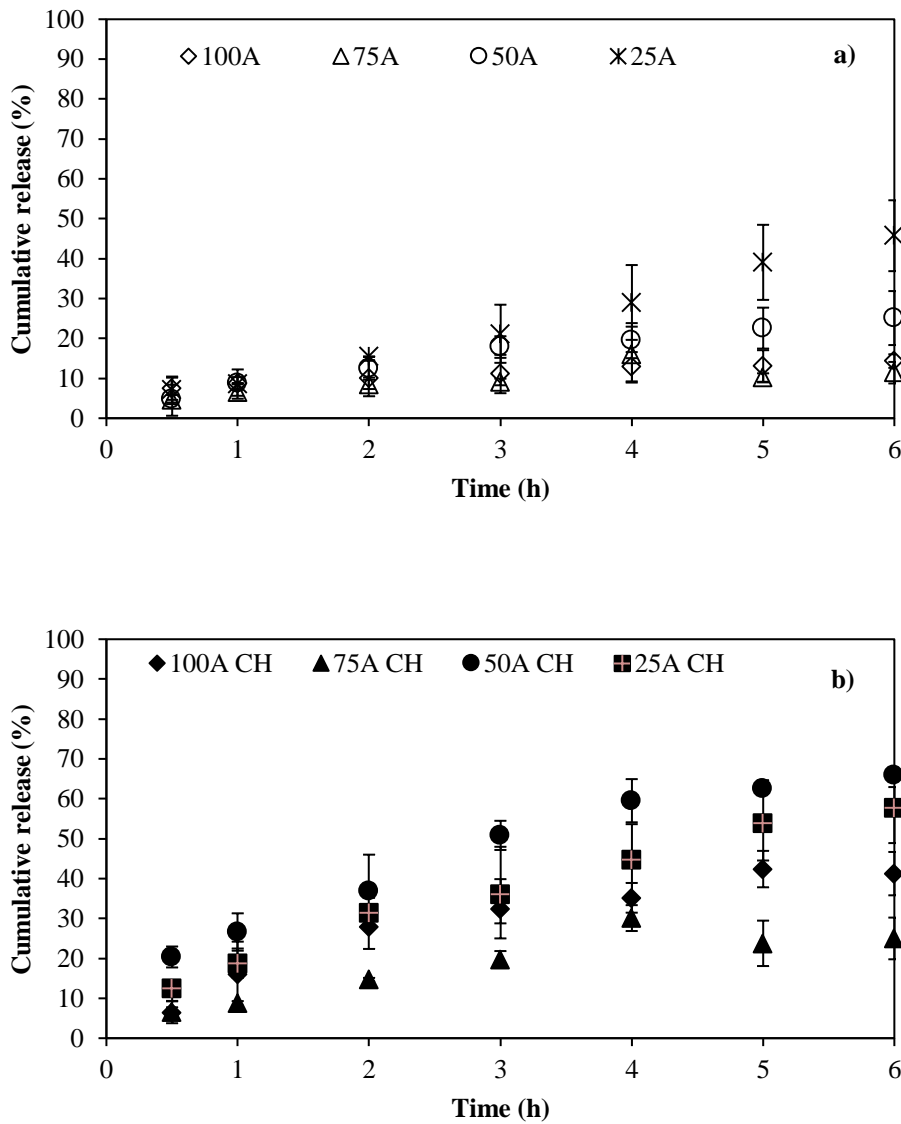


Figure 3.10. Release profile of hydrogels a) without CH coating b) with CH coating in SIF (pH 6.8).

ALG-GT hydrogels without CH exhibited a similar release profile during early times. Beginning from 3 h, distinction between samples began to appear in release percentages but significant difference occurred at the end of 5 h and 6 h ($p < 0.05$). After the end of 5 h, 25A hydrogels gave the highest release differing from other

samples ($p < 0.05$). As insulin was expelled from the gel, charge density differed and sample with high GT concentration, 25A, promoted higher insulin release. On the other hand, PEC with CH created differences between samples even at early times ($p < 0.05$). Unlike to standard hydrogels, PEC gels with CH showed a different release pattern with changing gum ratios ($p < 0.05$). Similar to ALG-GT gels, 75A-CH gels retarded release through all period and release of 50A-CH approached 25A-CH gels giving high and closer results, especially exhibiting the most similar results with 25A-CH at the end of 5 h ($p < 0.05$) (Fig.3.9b). Thereby, release time of 5 h was obtained as the critical time for differentiation of hydrogels formulations both with CH and without CH. It has been demonstrated that chitosan based formulations had easy paracellular transport of agents and good mucoadhesive property due to electrostatic interaction between negatively charged sialic acid of mucin and positively charged chitosan with abundant amino groups (L. Liu, Du, Zhao, Zeng, & Liu, 2015). Gel formulation with chitosan and anionic polymer could protect therapeutic agent from gastric degradation but allow the agent to release in intestine through electrostatic interaction. As gel moves to intestine, at alkaline pH, negative charge of ALG and GT was higher sequestering positive charge of CH, resulting in gel dissolution and acceleration of the drug release (Antunes et al., 2011).

In order to understand the reasons these results, pH of each gel solutions during preparation were also compared. They varied from 6.1 to 6.9 (from 25A to 100A) which showed that pH increased as GT ratio decreased. According to this finding, it was expected to occur higher repulsion due to higher negative charge in gel network as GT concentration decreased and so higher release in lower GT ratios. However, opposite behavior was observed. This showed that rather than the charge effect of polysaccharides, crosslinking between target protein-polysaccharides and gel internal structure through electrostatic interactions predominated the release pattern. GT is a branched and heterogeneous polysaccharide including both water soluble and water swellable units (Mostafavi et al., 2016). This high hydrophilicity of GT side residues

could have enhanced the interaction between gel and absorbed thus resulting in higher opening of the network.

In overall, the ranges of insulin release from PEC with CH in intestine were observed to be higher than that from gels without CH. PEC with CH weakened the gel structures leading structural defects within the hydrogels. This promoted faster release rates. It shows that binding solution with both calcium and CH was not strong enough to retain insulin in gel matrix as solution with only calcium. Crosslinking density was reduced and caused erosion of polymers in CH complex gels. At intestinal pH (> 6.5), CH could lose its positive charge and become weaker (Mokhammad Nur & Vasiljevic, 2017). Electrostatic interaction between the protein and the polyanion might also favor the retention of insulin within gel matrix in ALG-GT gels without CH complex (Martins et al., 2007). Opposite to our results, Lim et al. (2014), Reis et al. (2008) and Martins et al. (2007) revealed that CH as additional binding could achieve sustained insulin release due to action of CH as a barrier against insulin diffusion (Lim, Tey, & Chan, 2014; Martins et al., 2007; Reis et al., 2008). Xu and Dumont (2015) also found in protein based alginate gels that PEC with CH served prolonged release matrices reducing impact of loss of calcium ions on the hydrogel network. Although CH could have acted as a barrier, this did not overcome other polysaccharide interactions in each gel formulations. Control sample, 100A (GT free), exhibited immediate results in both gels with CH and without CH. This pointed out there was an optimum concentration for the desired ALG-GT interactions. It was observed that the zeta potential of binding solution with calcium chloride and CH was $+ 30.8$ mV proving positive charges in CH. As expected, opposite to CH solution, gelation solutions had the zeta potential in the range of $- 49.3$ mV and $- 42.4$ mV.

3.2.2. NMR / MRI Results

3.2.2.1. 0.32 T NMR relaxometry results

Non-destructive method, NMR for proton relaxation in gels, was conducted to comprehend internal structure of samples. T_1 and T_2 are parameters giving crucial information about water uptake and polymer-water/ polymer-polymer interactions, respectively. T_1 relaxation time is related to motional frequency. Since H protons in water have higher motional frequencies than in solids, water has higher T_1 values than solids (Cikrikci & Oztop, 2016). Vittadini et al. (2002) reported that T_1 and T_2 increased with moisture content due to higher mobility in samples (Vittadini, Dickinson, & Chinachoti, 2002). In the light of this approach, it is applicable to say that samples absorbed higher amount of water could give higher T_1 results. Fig. 3.11 represented T_1 values of all gels before and after immersed in SIF. Water uptake in all samples after immersion into intestinal fluid could be clearly understood from T_1 results of 6 h giving higher values than 0 h. However, this increase was lower in gels with CH than in gels without CH. This could be the sign of action of CH as a barrier for water absorption. Water uptake could decrease with the formation of ionic interaction between carboxylic groups of ALG and amine groups of CH and with formation of covalent links between macromolecular chains of ALG-GT and CH (Tahtat et al., 2013).

Another parameter, T_2 relaxation time gives information about interaction between water and polymer or between two polymers. As given in Fig. 3.12, T_2 's of gels were obtained before and after immersion into SIF through 6 h. Initially, all gels had shorter T_2 times and then they began to increase after 6 h immersion in solution. This was consistent with T_1 results. The main contribution for this increase was the amount of water present in gels and interaction between water and gel network (Ozel, Cikrikci, Aydin, & Oztop, 2017). Swelling of samples absorbing solvent and having more hydrogen molecules led to larger T_2 .

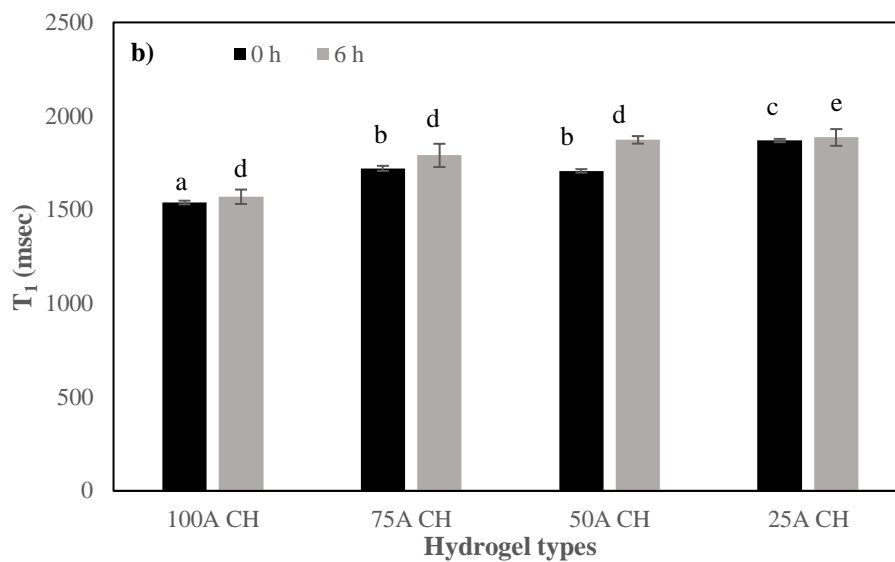
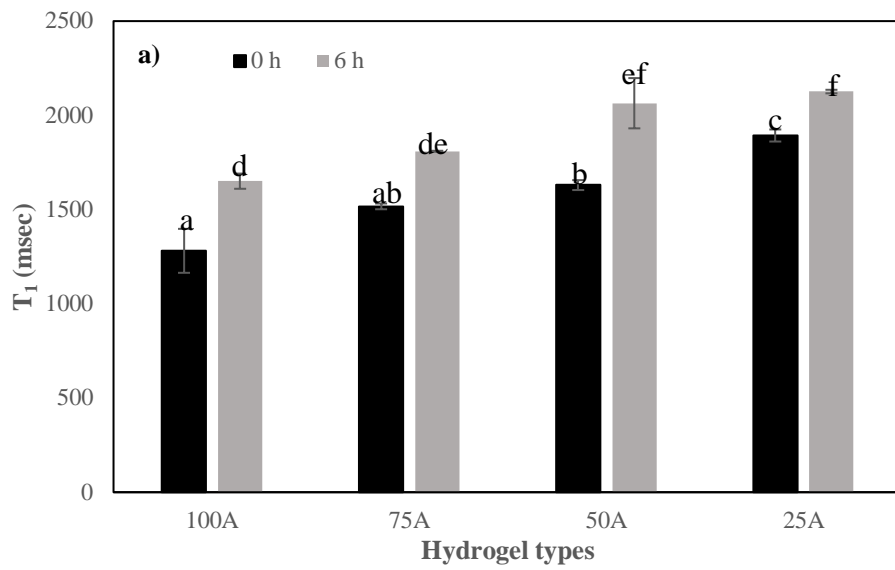


Figure 3.11. T₁ results of a) hydrogels without CH and b) hydrogels with CH. Lettering was done for each subgroup (0 h and 6 h) separately ($p < 0.05$).

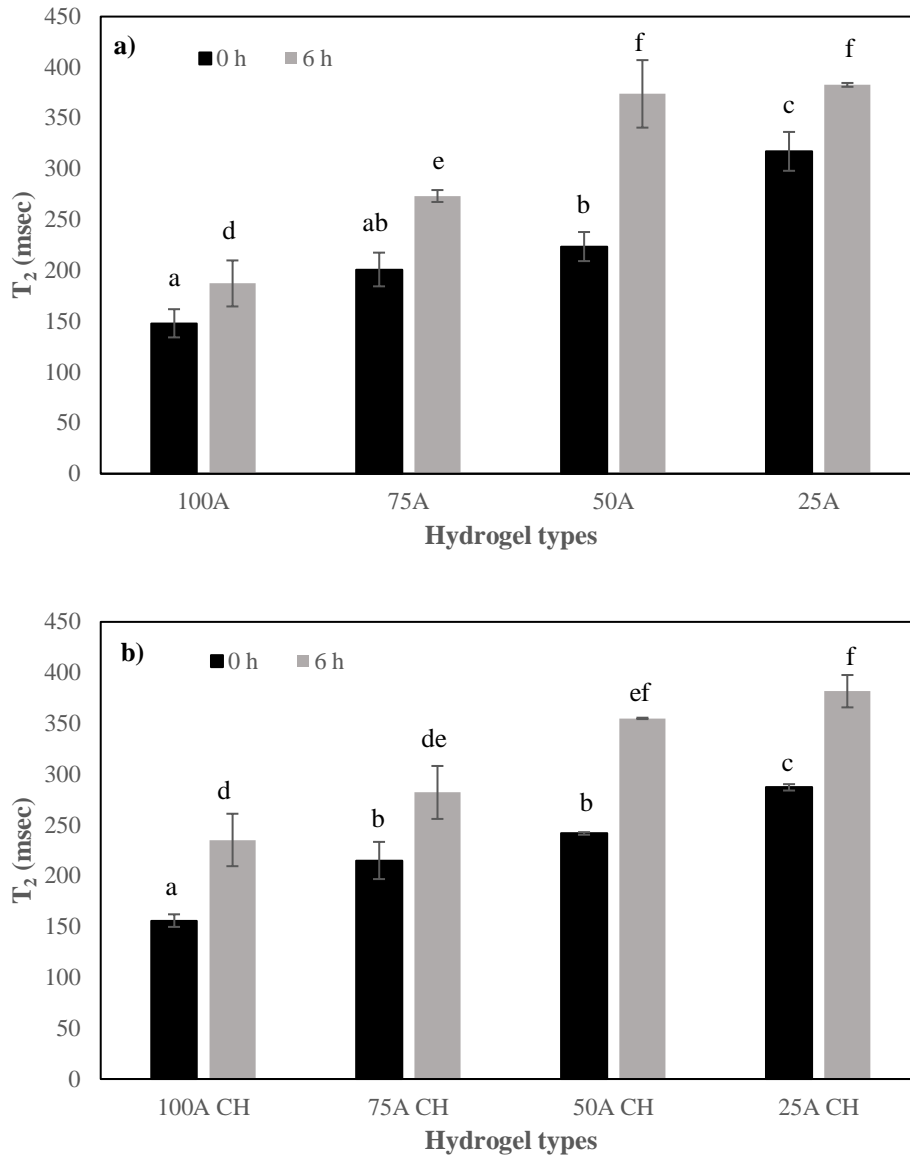


Figure 3.12. T_2 results of a) hydrogels without CH and b) hydrogels with CH. Lettering was done for each subgroup (0 h and 6 h) separately ($p < 0.05$).

0 h and 6 h T_2 results differed significantly but the presence of CH did not cause significant impact on T_2 values ($p < 0.05$). In both samples with CH and without CH, T_2 showed an increase as GT ratio increased. While 100A gel gave T_2 as 148.07 ms, T_2 of 25A gel was 317.31 ms giving significant difference at 0 h ($p < 0.05$). At the end of 6 h, T_2 of 100A and 25A increased to 155.93 ms and 287.11 ms, respectively.

Although the results of gels with CH were higher than samples without CH at the same ratio, they were not significantly different ($p < 0.05$). Unlike to T_1 results, CH complex gels gave closer profile with standard gels. Although the presence of CH reduced fluid uptake regarding to T_1 profile, it gave a similar increasing tendency in the absence of CH. It could be hypothesized that CH complex gels had weaker structures during uptake of water and led water molecules as free state diffusing in and out through gels (Ozel et al., 2017). This could have also caused weaker entrapment of insulin and easier release from the matrix consistent with release measurements.

Table 3.3. Self diffusion coefficient (SDC) values of gel samples. Results are mean values and errors are represented as standard deviation for at least two replicates in each gel sample. Lettering was done for each subgroup separately ($p < 0.05$).

	SDC 0 h (m ² /s)	SDC 6 h (m ² /s)
Hydrogels		
100A	(1.67 ± 0.24) x 10 ⁻⁹ a	(1.86 ± 0.24) x 10 ⁻⁹ a
75A	(2.06 ± 0.23) x 10 ⁻⁹ a	(2.07 ± 0.26) x 10 ⁻⁹ a
50A	(2.16 ± 0.05) x 10 ⁻⁹ a	(2.14 ± 0.18) x 10 ⁻⁹ a
25A	(2.13 ± 0.13) x 10 ⁻⁹ a	(1.81 ± 0.09) x 10 ⁻⁹ a
Hydrogels		
100A CH	(2.01 ± 0.17) x 10 ⁻⁹ a	(1.53 ± 0.05) x 10 ⁻⁹ a
75A CH	(2.30 ± 0.07) x 10 ⁻⁹ a	(1.72 ± 0.08) x 10 ⁻⁹ ab
50A CH	(1.98 ± 0.13) x 10 ⁻⁹ a	(1.79 ± 0.13) x 10 ⁻⁹ ab
25A CH	(2.25 ± 0.06) x 10 ⁻⁹ a	(2.04 ± 0.13) x 10 ⁻⁹ b

SDC of water molecules in gels varied from at around 2 x 10⁻⁹ to 1 x 10⁻⁹ m²/s (Table 3.3). They represented average data of water molecules coming from different parts within gels. SDC is related to self-diffusion of water in matrix and mobility of water molecules (Ozel et al., 2017). All gels except for 100 A-CH and 25 A-CH after 6 h immersion in intestine media gave different SDC ($p < 0.05$). Higher SDC value of 25

A-CH ($2.04 \times 10^{-9} \text{ m}^2/\text{s}$) than 100 A-CH ($1.53 \times 10^{-9} \text{ m}^2/\text{s}$) supported T_1 results indicating higher water uptake and more mobility of water molecules.

3.2.2.2. 1.4 T Benchtop NMR relaxometry results

As stated in the materials and methods section of NMR relaxation, experiments for the hydrogels were also performed at UC Berkeley using a higher field system than the one at METU. T_1 and T_2 results conducted at benchtop NMR were figured out in Figs. 3.13 and 3.14, respectively. This part was performed to establish NMR magnetic field strength dependency on T_1 and T_2 values. The magnetic field dependence of water-proton relaxation time constants is primarily dominated by magnetic coupling to protons of solid components in the molecule (Korb & Bryant, 2002). Dipole-dipole interactions contribute to chemical exchange phenomena in molecules hereby alteration in relaxation time constants (Korb & Bryant, 2002).

Regarding to degree of mobility of molecules, the effect of field strength shows differences. For molecules with low or intermediate mobility, shifting field strength to a higher value could reduce fraction of protons available to interact at that strength thereby causing an increase in T_1 value. Some empirical models represent this dependency for determined NMR frequency ranges. They have the curves of the form as (Bottomley, Foster, Argersinger, & Pfeifer, 1984):

$$T_1 = Av^B \quad (3.1)$$

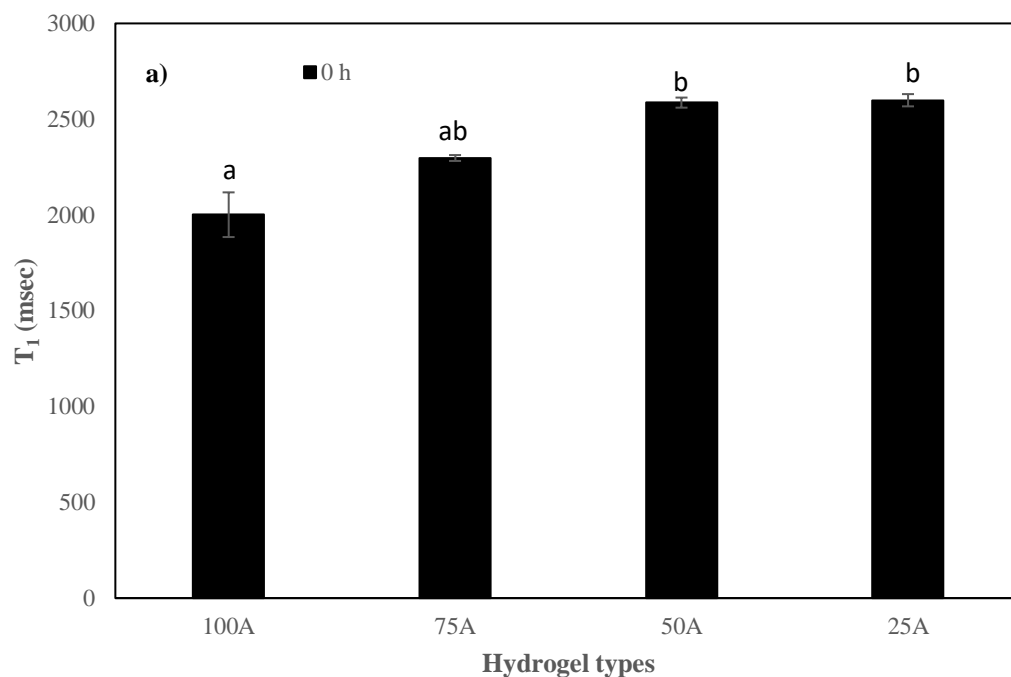
where A and B are the constants, v is the NMR frequency.

On the other hand, spin-spin relaxation time constant (T_2) is less dependent to magnetic field by considering the expression of T_2 dispersion including spectral density functions given below (Bottomley et al., 1984):

$$\frac{1}{T_2} = \frac{3}{4} \gamma^4 \bar{h}^2 \left[\frac{3}{8} J^0(0) + \frac{15}{4} J^1(v) + \frac{3}{8} J^2(2v) \right] \quad (3.2)$$

where $J^0(0)$ is the static component of the spectral density functions and contains the effects owing to microscopic and molecular level field heterogeneity in biological tissue and other parameters are constants (Bottomley et al., 1984).

T_2 can be said as frequency independent if latter two terms negligible compared to others. However, molecular diffusion or chemical exchange might have dominant effect at higher magnetic fields and they could shorten T_2 (De Graaf et al., 2006). To sum up, it could be concluded that T_2 is not highly affected by magnetic field at range of 0.2 T- 3 T but it can show a reduction at high fields (De Graaf et al., 2006). At that point, obtained results for samples without CH were good agreement with the literature. T_1 increase could be positively correlated with magnetic field (with pearson correlation of 0.886). Additionally, T_2 did not show magnetic field dependency at 0.32 T and 1.4 T, statistically ($p < 0.05$).



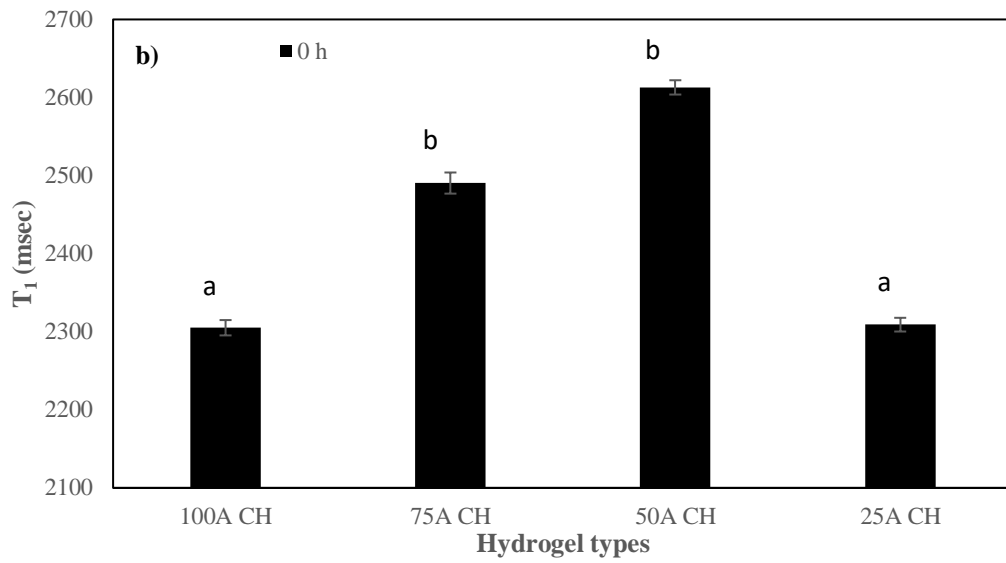
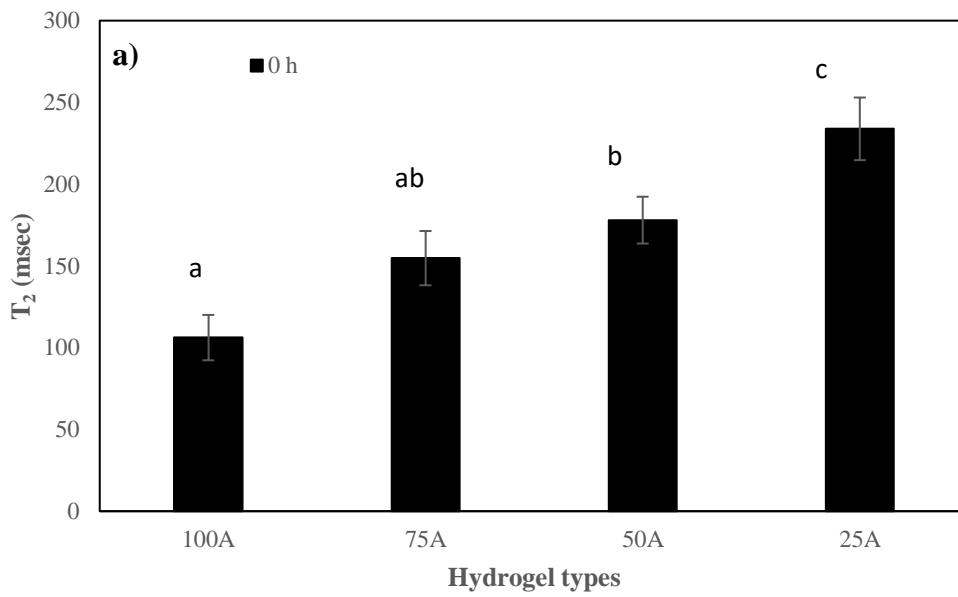


Figure 3.13. T₁ results of a) hydrogels without CH and b) hydrogels with CH.



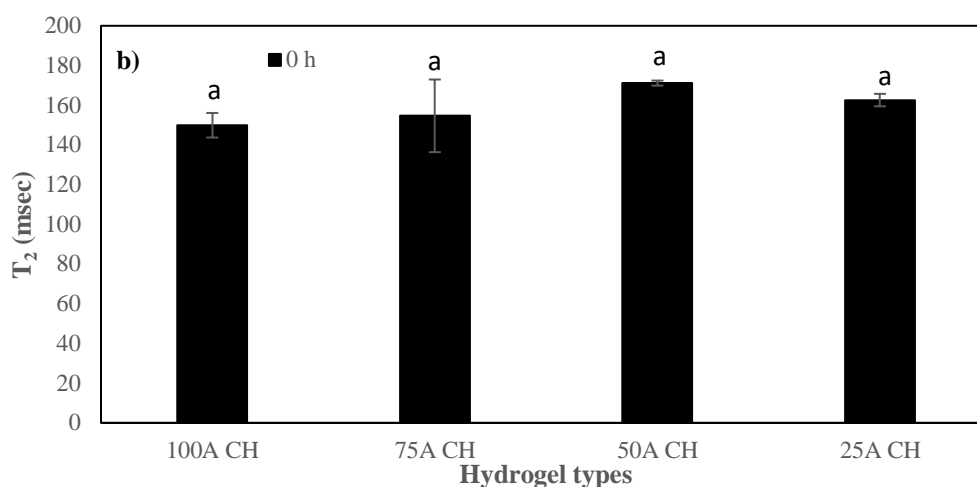
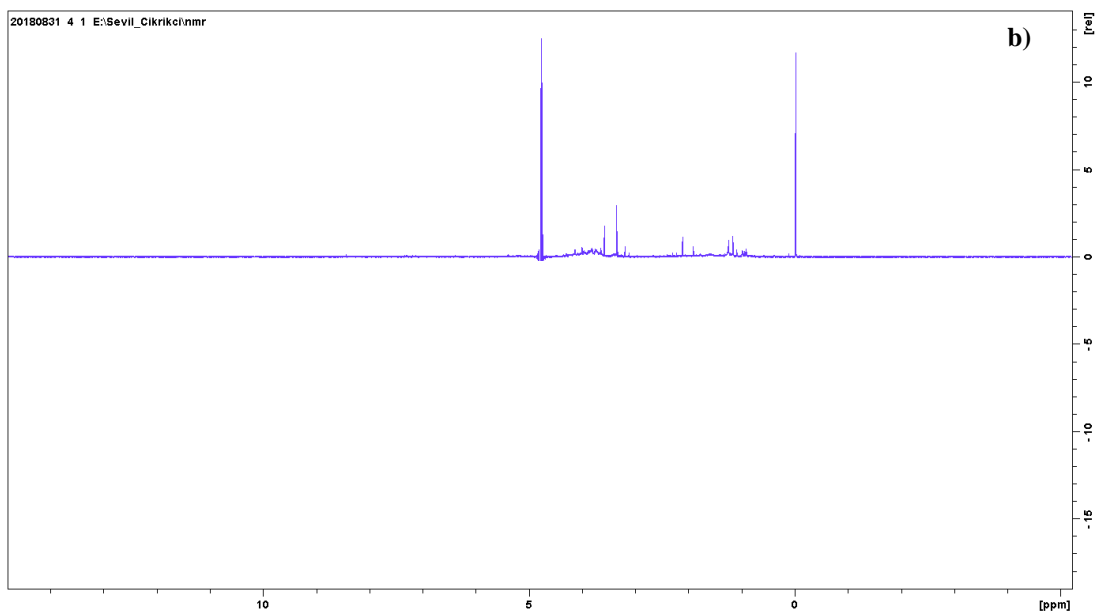
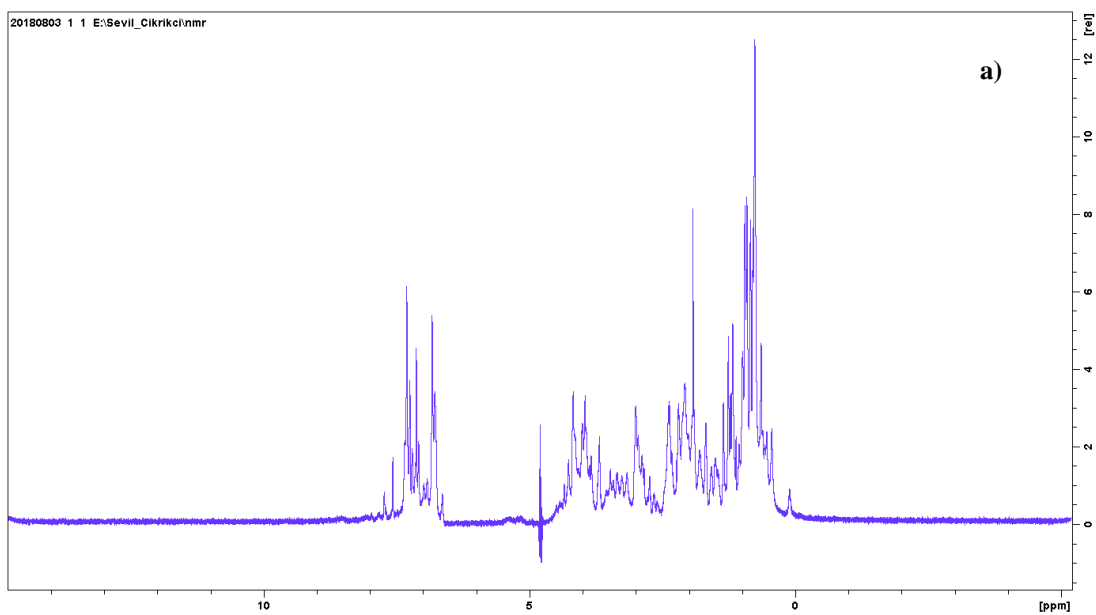


Figure 3.14. T₂ results of a) hydrogels without CH and b) hydrogels with CH.

3.2.2.3. High-Field NMR results

These experiments were just performed to obtain and confirm the presence of insulin on the used samples. Human insulin could have hexameric, tetrameric, dimeric and monomeric forms as well as hexamer aggregates undergoing conformational changes during aggregation (Roy et al., 1990). Fig. 3.15a give ¹H NMR spectrums for 1 mM human insulin at pH 9 in D₂O solution giving the aromatic region between 6 and 10 ppm. The findings were found as similar to the results of Lin and Larive (1995). The lowest peaks at around 7.57 and 7.70 ppm were related to C₂ proton resonance of His (B5) and His (B10), respectively. Chemical shift at around 4-5 ppm was correlated with H resonance of water (Olsen, 1996). On the other hand, in aliphatic region, particular linewidth and perturbation of signals between 0 and 1.4 ppm differentiates the monomeric state from higher aggregation part (Roy et al., 1990). Signal obtained at around 0.105 ppm was associated with the presence of monomers. Thus, spectrum proved the presence of mixture of different states in insulin at these conditions. At pH higher than 6.6, insulin dissolves as a mixture of dimers and aggregates, then it gradually dissociates with increase in pH (Olsen, 1996). Thus, different peaks were also obtained other than the study of Olsen (1996) in insulin spectrum at neutral pH.



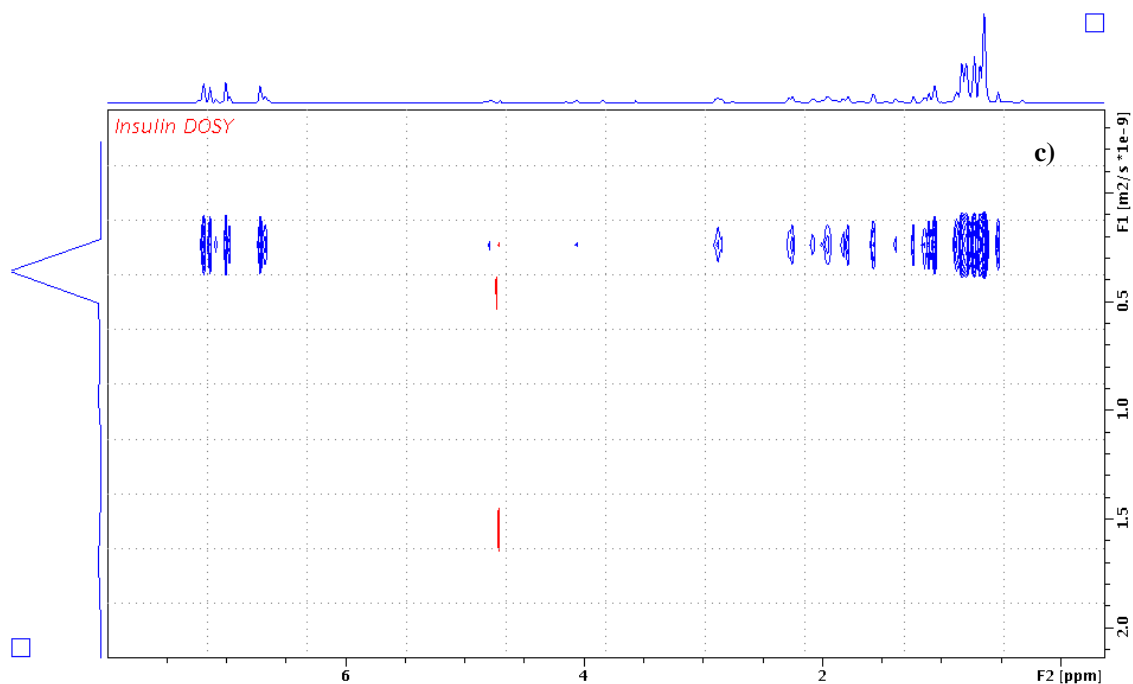


Figure 3.15. 18.8 T High-Field NMR results for insulin solution at pH 9 in D₂O a) Insulin spectra in the range of 0-15 ppm b) Insulin released buffer medium at pH 6.8 c) DOSY experiment of insulin solution.

Since large molecular protein aggregates give short T_1 and T_2 and loose intensity, parameter optimization is necessary for measurement of relaxation times. At around 7 and 7.1 ppm, broad signals were observed. T_1 and T_2 values of insulin by choosing peak around 7.1 ppm were obtained as 0.8 and 0.14 s, respectively. While T_1 value was found in the same order with results of Lin and Larive (1995), T_2 was obtained higher than their findings. These are acceptable because so many parameters in used sequences, sample preparation conditions, sensitivity and magnetic field of the instrument may affect the results. Self-diffusion coefficient was found in similar order as 10^{-6} cm²/s with Lin and Larive (1995).

3.2.2.4. MRI Results

MRI as a noninvasive technique enables the collection of the images of the system with respect to time without giving any harm to the sample and without interrupting the transport process (Oztop et al., 2010). 2D MR images of gels before and after immersion to simulated intestine medium were displayed in Fig. 3.16 to understand dynamic processes involved in gels. The image intensity was initially uniform in whole sample. After exposing the samples into the release medium, gel layer structure showed some irregularities due to solvent uptake. MR images supported negligible swelling by checking voxel number constancy, as well so any mathematical modelling for swelling was not conducted for the samples. However, a bright front was observed at the edge of gels. It could have potential to be seen as an erosion front. The advantage of MRI as giving spatial information could be used to differentiate dynamic fronts for detailed view on swelling dynamics on various swelling gel formulations. Additionally, MR images were not suitable to monitor and model insulin release from the hydrogels since MR signals coming from insulin were not specified. Thus, mathematical models were applied to only HPLC results which were very specific to insulin.

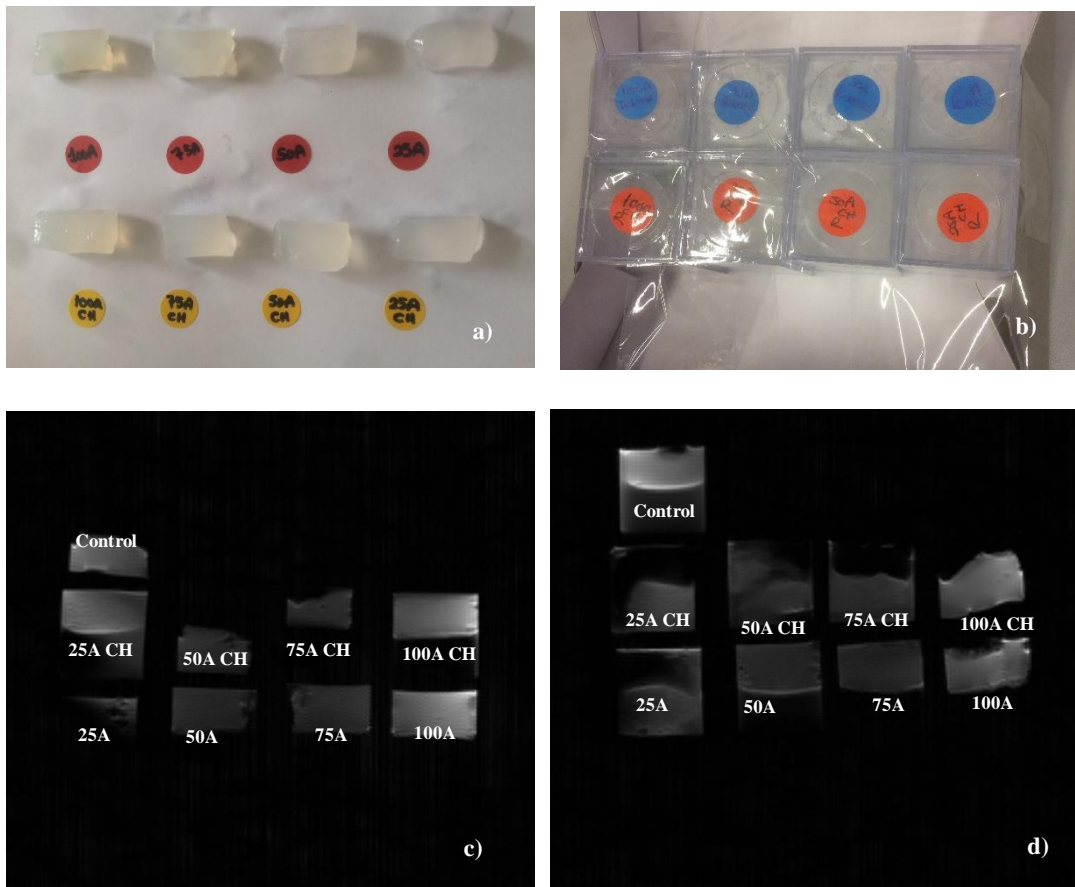


Figure 3.16. a) Gel samples b) gel samples prepared for MR analysis and 2D MR images of gel samples c) before and d) 6 hours after immersion into intestinal fluid (pH 6.8).

3.2.3. Texture Profiles

Hardness and springiness of all fresh gel samples were shown in Table 3.4. Replacement of ALG with GT reduced hardness of gels regardless of the presence of CH. This can be another reason of both NMR relaxometry and chromatographic release results. With increase in GT ratio, a weaker gel structure was obtained and tendency to absorb water became higher than tendency for interactions between biopolymer chains. Hence, it was meaningful to obtain high T_1 and T_2 values in these samples. Similarly, weak interaction between ALG and GT may be another reason for unsuccessful insulin entrapment in SIF. Nevertheless, these findings were different

than some studies such as reports of Belscak-Cvitanovic et al. (2015) (Belščak-Cvitanović et al., 2015). This may be due to unique structure of GT and its characteristic interactions with other biopolymer materials. Moreover, addition of CH decreased hardness values except for 25A formulation ($p < 0.05$) and this pointed out again weak structure of gels prepared with CH as previously obtained in other analyses.

Table 3.4. Textural properties of fresh gel samples. Results are mean values and errors are represented as standard deviation for at least two replicates in each gel sample ($n=5$). Lettering was done for each subgroup separately ($p < 0.05$).

	Hardness (g)*	Springiness
Hydrogels		
100A	888.27 ± 61.12 ^a	3.94 ± 0.18 ^a
75A	406.31 ± 27.69 ^b	8.24 ± 0.57 ^b
50A	241.75 ± 6.55 ^c	9.68 ± 0.51 ^c
25A	73.87 ± 10.59 ^d	7.45 ± 0.59 ^d
Hydrogels		
100A CH	505.05 ± 54.82 ^a	8.29 ± 0.97 ^a
75A CH	237.50 ± 34.80 ^b	12.73 ± 0.95 ^b
50A CH	157.82 ± 12.70 ^c	15.25 ± 0.77 ^c
25A CH	127.52 ± 13.47 ^d	6.52 ± 0.82 ^d

* “g” represents 0.0098 Newtons.

Springiness (elasticity) is a measure of how much the gel structure is broken down by the initial compression and is related to sensitivity of gel rubbery feeling in the mouth (Simi & Abraham, 2010). In gels with/out CH gave higher springiness as higher amount of ALG was replaced with GT up to 25A gel. Optimum concentration was found as 50 A and after this concentration, springiness began to decrease again ($p < 0.05$).

3.2.4. Mathematical Modelling of Hydrogels

Since diffusion was the rate limiting mechanism other than swelling in prepared hydrogels, Fickian based diffusion was only considered for mathematical modelling. As given in Table 1.3, by using HPLC results of SIF, exponent “n” value was found as 0.5 for cylinder gel samples confirming Fickian diffusion as rough estimation. Fick’s second law was used to model insulin release from gels in intestinal fluid and to estimate diffusion coefficient, D . When recent papers have been reviewed (Caccavo, 2019), it has been seen that most of the papers have been taken into account pure drug mass transport as similar to this study. Analytical solutions given in Eq. (2.15) was used to fit experimental data for D estimation, using MATLAB nonlinear curve fitting subroutine. Since diffusion became dominant rather than swelling in gels as seen during experiment, diffusion-controlled mechanism has been demonstrated in this study. To confirm this assumption, MR images of gels were performed before and after immersion into intestine as given in section 3.2.2.4. The negligible change in gel dimensions before and after release supported the applicability of negligible swelling assumption. Fitted D values for insulin release from the gel were in the order of 10^{-10} m^2/s . Results changed between 2.48 and 7.29×10^{-10} m^2/s (Table 3.5).

Table 3.5. Diffusion coefficients of gel samples. Results are mean values and errors are represented as standard deviation for at least two replicates in each gel sample. Lettering was done for each subgroup separately ($p < 0.05$).

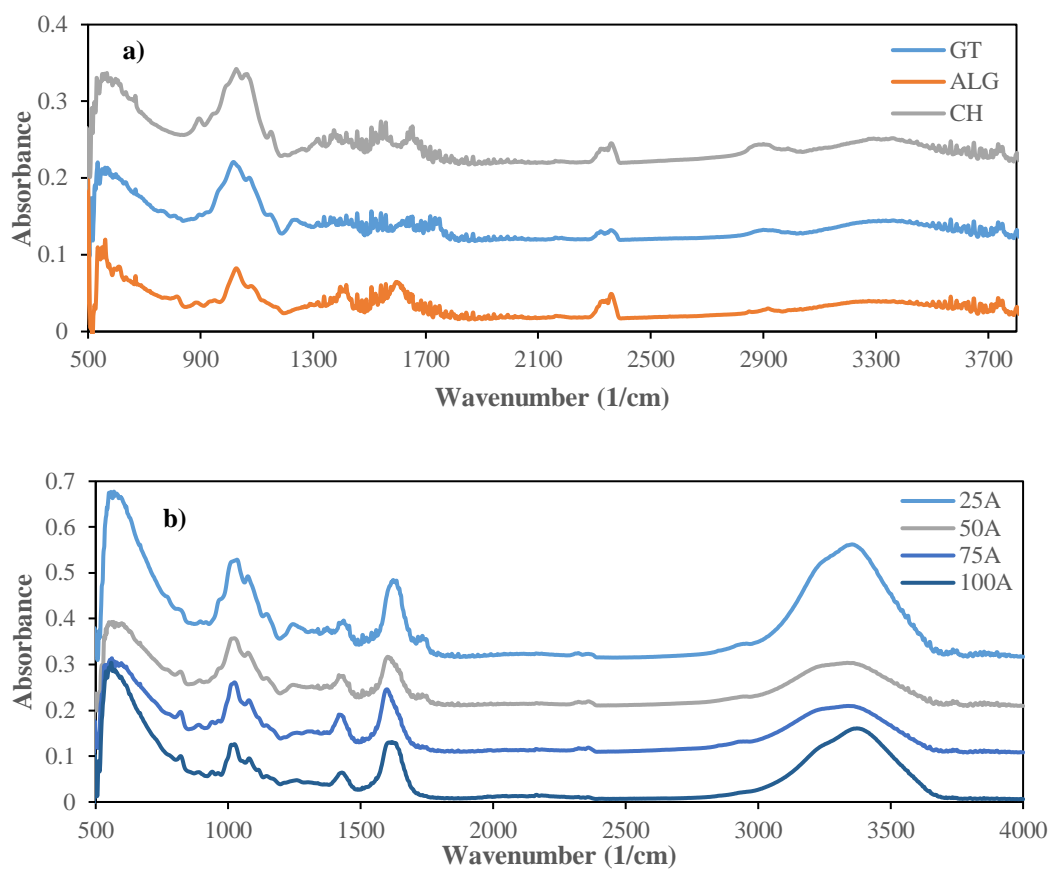
	D (m²/s)	R²
Hydrogels		
100A	$(7.29 \pm 0.95) \times 10^{-10b}$	≥ 0.87
75A	$(3.34 \pm 0.15) \times 10^{-10a}$	≥ 0.90
50A	$(2.98 \pm 0.25) \times 10^{-10a}$	≥ 0.80
25A	$(2.48 \pm 0.31) \times 10^{-10a}$	≥ 0.70
Hydrogels		
100A CH	$(2.75 \pm 0.92) \times 10^{-10a}$	≥ 0.80
75A CH	$(3.94 \pm 0.79) \times 10^{-10a}$	≥ 0.70
50A CH	$(3.45 \pm 0.21) \times 10^{-10a}$	≥ 0.90
25A CH	$(2.73 \pm 0.04) \times 10^{-10a}$	≥ 0.80

3.2.5. FTIR

In order to characterize possible chemical interactions between polymers in gel structure, FTIR measurements were conducted. Fig. 3.17 showed the FTIR spectra of each polymer and insulin loaded gels at different ratios over the range of 400-4000 cm^{-1} .

For common to all polysaccharides, the observed characteristic peak at around 1040 cm^{-1} was contributed to stretching of C-O bonds (Ebrahimi, Koocheki, Milani, & Mohebbi, 2016; H. Yang et al., 2015). Since this band could refer to the existence of galacturonic and guluronic units, ALG-GT based gels were more likely to have strengthened peaks (Blanco-Pascual, Montero, & Gómez-Guillén, 2014; Tonyali, Cikrikci, & Oztop, 2018). FTIR spectra of raw GT confirmed this hypothesis by giving considerable peak at that region (Figure 3.19a). Typical bands of polysaccharides in the spectral range of 3000-3680 cm^{-1} representing asymmetric stretching of the many

hydroxyl groups were observed in both ALG and GT. Since GT contains sugars like xylose, fucose and arabinose units, absorbance at around 1040 and 1070 cm^{-1} representing the existence of galactose such as arabinogalactans became higher in gels with higher GT content (Fattahi et al., 2013). Variations in pH could lead shifts of stretching groups and so differences in zeta potential of each sample could be the reason of small shifting in peaks but this did not affect absorbance values (M. Nur et al., 2016).



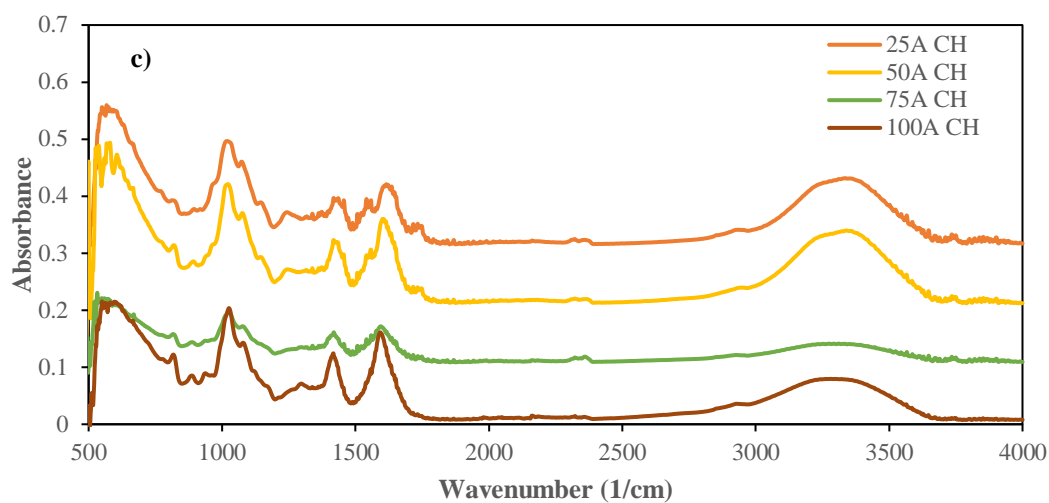


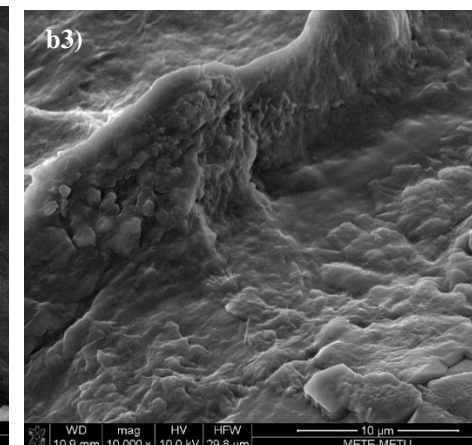
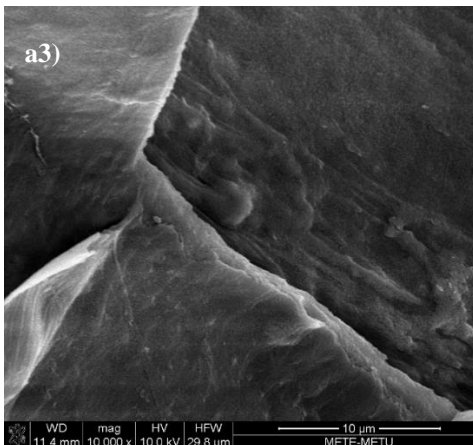
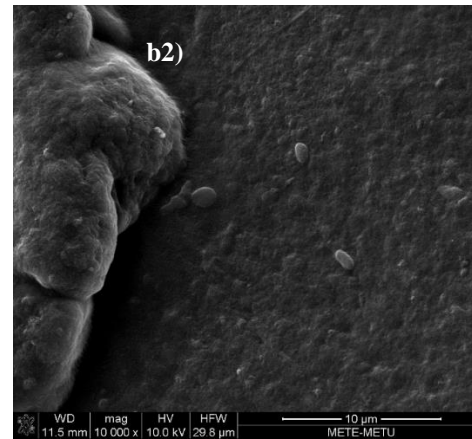
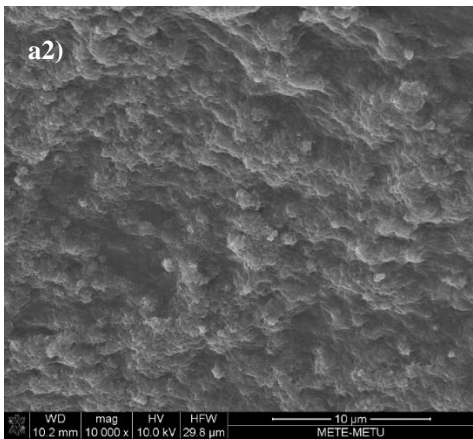
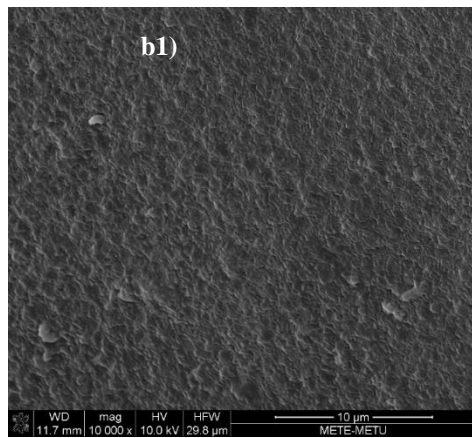
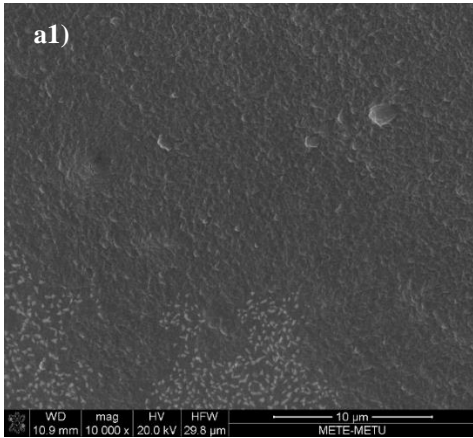
Figure 3.17. FTIR spectra corresponding to a) polymers in powder form and b-c) all gel formulations.

The broad bands at 1425 and 1640 cm^{-1} represent the symmetric and asymmetric stretching mode of the carboxyl groups (Dabiri et al., 2017; Ribeiro, Barrias, & Barbosa, 2004; Tahtat et al., 2013). Similar to ALG, GT as anionic polymer includes galacturonic acid indicating carboxyl group (COO^-) and it could interact with amino group (NH_3^+) of cationic polymer (protein or chitosan) forming ionic complex via polyelectrolytes interactions and peptide entrapment (Sarmiento, Martins, et al., 2006). Hereby, monitoring changes in carboxyl group in spectra would be helpful to get information about polymer interactions in gel network. FTIR spectra of insulin loaded gel samples were different than spectra of pure polymers due to these interactions during and after gelation process. After complexation with CH, especially the peak at range of $3000\text{--}3680\text{ cm}^{-1}$ belonging hydroxyl groups enlarged and peak intensity decreased. In addition, the peaks related to amino groups coming from CH and insulin at around 1153 cm^{-1} , 1650 cm^{-1} and 1540 cm^{-1} can be seen in the spectra. These observations agreed with previous studies (Lawrie et al., 2007; Sarmiento, Ferreira, et al., 2006; Sarmiento, Martins, et al., 2006; Xu & Dumont, 2015). More interestingly,

comparison in peak intensities with respect to each gel formulation showed same trend with release studies of these gel formulations. Since the sample with the high release rate also had higher peak amplitude, use of FTIR response of the samples was efficient to study interactions through the gels.

3.2.6. Microstructure of Hydrogels

SEM was used to examine internal gel structure and surface morphology of hydrogels. Insulin loaded freeze-dried hydrogels were displayed in Fig. 3.18. In the absence of CH, gels exhibited a relatively smooth and homogenous surface while gels with CH revealed irregular shape with fissures. Likely, the addition of GT created more heterogeneous structure in matrix. Plain ALG gel, 100A, had the straightest and smooth surface and the most regular shape, without irregular cavity and collapsed structure (Belščak-Cvitanović et al., 2015). These morphological changes in different samples pointed out different physicochemical interactions in each gels (Tahtat et al., 2013). With the presence of CH, strong crosslinking of ALG with calcium might have been prevented with cavities which were in agreement with the study of Belscak-Cvitanovic et al. (2015) and Popa, Gomes, and Reis (2011) (Popa, Gomes, & Reis, 2011). Less denser and more porous and tortuous flake structure in gels with CH explains the poor ability for slowing down insulin release and less firm gel structure obtained comparing the gels without CH (Martins et al., 2007; Tsai, Kitamura, & Kokawa, 2017; Zeeb, Saberi, Weiss, & McClements, 2015). These are also valid for GT effect in gel internal structures.



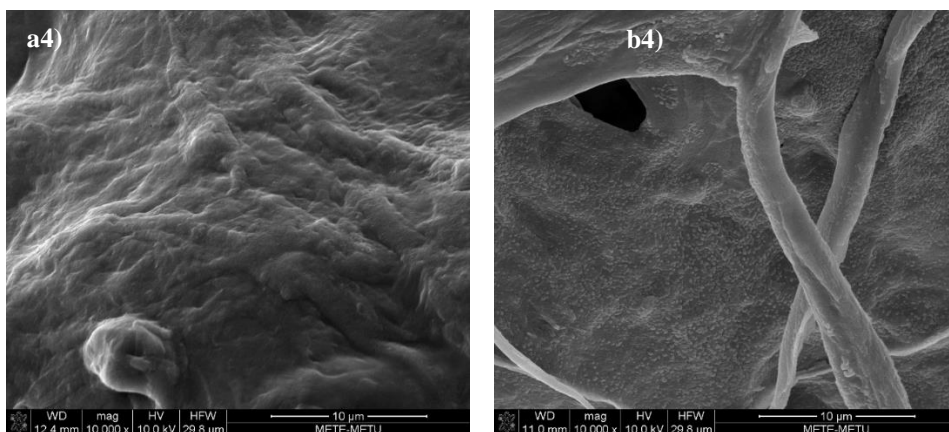


Figure 3.18. SEM images of hydrogels From a1) to a4): 100A, 75A, 50A, 25A. From b1) to b4): 100A CH, 75A CH, 50A CH, 25A CH, respectively.

CHAPTER 4

CONCLUSION AND RECOMMENDATIONS

This work supported the potential use of magnetic resonance for validation of transport processes, identification of molecular interactions and characterization of conformational changes occurred in a food and hydrogel matrix.

In the 1st part of the study, oil migration from hazelnut paste to dark chocolate was modelled using Fick's 2nd law. A new approach for boundary conditions using a logistic type boundary condition was proposed and modeling was evaluated. There was a net liquid fat migration from hazelnut paste to chocolate layer in contact with each other. The oil migration was modeled over 22 days of storage at 30 °C by an expression consistent with Fickian diffusion. Average diffusivities of all samples varied in the order of 10^{-11} m²/s. It was concluded that chocolate prepared with only stevia (F5) gave similar results with only sucrose formulation (F1) by leading higher diffusivity values. On the other hand, synergistic effect of sucrose and stevia reduced diffusion coefficient in F3 sample. Combination of sucrose with stevia presented much more barrier to penetrate liquid fat most probably leading to lower interstitial spaces and higher tortuosity owing to higher nonfat solid ratio when compared to sample with only sucrose. From these results, it was concluded that that sucrose-stevia combination in chocolate might be offered for less quality loss in two-layer chocolate systems. Chocolate matrix is very complex so some hypothesizes expressing interface migration and recrystallization form of fats, by phase separation could be said to explain the dark region zone at interface. As a further study, chemical shift imaging could be conducted to see signal intensity alterations.

It was also confirmed that MRI was a useful technique to differentiate different confectionery fillings/coatings based on their migration rates in chocolate systems.

This work is a step toward the design of confectionery products based on knowledge of mass transfer of oil migration during storage.

In the 2nd part of the study, alginate based hydrogels through cold set and ionotropic gelation in the presence of cross-linker Ca^{2+} were prepared. Additionally, polyelectrolyte complexation with an oppositely charged biopolymer CH was formulated. GT was used as additional polymer by replacing ALG at different ratios. ALG-GT blend gels with/out CH were prepared at different replacement ratios. Results of pH dependent release studies showed that, all gels retained insulin in gastric buffer however, PEC gels with CH showed more tendency to release entrapped insulin in intestinal conditions. Increase of GT ratio in formulation also pronounced less firm gel structure and weaker polymer-polymer interactions in gel network promoting release of insulin. Texture, FTIR and SEM analyses supported less firm structure, interactions between polymers and more heterogenous structure with the increase of GT ratio in the formulations. The current study could offer the use of GT as biodegradable and biocompatible natural polymer as carrier for insulin and other therapeutic proteins. *In-vivo* absorption studies of insulin from oral delivery system could be recommended for the future.

Under the light of conducted analyses and results, it could be referred that this study give an insight for further studies undergoing in food and biomedical applications.

REFERENCES

- Abrahamsén-Alami, S., Körner, A., Nilsson, I., & Larsson, A. (2007). New release cell for NMR microimaging of tablets. *International Journal of Pharmaceutics*, 342(1-2), 105–114. doi:10.1016/j.ijpharm.2007.05.005
- Afoakwa, E. O. (2010). *Chocolate Science and Technology*. *Chocolate Science and Technology*. doi:10.1002/9781444319880
- Afoakwa, E. O., Paterson, A., Fowler, M., & Vieira, J. (2008). Effects of tempering and fat crystallisation behaviour on microstructure, mechanical properties and appearance in dark chocolate systems. *Journal of Food Engineering*, 89(2), 128–136. doi:10.1016/j.jfoodeng.2008.04.021
- Afoakwa, E. O., Paterson, A., Fowler, M., & Vieira, J. (2009). Microstructure and mechanical properties related to particle size distribution and composition in dark chocolate. *International Journal of Food Science and Technology*, 44(2007), 111–119. doi:10.1111/j.1365-2621.2007.01677.x
- Aguiar, H. F., & Gut, J. a. W. (2014). Continuous HTST pasteurization of liquid foods with plate heat exchangers: Mathematical modeling and experimental validation using a time–temperature integrator. *Journal of Food Engineering*, 123, 78–86. doi:10.1016/j.jfoodeng.2013.09.022
- Aguilera, J. M., Michel, M., & Mayor, G. (2004). Fat Migration in Chocolate: Diffusion or Capillary Flow in a Particulate Solid?—A Hypothesis Paper. *Journal of Food Science*, 69(7), 167–174.
- Alfrey, T., Gurnee, E. F., & Lloyd, W. G. (2007). Diffusion in glassy polymers. *Journal of Polymer Science Part C: Polymer Symposia*, 12(1), 249–261. doi:10.1002/polc.5070120119
- Altan, A., Lavenson, D. M., Mccarthy, M. J., & Mccarthy, K. L. (2011). Oil Migration in Chocolate and Almond Product Confectionery Systems, 1–6. doi:10.1111/j.1750-3841.2011.02233.x
- Altimiras, P., Pyle, L., & Bouchon, P. (2007a). Structure–fat migration relationships during storage of cocoa butter model bars: Bloom development and possible mechanisms. *Journal of Food Engineering*, 80(2), 600–610. doi:10.1016/j.jfoodeng.2006.06.022
- Altimiras, P., Pyle, L., & Bouchon, P. (2007b). Structure–fat migration relationships during storage of cocoa butter model bars: Bloom development and possible mechanisms. *Journal of Food Engineering*, 80(2), 600–610. doi:10.1016/j.jfoodeng.2006.06.022
- Andrae-Nightingale, L. M., Lee, S. Y., & Engeseth, N. J. (2009). Textural changes in chocolate characterized by instrumental and sensory techniques. *Journal of*

Texture Studies, 40, 427–444. doi:10.1111/j.1745-4603.2009.00190.x

- Antunes, J. C., Pereira, C. L., Molinos, M., Ferreira-da-Silva, F., Dessi, M., Gloria, a, ... Barbosa, M. a. (2011). Layer-by-Layer Self-Assembly of Chitosan and Poly(γ -glutamic acid) into Polyelectrolyte Complexes. *Biomacromolecules*, 12, 4183–4195. doi:10.1021/bm2008235
- Arifin, D. Y., Lee, L. Y., & Wang, C. H. (2006). Mathematical modeling and simulation of drug release from microspheres: Implications to drug delivery systems. *Advanced Drug Delivery Reviews*, 58(12-13), 1274–1325. doi:10.1016/j.addr.2006.09.007
- Atkins, P., & Depaula, J. (2006). *Atkins' Physical Chemistry* (8th ed.). Oxford, UK: Oxford University Press.
- Baker, K., Dibildox-alvarado, E., Neves, J., & Marangoni, A. G. (2005). Monitoring and quantifying of oil migration in cocoa butter using a flatbed scanner and fluorescence light microscopy, 38, 1189–1197. doi:10.1016/j.foodres.2005.04.008
- Balaghi Sima, Mohammadifar Mohammad Amin, Zargaraan Azizollaah, Gavlighi Hassan Ahmadi, M. M. r. (2011). Tragacanth Gum : Structural Composition , Natural Functionality and Enzymatic Conversion as Source of Potential Prebiotic Activity Tragacanth Gum : Structural Composition , Natural Functionality and Enzymatic Conversion as Source of Potential Prebiotic Ac. *Food Hydrocolloids*, 25(2011), 1–83.
- Bayat, A., Larijani, B., Ahmadian, S., Junginger, H. E., & Rafiee-Tehrani, M. (2008). Preparation and characterization of insulin nanoparticles using chitosan and its quaternized derivatives. *Nanomedicine: Nanotechnology, Biology, and Medicine*, 4(2), 115–120. doi:10.1016/j.nano.2008.01.003
- Beckett, T. Stephen. (2008). "The Science of chocolate." *The Royal Society of Chemistry*. doi:10.1089/jam.2007.0571
- Belščak-Cvitanović, A., Dordević, V., Karlović, S., Pavlović, V., Komes, D., Ježek, D., ... Nedović, V. (2015). Protein-reinforced and chitosan-pectin coated alginate microparticles for delivery of flavan-3-ol antioxidants and caffeine from green tea extract. *Food Hydrocolloids*, 51, 361–374. doi:10.1016/j.foodhyd.2015.05.039
- Blanco-Pascual, N., Montero, M. P., & Gómez-Guillén, M. C. (2014). Antioxidant film development from unrefined extracts of brown seaweeds *Laminaria digitata* and *Ascophyllum nodosum*. *Food Hydrocolloids*, 37, 100–110. doi:10.1016/j.foodhyd.2013.10.021
- Bottomley, P. A., Foster, T. H., Argersinger, R. E., & Pfeifer, L. M. (1984). A review of normal tissue hydrogen NMR relaxation times and relaxation mechanisms

- from 1â€‘100 MHz: Dependence on tissue type, NMR frequency, temperature, species, excision, and age. *Medical Physics*, *11*(4), 425–448. doi:10.1118/1.595535
- Bouzidi, L., Omonov, T. S., Garti, N., & Narine, S. S. (2013). Relationships between molecular structure and kinetic and thermodynamic controls in lipid systems. Part I: propensity for oil loss of saturated triacylglycerols. *Food & Function*, *4*(1), 130–43. doi:10.1039/c2fo30164d
- Brake, N. C., & Fennema, O. R. (n.d.). Edible Coatings to Inhibit Lipid Migration in a Confectionery Product.
- Bricknell, J., & Hartel, R. W. (1998). Relation of Fat Bloom in Chocolate to Polymorphic Transition of Cocoa Butter, *75*(11), 1609–1615.
- Briones, V., & Aguilera, J. M. (2005). Image analysis of changes in surface color of chocolate. *Food Research International*, *38*(1), 87–94. doi:10.1016/j.foodres.2004.09.002
- Brown, S. P. (2018). Advanced solid-state NMR methods for characterising structure and self-assembly in supramolecular chemistry, polymers and hydrogels. *Current Opinion in Colloid and Interface Science*. doi:10.1016/j.cocis.2018.02.005
- Burey, P., Bhandari, B. R., Howes, T., & Gidley, M. J. (2008). Hydrocolloid gel particles: formation, characterization, and application. *Critical Reviews in Food Science and Nutrition*, *48*(5), 361–77. doi:10.1080/10408390701347801
- Caccavo, D. (2019). An overview on the mathematical modeling of hydrogels ' behavior for drug delivery systems. *International Journal of Pharmaceutics*. doi:10.1016/j.ijpharm.2019.01.076
- Caccavo, D., Lamberti, G., Barba, A. A., Abrahmsén-Alami, S., Viridén, A., & Larsson, A. (2017). Effects of HPMC substituent pattern on water up-take, polymer and drug release: An experimental and modelling study. *International Journal of Pharmaceutics*, *528*(1-2), 705–713. doi:10.1016/j.ijpharm.2017.06.064
- Campos, R., & Marangoni, A. G. (2014). Crystallization Dynamics of Shear Worked Cocoa Butter. *Crystal Growth & Design*, *14*(3), 1199–1210. doi:10.1021/cg4017273
- Chen, L., & Opara, U. L. (2013). Approaches to analysis and modeling texture in fresh and processed foods – A review. *Journal of Food Engineering*, *119*(3), 497–507. doi:10.1016/j.jfoodeng.2013.06.028
- Choi, Y. J., McCarthy, K. L., & McCarthy, M. J. (2005). Oil Migration in a Chocolate Confectionery System Evaluated by Magnetic Resonance Imaging. *Journal of Food Science*, *5*, e312–e317.

- Choi, Y. J., Mccarthy, K. L., Mccarthy, M. J., & Kim, M. H. (2007). Oil Migration in Chocolate. doi:10.1007/s00723-007-0013-4
- Chowdhury, M. A., Hill, D. J. T., & Whittaker, A. K. (2005). NMR imaging of the diffusion of water at 310 K into poly[(2-hydroxyethyl methacrylate)-co-(tetrahydrofurfuryl methacrylate)] containing vitamin B12 or aspirin. *Polymer International*, 54(2), 267–273. doi:10.1002/pi.1665
- Cikrikci, S., Mert, B., & Oztop, M. H. (2018). Development of pH Sensitive Alginate/Gum Tragacanth Based Hydrogels for Oral Insulin Delivery. *Journal of Agricultural and Food Chemistry*, 66(44), 11784–11796. research-article. doi:10.1021/acs.jafc.8b02525
- Cikrikci, S., & Oztop, M. H. (2016). Mathematical Modeling and Use of Magnetic Resonance Imaging (MRI) for Oil Migration in Chocolate Confectionery Systems. *Food Engineering Reviews*. doi:10.1007/s12393-016-9152-4
- Cikrikci, S., Yucekutlu, M., Mert, B., & Oztop, M. H. (2016). Physical characterization of low-calorie chocolate formulations. *Journal of Food Measurement and Characterization*, 1–9. doi:10.1007/s11694-016-9369-1
- Clercq, N. De, Depypere, F., Delbaere, C., Nopens, I., Bernaert, H., & Dewettinck, K. (2014). Influence of cocoa butter diacylglycerols on migration induced fat bloom in filled chocolates. *European Journal of Lipid Science and Technology*, 116(10), 1388–1399. doi:10.1002/ejlt.201300476
- Crank, J. (1975). THE MATHEMATICS OF DIFFUSION.
- Cukier, R. I. (1984). Diffusion of Brownian Spheres in Semidilute Polymer Solutions. *Macromolecules*, 17(2), 252–255. doi:10.1021/ma00132a023
- Cussler, E. L. (1997). *Diffusion: Mass Transfer in Fluid Systems*. Engineering (Vol. Second). Retrieved from <http://books.google.com/books?id=jpFgQgAACAAJ>
- d'Avila, M. A., Powell, R. L., Phillips, R. J., Shapley, N. C., Walton, J. H., & Dungan, S. R. (2005). Magnetic resonance imaging (MRI): A technique to study flow an microstructure of concentrated emulsions. *Brazilian Journal of Chemical Engineering*, 22(1), 49–60. Retrieved from <Go to ISI>://000225578800006
- Dabiri, S. M. H., Lagazzo, A., Barberis, F., Shayganpour, A., Finocchio, E., & Pastorino, L. (2017). New in-situ synthesized hydrogel composite based on alginate and brushite as a potential pH sensitive drug delivery system. *Carbohydrate Polymers*, 177(April), 324–333. doi:10.1016/j.carbpol.2017.08.046
- Dahlberg, C., Fureby, A., Schuleit, M., Dvinskikh, S. V., & Furó, I. (2007). Polymer mobilization and drug release during tablet swelling. A 1H NMR and NMR microimaging study. *Journal of Controlled Release*, 122(2), 199–205. doi:10.1016/j.jconrel.2007.07.007

- Dahlenborg, H., Millqvist-Fureby, A., Bergenståhl, B., & Kalnin, D. J. E. (2010). Investigation of Chocolate Surfaces Using Profilometry and Low Vacuum Scanning Electron Microscopy. *Journal of the American Oil Chemists' Society*, 88(6), 773–783. doi:10.1007/s11746-010-1721-8
- Dahlenborg, H., Millqvist-Fureby, A., Brandner, B. D., & Bergenstahl, B. (2012). Study of the porous structure of white chocolate by confocal Raman microscopy. *European Journal of Lipid Science and Technology*, 114(8), 919–926. doi:10.1002/ejlt.201200006
- De Graaf, R. A., Brown, P. B., McIntyre, S., Nixon, T. W., Behar, K. L., & Rothman, D. L. (2006). High magnetic field water and metabolite proton T1 and T2 relaxation in rat brain in vivo. *Magnetic Resonance in Medicine*, 56(2), 386–394. doi:10.1002/mrm.20946
- De Graef, V., Foubert, I., Agache, E., Bernaert, H., Landuyt, A., Vanrolleghem, P. a., & Dewettinck, K. (2005). Prediction of migration fat bloom on chocolate. *European Journal of Lipid Science and Technology*, 107(5), 297–306. doi:10.1002/ejlt.200401059
- Deka, K., MacMillan, B., Ziegler, G. R., Marangoni, A. G., Newling, B., & Balcom, B. J. (2006). Spatial mapping of solid and liquid lipid in confectionery products using a 1D centric SPRITE MRI technique. *Food Research International*, 39(3), 365–371. doi:10.1016/j.foodres.2005.08.009
- Depypere, F., De Clercq, N., Segers, M., Lewille, B., & Dewettinck, K. (2009). Triacylglycerol migration and bloom in filled chocolates: Effects of low-temperature storage. *European Journal of Lipid Science and Technology*, 111(3), 280–289. doi:10.1002/ejlt.200800179
- Du, H., Liu, M., Yang, X., & Zhai, G. (2015). The design of pH-sensitive chitosan-based formulations for gastrointestinal delivery. *Drug Discovery Today*, 20(8), 1004–1011. doi:10.1016/j.drudis.2015.03.002
- Duerk, J. L. (2007). MRI: The basics. Ray H Hashemi and William G Bradley, Jr. Williams & Wilkins, Baltimore, 1997 \$45.00 (softcover only), 443 illustrations, pp. 336. *Journal of Magnetic Resonance Imaging*, 7(3), 614–615. doi:10.1002/jmri.1880070330
- Duncan, D. C., & Whitten, D. G. (2000). 1H NMR investigation of the composition, structure, and dynamics of cholesterol-stilbene tethered dyad organogels. *Langmuir*, 16(16), 6445–6452. doi:10.1021/la0001631
- Ebrahimi, S. E., Koocheki, A., Milani, E., & Mohebbi, M. (2016). Interactions between *Lepidium perfoliatum* seed gum - Grass pea (*Lathyrus sativus*) protein isolate in composite biodegradable film. *Food Hydrocolloids*, 54, 302–314. doi:10.1016/j.foodhyd.2015.10.020

- Edmondson, P. T., Grammatika, M., Fryer, P. J., & Handy, B. (2005). Modelling of heat transfer, mass transfer and flavour development in chocolate crumb, (June).
- Erdemli, Ö. (2013). *No Title*. Middle East Technical University.
- Ergun, R., Lietha, R., & Hartel, R. W. (2010). Moisture and shelf life in sugar confections. *Critical Reviews in Food Science and Nutrition*, *50*(2), 162–92. doi:10.1080/10408390802248833
- Escuder, B., LLusar, M., & Miravet, J. F. (2006). Insight on the NMR study of supramolecular gels and its application to monitor molecular recognition on self-assembled fibers. *Journal of Organic Chemistry*, *71*(20), 7747–7752. doi:10.1021/jo0612731
- Farid, M. (2013). Heat and Mass Transfer in Food Processing. In *Handbook of Farm, Dairy and Food Machinery Engineering: Second Edition* (pp. 379–401). doi:10.1016/B978-0-12-385881-8.00014-8
- Fattahi, A., Petrini, P., Munarin, F., Shokohinia, Y., Golozar, M. A., Varshosaz, J., & Tanzi, M. C. (2013). Polysaccharides derived from tragacanth as biocompatible polymers and Gels. *Journal of Applied Polymer Science*, *129*(4), 2092–2102. doi:10.1002/app.38931
- Frazier, a., & Hartel, R. W. (2012). Bloom on chocolate chips baked in cookies. *Food Research International*, *48*(2), 380–386. doi:10.1016/j.foodres.2012.05.011
- Fyfe, C. a, & Blazek-Welsh, a I. (2000). Quantitative NMR imaging study of the mechanism of drug release from swelling hydroxypropylmethylcellulose tablets. *Journal of Controlled Release: Official Journal of the Controlled Release Society*, *68*(3), 313–33. doi:10.1016/S0168-3659(00)00245-5
- Galdámez, J. R., Szlachetka, K., Duda, J. L., & Ziegler, G. R. (2009). Oil migration in chocolate: A case of non-Fickian diffusion. *Journal of Food Engineering*, *92*(3), 261–268. doi:10.1016/j.jfoodeng.2008.11.003
- Ghosh, V., Duda, J. L., Ziegler, G. R., & Anantheswaran, R. C. (2004). Diffusion of moisture through chocolate- flavoured confectionery coatings, *82*(March), 35–43.
- Ghosh, V., Ziegler, G. R., & Anantheswaran, R. C. (2002). Fat, moisture, and ethanol migration through chocolates and confectionary coatings. *Critical Reviews in Food Science and Nutrition*, *42*(6), 583–626. doi:10.1080/20024091054265
- Ghosh, V., Ziegler, G. R., & Anantheswaran, R. C. (2005). Moisture migration through chocolate-flavored confectionery coatings, *66*, 177–186. doi:10.1016/j.jfoodeng.2004.03.012
- Glicerina, V., Balestra, F., Rosa, M. D., & Romani, S. (2013). Rheological, textural and calorimetric modifications of dark chocolate during process. *Journal of Food*

- Engineering*, 119(1), 173–179. doi:10.1016/j.jfoodeng.2013.05.012
- Green, N. L., & Rousseau, D. (2015). Oil diffusivity through fat crystal networks. *Soft Matter*, 11(27), 5523–30. doi:10.1039/c5sm01355k
- Grunin, L. Y., Grunin, Y. B., Nikolskaya, E. A., Sheveleva, N. N., & Nikolaev, I. A. (2017). An NMR relaxation and spin diffusion study of cellulose structure during water adsorption. *Biophysics*, 62(2), 198–206. doi:10.1134/s0006350917020087
- Grunin, Y. B., Grunin, L. Y., Talantsev, V. I., Nikolskaya, E. A., & Masas, D. S. (2015). Supramolecular reorganizations in cellulose during hydration. *Biophysics*, 60(1), 43–52. doi:10.1134/s0006350915010133
- Guiheneuf, T. M., Couzens, P. J., Wille, H., Hall, L. D., & Way, R. (1997). Visualisation of Liquid Triacylglycerol Migration in Chocolate by Magnetic Resonance Imaging, 00.
- Guo, M., Rong, W.-T., Hou, J., Wang, D.-F., Lu, Y., Wang, Y., ... Xu, Q. (2013). Mechanisms of chitosan-coated poly(lactic-co-glycolic acid) nanoparticles for improving oral absorption of 7-ethyl-10-hydroxycamptothecin. *Nanotechnology*, 24(24), 245101. doi:10.1088/0957-4484/24/24/245101
- Guti, T. J. (2018). *Polymers for Food Applications*. doi:10.1007/978-3-319-94625-2
- Hamraoui, A., & Nylander, T. (2002). Analytical approach for the Lucas-Washburn equation. *Journal of Colloid and Interface Science*, 250, 415–421. doi:10.1006/jcis.2002.8288
- Hara, M., & Miyake, J. (2001). Calcium alginate gel-entrapped liposomes. *Materials Science and Engineering C*, 17(1-2), 101–105. doi:10.1016/S0928-4931(01)00316-2
- Hartel, R. W. (1996). Applications of milk-fat fractions in confectionery products. *JAACS, Journal of the American Oil Chemists' Society*, 73(8), 945–953. doi:10.1007/BF02523401
- Haseeb, M. T., Hussain, M. A., Yuk, S. H., Bashir, S., & Nauman, M. (2016). Polysaccharides based superabsorbent hydrogel from Linseed: Dynamic swelling, stimuli responsive on-off switching and drug release. *Carbohydrate Polymers*, 136, 750–756. doi:10.1016/j.carbpol.2015.09.092
- Higuchi, T. (1961). Physical Chemical Analysis of percutaneous absorption process from creams and ointments. *Journal of the Society of Cosmetic Chemists*, 85–97.
- Higuchi, T. (1961). Rate of release of medicaments from ointment bases containing drugs in suspension. *Journal of Pharmaceutical Sciences*, 50(10), 874–875. doi:10.1002/jps.2600501018
- Ho, Q. T., Carmeliet, J., Datta, A. K., Defraeye, T., Delele, M. a., Herremans, E., ... Nicolai, B. M. (2013). Multiscale modeling in food engineering. *Journal of Food*

- Engineering*, 114(3), 279–291. doi:10.1016/j.jfoodeng.2012.08.019
- Hoare, T. R., & Kohane, D. S. (2008). Hydrogels in drug delivery: Progress and challenges. *Polymer*. doi:10.1016/j.polymer.2008.01.027
- Hondo, H. (2013). *Modeling of moisture migration through chocolate*. University of Technology, Göteborg.
- Hsieh, M. H., & Faculty, E. (2012). PhD Thesis. Mathematical modelling of controlled drug release from polymer micro-spheres : incorporating the effects of swelling , diffusion and dissolution via moving boundary problems, 190.
- James, B. J., & Smith, B. G. (2009a). Surface structure and composition of fresh and bloomed chocolate analysed using X-ray photoelectron spectroscopy, cryo-scanning electron microscopy and environmental scanning electron microscopy. *LWT - Food Science and Technology*, 42, 929–937. doi:10.1016/j.lwt.2008.12.003
- James, B. J., & Smith, B. G. (2009b). Surface structure and composition of fresh and bloomed chocolate analysed using X-ray photoelectron spectroscopy, cryo-scanning electron microscopy and environmental scanning electron microscopy. *LWT - Food Science and Technology*, 42(5), 929–937. doi:10.1016/j.lwt.2008.12.003
- Je Lee, S., & Rosenberg, M. (2000). Whey Protein-based Microcapsules Prepared by Double Emulsification and Heat Gelation. *LWT - Food Science and Technology*, 33(2), 80–88. doi:10.1006/fstl.1999.0619
- Karakosta, E., & McDonald, P. J. (2007). An MRI analysis of the dissolution of a soluble drug incorporated within an insoluble polymer tablet. *Applied Magnetic Resonance*, 32(1-2), 75–91. doi:10.1007/s00723-007-0001-8
- Kariduraganavar, M. Y., Kulkarni, S. B., & Aminabhavi, T. M. (2003). Molecular migration of aromatic liquids into a commercial fluoroelastomeric membrane at 30, 40, and 50°C. *Journal of Applied Polymer Science*, 88(11), 3100–3106. doi:10.1002/app.11724
- Khan, R. S., & Rousseau, D. (2006a). Hazelnut oil migration in dark chocolate - Kinetic, thermodynamic and structural considerations. *European Journal of Lipid Science and Technology*, 108(5), 434–443. doi:10.1002/ejlt.200501194
- Khan, R. S., & Rousseau, D. (2006b). Hazelnut oil migration in dark chocolate – kinetic, thermodynamic and structural considerations. *European Journal of Lipid Science and Technology*, 108(5), 434–443. doi:10.1002/ejlt.200501194
- Kikuchi, S., Onuki, Y., Kuribayashi, H., & Takayama, K. (2012). Relationship between diffusivity of water molecules inside hydrating tablets and their drug release behavior elucidated by magnetic resonance imaging. *Chemical & Pharmaceutical Bulletin*, 60(4), 536–42. doi:10.1248/cpb.60.536

- Kinta, Y., & Hartel, R. W. (2009). Bloom Formation on Poorly-Tempered Chocolate and Effects of Seed Addition. *Journal of the American Oil Chemists' Society*, 87(1), 19–27. doi:10.1007/s11746-009-1473-5
- Kirtil, E., & Oztop, M. H. (2016). ¹H Nuclear Magnetic Resonance Relaxometry and Magnetic Resonance Imaging and Applications in Food Science and Processing. *Food Engineering Reviews*, 1–22. doi:10.1007/s12393-015-9118-y
- Koetting, M. C., Peters, J. T., Steichen, S. D., & Peppas, N. A. (2015). Stimulus-responsive hydrogels: Theory, modern advances, and applications. *Materials Science and Engineering: R: Reports*, 93, 1–49. doi:10.1016/j.mser.2015.04.001
- Korb, J. P., & Bryant, R. G. (2002). Magnetic field dependence of proton spin-lattice relaxation times. *Magnetic Resonance in Medicine*, 48(1), 21–26. doi:10.1002/mrm.10185
- Lawrie, G., Keen, I., Drew, B., Chandler-Temple, A., Rintoul, L., Fredericks, P., & Grøndahl, L. (2007). Interactions between alginate and chitosan biopolymers characterized using FTIR and XPS. *Biomacromolecules*, 8(8), 2533–2541. doi:10.1021/bm070014y
- Lee, K., Cho, K., Park, I., Lee, B. H., Rana, D., Choe, S., & Al, L. E. E. E. T. (1999). Migration Phenomena of Surfactants in Polyethylene Film, 1387–1395.
- Lee, W. L., McCarthy, M. J., & McCarthy, K. L. (2010a). Oil migration in 2-component confectionery systems. *Journal of Food Science*, 75. doi:10.1111/j.1750-3841.2009.01454.x
- Lee, W. L., McCarthy, M. J., & McCarthy, K. L. (2010b). Oil migration in 2-component confectionery systems. *Journal of Food Science*, 75(1), 83–89. doi:10.1111/j.1750-3841.2009.01454.x
- Lim, H. P., Tey, B. T., & Chan, E. S. (2014). Particle designs for the stabilization and controlled-delivery of protein drugs by biopolymers: A case study on insulin. *Journal of Controlled Release*, 186, 11–21. doi:10.1016/j.jconrel.2014.04.042
- Lin, M., & Larive, C. K. (1995). Detection of insulin aggregates with pulsed-field gradient nuclear magnetic resonance spectroscopy. *Analytical Biochemistry*. doi:10.1006/abio.1995.1405
- Lipp, M., & Anklam, E. (1998). Review of cocoa butter and alternative fats for use in chocolate-Part B . Analytical approaches for identification and determination, 62(1), 99–108.
- Liu, J., Gong, T., Wang, C., Zhong, Z., & Zhang, Z. (2007). Solid lipid nanoparticles loaded with insulin by sodium cholate-phosphatidylcholine-based mixed micelles: Preparation and characterization. *International Journal of Pharmaceutics*, 340(1-2), 153–162. doi:10.1016/j.ijpharm.2007.03.009

- Liu, L., Du, P., Zhao, X., Zeng, J., & Liu, P. (2015). Independent temperature and pH dual-stimuli responsive yolk/shell polymer microspheres for controlled release: Structural effect. *European Polymer Journal*, *69*, 540–551. doi:10.1016/j.eurpolymj.2015.03.026
- Loisel, C., Lecq, G., Ponchel, G., Keller, G., & Ollivon, M. (1997). Fat bloom and chocolate structure studied by mercury porosimetry. *Journal of Food Science*, *62*, 781–788. doi:10.1111/j.1365-2621.1997.tb15455.x
- Lonchamp, P., & Hartel, R. W. (2004). Fat bloom in chocolate and compound coatings. *European Journal of Lipid Science and Technology*, *106*(4), 241–274. doi:10.1002/ejlt.200400938
- Lonchamp, P., & Hartel, R. W. (2006). Surface bloom on improperly tempered chocolate. *European Journal of Lipid Science and Technology*, *108*(2), 159–168. doi:10.1002/ejlt.200500260
- López-Cebral, R., Martin-Pastor, M., Paolicelli, P., Casadei, M. A., Seijo, B., & Sanchez, A. (2014). Application of NMR spectroscopy in the development of a biomimetic approach for hydrophobic drug association with physical hydrogels. *Colloids and Surfaces B: Biointerfaces*, *115*, 391–399. doi:10.1016/j.colsurfb.2013.12.022
- Maleky, F., & Marangoni, A. (2011a). Nanoscale effects on oil migration through triacylglycerol polycrystalline colloidal networks. *Soft Matter*, *7*(13), 6012. doi:10.1039/c1sm05154g
- Maleky, F., & Marangoni, A. (2011b). Thermal and mechanical properties of Cocoa butter crystallized under an external laminar shear field. *Crystal Growth and Design*, *11*, 2429–2437. doi:10.1021/cg200202u
- Maleky, F., Smith, A. K., & Marangoni, A. (2011). Laminar shear effects on crystalline alignments and nanostructure of a triacylglycerol crystal network. *Crystal Growth and Design*, *11*, 2335–2345. doi:10.1021/cg200014w
- Mani, S., & Tulsi, G. (2016). Intelligent Hydrogels for Controlled Drug Delivery System: A Review, (January). doi:10.13140/RG.2.1.3098.2564
- Mantle, M. D. (2013). Current Opinion in Colloid & Interface Science NMR and MRI studies of drug delivery systems. *Current Opinion in Colloid & Interface Science*, *18*(3), 214–227. doi:10.1016/j.cocis.2013.03.006
- Martins, S., Sarmiento, B., Souto, E. B., & Ferreira, D. C. (2007). Insulin-loaded alginate microspheres for oral delivery - Effect of polysaccharide reinforcement on physicochemical properties and release profile. *Carbohydrate Polymers*, *69*(4), 725–731. doi:10.1016/j.carbpol.2007.02.012
- Marty, S., & Marangoni, A. G. (2009). Effects of Cocoa Butter Origin, Tempering Procedure, and Structure on Oil Migration Kinetics. *Crystal Growth & Design*,

9(10), 4415–4423. doi:10.1021/cg9004505

- Marty, S., Schroeder, M., Baker, K. W., Mazzanti, G., & Marangoni, A. G. (2009). Small-molecule diffusion through polycrystalline triglyceride networks quantified using fluorescence recovery after photobleaching. *Langmuir: The ACS Journal of Surfaces and Colloids*, 25(15), 8780–5. doi:10.1021/la900255u
- Maus, A., Hertlein, C., & Saalwächter, K. (2006). A robust proton NMR method to investigate hard/soft ratios, crystallinity, and component mobility in polymers. *Macromolecular Chemistry and Physics*, 207(13), 1150–1158. doi:10.1002/macp.200600169
- McCarthy, K. L., & McCarthy, M. J. (2008). Oil migration in chocolate-peanut butter paste confectionery as a function of chocolate formulation. *Journal of Food Science*, 73. doi:10.1111/j.1750-3841.2008.00797.x
- McConville, P., & Pope, J. M. (2000). A comparison of water binding and mobility in contact lens hydrogels from NMR measurements of the water self-diffusion coefficient. *Polymer*, 41(26), 9081–9088. doi:10.1016/S0032-3861(00)00295-0
- Mikac, U., Sepe, A., Kristl, J., & Baumgartner, S. (2010). A new approach combining different MRI methods to provide detailed view on swelling dynamics of xanthan tablets influencing drug release at different pH and ionic strength. *Journal of Controlled Release*, 145(3), 247–256. doi:10.1016/j.jconrel.2010.04.018
- Milani, J., & Maleki, G. (2012). Hydrocolloids in Food Industry. *Food Industrial Processes*, 418. doi:10.5772/2491
- Miquel, M. E., Carli, S., Couzens, P. J., Wille, H., & Hall, D. (2001a). Kinetics of the migration of lipids in composite chocolate measured by magnetic resonance imaging, 34, 773–781.
- Miquel, M. E., Carli, S., Couzens, P. J., Wille, H. J., & Hall, L. D. (2001b). Kinetics of the migration of lipids in composite chocolate measured by magnetic resonance imaging. *Food Research International*, 34(9), 773–781. doi:10.1016/S0963-9969(00)00162-9
- Miquel, M. E., & Hall, L. D. (1998). A General Survey of Chocolate Confectionery by Magnetic Resonance Imaging, 99, 93–99.
- Miquel, M. E., & Hall, L. D. (2002a). Measurement by MRI of storage changes in commercial chocolate confectionery products, 35, 993–998.
- Miquel, M. E., & Hall, L. D. (2002b). Measurement by MRI of storage changes in commercial chocolate confectionery products. *Food Research International*, 35(10), 993–998. doi:10.1016/S0963-9969(02)00160-6
- Mostafavi, F. S., Kadkhodae, R., Emadzadeh, B., & Koocheki, A. (2016). Preparation and characterization of tragacanth-locust bean gum edible blend

- films. *Carbohydrate Polymers*, 139, 20–27. doi:10.1016/j.carbpol.2015.11.069
- Motwani, T., Hanselmann, W., & Anantheswaran, R. C. (2011). Diffusion, counter-diffusion and lipid phase changes occurring during oil migration in model confectionery systems. *Journal of Food Engineering*, 104(2), 186–195. doi:10.1016/j.jfoodeng.2010.11.032
- Mukhopadhyay, P., Mishra, R., Rana, D., & Kundu, P. P. (2012). Strategies for effective oral insulin delivery with modified chitosan nanoparticles: A review. *Progress in Polymer Science*, 37(11), 1457–1475. doi:10.1016/j.progpolymsci.2012.04.004
- Mukhopadhyay, P., Sarkar, K., Soam, S., & Kundu, P. P. (2013). Formulation of pH-responsive carboxymethyl chitosan and alginate beads for the oral delivery of insulin. *Journal of Applied Polymer Science*, 129(2), 835–845. doi:10.1002/app.38814
- Nattress, L. A., Ziegler, G. R., Hollender, R., & Peterson, D. G. (2003). PROPERTIES AND SHELF-LIFE OF DARK CHOCOLATE, 19(2004), 133–148.
- Nokhodchi, A., Raja, S., Patel, P., & Asare-Addo, K. (2012). The role of oral controlled release matrix tablets in drug delivery systems. *BioImpacts : BI*, 2(4), 175–87. doi:10.5681/bi.2012.027
- Nur, M., Ramchandran, L., & Vasiljevic, T. (2016). Tragacanth as an oral peptide and protein delivery carrier: Characterization and mucoadhesion. *Carbohydrate Polymers*, 143, 223–230. doi:10.1016/j.carbpol.2016.01.074
- Nur, M., & Vasiljevic, T. (2017). Can natural polymers assist in delivering insulin orally? *International Journal of Biological Macromolecules*, 103, 889–901. doi:10.1016/j.ijbiomac.2017.05.138
- Olsen, H. B. (1996). Investigations of Structure and Dynamics of Insulin Mutants using NMR Spectroscopy Investigations of Structure and Dynamics of Insulin Mutants using NMR Spectroscopy, (february).
- Omonov, T. S., Bouzidi, L., & Narine, S. S. (2010). Quantification of oil binding capacity of structuring fats: A novel method and its application. *Chemistry and Physics of Lipids*, 163(7), 728–40. doi:10.1016/j.chemphyslip.2010.07.003
- Ozel, B., Cikrikci, S., Aydin, O., & Oztop, M. H. (2017). Polysaccharide blended whey protein isolate-(WPI) hydrogels: A physicochemical and controlled release study. *Food Hydrocolloids*, 71, 35–46. doi:10.1016/j.foodhyd.2017.04.031
- Ozel, B., Uguz, S. S., Kilercioglu, M., Grunin, L., & Oztop, M. H. (2016). Effect of different polysaccharides on swelling of composite whey protein hydrogels: A low field (LF) NMR relaxometry study. *Journal of Food Process Engineering*, (July), 1–9. doi:10.1111/jfpe.12465

- Oztop, M. H., Rosenberg, M., Rosenberg, Y., McCarthy, K. L., & McCarthy, M. J. (2010). Magnetic resonance imaging (MRI) and relaxation spectrum analysis as methods to investigate swelling in whey protein gels. *Journal of Food Science*, 75(8), E508–15. doi:10.1111/j.1750-3841.2010.01788.x
- Östlund, Å., Bernin, D., Nordstierna, L., & Nydén, M. (2010). Chemical shift imaging NMR to track gel formation. *Journal of Colloid and Interface Science*, 344(1), 238–240. doi:10.1016/j.jcis.2009.12.027
- Pareek, A., Maheshwari, S., Cherlo, S., Thavva, R. S. R., & Runakana, V. (2017). Modeling drug release through stimuli responsive polymer hydrogels. *International Journal of Pharmaceutics*, 532(1), 502–510. doi:10.1016/j.ijpharm.2017.09.001
- Park, K. S. (2004). Prevention of type 2 diabetes mellitus from the viewpoint of genetics. In *Diabetes Research and Clinical Practice* (Vol. 66). doi:10.1016/j.diabres.2003.11.023
- Peppas, N. (2000). Hydrogels in pharmaceutical formulations. *European Journal of Pharmaceutics and Biopharmaceutics*, 50(1), 27–46. doi:10.1016/S0939-6411(00)00090-4
- Peppas, N. A., & Brannon-Peppas, L. (1994). Water diffusion and sorption in amorphous macromolecular systems and foods. *Journal of Food Engineering*. doi:10.1016/0260-8774(94)90030-2
- Peppas, N. A., & Kavimandan, N. J. (2006). Nanoscale analysis of protein and peptide absorption: Insulin absorption using complexation and pH-sensitive hydrogels as delivery vehicles. *European Journal of Pharmaceutical Sciences*, 29(3-4 SPEC. ISS.), 183–197. doi:10.1016/j.ejps.2006.04.014
- Peralta, J. M., Rubiolo, A. C., & Zorrilla, S. E. (2012). Mathematical modeling of the heat and mass transfer in a stationary potato sphere impinged by a single round liquid jet in a hydrofluidization system. *Journal of Food Engineering*, 109(3), 501–512. doi:10.1016/j.jfoodeng.2011.10.032
- Pham, Q. T. (2006). Modelling heat and mass transfer in frozen foods: a review. *International Journal of Refrigeration*, 29(6), 876–888. doi:10.1016/j.ijrefrig.2006.01.013
- Pinardag, F. E. (2006). Modified Acrylic Hydrogels As Controlled Release Systems a Thesis Submitted To the Graduate School of Natural and Applied Sciences of Middle East Technical University By Fatma Esra Pinardağ in Partial Fulfillment of the Requirements for the Degree of Mast, (May).
- Popa, E. G., Gomes, M. E., & Reis, R. L. (2011). Cell delivery systems using alginate-carrageenan hydrogel beads and fibers for regenerative medicine applications. *Biomacromolecules*, 12(11), 3952–3961. doi:10.1021/bm200965x

- Quevedo, R., Brown, C., Bouchon, P., & Aguilera, J. M. (2005). Surface roughness during storage of chocolate: Fractal analysis and possible mechanisms. *JAOCS, Journal of the American Oil Chemists' Society*, 82(6), 457–462. doi:10.1007/s11746-005-1093-2
- Reinke, S. K., Roth, S. V., Santoro, G., Vieira, J., Heinrich, S., & Palzer, S. (2015). Tracking Structural Changes in Lipid-based Multicomponent Food Materials due to Oil Migration by Microfocus Small-Angle X-ray Scattering. *ACS Applied Materials & Interfaces*, 7(18), 9929–36. doi:10.1021/acsami.5b02092
- Reis, C. P., Ribeiro, A. J., Veiga, F., Neufeld, R. J., & Damgé, C. (2008). Polyelectrolyte biomaterial interactions provide nanoparticulate carrier for oral insulin delivery. *Drug Delivery*, 15(2), 127–39. doi:10.1080/10717540801905165
- Ribeiro, C. C., Barrias, C. C., & Barbosa, M. A. (2004). Calcium phosphate-alginate microspheres as enzyme delivery matrices. *Biomaterials*, 25(18), 4363–4373. doi:10.1016/j.biomaterials.2003.11.028
- Roy, M., Lee, R. W., Brange, J., Dunn, M. F., Lee, W. K., Brangeli, J., & Dun, F. (1990). ¹H NMR Spectrum of the Native Human Insulin Monomer. *Journal of Biological Chemistry*, 265(10).
- Ruiz-López, I. I., Martínez-Sánchez, C. E., Cobos-Vivaldo, R., & Herman-Lara, E. (2008). Mathematical modeling and simulation of batch drying of foods in fixed beds with airflow reversal. *Journal of Food Engineering*, 89(3), 310–318. doi:10.1016/j.jfoodeng.2008.05.009
- Rumsey, T. R., & McCarthy, K. L. (2012). Modeling oil migration in two-layer chocolate – almond confectionery products. *Journal of Food Engineering*, 111(1), 149–155. doi:10.1016/j.jfoodeng.2012.01.006
- Saha, D., & Bhattacharya, S. (2010). Hydrocolloids as thickening and gelling agents in food: A critical review. *Journal of Food Science and Technology*, 47(6), 587–597. doi:10.1007/s13197-010-0162-6
- Sankalia, M. G., Mashru, R. C., Sankalia, J. M., & Sutariya, V. B. (2007). Reversed chitosan-alginate polyelectrolyte complex for stability improvement of alpha-amylase: Optimization and physicochemical characterization. *European Journal of Pharmaceutics and Biopharmaceutics*, 65(2), 215–232. doi:10.1016/j.ejpb.2006.07.014
- Sarmiento, B., Ferreira, D., Veiga, F., & Ribeiro, A. (2006). Characterization of insulin-loaded alginate nanoparticles produced by ionotropic pre-gelation through DSC and FTIR studies. *Carbohydrate Polymers*, 66(1), 1–7. doi:10.1016/j.carbpol.2006.02.008
- Sarmiento, B., Martins, S., Ribeiro, A., Veiga, F., Neufeld, R., & Ferreira, D. (2006).

- Development and comparison of different nanoparticulate polyelectrolyte complexes as insulin carriers. *International Journal of Peptide Research and Therapeutics*, 12(2), 131–138. doi:10.1007/s10989-005-9010-3
- Shiroodi, S. G., Mohammadifar, M. A., Gorji, E. G., Ezzatpanah, H., & Zohouri, N. (2012). Influence of gum tragacanth on the physicochemical and rheological properties of kashk. *Journal of Dairy Research*, 79(01), 93–101. doi:10.1017/S0022029911000872
- Siepmann, J., & Peppas, N. A. (2000). Hydrophilic matrices for controlled drug delivery: An improved mathematical model to predict the resulting drug release kinetics the “sequential layer” model). *Pharmaceutical Research*, 17(10), 1290–1298. doi:10.1023/A:1026455822595
- Siepmann, J., & Peppas, N. A. (2001). Modeling of drug release from delivery systems based on hydroxypropyl methylcellulose (HPMC). *Advanced Drug Delivery Reviews*. doi:10.1016/S0169-409X(01)00112-0
- Siepmann, J., & Siepmann, F. (2008). Mathematical modeling of drug delivery, 364, 328–343. doi:10.1016/j.ijpharm.2008.09.004
- Simi, C. K., & Abraham, T. E. (2010). Transparent xyloglucan-chitosan complex hydrogels for different applications. *Food Hydrocolloids*, 24(1), 72–80. doi:10.1016/j.foodhyd.2009.08.007
- Sinha, V. R., Singla, A. K., Wadhawan, S., Kaushik, R., Kumria, R., Bansal, K., & Dhawan, S. (2004). Chitosan microspheres as a potential carrier for drugs. *International Journal of Pharmaceutics*, 274(1-2), 1–33. doi:10.1016/j.ijpharm.2003.12.026
- Smith, K. . (1998). Chocolate Technology. In *Zentralfachschule Deutschen Susswarrenwirtschaft*. Cologne.
- Smith, K., Cain, F., & Talbot, G. (2007). Effect of nut oil migration on polymorphic transformation in a model system. *Food Chemistry*, 102(3), 656–663. doi:10.1016/j.foodchem.2006.05.045
- Sonaje, K., Lin, K. J., Wey, S. P., Lin, C. K., Yeh, T. H., Nguyen, H. N., ... Sung, H. W. (2010). Biodistribution, pharmacodynamics and pharmacokinetics of insulin analogues in a rat model: Oral delivery using pH-Responsive nanoparticles vs. subcutaneous injection. *Biomaterials*, 31(26), 6849–6858. doi:10.1016/j.biomaterials.2010.05.042
- Sonia, T. A., & Sharma, C. P. (2012). An overview of natural polymers for oral insulin delivery. *Drug Discovery Today*, 17(13-14), 784–792. doi:10.1016/j.drudis.2012.03.019
- Sonwai, S., & Rousseau, D. (2008). Fat crystal growth and microstructural evolution in industrial milk chocolate. *Crystal Growth and Design*, 8, 3165–3174.

doi:10.1021/cg070503h

- Strübing, S., Metz, H., & Mäder, K. (2008). Characterization of poly(vinyl acetate) based floating matrix tablets. *Journal of Controlled Release*, *126*(2), 149–155. doi:10.1016/j.jconrel.2007.11.013
- Svanberg, L., Ahrné, L., Lorén, N., & Windhab, E. (2011a). Effect of pre-crystallization process and solid particle addition on microstructure in chocolate model systems. *Food Research International*, *44*(5), 1339–1350. doi:10.1016/j.foodres.2011.01.018
- Svanberg, L., Ahrné, L., Lorén, N., & Windhab, E. (2011b). Effect of sugar, cocoa particles and lecithin on cocoa butter crystallisation in seeded and non-seeded chocolate model systems. *Journal of Food Engineering*, *104*(1), 70–80. doi:10.1016/j.jfoodeng.2010.09.023
- Svanberg, L., Ahrné, L., Lorén, N., & Windhab, E. (2012). a Method To Assess Changes in Mechanical Properties of Chocolate Confectionery Systems Subjected To Moisture and Fat Migration During Storage. *Journal of Texture Studies*, *43*(2), 106–114. doi:10.1111/j.1745-4603.2011.00320.x
- Svanberg, L., Ahrné, L., Lorén, N., & Windhab, E. (2013). Impact of pre-crystallization process on structure and product properties in dark chocolate. *Journal of Food Engineering*, *114*(1), 90–98. doi:10.1016/j.jfoodeng.2012.06.016
- Svanberg, L., Lorén, N., & Ahrné, L. (2012). Chocolate swelling during storage caused by fat or moisture migration. *Journal of Food Science*, *77*(11), E328–34. doi:10.1111/j.1750-3841.2012.02945.x
- Svanberg, L., Lorén, N., Ahrné, L., & Windhab, E. (2013). Pre-crystallization to control the fat crystal structure and its relation to storage stability in dark chocolate, (April), 9–12.
- Swarbrick, J., Hill, C., & Carolina, N. (2000). *Controlled Drug Delivery* (Vol. 752). doi:10.1021/bk-2000-0752
- Tahtat, D., Mahlous, M., Benamer, S., Khodja, A. N., Oussedik-Oumehdi, H., & Laraba-Djebari, F. (2013). Oral delivery of insulin from alginate/chitosan crosslinked by glutaraldehyde. *International Journal of Biological Macromolecules*, *58*, 160–168. doi:10.1016/j.ijbiomac.2013.03.064
- Tajarobi, F., Abrahmsén-Alami, S., Carlsson, A. S., & Larsson, A. (2009). Simultaneous probing of swelling, erosion and dissolution by NMR-microimaging-Effect of solubility of additives on HPMC matrix tablets. *European Journal of Pharmaceutical Sciences*, *37*(2), 89–97. doi:10.1016/j.ejps.2009.01.008
- Talbot, G. (2010). Bloom and migration. *Confectionery Production*.

- Tirilmasi, A. R. A. Ş. (2013). Mayıs 2013 KAYSER İ.
- Tonyali, B., Cikrikci, S., & Oztop, M. H. (2018). Physicochemical and microstructural characterization of gum tragacanth added whey protein based films. *Food Research International*, *105*, 1–9. doi:10.1016/j.foodres.2017.10.071
- Toro-vazquez, J. F., & Marangoni, A. G. (2004). Effects of Crystalline Microstructure on Oil Migration in a Semisolid Fat Matrix 2004, 4–9.
- Trystram, G. (2012). Modelling of food and food processes. *Journal of Food Engineering*, *110*(2), 269–277. doi:10.1016/j.jfoodeng.2011.05.001
- Tsai, F. H., Kitamura, Y., & Kokawa, M. (2017). Effect of gum arabic-modified alginate on physicochemical properties, release kinetics, and storage stability of liquid-core hydrogel beads. *Carbohydrate Polymers*, *174*, 1069–1077. doi:10.1016/j.carbpol.2017.07.031
- Van Der Weeën, P., De Clercq, N., Baetens, J. M., Delbaere, C., Dewettinck, K., & De Baets, B. (2013). A discrete stochastic model for oil migration in chocolate-coated confectionery. *Journal of Food Engineering*, *119*(3), 602–610. doi:10.1016/j.jfoodeng.2013.06.031
- Van der Weeën, P., De Clercq, N., Baetens, J. M., Delbaere, C., Dewettinck, K., & De Baets, B. (2013). A discrete stochastic model for oil migration in chocolate-coated confectionery. *Journal of Food Engineering*, *119*(3), 602–610. doi:10.1016/j.jfoodeng.2013.06.031
- Viridén, A., Abrahmsén-Alami, S., Wittgren, B., & Larsson, A. (2011). Release of theophylline and carbamazepine from matrix tablets - Consequences of HPMC chemical heterogeneity. *European Journal of Pharmaceutics and Biopharmaceutics*, *78*(3), 470–479. doi:10.1016/j.ejpb.2011.02.003
- Vittadini, E., Dickinson, L. C., & Chinachoti, P. (2002). NMR water mobility in xanthan and locust bean gum mixtures: Possible explanation of microbial response. *Carbohydrate Polymers*, *49*(3), 261–269. doi:10.1016/S0144-8617(01)00330-7
- Walter, P., & Cornillon, P. (2002a). Lipid migration in two-phase chocolate systems investigated by NMR and DSC. *Food Research International*, *35*(8), 761–767. doi:10.1016/S0963-9969(02)00072-8
- Walter, P., & Cornillon, P. (2002b). Lipid migration in two-phase chocolate systems investigated by NMR and DSC §, *35*, 761–767.
- Williams, H. D., Nott, K. P., Barrett, D. A., Ward, R., Hardy, I. J., & Melia, C. D. (2011). Drug release from HPMC matrices in milk and fat-rich emulsions. *Journal of Pharmaceutical Sciences*, *100*(11), 4823–4835. doi:10.1002/jps.22689

- Williams, P. D., Oztop, M. H., McCarthy, M. J., McCarthy, K. L., & Lo, Y. M. (2011). Characterization of water distribution in xanthan-curdlan hydrogel complex using magnetic resonance imaging, nuclear magnetic resonance relaxometry, rheology, and scanning electron microscopy. *Journal of Food Science*, 76(6), E472–8. doi:10.1111/j.1750-3841.2011.02227.x
- Woitiski, C. B., Neufeld, R. J., Ribeiro, A. J., & Veiga, F. (2009). Colloidal carrier integrating biomaterials for oral insulin delivery: Influence of component formulation on physicochemical and biological parameters. *Acta Biomaterialia*, 5(7), 2475–2484. doi:10.1016/j.actbio.2009.03.007
- Wong, T. W. (2010). Design of oral insulin delivery systems. *Journal of Drug Targeting*, 18(2), 79–92. doi:10.3109/10611860903302815
- Xu, M., & Dumont, M. J. (2015). Evaluation of the stability of pea and canola protein-based hydrogels in simulated gastrointestinal fluids. *Journal of Food Engineering*, 165, 52–59. doi:10.1016/j.jfoodeng.2015.04.033
- Yang, H., Li, J. G., Wu, N. F., Fan, M. M., Shen, X. L., Chen, M. T., ... Lai, L. S. (2015). Effect of hsian-tsao gum (HG) content upon rheological properties of film-forming solutions (FFS) and physical properties of soy protein/hsian-tsao gum films. *Food Hydrocolloids*, 50, 211–218. doi:10.1016/j.foodhyd.2015.03.028
- Yang, W. W., & Pierstorff, E. (2012). Reservoir-based polymer drug delivery systems. *Journal of Laboratory Automation*. doi:10.1177/2211068211428189
- Yoon, J. A., Gayathri, C., Gil, R. R., Kowalewski, T., & Matyjaszewski, K. (2010). Comparison of the thermoresponsive deswelling kinetics of poly(2-(2-methoxyethoxy)ethyl methacrylate) hydrogels prepared by ATRP and FRP. *Macromolecules*, 43(10), 4791–4797. doi:10.1021/ma1004953
- Zarzycki, R., Modrzejewska, Z., Nawrotek, K., & Lek, U. (2010). Drug Release From Hydrogel Matrices. *Ecological Chemistry and Engineering S*, 17(2), 117–136.
- Zeeb, B., Saberi, A. H., Weiss, J., & McClements, D. J. (2015). Formation and characterization of filled hydrogel beads based on calcium alginate: Factors influencing nanoemulsion retention and release. *Food Hydrocolloids*, 50, 27–36. doi:10.1016/j.foodhyd.2015.02.041
- Zeng, R., Feng, Z. C., Smith, R., Shao, Z. Z., Chen, X., & Yang, Y. H. (2007). Exploring study of chitosan/glycerophosphate thermosensitive hydrogel with variable-temperature NMR. *Acta Chimica Sinica*, 65(21), 2459–2465.
- Zhang, Y., Wei, W., Lv, P., Wang, L., & Ma, G. (2011). Preparation and evaluation of alginate-chitosan microspheres for oral delivery of insulin. *European Journal of Pharmaceutics and Biopharmaceutics*, 77(1), 11–19. doi:10.1016/j.ejpb.2010.09.016

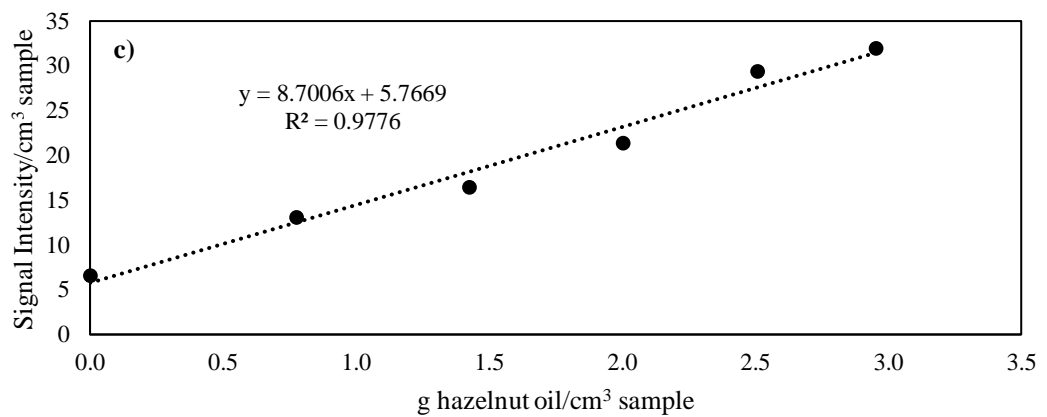
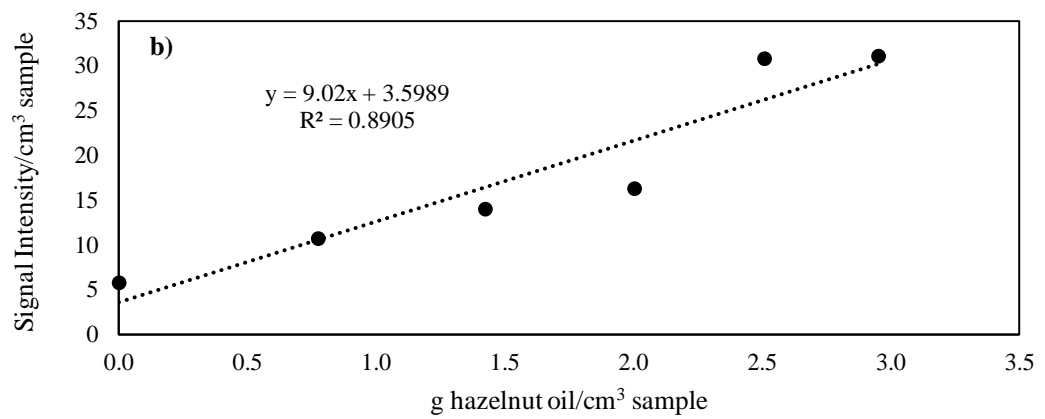
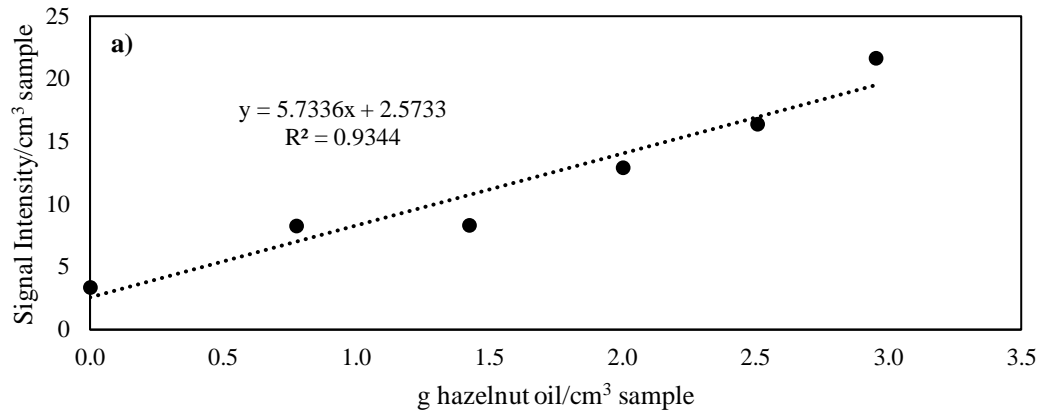
Ziegleder, G. R. (2000). Chocolate Technology. In *Zentralfachschule Deutschen Susswarenwirtschaft*. Cologne.

Ziegleder, G. R. (2009). Product design and shelf life issues: oil migration and fat bloom. In G. Talbot (Ed.), *Technology of coated and filled chocolate, confectionery, bakery products and ice cream, Part II: Product Design* (pp. 185–210). Cambridge, U.K.: Woodhead Publishing.

Ziegler, G. (2009). Product design Product design and shelf-life issues : oil migration and fat bloom. *Science and Technology of Enrobed and Filled Chocolate, Confectionery and Bakery Products*, 185–210. doi:10.1533/9781845696436.2.185

APPENDICES

A. Additional Results for Chocolate System



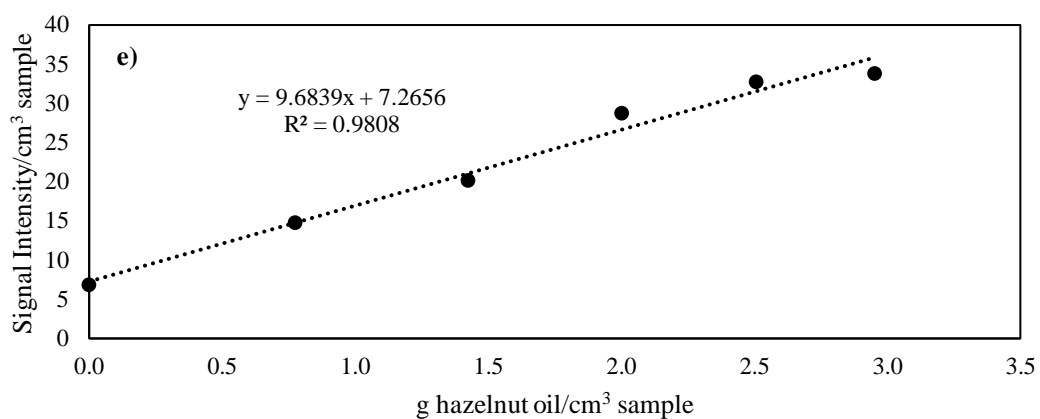
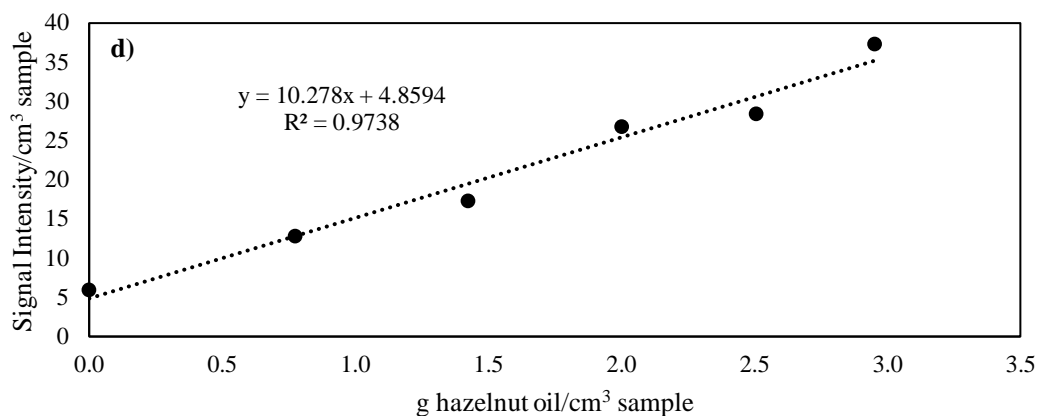


Figure A.1 Calibration curves to relate MR signal intensity to peanut oil content for different chocolate formulations. The coefficients of linear regression were represented. (a) F1 ($y=5.7336x+2.5733$, $R^2 = 0.9344$). (b) F2 ($y=9.02x+3.5989$, $R^2 = 0.8905$). (c) F3 ($y=8.7006x+5.7669$, $R^2 = 0.9776$). (d) F4 ($y=10.278x+4.8594$, $R^2 = 0.9738$). (e) F5 ($y=9.6839x+7.2656$, $R^2 = 0.9808$).

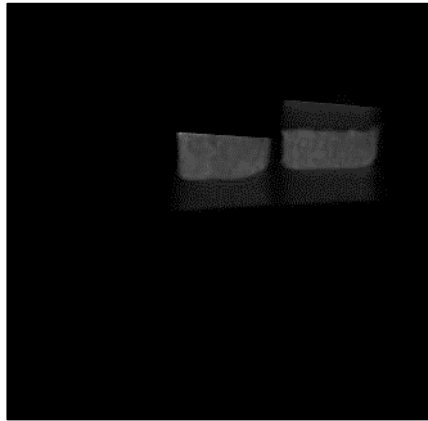
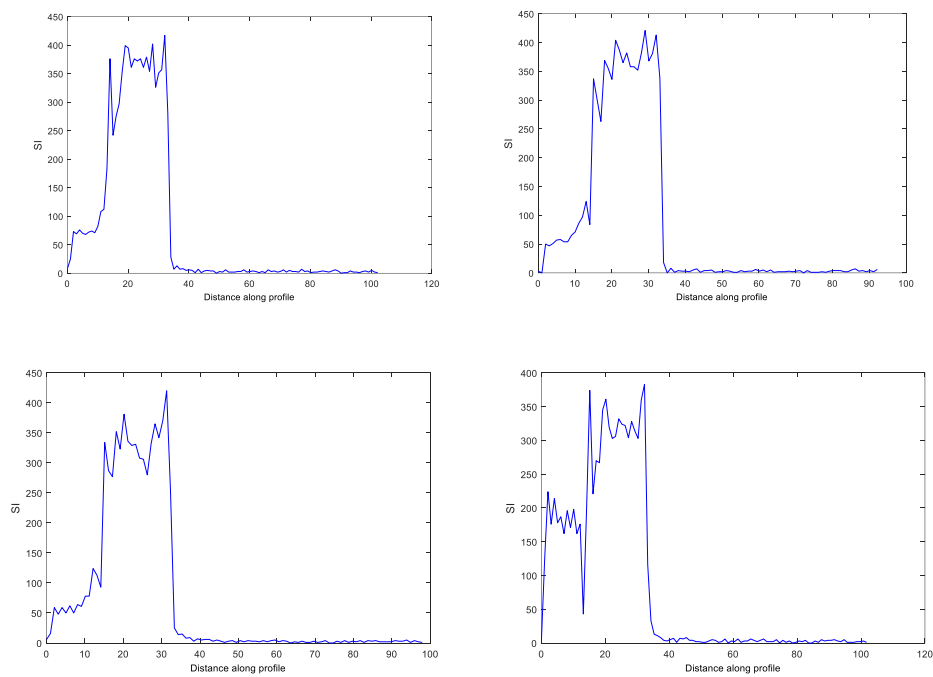


Figure A.2 MR image of chocolate interface in two (left) and three layer system (right).



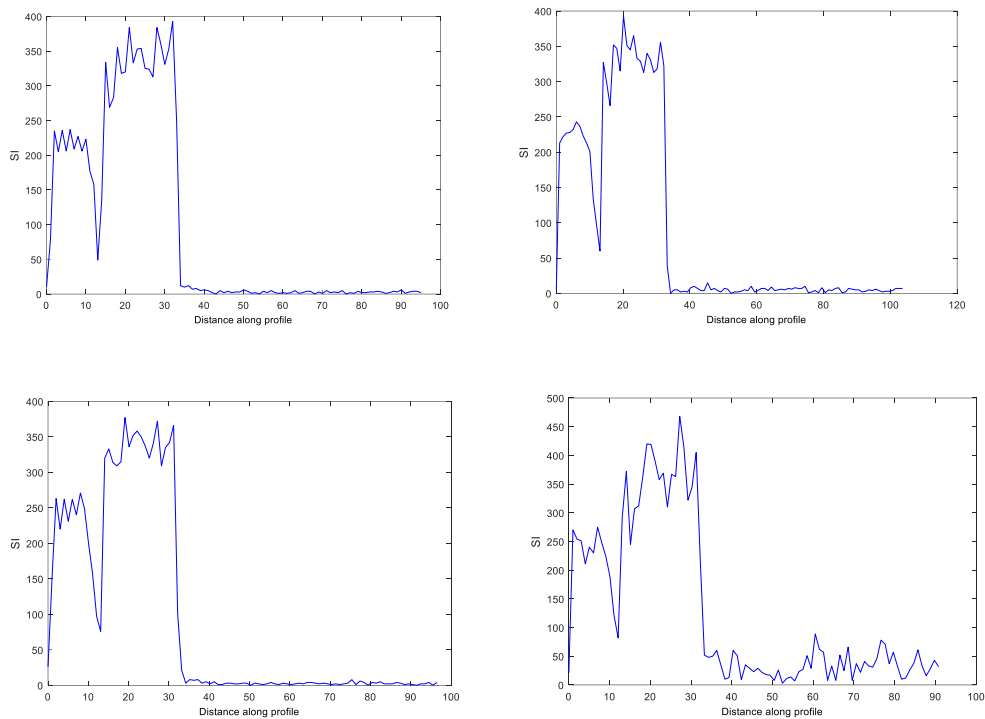
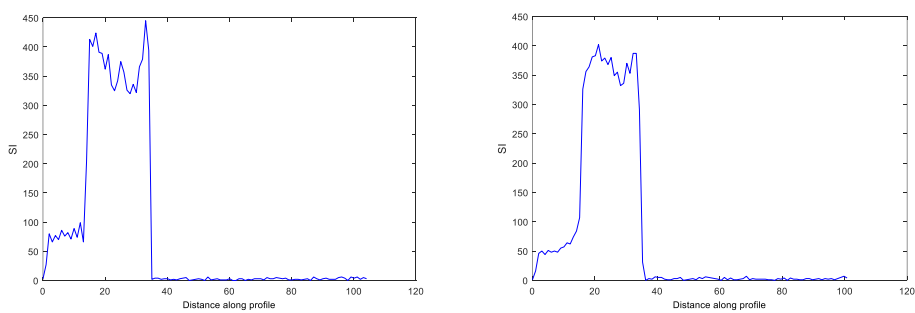


Figure A.3 Representative 1D signal intensity profile for one set of 2-layer chocolate sample F2 stored at 30 °C. (a) at day 1. (b) at day 2. (c) at day 3. (d) at day 4. (e) at day 5. (f) at day 11. (g) at day 15. (h) at day 22. HP: hazelnut paste. CH: chocolate. HO: hazelnut oil.



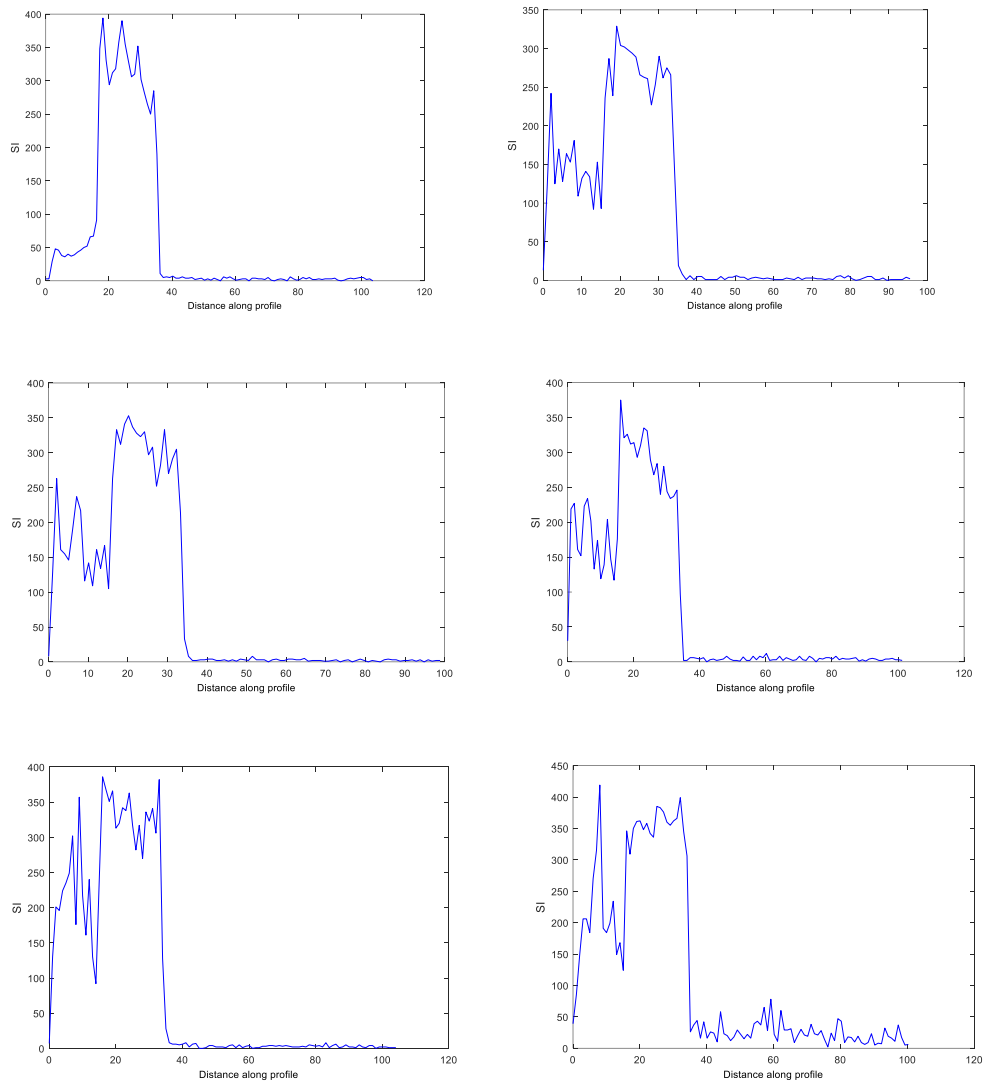


Figure A.4 Representative 1D signal intensity profile for one set of 2-layer chocolate sample F3 stored at 30 °C. (a) at day 1. (b) at day 2. (c) at day 3. (d) at day 4. (e) at day 5. (f) at day 11. (g) at day 15. (h) at day 22. HP: hazelnut paste. CH: chocolate. HO: hazelnut oil.

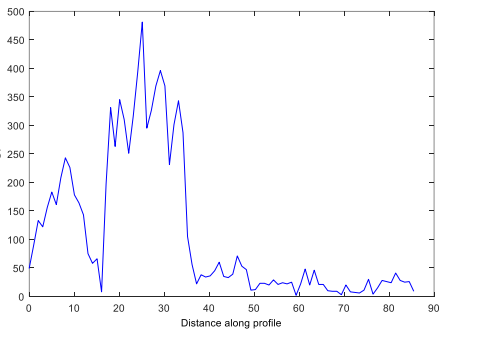
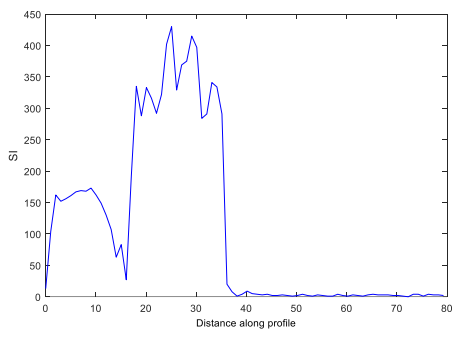
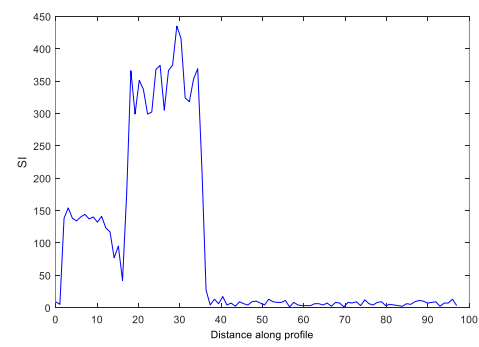
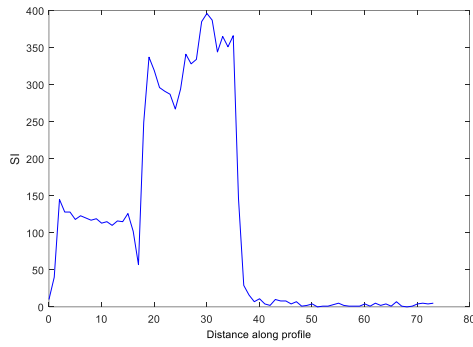
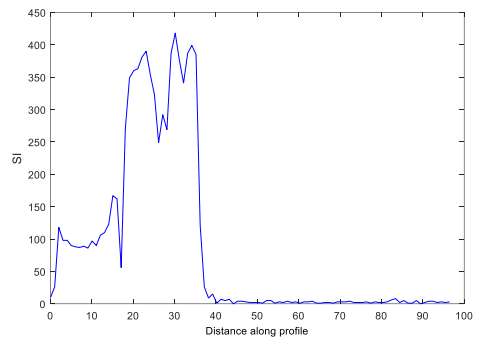
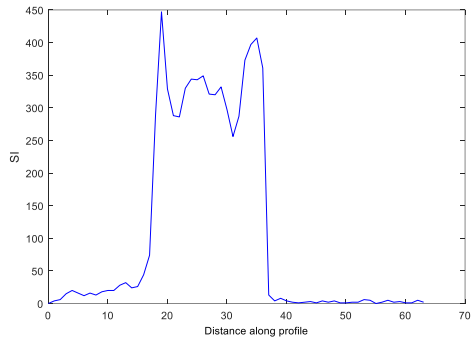
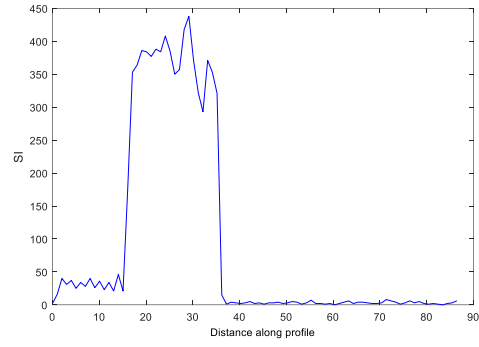
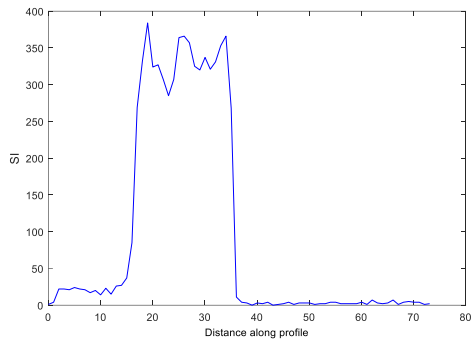
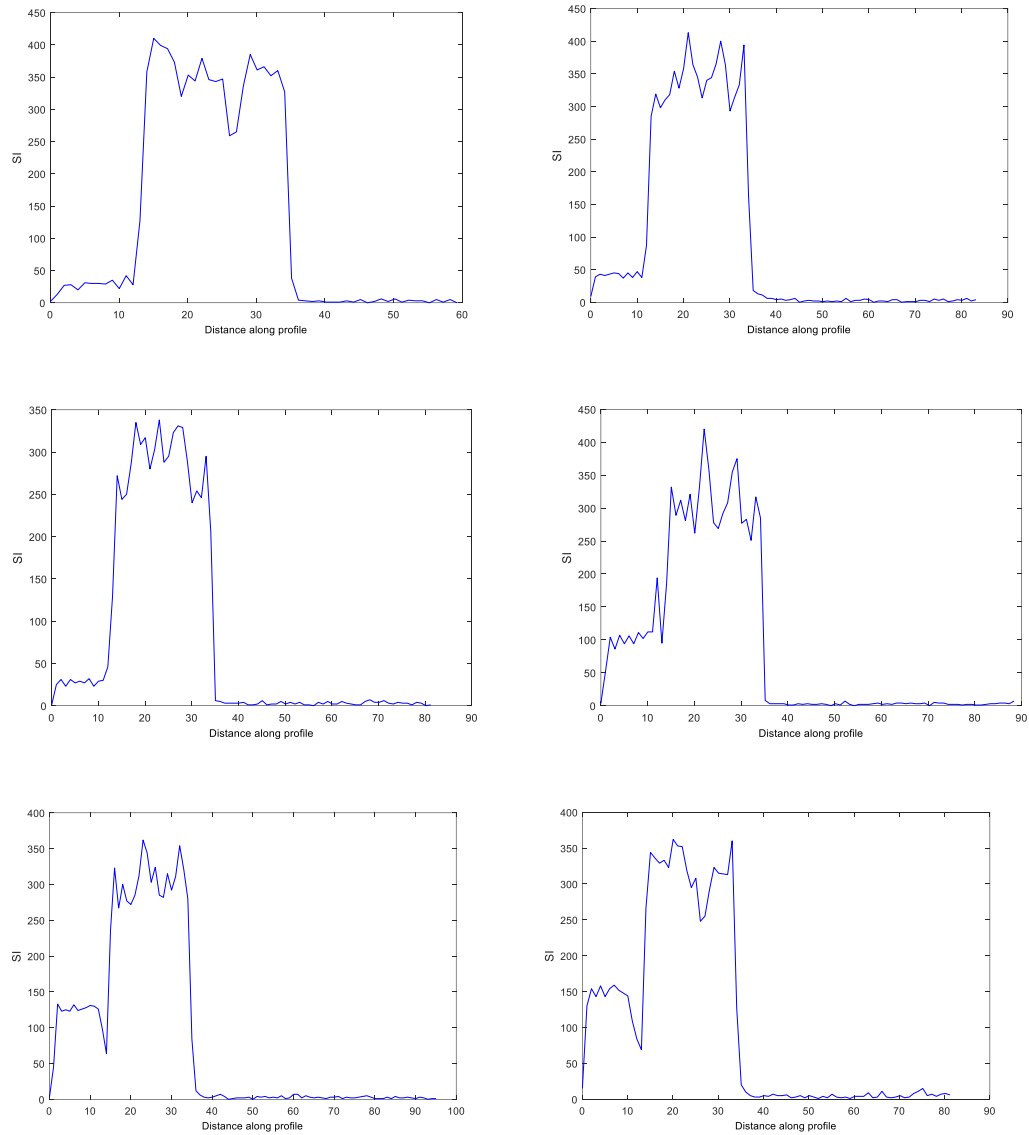


Figure A.5 Representative 1D signal intensity profile for one set of 2-layer chocolate sample F4 stored at 30 °C. (a) at day 1. (b) at day 2. (c) at day 3. (d) at day 4. (e) at day 5. (f) at day 11. (g) at day 15. (h) at day 22. HP: hazelnut paste. CH: chocolate. HO: hazelnut oil.



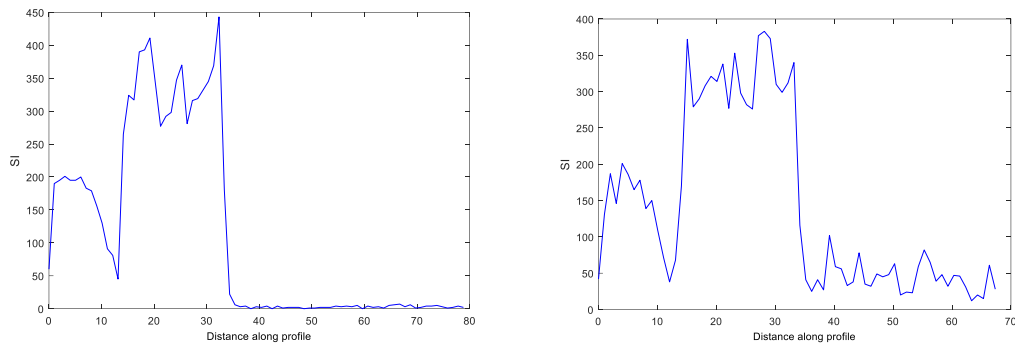


Figure A.6 Representative 1D signal intensity profile for one set of 2-layer chocolate sample F5 stored at 30 °C. (a) at day 1. (b) at day 2. (c) at day 3. (d) at day 4. (e) at day 5. (f) at day 11. (g) at day 15. (h) at day 22. HP: hazelnut paste. CH: chocolate. HO: hazelnut oil.

B. Statistical Analysis

Table B.1 Results for Tukey’s mean comparison test for model 1 constants of two layer chocolate systems

One-way ANOVA: D versus formulation

Source	DF	SS	MS	F	P
formulation	4	11,35	2,84	1,87	0,168
Error	15	22,72	1,51		
Total	19	34,07			

S = 1,231 R-Sq = 33,31% R-Sq(adj) = 15,52%

Individual 95% CIs For Mean Based on Pooled StDev

Level	N	Mean	StDev
1	4	2,542	1,546
2	4	1,382	0,321
3	4	0,647	0,237
4	4	2,265	0,680
5	4	2,574	2,136

0,0 1,2 2,4 3,6

Pooled StDev = 1,231

Grouping Information Using Tukey Method

formulation	N	Mean	Grouping
1	4	2,542	
2	4	1,382	
3	4	0,647	
4	4	2,265	
5	4	2,574	

5	4	2,574	A
1	4	2,542	A
4	4	2,265	A
2	4	1,382	A
3	4	0,647	A

Means that do not share a letter are significantly different.

Tukey 95% Simultaneous Confidence Intervals
All Pairwise Comparisons among Levels of formulation

Individual confidence level = 99,25%

formulation = 1 subtracted from:

formulation	Lower	Center	Upper	
2	-3,849	-1,160	1,529	(-----*-----)
3	-4,584	-1,895	0,794	(-----*-----)
4	-2,966	-0,276	2,413	(-----*-----)
5	-2,657	0,032	2,721	(-----*-----)

-----+-----+-----+-----
+-
-2,5 0,0 2,5 5,0

formulation = 2 subtracted from:

formulation	Lower	Center	Upper	
3	-3,424	-0,735	1,954	(-----*-----)
4	-1,806	0,884	3,573	(-----*-----)
5	-1,497	1,192	3,881	(-----*-----)

-----+-----+-----+-----
+-
-2,5 0,0 2,5 5,0

formulation = 3 subtracted from:

formulation	Lower	Center	Upper	
4	-1,071	1,619	4,308	(-----*-----)
5	-0,762	1,927	4,616	(-----*-----)

-----+-----+-----+-----
+-
-2,5 0,0 2,5 5,0

formulation = 4 subtracted from:

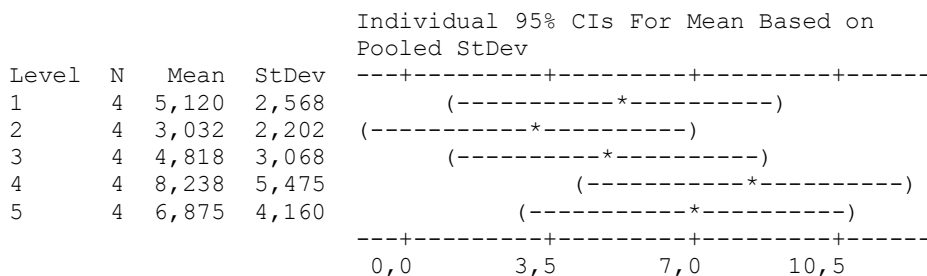
formulation	Lower	Center	Upper	
5	-2,380	0,309	2,998	(-----*-----)

-----+-----+-----+-----
+-
-2,5 0,0 2,5 5,0

One-way ANOVA: Co versus formulation

Source	DF	SS	MS	F	P
formulation	4	64,1	16,0	1,18	0,361
Error	15	204,4	13,6		
Total	19	268,5			

S = 3,691 R-Sq = 23,86% R-Sq(adj) = 3,56%



Pooled StDev = 3,691

Grouping Information Using Tukey Method

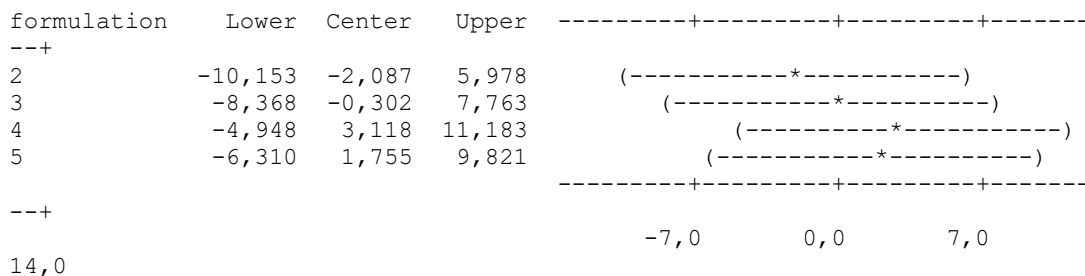
formulation	N	Mean	Grouping
4	4	8,238	A
5	4	6,875	A
1	4	5,120	A
3	4	4,818	A
2	4	3,032	A

Means that do not share a letter are significantly different.

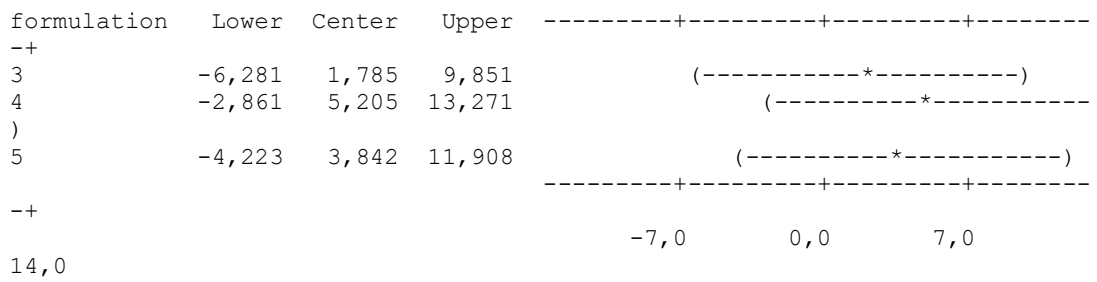
Tukey 95% Simultaneous Confidence Intervals All Pairwise Comparisons among Levels of formulation

Individual confidence level = 99,25%

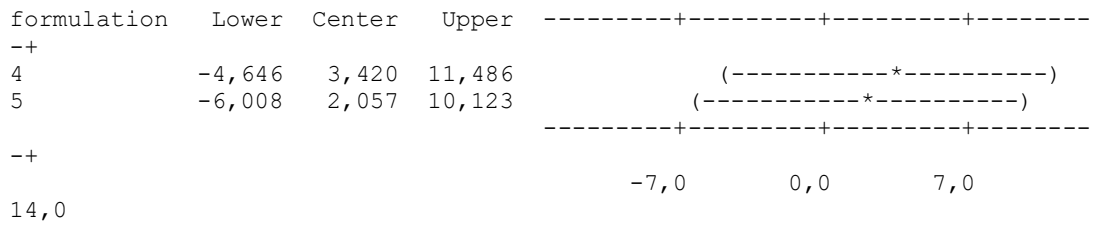
formulation = 1 subtracted from:



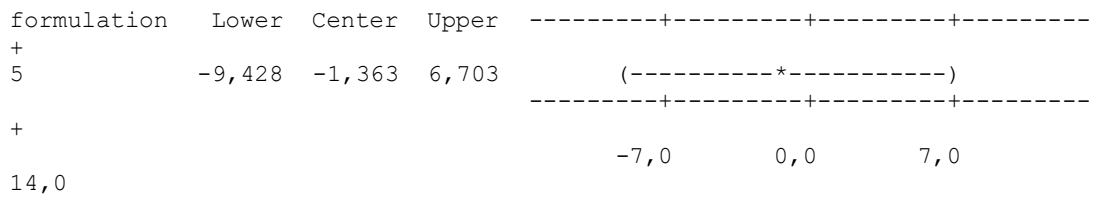
formulation = 2 subtracted from:



formulation = 3 subtracted from:



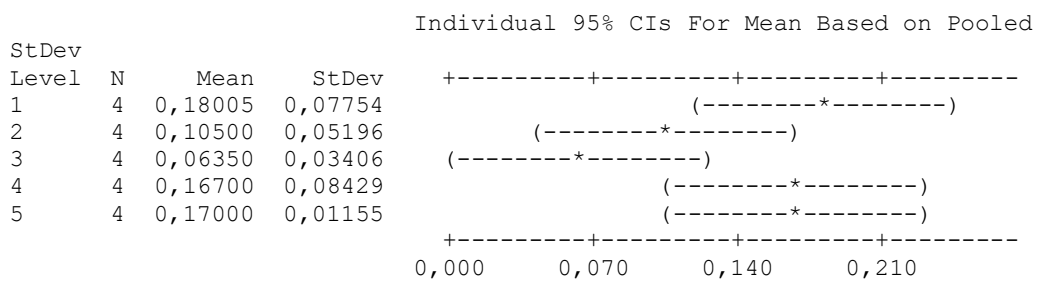
formulation = 4 subtracted from:



One-way ANOVA: b versus formulation

Source	DF	SS	MS	F	P
formulation	4	0,04107	0,01027	3,00	0,053
Error	15	0,05133	0,00342		
Total	19	0,09241			

S = 0,05850 R-Sq = 44,45% R-Sq(adj) = 29,64%



Pooled StDev = 0,05850

Grouping Information Using Tukey Method

formulation	N	Mean	Grouping
1	4	0,18005	A
5	4	0,17000	A
4	4	0,16700	A
2	4	0,10500	A
3	4	0,06350	A

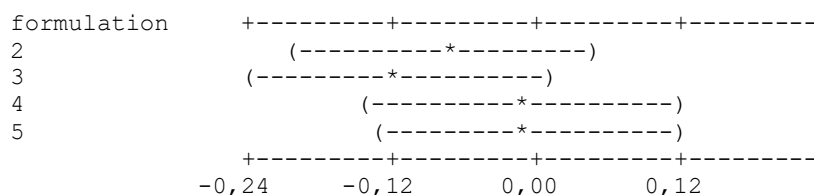
Means that do not share a letter are significantly different.

Tukey 95% Simultaneous Confidence Intervals
All Pairwise Comparisons among Levels of formulation

Individual confidence level = 99,25%

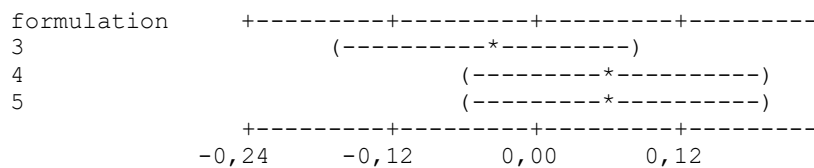
formulation = 1 subtracted from:

formulation	Lower	Center	Upper
2	-0,20287	-0,07505	0,05277
3	-0,24437	-0,11655	0,01127
4	-0,14087	-0,01305	0,11477
5	-0,13787	-0,01005	0,11777



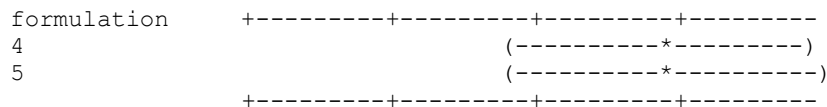
formulation = 2 subtracted from:

formulation	Lower	Center	Upper
3	-0,16932	-0,04150	0,08632
4	-0,06582	0,06200	0,18982
5	-0,06282	0,06500	0,19282



formulation = 3 subtracted from:

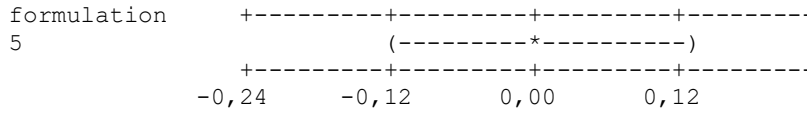
formulation	Lower	Center	Upper
4	-0,02432	0,10350	0,23132
5	-0,02132	0,10650	0,23432



-0,24 -0,12 0,00 0,12

formulation = 4 subtracted from:

formulation	Lower	Center	Upper
5	-0,12482	0,00300	0,13082

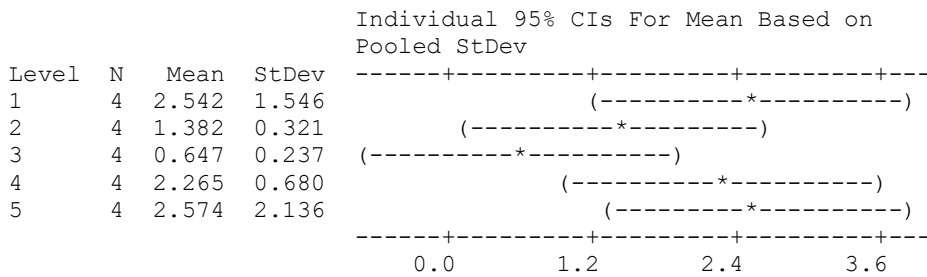


Box-Cox Plot of D

One-way ANOVA: D versus formulation

Source	DF	SS	MS	F	P
formulation	4	11.35	2.84	1.87	0.168
Error	15	22.72	1.51		
Total	19	34.07			

S = 1.231 R-Sq = 33.31% R-Sq(adj) = 15.52%



Pooled StDev = 1.231

Grouping Information Using Tukey Method

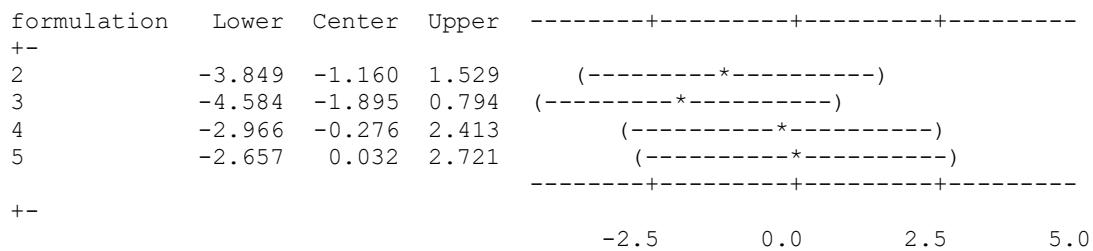
formulation	N	Mean	Grouping
5	4	2.574	A
1	4	2.542	A
4	4	2.265	A
2	4	1.382	A
3	4	0.647	A

Means that do not share a letter are significantly different.

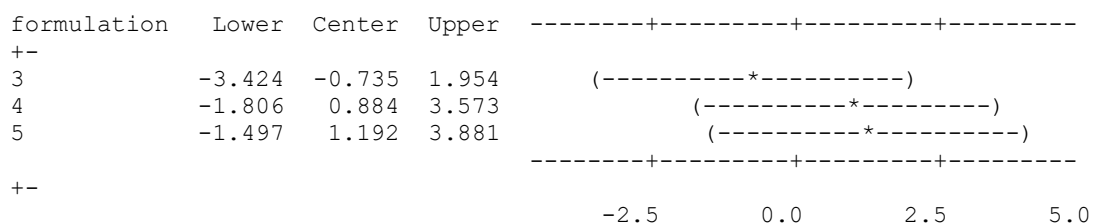
Tukey 95% Simultaneous Confidence Intervals
All Pairwise Comparisons among Levels of formulation

Individual confidence level = 99.25%

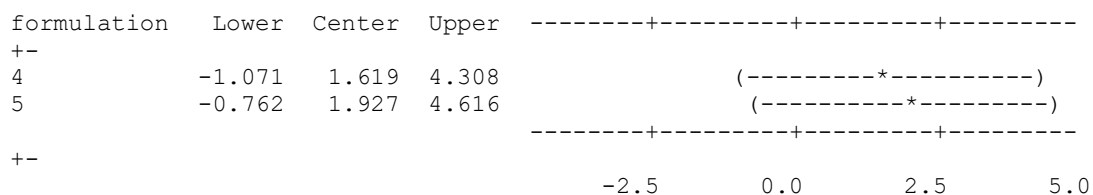
formulation = 1 subtracted from:



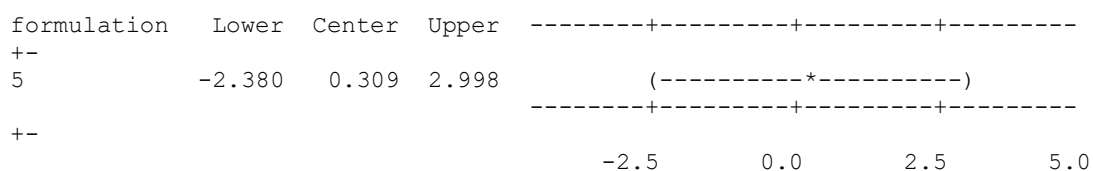
formulation = 2 subtracted from:



formulation = 3 subtracted from:



formulation = 4 subtracted from:



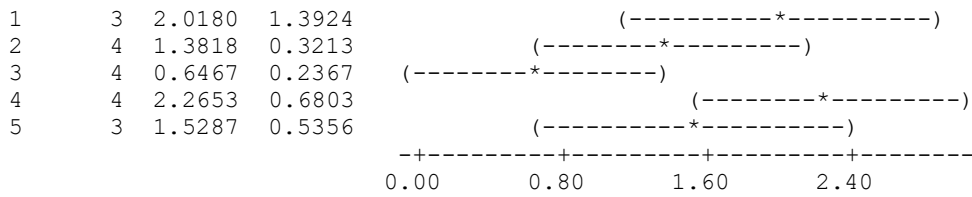
One-way ANOVA: D versus formulation

Source	DF	SS	MS	F	P
formulation	4	6.081	1.520	3.13	0.052
Error	13	6.318	0.486		
Total	17	12.399			

S = 0.6971 R-Sq = 49.05% R-Sq(adj) = 33.37%

Individual 95% CIs For Mean Based on Pooled StDev

Level	N	Mean	StDev



Pooled StDev = 0.6971

Grouping Information Using Tukey Method

formulation	N	Mean	Grouping
4	4	2.2653	A
1	3	2.0180	A B
5	3	1.5287	A B
2	4	1.3818	A B
3	4	0.6467	B

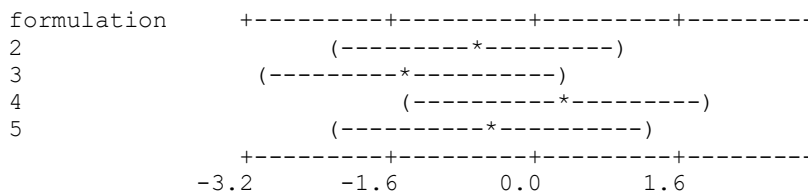
Means that do not share a letter are significantly different.

Tukey 95% Simultaneous Confidence Intervals
All Pairwise Comparisons among Levels of formulation

Individual confidence level = 99.23%

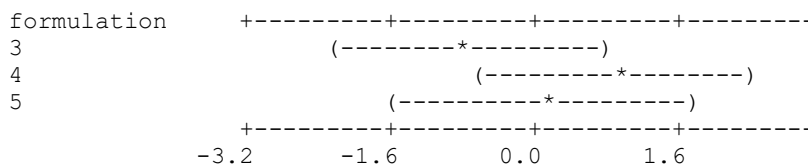
formulation = 1 subtracted from:

formulation	Lower	Center	Upper
2	-2.3116	-0.6363	1.0391
3	-3.0466	-1.3713	0.3041
4	-1.4281	0.2472	1.9226
5	-2.2804	-0.4893	1.3017



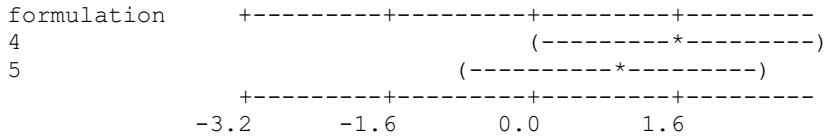
formulation = 2 subtracted from:

formulation	Lower	Center	Upper
3	-2.2861	-0.7350	0.8161
4	-0.6676	0.8835	2.4346
5	-1.5284	0.1469	1.8223



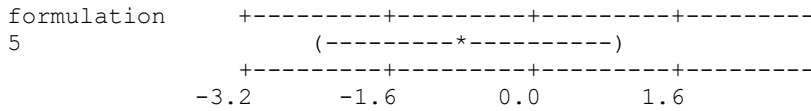
formulation = 3 subtracted from:

formulation	Lower	Center	Upper
4	0.0674	1.6185	3.1696
5	-0.7934	0.8819	2.5573



formulation = 4 subtracted from:

formulation	Lower	Center	Upper
5	-2.4119	-0.7366	0.9388



Test for Equal Variances: D versus formulation

95% Bonferroni confidence intervals for standard deviations

formulation	N	Lower	StDev	Upper
1	3	0.604922	1.39241	19.6671
2	4	0.155314	0.32129	2.0780
3	4	0.114413	0.23668	1.5307
4	4	0.328871	0.68032	4.4000
5	3	0.232673	0.53557	7.5646

Bartlett's Test (Normal Distribution)
Test statistic = 8.24, p-value = 0.083

Levene's Test (Any Continuous Distribution)
Test statistic = 0.96, p-value = 0.463

Test for Equal Variances: D versus formulation

Regression Analysis: D versus formulation

The regression equation is
 $D = 1.49 + 0.019 \text{ formulation}$

18 cases used, 2 cases contain missing values

Predictor	Coef	SE Coef	T	P
Constant	1.4892	0.5106	2.92	0.010

formulation 0.0187 0.1555 0.12 0.906

S = 0.879895 R-Sq = 0.1% R-Sq(adj) = 0.0%

Analysis of Variance

Source	DF	SS	MS	F	P
Regression	1	0.0112	0.0112	0.01	0.906
Residual Error	16	12.3874	0.7742		
Total	17	12.3986			

Unusual Observations

Obs	formulation	D	Fit	SE Fit	Residual	St Resid
2	1.00	3.613	1.508	0.374	2.105	2.64R

R denotes an observation with a large standardized residual.

Residual Plots for D

Regression Analysis: D versus formulation

The regression equation is
 $D = 1.49 + 0.019 \text{ formulation}$

18 cases used, 2 cases contain missing values

Predictor	Coef	SE Coef	T	P
Constant	1.4892	0.5106	2.92	0.010
formulation	0.0187	0.1555	0.12	0.906

S = 0.879895 R-Sq = 0.1% R-Sq(adj) = 0.0%

Analysis of Variance

Source	DF	SS	MS	F	P
Regression	1	0.0112	0.0112	0.01	0.906
Residual Error	16	12.3874	0.7742		
Total	17	12.3986			

Unusual Observations

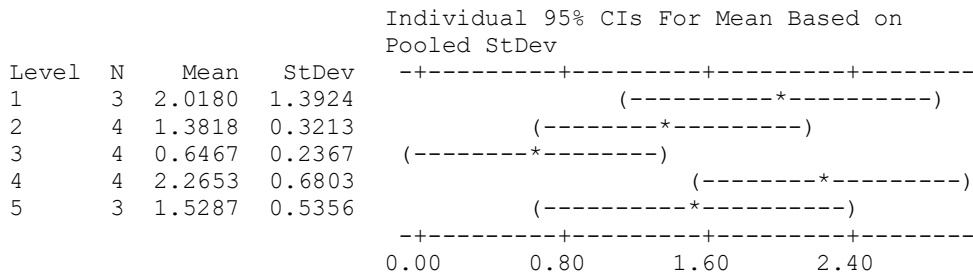
Obs	formulation	D	Fit	SE Fit	Residual	St Resid
2	1.00	3.613	1.508	0.374	2.105	2.64R

R denotes an observation with a large standardized residual.

One-way ANOVA: D versus formulation

Source	DF	SS	MS	F	P
formulation	4	6.081	1.520	3.13	0.052
Error	13	6.318	0.486		
Total	17	12.399			

S = 0.6971 R-Sq = 49.05% R-Sq(adj) = 33.37%



Pooled StDev = 0.6971

Grouping Information Using Tukey Method

formulation	N	Mean	Grouping
4	4	2.2653	A
1	3	2.0180	A B
5	3	1.5287	A B
2	4	1.3818	A B
3	4	0.6467	B

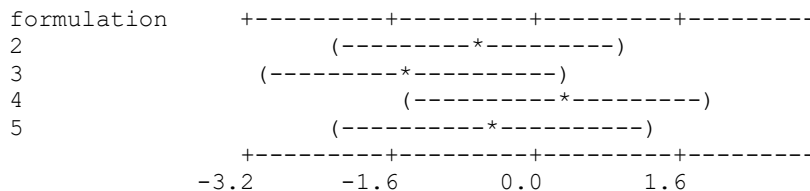
Means that do not share a letter are significantly different.

Tukey 95% Simultaneous Confidence Intervals All Pairwise Comparisons among Levels of formulation

Individual confidence level = 99.23%

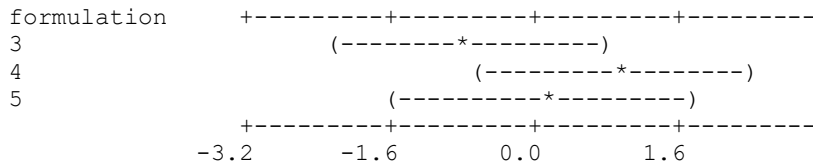
formulation = 1 subtracted from:

formulation	Lower	Center	Upper
2	-2.3116	-0.6363	1.0391
3	-3.0466	-1.3713	0.3041
4	-1.4281	0.2472	1.9226
5	-2.2804	-0.4893	1.3017



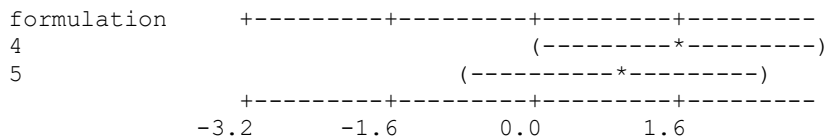
formulation = 2 subtracted from:

formulation	Lower	Center	Upper
3	-2.2861	-0.7350	0.8161
4	-0.6676	0.8835	2.4346
5	-1.5284	0.1469	1.8223



formulation = 3 subtracted from:

formulation	Lower	Center	Upper
4	0.0674	1.6185	3.1696
5	-0.7934	0.8819	2.5573



formulation = 4 subtracted from:

formulation	Lower	Center	Upper
5	-2.4119	-0.7366	0.9388

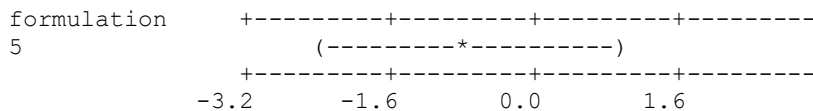
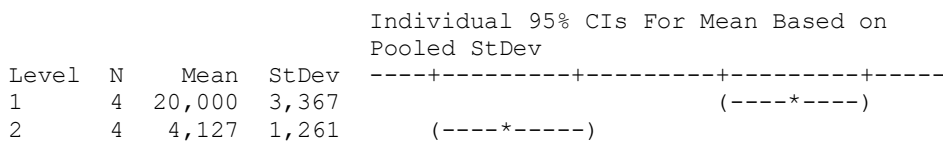


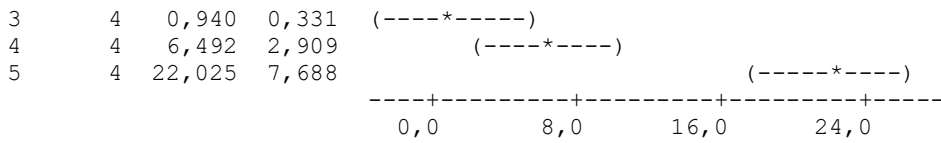
Table B.2 Results for Tukey's mean comparison test for model 2 constants of two layer chocolate systems

One-way ANOVA: D versus formulation

Source	DF	SS	MS	F	P
formulation	4	1483,6	370,9	23,01	0,000
Error	15	241,8	16,1		
Total	19	1725,4			

S = 4,015 R-Sq = 85,99% R-Sq(adj) = 82,25%





Pooled StDev = 4,015

Grouping Information Using Tukey Method

formulation	N	Mean	Grouping
5	4	22,025	A
1	4	20,000	A
4	4	6,492	B
2	4	4,127	B
3	4	0,940	B

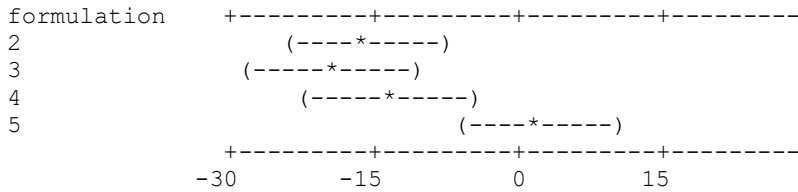
Means that do not share a letter are significantly different.

Tukey 95% Simultaneous Confidence Intervals
All Pairwise Comparisons among Levels of formulation

Individual confidence level = 99,25%

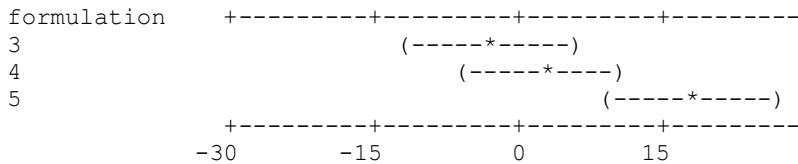
formulation = 1 subtracted from:

formulation	Lower	Center	Upper
2	-24,645	-15,873	-7,100
3	-27,832	-19,060	-10,288
4	-22,280	-13,508	-4,735
5	-6,747	2,025	10,797



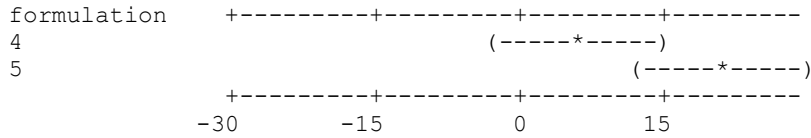
formulation = 2 subtracted from:

formulation	Lower	Center	Upper
3	-11,960	-3,188	5,585
4	-6,407	2,365	11,137
5	9,125	17,898	26,670

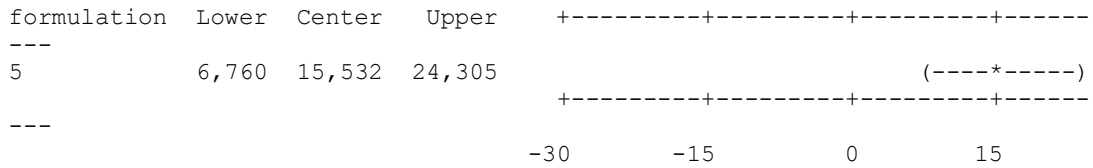


formulation = 3 subtracted from:

formulation	Lower	Center	Upper
4	-3,220	5,553	14,325
5	12,313	21,085	29,857



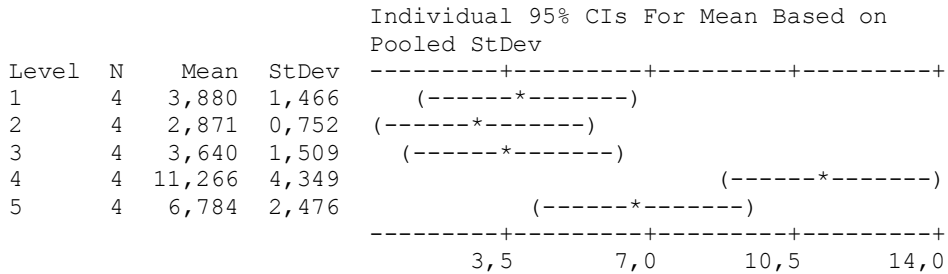
formulation = 4 subtracted from:



One-way ANOVA: Co versus formulation

Source	DF	SS	MS	F	P
formulation	4	190,89	47,72	7,94	0,001
Error	15	90,12	6,01		
Total	19	281,01			

S = 2,451 R-Sq = 67,93% R-Sq(adj) = 59,38%



Pooled StDev = 2,451

Grouping Information Using Tukey Method

formulation	N	Mean	Grouping
4	4	11,266	A
5	4	6,784	A B
1	4	3,880	B
3	4	3,640	B
2	4	2,871	B

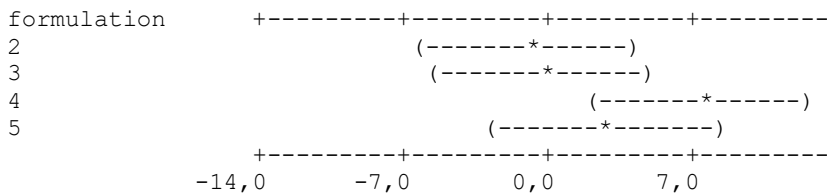
Means that do not share a letter are significantly different.

Tukey 95% Simultaneous Confidence Intervals
All Pairwise Comparisons among Levels of formulation

Individual confidence level = 99,25%

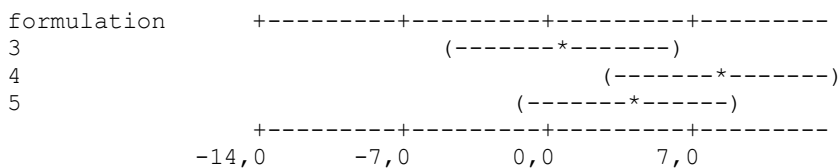
formulation = 1 subtracted from:

formulation	Lower	Center	Upper
2	-6,365	-1,009	4,347
3	-5,596	-0,240	5,116
4	2,031	7,387	12,742
5	-2,451	2,904	8,260



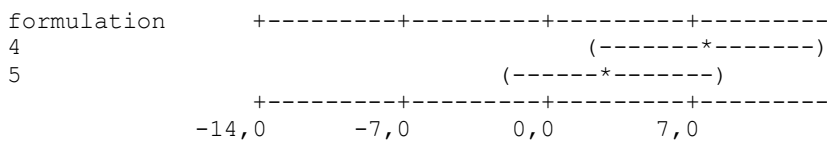
formulation = 2 subtracted from:

formulation	Lower	Center	Upper
3	-4,587	0,769	6,125
4	3,040	8,396	13,751
5	-1,443	3,913	9,269



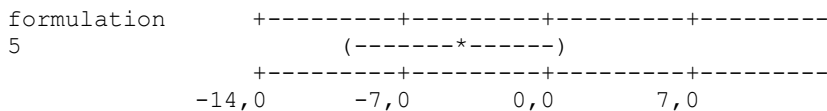
formulation = 3 subtracted from:

formulation	Lower	Center	Upper
4	2,271	7,627	12,982
5	-2,211	3,144	8,500



formulation = 4 subtracted from:

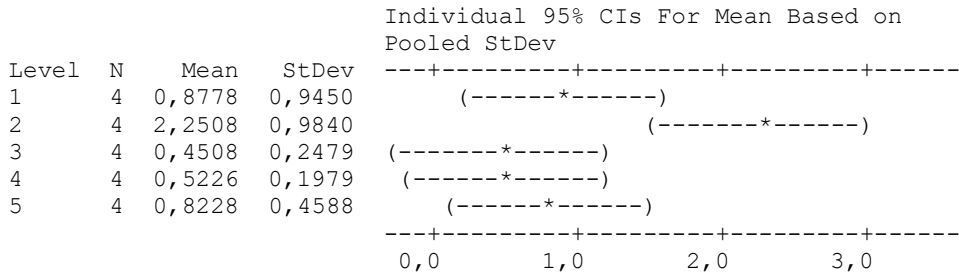
formulation	Lower	Center	Upper
5	-9,838	-4,482	0,873



One-way ANOVA: b versus formulation

Source	DF	SS	MS	F	P
formulation	4	8,557	2,139	4,92	0,010
Error	15	6,517	0,434		
Total	19	15,074			

S = 0,6591 R-Sq = 56,77% R-Sq(adj) = 45,24%



Pooled StDev = 0,6591

Grouping Information Using Tukey Method

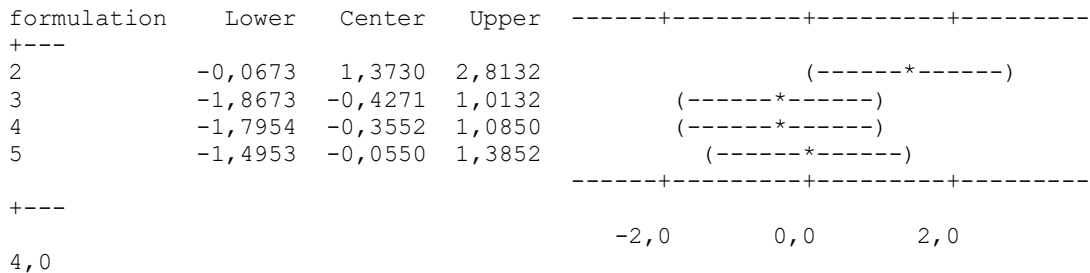
formulation	N	Mean	Grouping
2	4	2,2508	A
1	4	0,8778	A B
5	4	0,8228	A B
4	4	0,5226	B
3	4	0,4508	B

Means that do not share a letter are significantly different.

Tukey 95% Simultaneous Confidence Intervals
All Pairwise Comparisons among Levels of formulation

Individual confidence level = 99,25%

formulation = 1 subtracted from:



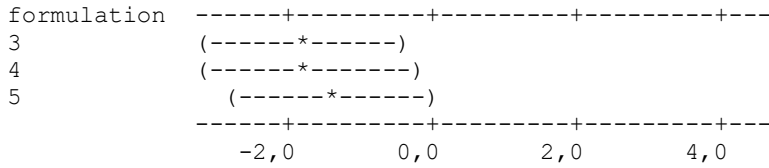
formulation = 2 subtracted from:

formulation	Lower	Center	Upper
-------------	-------	--------	-------

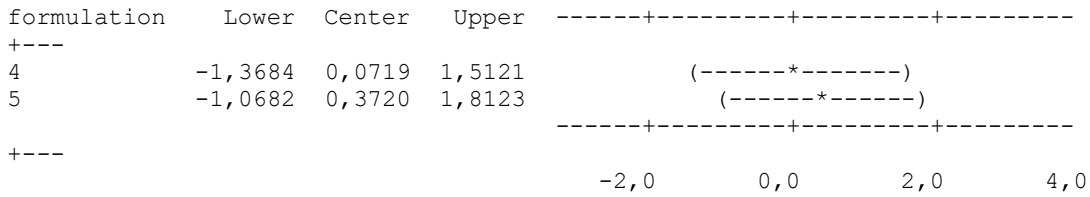
```

3      -3,2403  -1,8001  -0,3598
4      -3,1684  -1,7282  -0,2879
5      -2,8683  -1,4280   0,0122

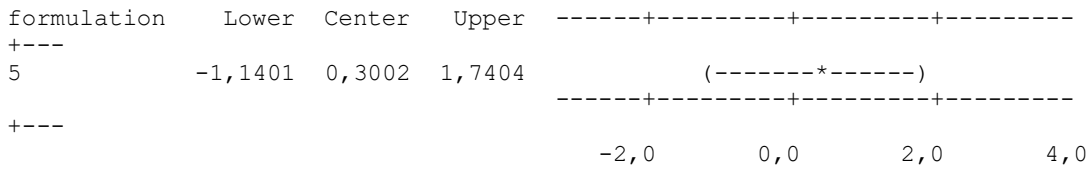
```



formulation = 3 subtracted from:



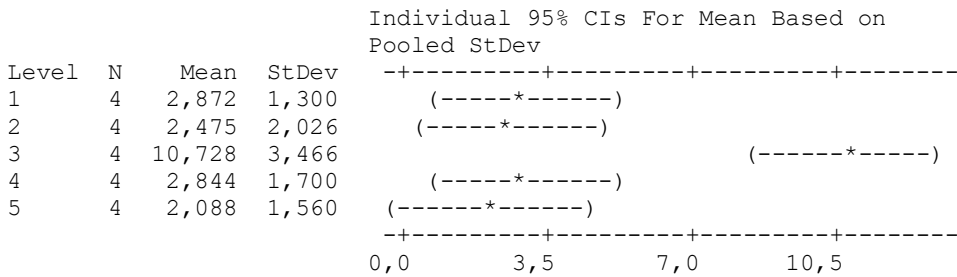
formulation = 4 subtracted from:



One-way ANOVA: to versus formulation

Source	DF	SS	MS	F	P
formulation	4	214,59	53,65	11,60	0,000
Error	15	69,39	4,63		
Total	19	283,98			

S = 2,151 R-Sq = 75,57% R-Sq(adj) = 69,05%



Pooled StDev = 2,151

Grouping Information Using Tukey Method

formulation	N	Mean	Grouping
3	4	10,728	A
1	4	2,872	B
4	4	2,844	B
2	4	2,475	B
5	4	2,088	B

Means that do not share a letter are significantly different.

Tukey 95% Simultaneous Confidence Intervals
All Pairwise Comparisons among Levels of formulation

Individual confidence level = 99,25%

formulation = 1 subtracted from:

formulation	Lower	Center	Upper	
-+				-----+-----+-----+-----
2	-5,097	-0,397	4,302	(-----*-----)
3	3,156	7,855	12,555	(-----*-----)
4	-4,728	-0,029	4,671	(-----*-----)
5	-5,483	-0,784	3,915	(-----*-----)
-+				-----+-----+-----+-----
14,0				-7,0 0,0 7,0

formulation = 2 subtracted from:

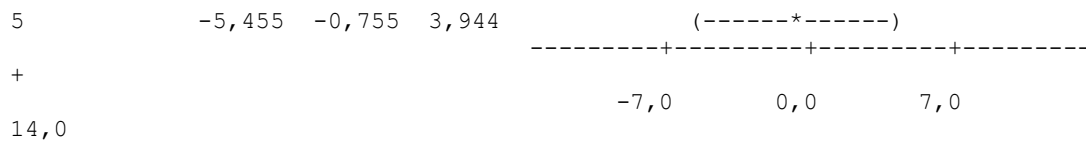
formulation	Lower	Center	Upper	
-+				-----+-----+-----+-----
3	3,553	8,253	12,952	(-----*-----)
4	-4,330	0,369	5,068	(-----*-----)
5	-5,086	-0,386	4,313	(-----*-----)
-+				-----+-----+-----+-----
14,0				-7,0 0,0 7,0

formulation = 3 subtracted from:

formulation	Lower	Center	Upper	
--+				-----+-----+-----+-----
4	-12,583	-7,884	-3,184	(-----*-----)
5	-13,339	-8,639	-3,940	(-----*-----)
--+				-----+-----+-----+-----
14,0				-7,0 0,0 7,0

formulation = 4 subtracted from:

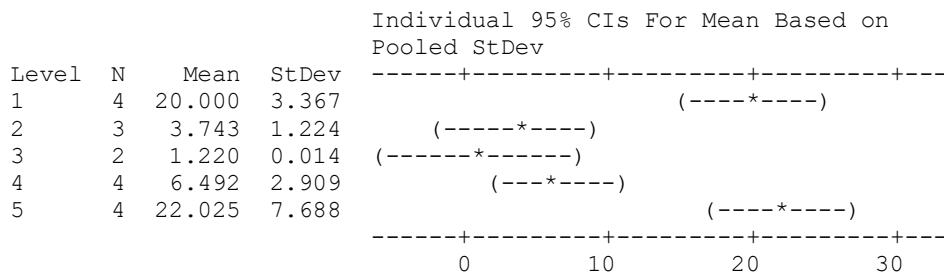
formulation	Lower	Center	Upper	
+				-----+-----+-----+-----



One-way ANOVA: D versus formulation

Source	DF	SS	MS	F	P
formulation	4	1215.4	303.9	15.21	0.000
Error	12	239.7	20.0		
Total	16	1455.1			

S = 4.469 R-Sq = 83.53% R-Sq(adj) = 78.04%



Pooled StDev = 4.469

Grouping Information Using Tukey Method

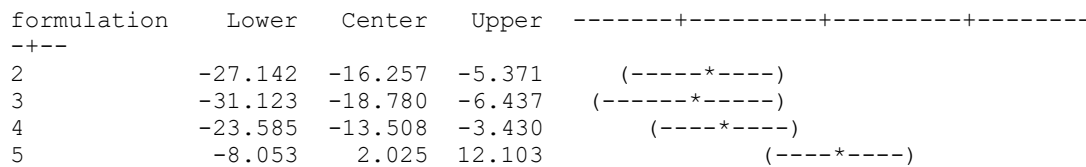
formulation	N	Mean	Grouping
5	4	22.025	A
1	4	20.000	A
4	4	6.492	B
2	3	3.743	B
3	2	1.220	B

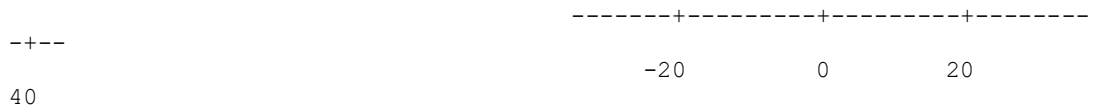
Means that do not share a letter are significantly different.

Tukey 95% Simultaneous Confidence Intervals All Pairwise Comparisons among Levels of formulation

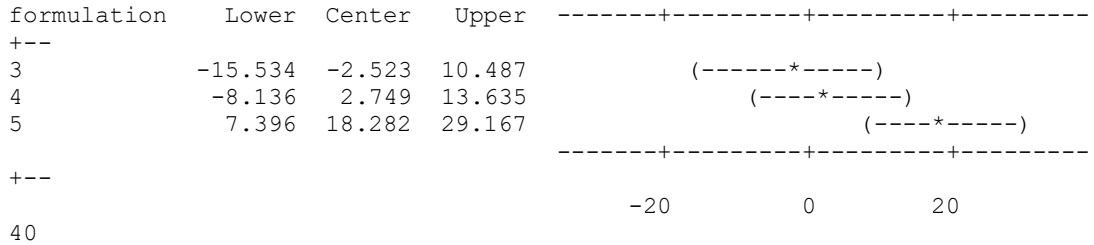
Individual confidence level = 99.22%

formulation = 1 subtracted from:

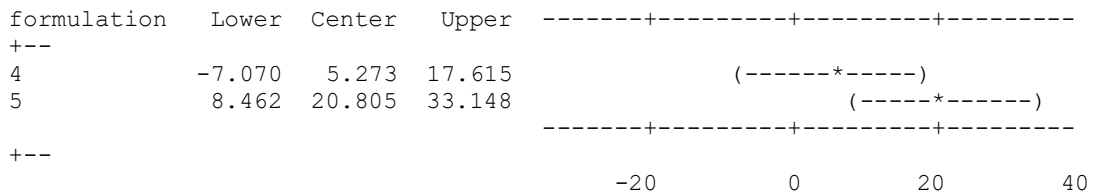




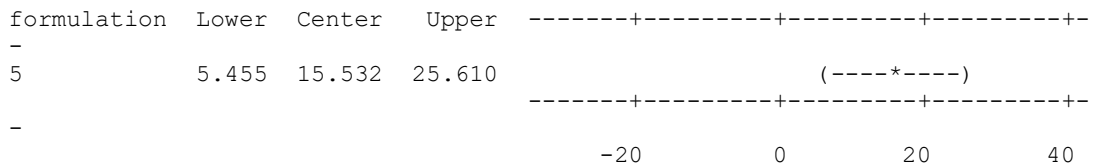
formulation = 2 subtracted from:



formulation = 3 subtracted from:



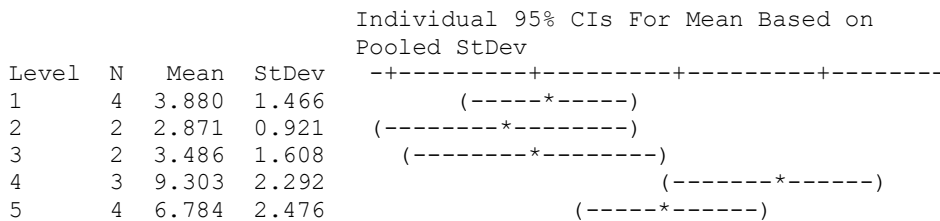
formulation = 4 subtracted from:

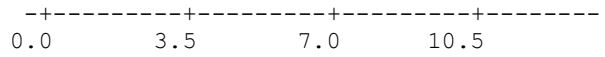


One-way ANOVA: Co versus formulation

Source	DF	SS	MS	F	P
formulation	4	82.39	20.60	5.31	0.015
Error	10	38.79	3.88		
Total	14	121.18			

S = 1.970 R-Sq = 67.99% R-Sq(adj) = 55.18%





Pooled StDev = 1.970

Grouping Information Using Tukey Method

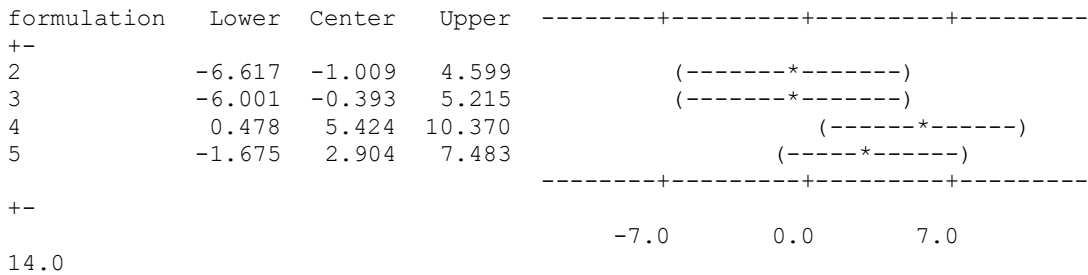
formulation	N	Mean	Grouping
4	3	9.303	A
5	4	6.784	A B
1	4	3.880	B
3	2	3.486	A B
2	2	2.871	B

Means that do not share a letter are significantly different.

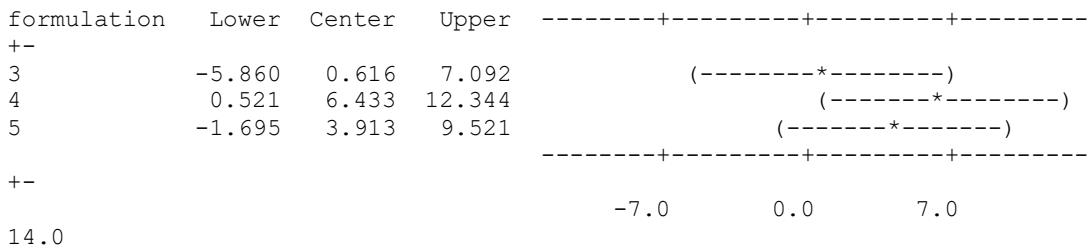
Tukey 95% Simultaneous Confidence Intervals
All Pairwise Comparisons among Levels of formulation

Individual confidence level = 99.18%

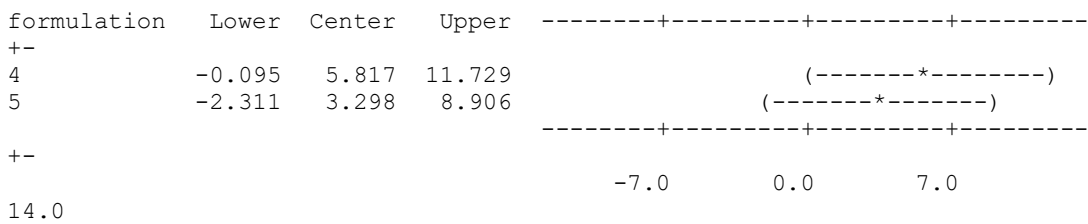
formulation = 1 subtracted from:



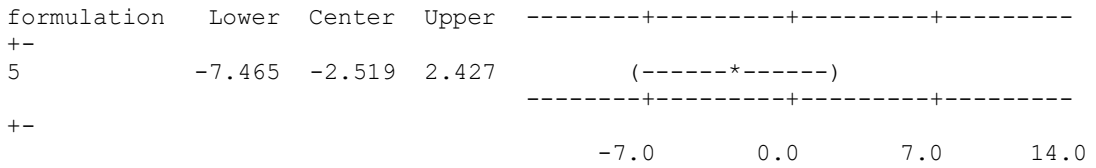
formulation = 2 subtracted from:



formulation = 3 subtracted from:



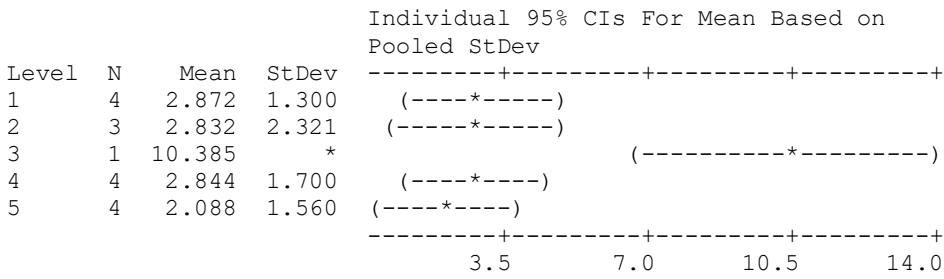
formulation = 4 subtracted from:



One-way ANOVA: to versus formulation

Source	DF	SS	MS	F	P
formulation	4	57.83	14.46	5.00	0.015
Error	11	31.82	2.89		
Total	15	89.65			

S = 1.701 R-Sq = 64.51% R-Sq(adj) = 51.60%



Pooled StDev = 1.701

Grouping Information Using Tukey Method

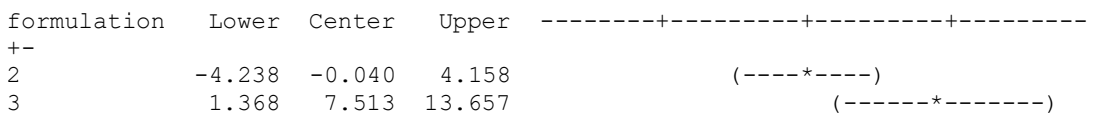
formulation	N	Mean	Grouping
3	1	10.385	A
1	4	2.872	B
4	4	2.844	B
2	3	2.832	B
5	4	2.088	B

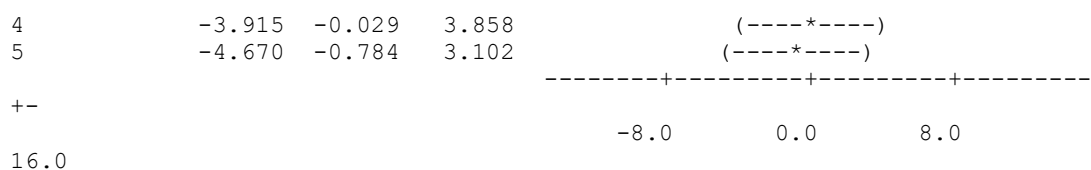
Means that do not share a letter are significantly different.

Tukey 95% Simultaneous Confidence Intervals
All Pairwise Comparisons among Levels of formulation

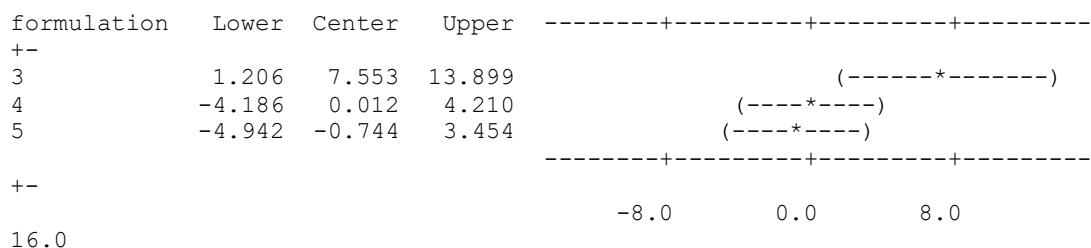
Individual confidence level = 99.20%

formulation = 1 subtracted from:

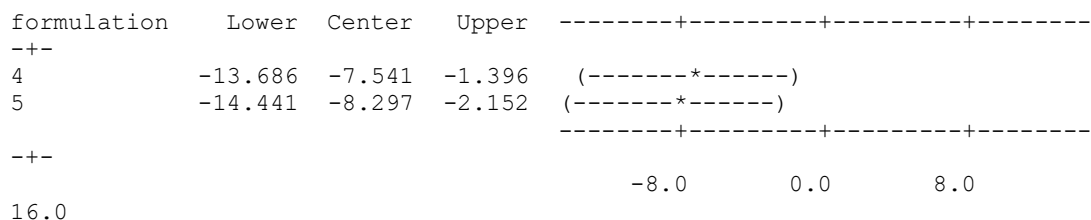




formulation = 2 subtracted from:



formulation = 3 subtracted from:



formulation = 4 subtracted from:

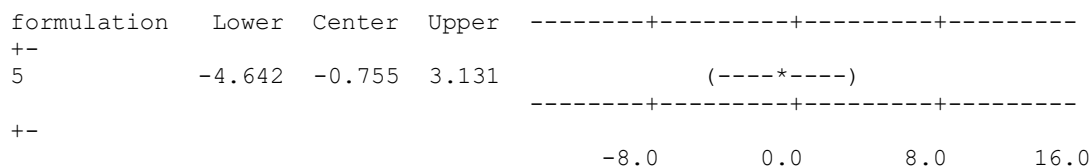


Table B.3 Results for Tukey's mean comparison test for NMR release data of hydrogels

General Linear Model: R at 0.5h versus sample; CH

Factor	Type	Levels	Values
sample	fixed	4	100A; 25A; 50A; 75A
CH	fixed	2	ch; no ch

Analysis of Variance for R at 0.5h, using Adjusted SS for Tests

Source	DF	Seq SS	Adj SS	Adj MS	F	P
--------	----	--------	--------	--------	---	---

sample	3	153,33	154,08	51,36	3,30	0,052
CH	1	196,11	159,04	159,04	10,23	0,006
sample*CH	3	222,35	222,35	74,12	4,77	0,017
Error	14	217,68	217,68	15,55		
Total	21	789,47				

S = 3,94314 R-Sq = 72,43% R-Sq(adj) = 58,64%

Unusual Observations for R at 0.5h

Obs	R at 0.5h	Fit	SE Fit	Residual	St Resid
3	16,6000	6,4100	2,2766	10,1900	3,17 R

R denotes an observation with a large standardized residual.

Grouping Information Using Tukey Method and 95,0% Confidence

sample	N	Mean	Grouping
50A	6	12,5	A
25A	6	9,8	A
100A	5	7,0	A
75A	5	5,6	A

Means that do not share a letter are significantly different.

Grouping Information Using Tukey Method and 95,0% Confidence

CH	N	Mean	Grouping
ch	12	11,4	A
no ch	10	6,0	B

Means that do not share a letter are significantly different.

Grouping Information Using Tukey Method and 95,0% Confidence

sample	CH	N	Mean	Grouping
50A	ch	3	20,4	A
25A	ch	3	12,5	A B
100A	no ch	2	7,5	B
25A	no ch	3	7,0	B
75A	ch	3	6,5	B
100A	ch	3	6,4	B
50A	no ch	3	4,7	B
75A	no ch	2	4,6	B

Means that do not share a letter are significantly different.

General Linear Model: R at 1h versus sample; CH

Factor	Type	Levels	Values
sample	fixed	4	100A; 25A; 50A; 75A
CH	fixed	2	ch; no ch

Analysis of Variance for R at 1h, using Adjusted SS for Tests

Source	DF	Seq SS	Adj SS	Adj MS	F	P
sample	3	304,18	323,88	107,96	4,08	0,028
CH	1	505,12	443,48	443,48	16,78	0,001
sample*CH	3	177,41	177,41	59,14	2,24	0,129
Error	14	370,09	370,09	26,44		
Total	21	1356,80				

S = 5,14153 R-Sq = 72,72% R-Sq(adj) = 59,08%

Unusual Observations for R at 1h

Obs	R at 1h	Fit	SE Fit	Residual	St Resid
2	2,1700	13,4533	2,9685	-11,2833	-2,69 R
3	25,2900	13,4533	2,9685	11,8367	2,82 R

R denotes an observation with a large standardized residual.

Grouping Information Using Tukey Method and 95,0% Confidence

sample	N	Mean	Grouping
50A	6	17,6	A
25A	6	13,7	A B
100A	5	11,1	A B
75A	5	6,9	B

Means that do not share a letter are significantly different.

Grouping Information Using Tukey Method and 95,0% Confidence

CH	N	Mean	Grouping
ch	12	16,9	A
no ch	10	7,8	B

Means that do not share a letter are significantly different.

Grouping Information Using Tukey Method and 95,0% Confidence

sample	CH	N	Mean	Grouping
50A	ch	3	26,6	A
25A	ch	3	18,8	A B
100A	ch	3	13,5	A B
100A	no ch	2	8,8	B
75A	ch	3	8,7	B
50A	no ch	3	8,7	B
25A	no ch	3	8,6	B
75A	no ch	2	5,1	B

Means that do not share a letter are significantly different.

General Linear Model: R at 2h versus sample; CH

Factor	Type	Levels	Values
sample	fixed	4	100A; 25A; 50A; 75A
CH	fixed	2	ch; no ch

Analysis of Variance for R at 2h, using Adjusted SS for Tests

Source	DF	Seq SS	Adj SS	Adj MS	F	P
sample	3	427,26	461,35	153,78	30,68	0,000
CH	1	1120,45	995,92	995,92	198,70	0,000
sample*CH	3	317,20	317,20	105,73	21,09	0,000
Error	11	55,13	55,13	5,01		
Total	18	1920,04				

S = 2,23880 R-Sq = 97,13% R-Sq(adj) = 95,30%

Grouping Information Using Tukey Method and 95,0% Confidence

sample	N	Mean	Grouping
50A	6	24,6	A
100A	4	20,3	A B
25A	4	19,2	B
75A	5	11,6	C

Means that do not share a letter are significantly different.

Grouping Information Using Tukey Method and 95,0% Confidence

CH	N	Mean	Grouping
ch	10	26,3	A
no ch	9	11,6	B

Means that do not share a letter are significantly different.

Grouping Information Using Tukey Method and 95,0% Confidence

sample	CH	N	Mean	Grouping
50A	ch	3	36,9	A
100A	ch	2	30,7	A B
25A	ch	2	23,0	B C
25A	no ch	2	15,4	C D
75A	ch	3	14,7	D
50A	no ch	3	12,4	D
100A	no ch	2	10,0	D
75A	no ch	2	8,5	D

Means that do not share a letter are significantly different.

General Linear Model: R at 3h versus sample; CH

Factor	Type	Levels	Values
sample	fixed	4	100A; 25A; 50A; 75A
CH	fixed	2	ch; no ch

Analysis of Variance for R at 3h, using Adjusted SS for Tests

Source	DF	Seq SS	Adj SS	Adj MS	F	P
sample	3	1040,14	1131,20	377,07	9,88	0,001
CH	1	2294,63	2183,87	2183,87	57,23	0,000
sample*CH	3	413,81	413,81	137,94	3,61	0,043
Error	13	496,05	496,05	38,16		
Total	20	4244,63				

S = 6,17718 R-Sq = 88,31% R-Sq(adj) = 82,02%

Unusual Observations for R at 3h

Obs	R at 3h	Fit	SE Fit	Residual	St Resid
10	49,1900	36,0700	3,5664	13,1200	2,60 R

R denotes an observation with a large standardized residual.

Grouping Information Using Tukey Method and 95,0% Confidence

sample	N	Mean	Grouping
50A	6	34,3	A
25A	6	28,6	A
100A	4	23,4	A B
75A	5	14,4	B

Means that do not share a letter are significantly different.

Grouping Information Using Tukey Method and 95,0% Confidence

CH	N	Mean	Grouping
ch	11	35,6	A
no ch	10	14,8	B

Means that do not share a letter are significantly different.

Grouping Information Using Tukey Method and 95,0% Confidence

sample	CH	N	Mean	Grouping
50A	ch	3	50,8	A
25A	ch	3	36,1	A B
100A	ch	2	35,7	A B C
25A	no ch	3	21,2	B C D
75A	ch	3	19,7	B C D
50A	no ch	3	17,8	C D
100A	no ch	2	11,1	D
75A	no ch	2	9,1	D

Means that do not share a letter are significantly different.

General Linear Model: R at 4h versus sample; CH

Factor	Type	Levels	Values
sample	fixed	4	100A; 25A; 50A; 75A
CH	fixed	2	ch; no ch

Analysis of Variance for R at 4h, using Adjusted SS for Tests

Source	DF	Seq SS	Adj SS	Adj MS	F	P
sample	3	1266,47	1117,61	372,54	8,36	0,002
CH	1	2906,07	2685,16	2685,16	60,24	0,000
sample*CH	3	609,77	609,77	203,26	4,56	0,022
Error	13	579,43	579,43	44,57		
Total	20	5361,74				

S = 6,67619 R-Sq = 89,19% R-Sq(adj) = 83,37%

Grouping Information Using Tukey Method and 95,0% Confidence

sample	N	Mean	Grouping
50A	6	39,5	A
25A	6	36,9	A
100A	4	24,0	B
75A	5	23,0	B

Means that do not share a letter are significantly different.

Grouping Information Using Tukey Method and 95,0% Confidence

CH	N	Mean	Grouping
ch	10	42,4	A
no ch	11	19,3	B

Means that do not share a letter are significantly different.

Grouping Information Using Tukey Method and 95,0% Confidence

sample	CH	N	Mean	Grouping
50A	ch	3	59,5	A
25A	ch	3	44,7	A B
100A	ch	2	35,2	B C
75A	ch	2	30,1	B C
25A	no ch	3	29,0	B C
50A	no ch	3	19,4	C
75A	no ch	3	15,9	C
100A	no ch	2	12,9	C

Means that do not share a letter are significantly different.

General Linear Model: R at 5h versus sample; CH

Factor	Type	Levels	Values
sample	fixed	4	100A; 25A; 50A; 75A
CH	fixed	2	ch; no ch

Analysis of Variance for R at 5h, using Adjusted SS for Tests

Source	DF	Seq SS	Adj SS	Adj MS	F	P
sample	3	3489,7	3285,0	1095,0	26,87	0,000
CH	1	3296,5	3330,6	3330,6	81,74	0,000
sample*CH	3	694,2	694,2	231,4	5,68	0,008
Error	15	611,2	611,2	40,7		
Total	22	8091,5				

S = 6,38334 R-Sq = 92,45% R-Sq(adj) = 88,92%

Unusual Observations for R at 5h

Obs	R at 5h	Fit	SE Fit	Residual	St Resid
10	66,3000	53,9433	3,6854	12,3567	2,37 R
22	49,9200	39,0700	3,6854	10,8500	2,08 R

R denotes an observation with a large standardized residual.

Grouping Information Using Tukey Method and 95,0% Confidence

sample	N	Mean	Grouping
25A	6	46,5	A
50A	6	42,5	A
100A	5	28,0	B
75A	6	17,0	B

Means that do not share a letter are significantly different.

Grouping Information Using Tukey Method and 95,0% Confidence

CH	N	Mean	Grouping
ch	11	45,6	A
no ch	12	21,4	B

Means that do not share a letter are significantly different.

Grouping Information Using Tukey Method and 95,0% Confidence

sample	CH	N	Mean	Grouping
50A	ch	3	62,5	A
25A	ch	3	53,9	A B
100A	ch	2	42,4	A B C
25A	no ch	3	39,1	B C
75A	ch	3	23,8	C D
50A	no ch	3	22,6	C D
100A	no ch	3	13,6	D
75A	no ch	3	10,2	D

Means that do not share a letter are significantly different.

General Linear Model: R at 6h versus sample; CH

Factor	Type	Levels	Values
sample	fixed	4	100A; 25A; 50A; 75A
CH	fixed	2	ch; no ch

Analysis of Variance for R at 6h, using Adjusted SS for Tests

Source	DF	Seq SS	Adj SS	Adj MS	F	P
sample	3	4290,2	4105,1	1368,4	39,74	0,000
CH	1	2832,6	2813,6	2813,6	81,71	0,000
sample*CH	3	784,7	784,7	261,6	7,60	0,003
Error	15	516,5	516,5	34,4		
Total	22	8424,1				

S = 5,86806 R-Sq = 93,87% R-Sq(adj) = 91,01%

Unusual Observations for R at 6h

Obs	R at 6h	Fit	SE Fit	Residual	St Resid
22	56,0000	45,7433	3,3879	10,2567	2,14 R

R denotes an observation with a large standardized residual.

Grouping Information Using Tukey Method and 95,0% Confidence

sample	N	Mean	Grouping
25A	6	51,8	A
50A	6	45,5	A
100A	5	29,8	B
75A	6	18,2	C

Means that do not share a letter are significantly different.

Grouping Information Using Tukey Method and 95,0% Confidence

CH	N	Mean	Grouping
ch	11	47,5	A
no ch	12	25,2	B

Means that do not share a letter are significantly different.

Grouping Information Using Tukey Method and 95,0% Confidence

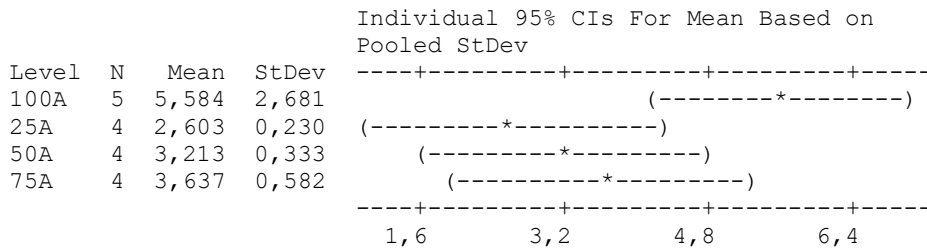
sample	CH	N	Mean	Grouping
50A	ch	3	65,9	A
25A	ch	3	57,8	A B
25A	no ch	3	45,7	B
100A	ch	2	41,2	B C
50A	no ch	3	25,1	C D
75A	ch	3	25,0	C D
100A	no ch	3	18,4	D
75A	no ch	3	11,4	D

Means that do not share a letter are significantly different.

One-way ANOVA: D versus sample

Source	DF	SS	MS	F	P
sample	3	23,06	7,69	3,30	0,054
Error	13	30,25	2,33		
Total	16	53,31			

S = 1,525 R-Sq = 43,26% R-Sq(adj) = 30,17%



Pooled StDev = 1,525

Grouping Information Using Tukey Method

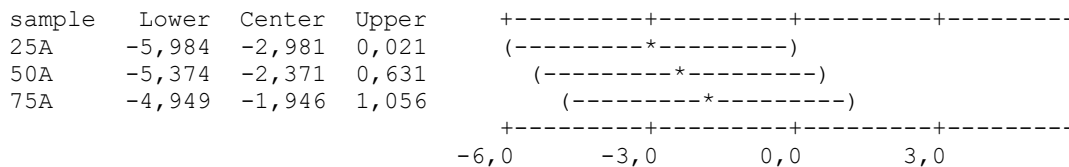
sample	N	Mean	Grouping
100A	5	5,584	A
75A	4	3,637	A
50A	4	3,213	A
25A	4	2,603	A

Means that do not share a letter are significantly different.

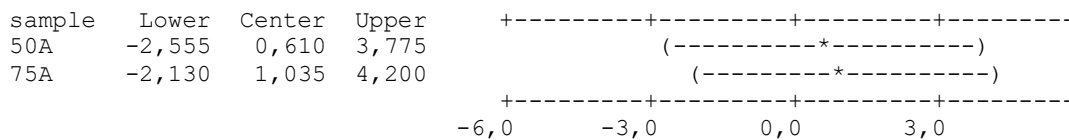
Tukey 95% Simultaneous Confidence Intervals All Pairwise Comparisons among Levels of sample

Individual confidence level = 98,84%

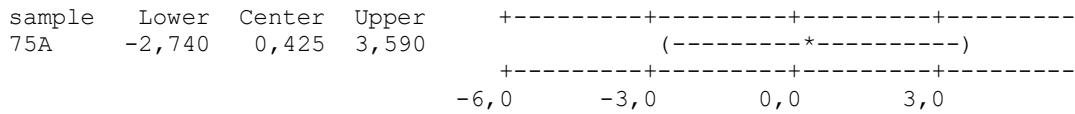
sample = 100A subtracted from:



sample = 25A subtracted from:



sample = 50A subtracted from:



General Linear Model: D versus sample; CH

Factor	Type	Levels	Values
sample	fixed	4	100A; 25A; 50A; 75A
CH	fixed	2	ch; no ch

Analysis of Variance for D, using Adjusted SS for Tests

Source	DF	Seq SS	Adj SS	Adj MS	F	P
sample	3	23,060	27,469	9,156	4,13	0,043
CH	1	1,027	0,595	0,595	0,27	0,617
sample*CH	3	9,269	9,269	3,090	1,39	0,307
Error	9	19,950	19,950	2,217		
Total	16	53,307				

S = 1,48884 R-Sq = 62,58% R-Sq(adj) = 33,47%

Unusual Observations for D

Obs	D	Fit	SE Fit	Residual	St Resid
3	7,85000	4,45000	0,85958	3,40000	2,80 R

R denotes an observation with a large standardized residual.

Grouping Information Using Tukey Method and 95,0% Confidence

sample	N	Mean	Grouping
100A	5	5,9	A
75A	4	3,6	A B
50A	4	3,2	A B
25A	4	2,6	B

Means that do not share a letter are significantly different.

Grouping Information Using Tukey Method and 95,0% Confidence

CH	N	Mean	Grouping
no ch	8	4,0	A
ch	9	3,6	A

Means that do not share a letter are significantly different.

Grouping Information Using Tukey Method and 95,0% Confidence

sample	CH	N	Mean	Grouping
--------	----	---	------	----------

100A	no ch	2	7,3	A
100A	ch	3	4,4	A
75A	ch	2	3,9	A
50A	ch	2	3,4	A
75A	no ch	2	3,3	A
50A	no ch	2	3,0	A
25A	ch	2	2,7	A
25A	no ch	2	2,5	A

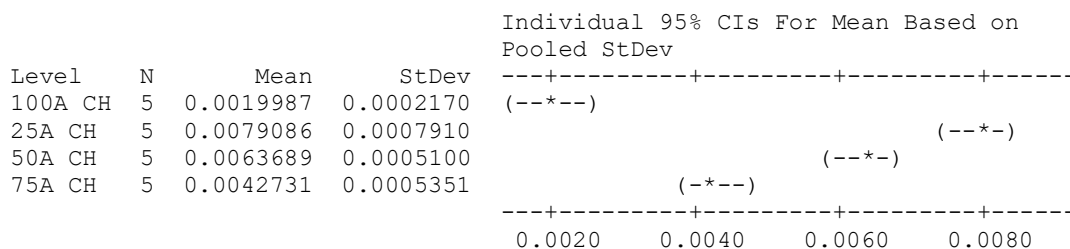
Means that do not share a letter are significantly different.

Table B.4 Results for Tukey’s mean comparison test for texture results of hydrogels

One-way ANOVA: firmness versus sample

Source	DF	SS	MS	F	P
sample	3	0.0000990	0.0000330	108.23	0.000
Error	16	0.0000049	0.0000003		
Total	19	0.0001038			

S = 0.0005521 R-Sq = 95.30% R-Sq(adj) = 94.42%



Pooled StDev = 0.0005521

Grouping Information Using Tukey Method

sample	N	Mean	Grouping
25A CH	5	0.0079086	A
50A CH	5	0.0063689	B
75A CH	5	0.0042731	C
100A CH	5	0.0019987	D

Means that do not share a letter are significantly different.

Tukey 95% Simultaneous Confidence Intervals
All Pairwise Comparisons among Levels of sample

Individual confidence level = 98.87%

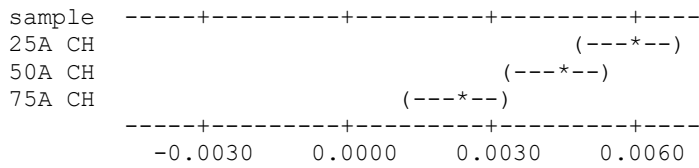
sample = 100A CH subtracted from:

sample	Lower	Center	Upper
25A CH	0.0049098	0.0059098	0.0069098

```

50A CH  0.0033702  0.0043702  0.0053702
75A CH  0.0012744  0.0022744  0.0032744

```

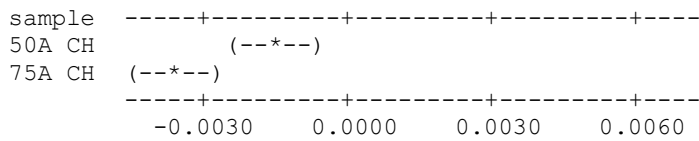


sample = 25A CH subtracted from:

```

sample      Lower      Center      Upper
50A CH  -0.0025396  -0.0015397  -0.0005397
75A CH  -0.0046354  -0.0036354  -0.0026354

```

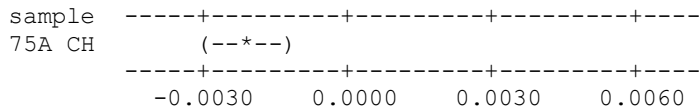


sample = 50A CH subtracted from:

```

sample      Lower      Center      Upper
75A CH  -0.0030958  -0.0020958  -0.0010958

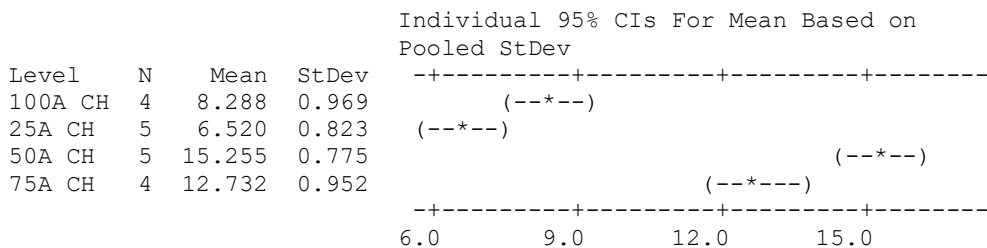
```



One-way ANOVA: springiness versus sample

Source	DF	SS	MS	F	P
sample	3	230.855	76.952	101.16	0.000
Error	14	10.649	0.761		
Total	17	241.504			

S = 0.8722 R-Sq = 95.59% R-Sq(adj) = 94.65%



Pooled StDev = 0.872

Grouping Information Using Tukey Method

sample	N	Mean	Grouping
50A CH	5	15.255	A
75A CH	4	12.732	B
100A CH	4	8.288	C
25A CH	5	6.520	D

Means that do not share a letter are significantly different.

Tukey 95% Simultaneous Confidence Intervals
All Pairwise Comparisons among Levels of sample

Individual confidence level = 98.85%

sample = 100A CH subtracted from:

sample	Lower	Center	Upper	
25A CH	-3.469	-1.768	-0.068	(--*--)
50A CH	5.266	6.966	8.667	(--*--)
75A CH	2.651	4.443	6.236	(--*--)

-----+-----+-----+-----+-----
-6.0 0.0 6.0 12.0

sample = 25A CH subtracted from:

sample	Lower	Center	Upper	
50A CH	7.132	8.735	10.338	(--*--)
75A CH	4.511	6.212	7.912	(--*--)

-----+-----+-----+-----+-----
-6.0 0.0 6.0 12.0

sample = 50A CH subtracted from:

sample	Lower	Center	Upper	
75A CH	-4.223	-2.523	-0.823	(--*--)

-----+-----+-----+-----+-----
-6.0 0.0 6.0 12.0

CURRICULUM VITAE

PERSONAL INFORMATION

Surname, Name : ÇIKRIKCI, SEVİL
Nationality : Turkish (TC)
Date and Place of Birth : 24 May 1988, Bartın
Phone : +90 312 210 56 26
E-mail : e156202@metu.edu.tr

EDUCATION

Degree	Institution	Year of Graduation
MS	METU Food Engineering	2013
BS	METU Food Engineering	2011
High School	Davut Fırıncıoğlu Anadolu High School, Bartın	2006

WORK EXPERIENCE

Year	Place	Enrollment
2018-2019	UC Berkeley, Bioscience Dept.	Visiting Student Researcher
2012-2018	METU Dept. of Food Eng.	Research Assistant
2011-2012	ETI Food Ind. And Trade Co.	Product Development Engineer

FOREIGN LANGUAGES

Advanced English, Beginner German

PUBLICATIONS

1. Barskiy, D., Tayler, M., Marco, I., Kentner, A., Vigneron, D., **Cikrikci, S.**, Aydogdu, A., Reh, M., Pravdivtsev, A., Hovener, J., Blanchard, J., Wu, T., Budker, D., & Pines, A. (2019). Zero-Field Nuclear Magnetic Resonance of Chemically Exchanging Systems. *Nature Communications*.

2. **Cikrikci, S., & Oztop M.H. (2018).** Development of pH Sensitive Alginate/Gum Tragacanth Based Hydrogels for Oral Insulin Delivery. *Journal of Agricultural and Food Chemistry, Article ASAP*, <http://doi.org/10.1021/acs.jafc.8b02525>
3. **Cikrikci, S., & Oztop, M. H. (2018).** Oil Migration in Hazelnut Paste/Chocolate Systems Using Magnetic Resonance Imaging. *Journal of Food Measurement and Characterization*, 12(3), 1460-1472. <https://doi.org/10.1007/s11694-018-9761-0>
4. 4. Tonyali, B., **Cikrikci, S., & Oztop, M. H. (2018).** Physicochemical and Microstructural Characterization of Gum Tragacanth Added Whey Protein Based Films. *Food Research International*, 105, 1–9. <http://doi.org/10.1016/j.foodres.2017.10.071>
5. Ozel B., **Cikrikci S., Aydın O., & Oztop M.H. (2017).** Polysaccharide Blended Whey Protein Isolate-(WPI) Hydrogels: A Physicochemical and Controlled Release Study. *Food Hydrocolloids*, 71, 35-46.
6. Kirtil E., **Cikrikci S., & Oztop M.H. (2017).** Recent Advances in TD NMR & MRI Sensors. *Current Opinion in Food Science*, 17, 9-15.
7. **Cikrikci, S., & Oztop, M.H. (2017).** Mathematical Modeling and Use of Magnetic Resonance Imaging (MRI) for Oil Migration in Chocolate Confectionery Systems. *Food Engineering Reviews*, 9(1), 50-70.
8. **Cikrikci, S., Yucekutlu, M., Mert, B., & Oztop, M.H. (2016).** Physical Characterization of Low-Calorie Chocolate Formulations. *Journal of Food Measurement and Characterization*, 11(1), 41-49.
9. **Cikrikci, S., Demirkesen, I., & Mert, B. (2016).** Production of Hazelnut Skin Fibres and Utilisation in a Model Bakery Product. *Quality Assurance and Safety of Crops & Foods*, 8(2), 195-206.

HOBBIES

Ceramics, Guitar, Tennis)